An Abstract of the Thesis of

Theodore A. Hammer for the degree of Master of Science in

Civil Engineering presented on November 3, 1983.

Title: DYNAMIC PROPERTIES OF NATURALLY FROZEN ICE

Abstract approved: Redacted for privacy

Ted S. Vinson

In recognition of the need to determine dynamic properties of naturally frozen materials, a research project was conducted to measure the dynamic properties (dynamic moduli and damping ratio) of naturally frozen wedge ice samples obtained from the Fairbanks, Alaska area. Cyclic triaxial and resonant column test systems were employed to subject the samples to a range of conditions associated with dynamic loading of frozen ground deposits. Test parameters considered in the program included temperature, confining pressure, strain amplitude, and frequency of loading. Material properties considered were density and sample core orientation.

A preliminary laboratory investigation was performed on laboratory prepared ice specimens to develop methods for attaching the naturally frozen ice specimens to the cyclic triaxial and resonant column test systems. Time effects were also evaluated on laboratory prepared

ice specimens to determine the time required for dynamic properties to stabilize following temperature and confining pressure changes. The orientation of ice crystals was determined and mapped to establish if the core samples were anisotropic. A preferred crystal orientation was noted for all the naturally frozen ice samples.

All naturally frozen ice specimens were tested in the resonant column test apparatus first, due to the potential for specimen damage during cyclic triaxial testing at high strain amplitudes. During resonant column testing the specimens were subjected to both longitudinal and torsional excitation under various confining pressures (0, 30 and 70 psi (0, 207 and 482 KN/m^2)), under controlled temperatures of -1, -4 and -10°C (30, 25 and 14°F). During cyclic triaxial testing, dynamic properties were measured at various confining pressures (0, 30 and 70 psi (0, 207 and 482 KN/m^2)) strain amplitudes (.0009, .005 and .01%) and loading frequencies (.05, .5 and 5 cps) under controlled temperature conditions of -1, -4 and -10°C (30, 25 and 14°F.

Measurements of the dynamic properties of the naturally frozen ice samples under varying conditions of temperature, confining pressure, strain amplitude, and loading frequency indicated that the parameters considered in the program have an influence on the dynamic properties. Specifically, it was found that: (1) the dynamic moduli increased with increased frequency of loading and strain amplitude, but showed a decrease with ascending temperature, and (2) in general, the damping ratio decreased with increased frequency of loading and strain amplitude but showed an increased with ascending temperature. Sample core orientation had little affect on the dynamic properties for the wedge ice samples employed in the test program. It was also found that the dynamic properties were influenced to a greater extent by changes in temperature and confining pressure when the test specimen were subjected to strong motion loading conditions (low frequency, high strain amplitude) rather than weak motion conditions (high frequency, low strain amplitude).

DYNAMIC PROPERTIES OF NATURALLY FROZEN ICE

by

Theodore A. Hammer

A THESIS

submitted to
Oregon State University

in partial fulfillment of
the requirements for the
degree of

Master of Science

Completed November 3, 1983

Commencement June, 1984

APPROVED:

Redacted for privacy

Professor of Civil Engineering in charge of major

Redacted for privacy

Head of Department of Civil Engineering

Redacted for privacy

Dean of Graduate School

Date thesis presented: November 3, 1983

Typed by Nancy Brost for Theodore A. Hammer

ACKNOWLEDGEMENTS

I would like to extend my thanks to the National Science Foundation which provided the financial assistance necessary to perform the work documented in this thesis under Grant 77-04437: "Dynamic Properties of Naturally Frozen Soils".

I would also like to express my thanks to the following people for their support during the research project:

T.S. Vinson	W.L. Schroeder	A. Brickman
R. Rieke	T. Allen	C. Wilson
P. Bolander	K. Mills	L. Wilchman

TABLE OF CONTENTS

TABLE OF CONTENTS (continued)

TABLE OF CONTENTS (continued)

LIST OF FIGURES

LIST OF FIGURES (continued)

Page

LIST OF FIGURES (continued)

LIST OF FIGURES (continued)

LIST OF FIGURES (continued)

LIST OF TABLES

DYNAMIC PROPTERTIES OF NATURALLY FROZEN ICE

by

Theodore A. Hammer

1. INTRODUCTION

1.1 Statement of Problem

In the early 1900's gold was discovered in the Klondike which instigated a gold rush and the first significant population boom in the arctic regions of Alaska and Western Canada. From that time the population of Alaska grew and expanded steadily. The discovery of oil in Cook Inlet in the 1950's was influential in Alaska becoming the 49th state in the United States in 1959. Since that time the discovery of additional natural resources in arctic and subarctic regions has created significant interest in the development of civil engineering and industrial works. With recent discoveries of oil and natural gas in Alaska many new engineering projects have been constructed. Since 85% of Alaska lies within either continuous or discontinuous permafrost, and much of Alaska is also located within one of the world's most active seismic zones, a knowledge of the dynamic behavior of frozen ground is essential to the solution of engineering problems associated with dynamic loading of permafrost.

To solve engineering problems involving dynamic material responses, two soil properties are required: (1) The dynamic shear modulus, and (2) the damping ratio. With a knowledge of these soil properties, ground surface motions during earthquakes and ground response to other vibratory loading conditions may be predicted by several analytical techniques (Seed, et al., 1974, Idriss and Seed, 1968; Lysmer et al., 1974; Schnabel et al., 1972; Streeter et al., 1974.) To date, the measurement of dynamic properties of naturally frozen ground has been directed primarily toward high frequency, low strain amplitude testing (Stevens, 1966; Kaplar 1969). With recent advancements in laboratory test equipment (Bolander, 1980; Vinson, et. al., 1978; Kaplar, 1981) it is now possible to test naturally frozen ground at loading frequencies and strain amplitudes equivalent to earthquake loading, blasting, foundation vibration loading and other strong motion loading conditions.

The research program presented herein was conducted simultaneously with another research program (Wilson, 1982) to evaluate the dynamic properties of naturally frozen ground. This research program involved the preparation of naturally frozen ice samples which were obtained from the Fairbanks, Alaska area (Bolander, 1980), and the measurement of dynamic properties under controlled conditions to evaluate the effects of a number of material and test condition parameters which are associated with dynamic loading of permafrost deposits.

1.2 Purpose and Scope

The purpose of the research work reported herein is to evaluate the dynamic properties of naturally frozen ice over a range of test and material condition parameters associated with dynamic loading of frozen ground deposits. The test parameters considered in the research work include temperature, frequency of loading, strain amplitude and confining pressure. Material and sample properties considered include density, crystal size, crystal structure and anisotropy.

The scope of this research is limited to the evaluation of dynamic properties of eight ice samples obtained in 1977 from the Fairbanks Alaska area, (Bolander, 1980) transported to Oregon State University and stored in a walk-in freezer (Baker, 1975). The material included in this thesis is presented in the following order: Chapter 2 provides a brief background on the mechanical properties of ice and test systems to evaluate dynamic properties of ice; Chapters 3 and 4 summarize the procedures used to prepare ice samples for dynamic testing together with procedures for attaching the ice specimens to the two test systems (resonant column and cyclic triaxial); Chapter 5 presents and summarizes the data obtained during the test program, and provides an interpretation of the test results; Chapter 6 gives conclusions and recommendations to be considered in future research work.

2. PHYSICS AND MECHANICS OF ICE AND TEST SYSTEMS TO EVALUATE DYNAMIC PROPTERTIES OF ICE

2.1 Physics and Mechanics of Ice

Stable and metastable ice exists in eight different spacial configurations (Glenn, 1974), as indicated on Figure 2-1. At the low pressures of interest to cold regions engineers, ice is found to be stable in the configuration referred to as ice I. Ice I has two structural variants which are closely related to each other. One is hexagonal in crystal symmetry and is referred to as ice Ih, the other is cubic in crystal symmetry and is referred to as ice Ic (See Figures 2-2 through 2-5). Since ice Ic is a metastable form of ice I, requiring very low temperatures during its formation (Glen, 1974), only the hexagonal form of ice I will be considered in this report.

The mechanical properties of ice are very temperature dependent in the range of interest to most engineers. At temperatures warmer than -8°C, the viscoelastic properties vary dramatically with temperature.

Creep, the plastic response of a material to an applied stress, is evident in ice at all temperatures, but is most pronounced at temperatures associated with engineering practice (warmer than -6°C). The elastic response of ice is also very temperature dependent at warmer temperatures, as evidenced by the changes in dynamic Young's modulus (Vinson and Chaichanavong, 1976). When small stresses are applied over short time periods the strain may lag the applied stress. This process in which no permanent deformation occurs, but there is a

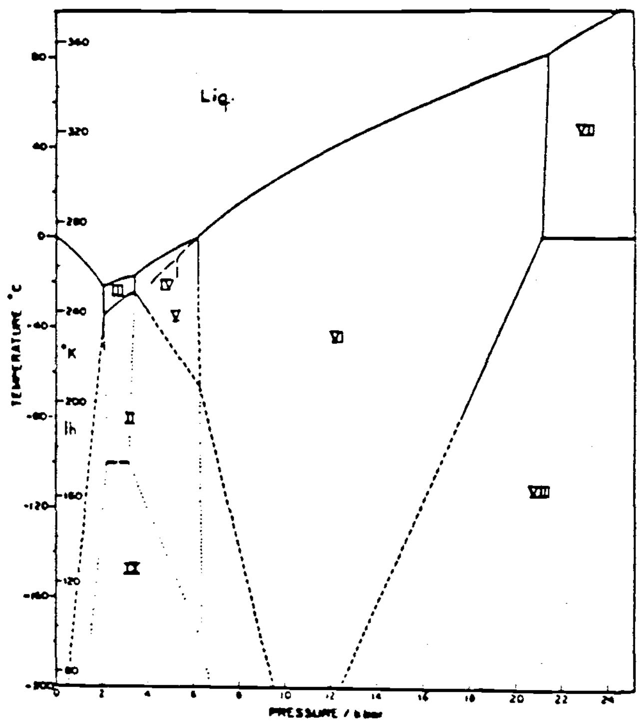

FIGURE 2-1 Phase Diagram of Ice. Dashed Lines Are Extrapolated Or Calculated Boundaries. Metastable Phases Apart From Ice Ih and Ic Are Shown By Light Lines. (From Ref. 271.)

(after Glen, 1974)

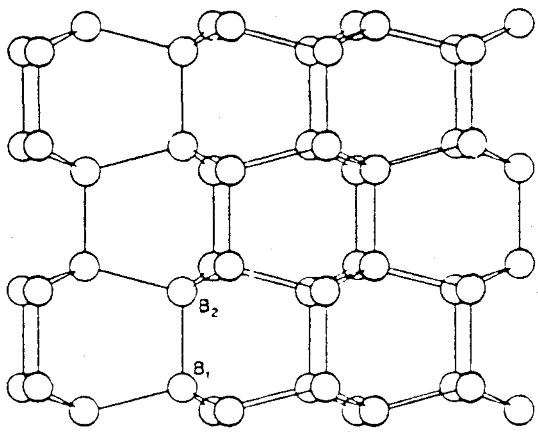

FIGURE 2-2 The Arrangement Of Water Molecules In Ice Ih. Note That The Three Water Molecules Bonded To B_2 Are Vertically Above Those Bonded To B_1.

(after Glen, 1974)

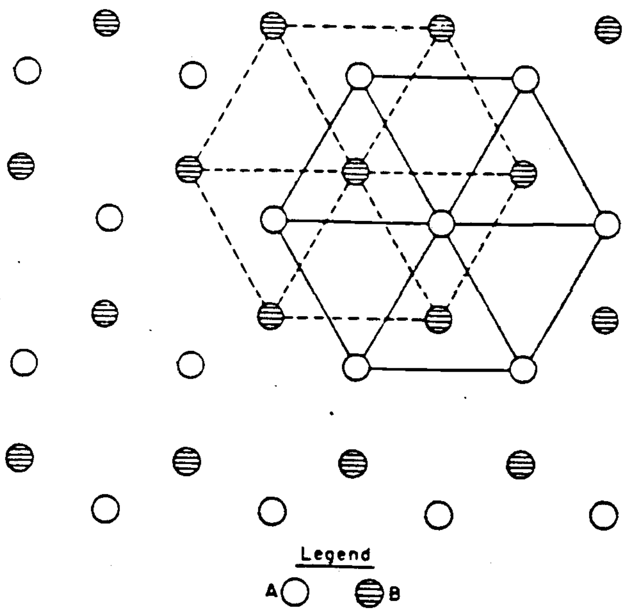

FIGURE 2-3 Projection Of The Structure Of Ice Ih Onto The Basal Plane. Molecules Are Arranged In The Stacking Sequence ABBAABBAABBAA... Large Straight Hexagonal Holes Penetrate The Structure.

(after Glen, 1974)

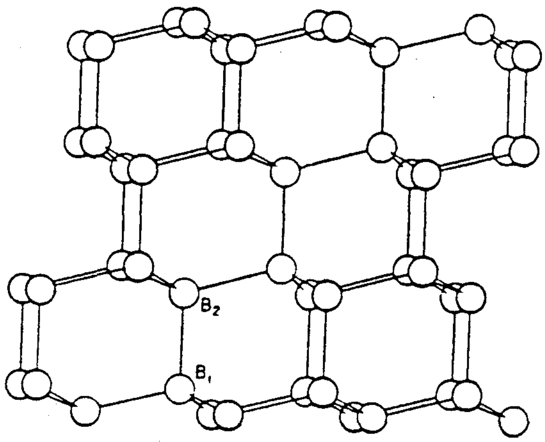

FIGURE 2-4 The Arrangement Of Water Molecules In Ice Ic. Compare With Figure 2-2. Note That The Three Water Molecules Bonded To B_2 Are Not Vertically Above Those Bonded To B_1 But Are Rotated 60° Around The Line B_1B_2 From The Positions That They Had in Figure 2-3.

(after Glen, 1974)

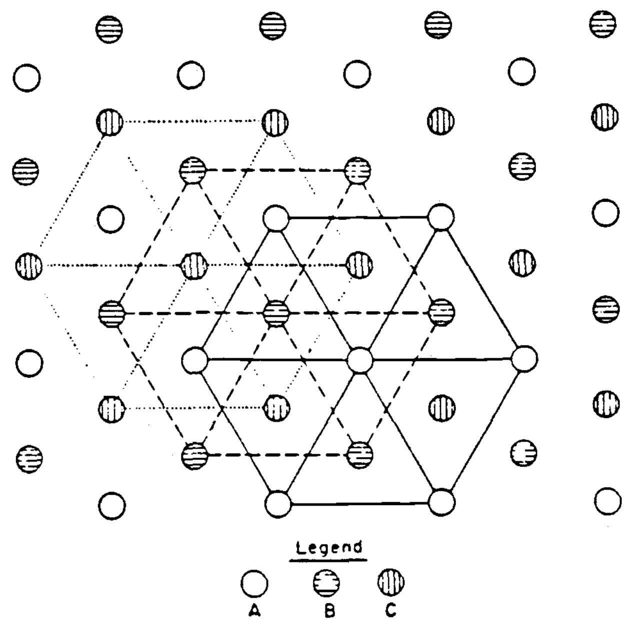

FIGURE 2-5 Projection Of The Structure Of Ice Ic Onto The (111) Plane. Compare With Figure 2-4. Molecules Are Arranged In The Stacking Sequence AFFCCAABB-CCAABBCC... .

(after Glen, 1974)

loss of energy, is known as anelasticity and is responsible for the damping observed in ice (Glen, 1975). Damping is also a temperature dependent phenomena (Vinson and Chaichanavong, 1976). Since a significant portion of the surficial material in Alaska exists in a temperature range of 0°C to -6°C, great emphasis should be placed on temperatures in this range (Vinson, 1975). In addition to temperature, Vinson and Chaichanavong (1976) found the mechanical properties of ice to be dependent on stain amplitude, frequency of loading, and confining pressure.

Ice crystals undergo plastic deformation (creep) because ice crystals slip readily on the basal planes (planes perpendicular to the c-axis) when a shear stress is applied. A misconception that ice is a brittle substance which is hard to deform arises from the fact that most naturally occurring ice crystals are oriented in such a way that it is not easy to apply shear stresses on the basal plane (Glen, 1975). For example, lake ice normally forms such that the c-axis is normal to the ice sheet. Loading of lake ice causes bending which results mainly in tension and compression normal to the c-axis. Little shear stress is applied to the basal plane during the bending stress.

Even if isotropic ice is formed (ice with randomly oriented grains) directional stresses applied to the ice mass will cause a shift of the ice grains, in time, towards a nonisotropic condition (preferred orientation of the ice crystals). The shift mechanism is through recrystallization and grain growth and is explained in detail by Glen (1975). To date, no studies have been conducted which compare dynamic engineering properties of ice to its degree of anisotropy.

2.2 Test Systems to Evaluate Dynamic Properties of Ice

For reasons previously noted by Bolander (1980), both the resonant column and the cyclic triaxial test systems must be employed to evaluate the dynamic properties of frozen soils over a range of strain amplitudes and frequencies of interest to engineers. As indicated by Figure 2-6, the cyclic triaxial and resonant column test systems simulate the strain amplitudes expected for most field loading conditions. Further, to date, no naturally occurring ice samples have been tested over such a wide range of strain amplitudes.

2.2.1 Resonant Column Testing of Ice

Laboratory prepared ice specimens were fabricated and tested by Stevens (1974 and 1975) in a resonant column test system similar to the test system employed in this research program. Right cylindrical test specimens were subjected to steady state sinusoidal vibrations in both the longitudinal and torsional mode through a fixed base plate. Accelerometers attached to the base (driven end) and the free end of the test specimen were monitored in both the longitudinal and torsional directions. Figure 2-7 shows a schematic of the test system used by Stevens which was located inside a walk-in cold room. A plexiglas environmental chamber was used to control the temperature of the test specimen. Details of the specimen preparation and testing have been given by Stevens (1975). The validity of the resonant column test system under fixed-free end conditions has been evaluated by Chung and Tyler (1979).

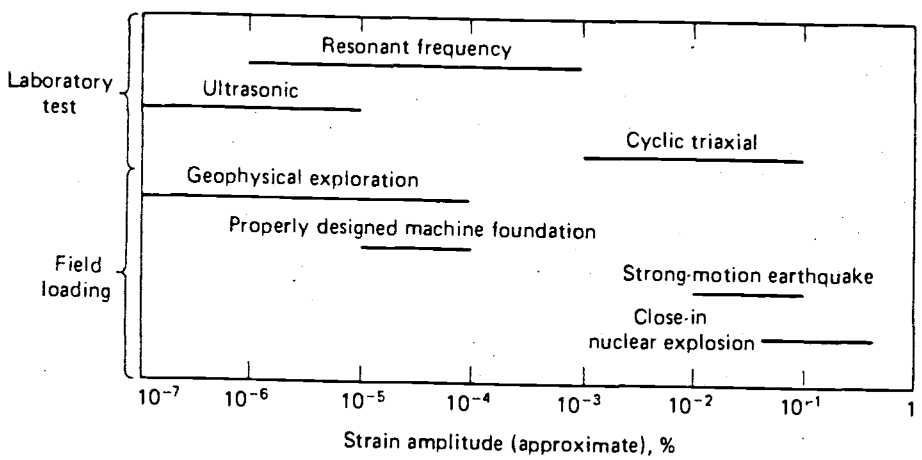

FIGURE 2-6 Relationship Between Laboratory And Field Strain Amplitudes

(after Vinson, 1978)

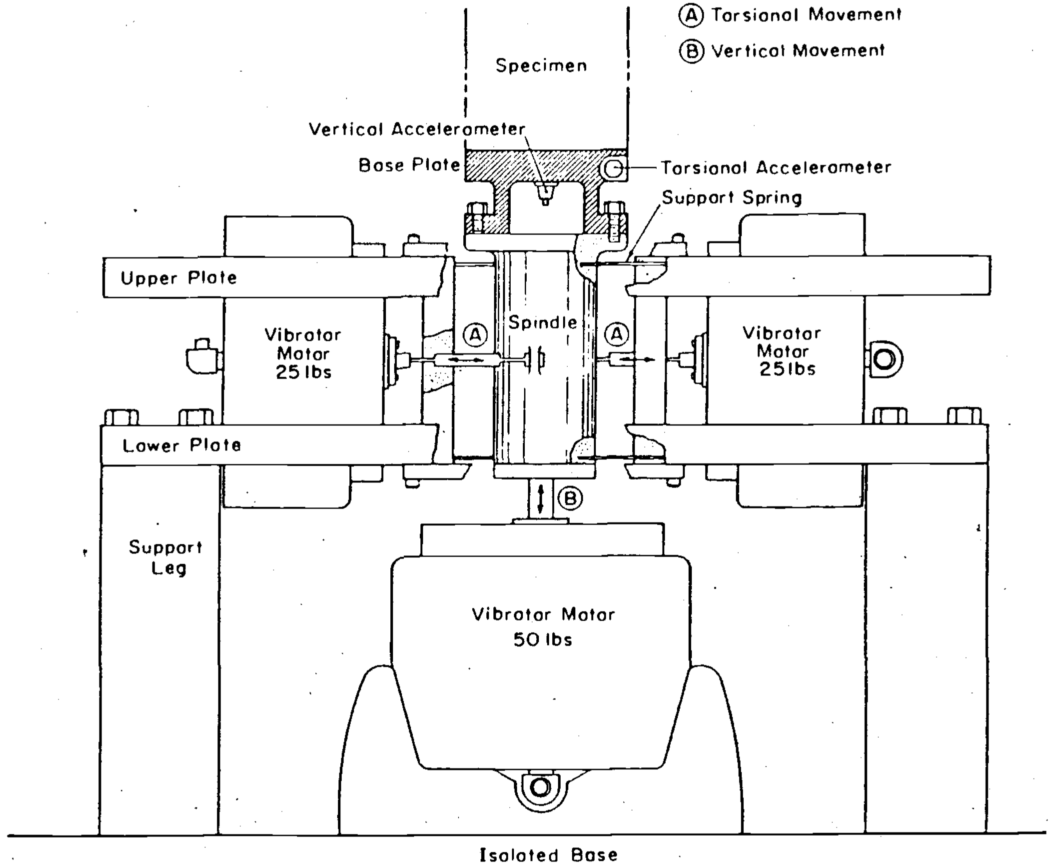

FIGURE 2-7 The Resonant Column Test System Employed By Stevens (1975)

2.2.2 Cyclic Triaxial Testing of Ice

The fundamentals of cyclic triaxial testing have been covered by Vinson and Chaichanavong (1976). Right cylindrical test specimens are attached to the cyclic triaxial test frame so they can be subjected to both compressive and tensile axial deviator stresses. The temperature and confining pressure are adjusted and the specimen is subjected to a steady state sinusoidal deviator stress of various frequencies and strain amplitudes. By cycling through equal tensile and compressive stresses during each cycle, the shear stresses are reversed causing the principal stresses to rotate through 90 degrees with each half cycle of loading. Figure 2-8 shows typical test results obtained from one cycle of loading. From these results dynamic Young's modulus (E_d) and damping ratio (D) can be determined using equations (1) and (2).

$$E_d = \frac{\sigma_{max,\ deviator}}{\varepsilon_{max,\ axial}} \tag{1}$$

$$D = \frac{A_L}{4\pi A_T} \tag{2}$$

The terms used in equations (1) and (2) are defined in Figure 2-8.

2.2.3 Unconfined Compressive Strength Testing of Ice

After testing was completed with the resonant column and cyclic triaxial test systems, unconfined compressive strength tests were performed. To minimize end constraint during unconfined

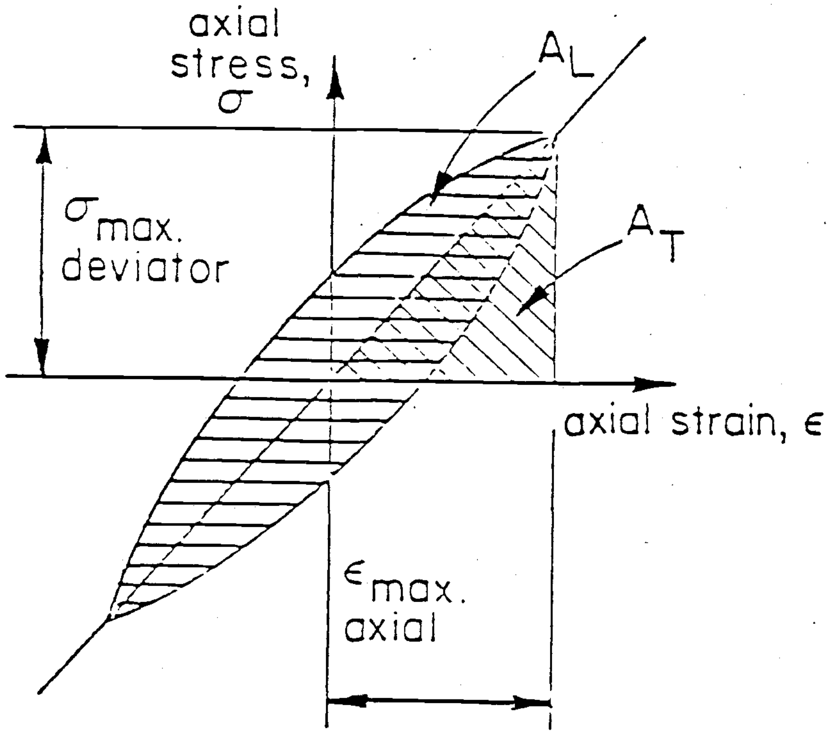

FIGURE 2-8 Deviator Stress Versus Axial Strain For One Load Cycle

(after Vinson & Chaichanavong, 1976)

compressive strength testing the samples were lathed to a dumbell shape. All unconfined compressive strength tests were conducted at the ambient coldroom temperature of -11°C ± 2°C.

3. TEST SPECIMEN PREPARATION FOR DYNAMIC AND STATIC TESTING AND ICE CRYSTALLOGRAPHY

This chapter provides details on the laboratory preparation of reconstituted, artificially frozen ice samples, and the trimming of test specimens from larger diameter samples (both naturally occurring and laboratory prepared) for use in the resonant column and cyclic triaxial test systems. The attachment of test specimens to the two test systems is also described, followed by a description of preparing specimens for unconfined compressive strength testing. Finally the preparation of ice thin-sections for the evaluation of crystal orientation is described.

3.1 Laboratory Fabrication of Ice Specimens

Right cylindrical polycrystalline ice samples were prepared in the laboratory using natural snow and distilled water. These samples were used to develop specimen preparation and testing procedures for the naturally frozen ice samples. An 18 in. (46.7 cm) long, 3.0 in. inside diameter (7.6 cm) polyvinyl chloride (PVC) pipe was used as a mold to fabricate the samples. The mold was split down the side to facilitate removal of prepared samples. The samples were prepared as follows:

(1) The PVC mold was taped along the split seam using plastic "electrician's" tape

(2) A plastic end cap was taped to one end of the mold using "electrician's" tape.

(3) Seven hose clamps were placed along the sides of the mold to reduce lateral expansion during the freezing process.

(4) Dry clean snow crystals passing the #4 sieve were placed in the plastic mold, while the side of the mold was tapped to densify the snow crystals.

(5) Distilled water, cooled to near 0°C, was added to the mold. The side of the mold was again tapped to remove entrapped air bubbles. Figure 3-1 shows the PVC mold with a prepared ice sample.

The resulting polycrystalline ice samples were cloudy in appearance with an average density of 56.5 pcf (0.9 gm/cc). Figure 3-2 shows a typical sample after extraction from the PVC mold. Approximately two out of three samples were rejected due to the presence of visible cracks incurred during the freezing process. The resulting test specimens, following visual inspection, appeared to be homogeneous in composition.

3.2 Specimen Trimming for Dynamic Testing

A South Bend 13 in. (33 cm) swing metal lathe was used to trim the ice samples to a right cylinder of the desired dimensions. The test systems used in this research program were designed to test right cylindrical specimens with a diameter of 2.83 in. (7.91 cm). Previous researchers have determined desired specimen height to diameter (H:D) ratios for both the resonant column and the cyclic triaxial test systems (Bolander, 1980). Based on their findings, a 2.83 in. (7.91 cm) diameter specimen should have a length between 8.5 in. (21.6 cm) and 17.0 in. (43.2 cm) for the resonant column test system, and

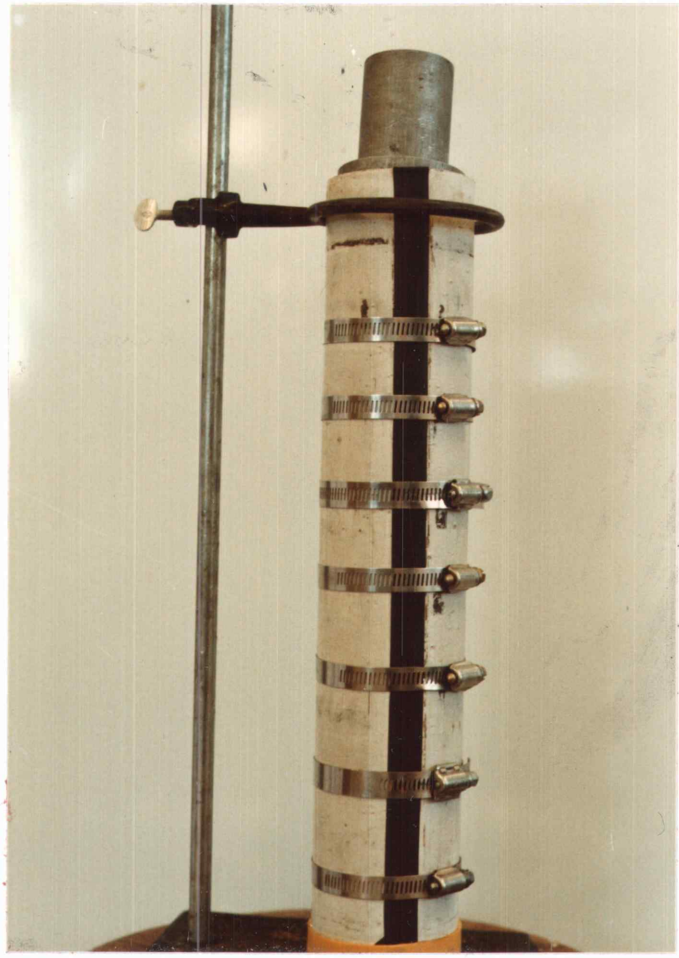

FIGURE 3-1 Laboratory Prepared Ice Specimen In PVC Mold
Before Extrusion

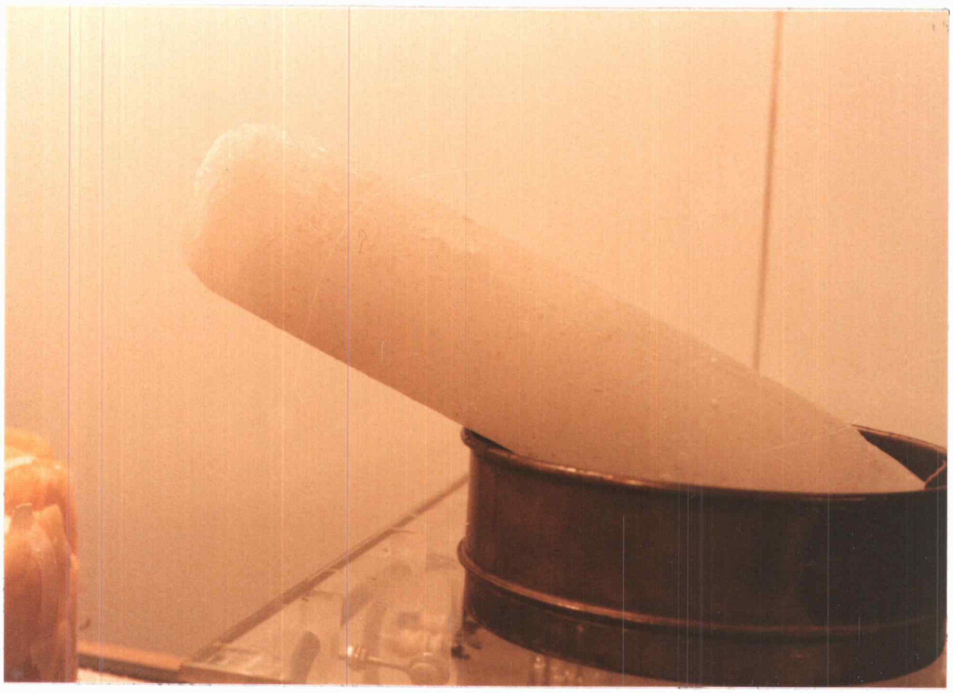

FIGURE 3-2 Laboratory Prepared Ice Specimen Before Trimming

between 5.7 in. (14.5 cm) and 8.5 in. (21.6 cm) for the cyclic triaxial test system. Since end caps are used to attach the specimen to the resonant column test system (see Section 3.3), the total length of the specimen enters into the H:D ratio. For the cyclic triaxial test system, however, the length is reduced by the height of the grips (see Section 3.4) when determining the H:D ratio, since the portion of the specimen within the grips is held rigidly in place during testing.

Therefore, by taking the grip length into account (3.75 in., or 9.53 cm) for the cyclic triaxial test system, a sample length of 9.4 in. to 12.2 in. (23.9 to 31.0 cm) satisfies the height to diameter ratio criteria for both test systems.

With a knowledge of the dimensions required, an outline of the machining procedure used follows:

(1) The ice sample was attached to the lathe using the end grips as shown in Figure 3-3.

(2) The ice sample was turned to a diameter of 2.83 in. (7.19 cm) as shown in Figure 3-4.

(3) One end was faced off with the lathe to a plane surface as shown on Figure 3-5.

(4) The sample was reversed in the lathe and the other end was faced off to the desired length.

(5) The average diameter, average height and weight of the trimmed specimen are measured and recorded.

A complete guide to the machining of frozen samples is given by O'Brian and O'Brian (1942), and Bolander (1980).

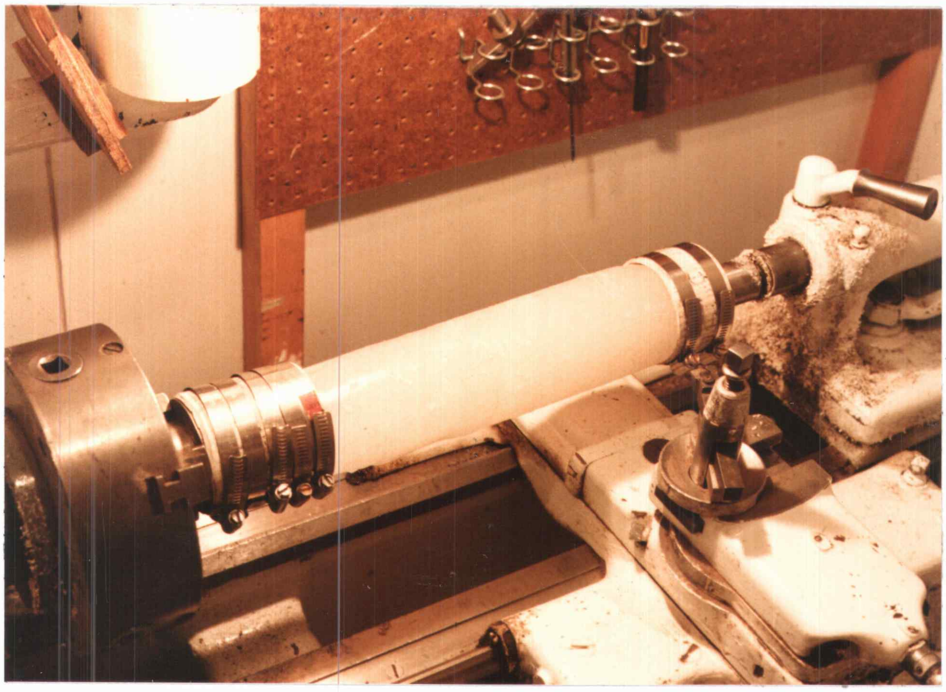

FIGURE 3-3 Ice Specimen Secured In Lathe Before Trimming

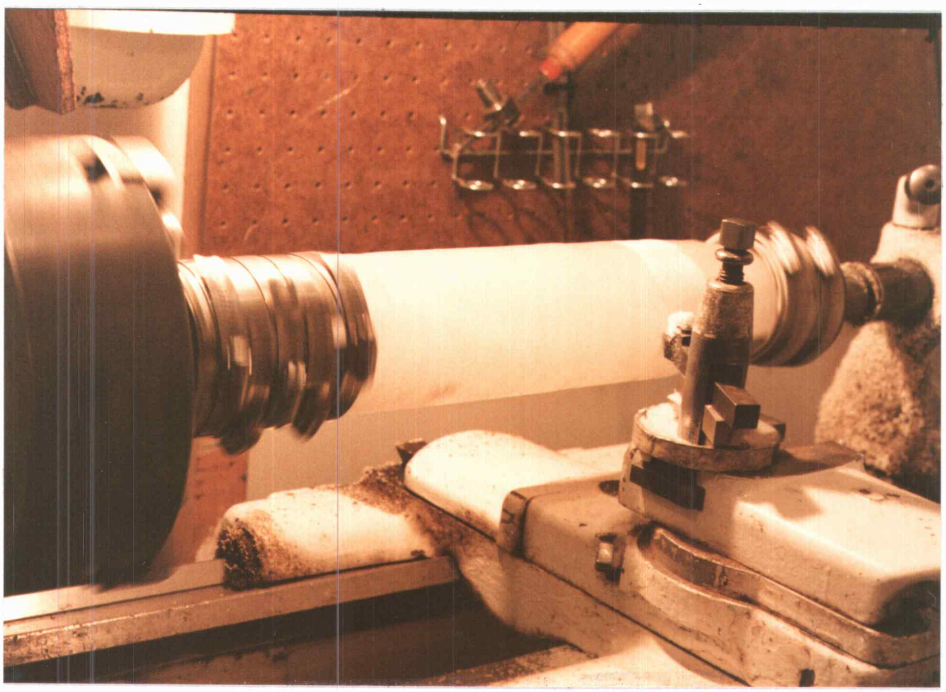

FIGURE 3-4 Ice Specimen Lathed To 2.83 In. Diameter

FIGURE 3-5 Facing Off End Of Ice Specimen To Create A Right Cylinder

3.3 Attaching Specimen to the Resonant Column Test System

The end caps (top cap and bottom platen) were attached to the test specimen using a freeze bond. The attachment procedure involves spraying precooled water on the end caps and using an alignment stand to insure correct alignment of the ice specimen. The attachment procedure has been described in detail by Bolander (1980). Figure 3-6 shows a specimen attached to the resonant column test system, with the end caps attached, before the confining pressure cylinder and environmental chamber have been secured. Figure 3-7 shows the resonant column test system as it appears during testing.

3.4 Attaching Specimen to the Cyclic Triaxial Test System

Due to the brittle behavior exhibited by ice under rapid loading conditions, a special grip was designed to couple the ice specimen to the cyclic triaxial test frame. An oversized grip was developed such that an ice to ice bond could be formed between the test specimen and the grip. Figure 3-8 shows the design of the grip used for ice specimens. The procedure used to attach the test specimen to the grip was as follows:

(1) The top cap was freeze-bonded to the test specimen using the alignment stand (see Figure 3-9).

(2) The specimen was placed on the top plate of the cyclic triaxial test system and one of the grips was aligned over the top cap and top plate.

(3) The top half of the anti-tilt device was attached.

(4) Ice shavings, which are produced while lathing the specimen,

FIGURE 3-6 Ice Specimen In The Resonant Column Test System Before The Confining Pressure Cylinder And Environmental Chamber Are Secured

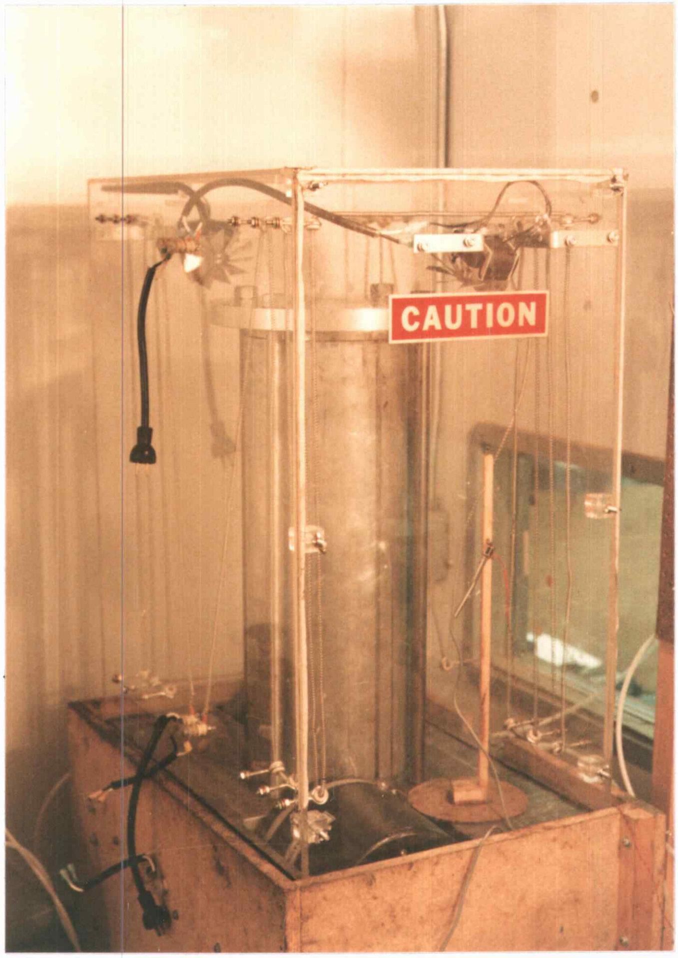

FIGURE 3-7 Ice Specimen In Resonant Column Test System During Testing

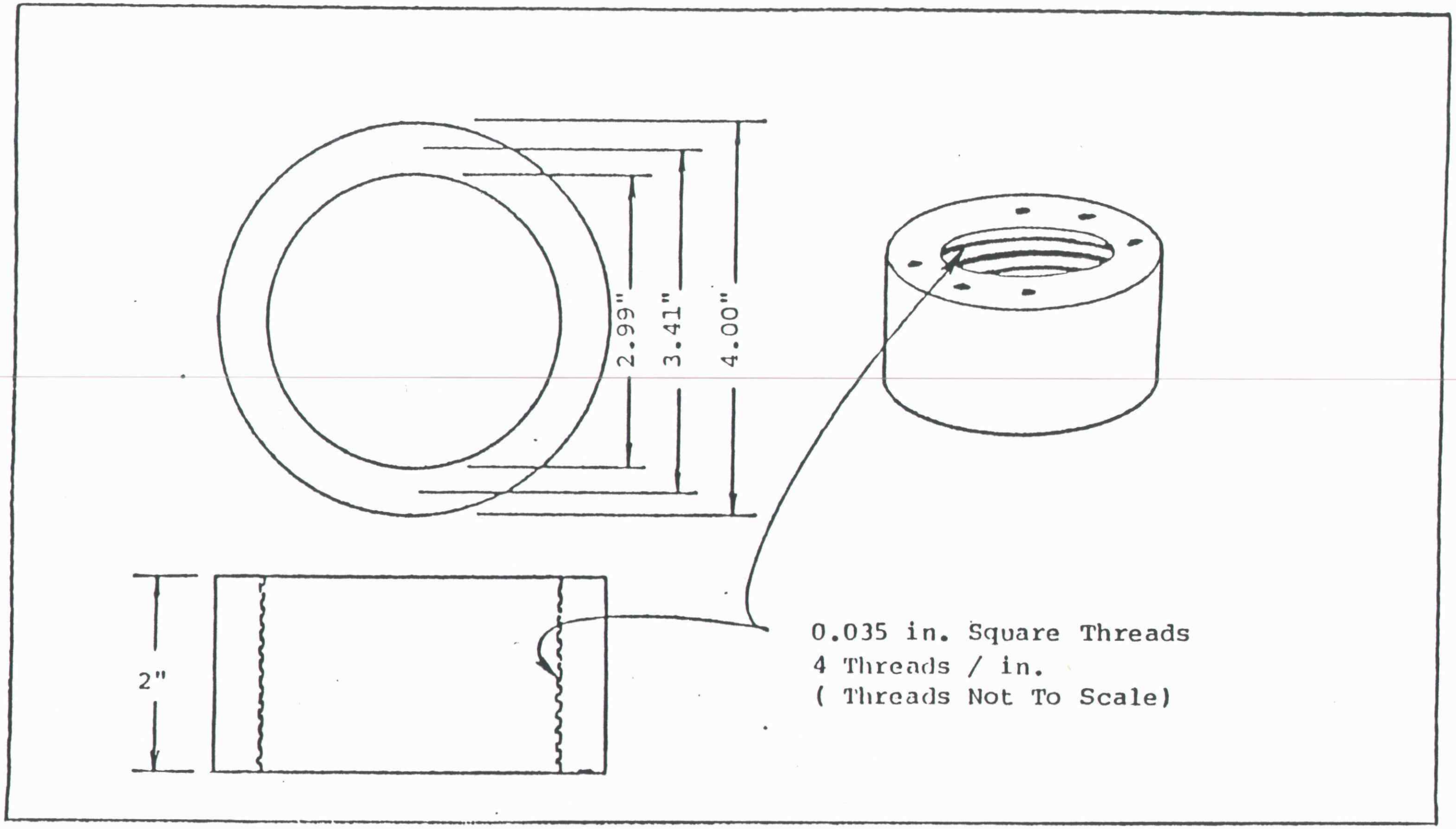

FIGURE 3-8 Ice Specimen Grip Design For The Cyclic Triaxial Test System

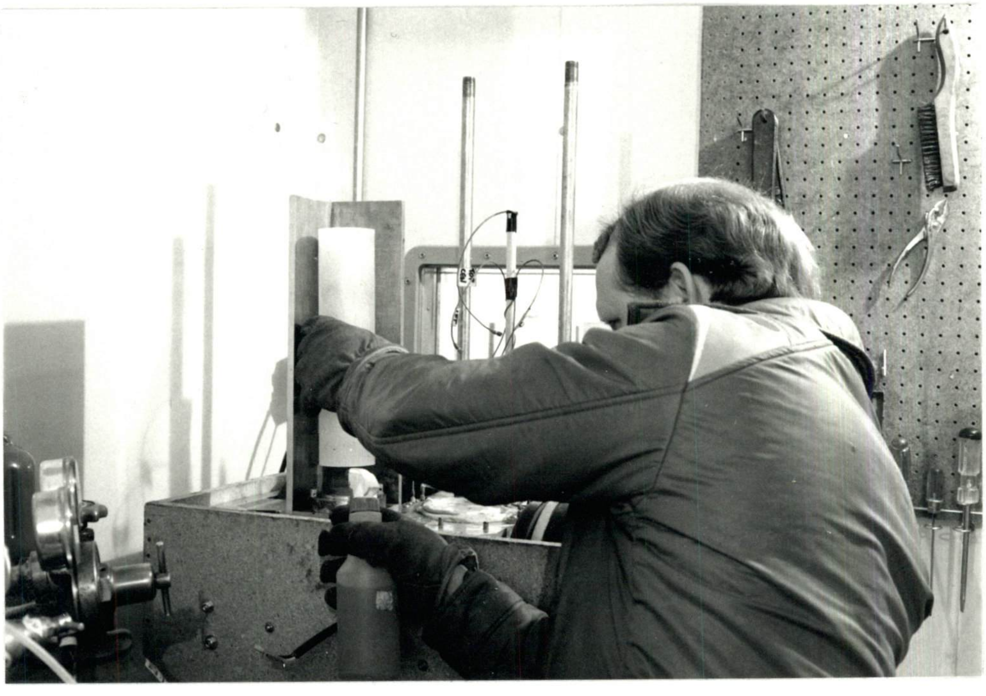

FIGURE 3-9 Attaching The Top Cap To Specimen Using The Alignment Stand

were forced between the grip and the test specimen.

(5) Using a hypodermic needle, 2-3 cc of distilled, precooled water (near 0°C) was injected between the specimen and the grip and allowed to freeze.

(6) Step 5 was repeated every 15 minutes until the space between the grip and the specimen was completely filled with ice.

(7) The specimen, firmly attached to the top plate, was inverted and placed in the cyclic triaxial test system with the base cap and base grip in place. The bottom half of the anti-tilt device was attached.

(8) Ice shavings were forced between the lower grip and the specimen; steps (5) and (6) were repeated.

Once attached to the cyclic triaxial test system the specimen was allowed to remain undisturbed for a minimum of 24 hours prior to testing. Figure 3-10 shows a specimen attached to the cyclic triaxial test system before the confining pressure cylinder and environmental chamber were attached. Figure 3-11 shows the cyclic triaxial test system as it appeared during testing.

3.5 Specimen Trimming in Preparation for Unconfined Compressive Strength Testing

In order to minimize end effects during unconfined compressive strength testing without removing the cyclic triaxial grips, specimens were lathed down to a dumbell shape as shown in Figure 3-12.

The effective length was taken as that length along which the diameter was a minimum. The length was maintained within ASTM stan-

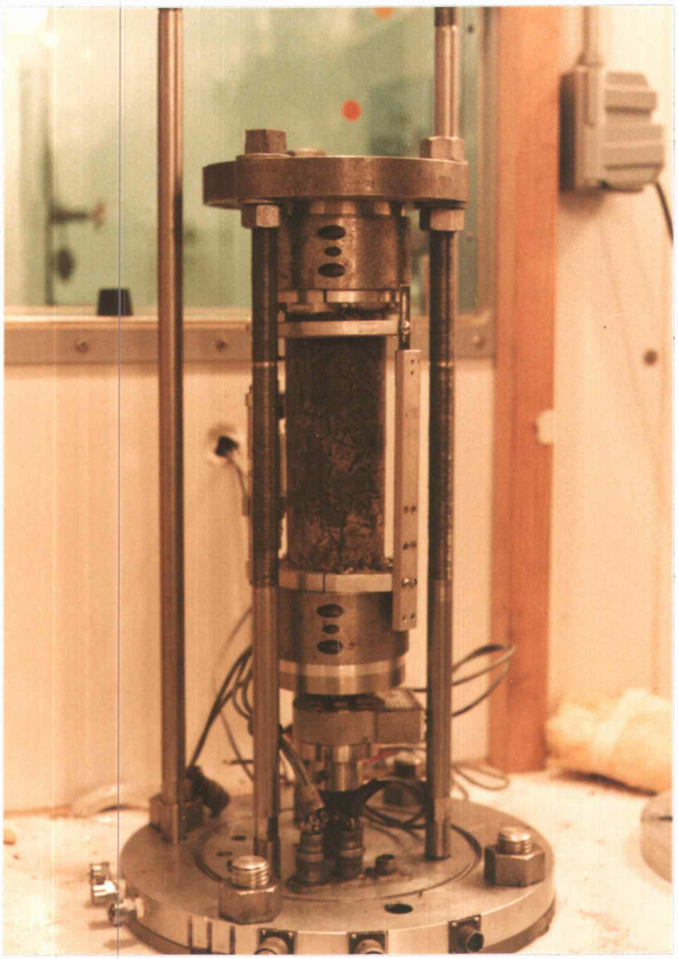

FIGURE 3-10 Specimen In Cyclic Triaxial Test System Before The Confining Pressure Cylinder And Environmental Chamber Are Secured

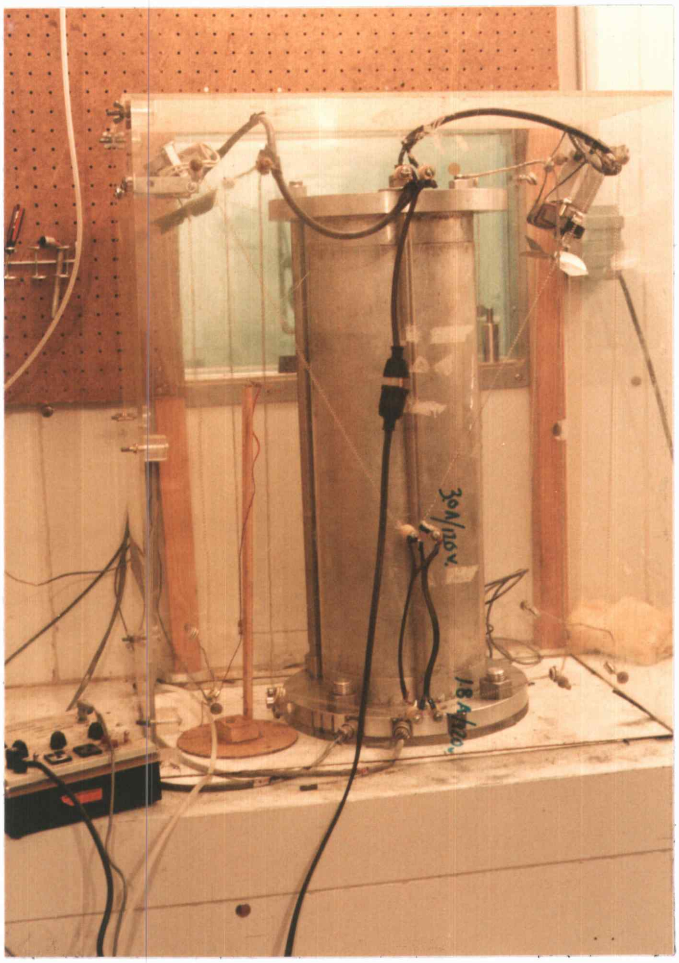

FIGURE 3-11 Ice Specimen In Cyclic Triaxial Test System During Testing

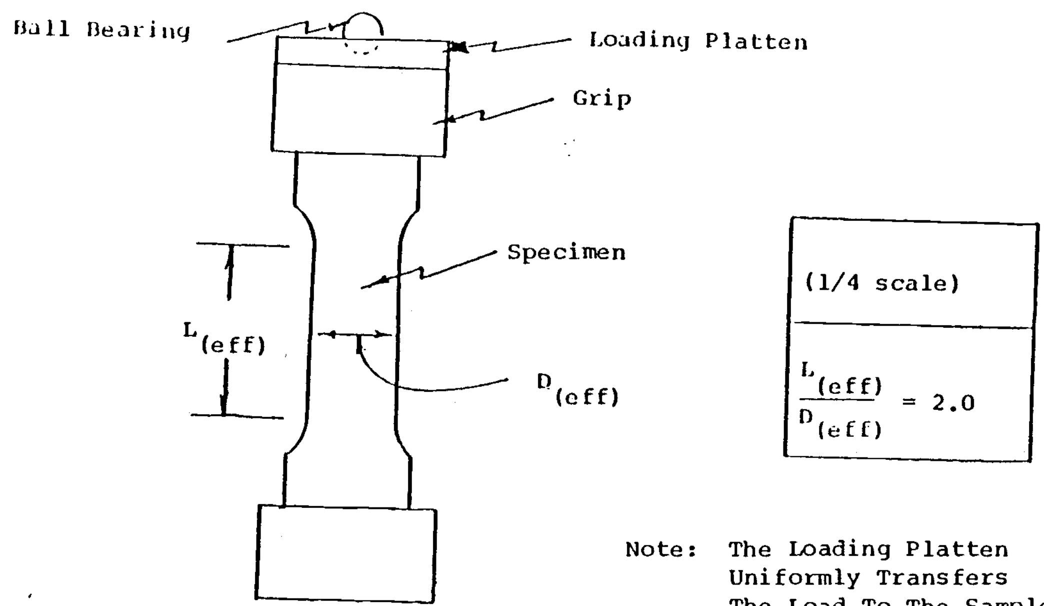

Note: The Loading Platten Uniformly Transfers The Load To The Sample Through The Ball Bearing

FIGURE 3-12 Ice Specimen Lathed To A "Dumbell" Shape In Preparation For Unconfined Compressive Strength Testing dards (D-2166) by setting the effective diameter at 2 inches (5 cm) and effective length at 4 inches (10 cm). Details of the lathing and test procedure are given by Wilson (1982).

3.6 Preparation of Thin Sections of Ice for the Evaluation of Crystal Orientation

Thin sections of ice were prepared in the coldroom (set at -10°C) for the purpose of measuring the orientation and size of the ice crystals. The crystal orientations were plotted on a fabric diagram to determine if the ice crystals within the sample were isotropic.

The procedure used to prepare thin sections may be summarized as follows:

(1) A plane surface was cut normal to the axis of the cylindrical ice specimen with compressed air (at -10°C) acting as the cooling fluid at the cutting surface. Figure 3-13 shows the cutting system employed for the test program (a Dresser diamond blade rock-saw).

(2) A glass plate was attached to the plane surface of the sample by first warming the plate with the palm of the hand and placing it on the plane surface where attachment occurred through freeze bonding.

(3) A thin section was cut parallel to the glass plate using a microtome.

(4) The thin section thickness was reduced, if required, using sand paper.

(5) A cover glass was attached as per step (2) to protect the

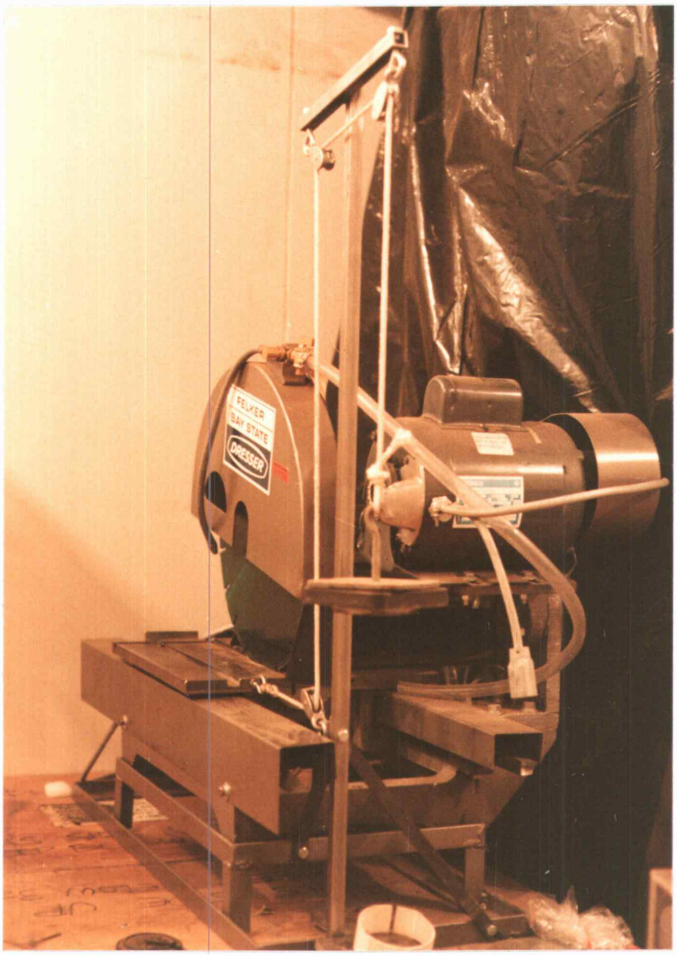

FIGURE 3-13 Dresser 14 In. Diamond Blade Rock Saw Used To Prepare Ice Thin Sections

specimen from sublimitation.

Details of the preparation and preservation of thin sections are given in CRREL Technical Report 62 (Langway, 1958).

4. DYNAMIC TESTING AND ICE CRYSTALLOGRAPHY PROCEDURES

4.1 Influence of Time on Test Procedures and Dynamic Properties

Before dynamic testing of ice could be performed, the effects of time on the test parameters considered had to be determined. The effect of time on dynamic properties was investigated by performing the following control tests:

(1) Temperature vs. time

(2) Confining pressure vs. time

(3) Dynamic property changes with time after grips and end caps were attached to the test specimen.

4.1.1 Temperature-Time Effects

To determine the influence of temperature on the dynamic properties of ice, three test temperatures were considered, namely, -10°C, -4°C and -1°C. Temperature equilibrium within the test specimen was investigated by placing three thermistors at the midpoint of a laboratory prepared ice specimen. One thermistor was freeze bonded to the surface of the ice specimen, one was freezed bonded to a quarter point within the ice specimen, and one was frozen at the center as shown in Figure 4-1. The temperature of each thermistor was monitored as a function of time following temperature control changes. Throughout the test, the temperature difference between thermistors (temperature lag) was monitored. The maximum temperature lag observed was 0.1°C

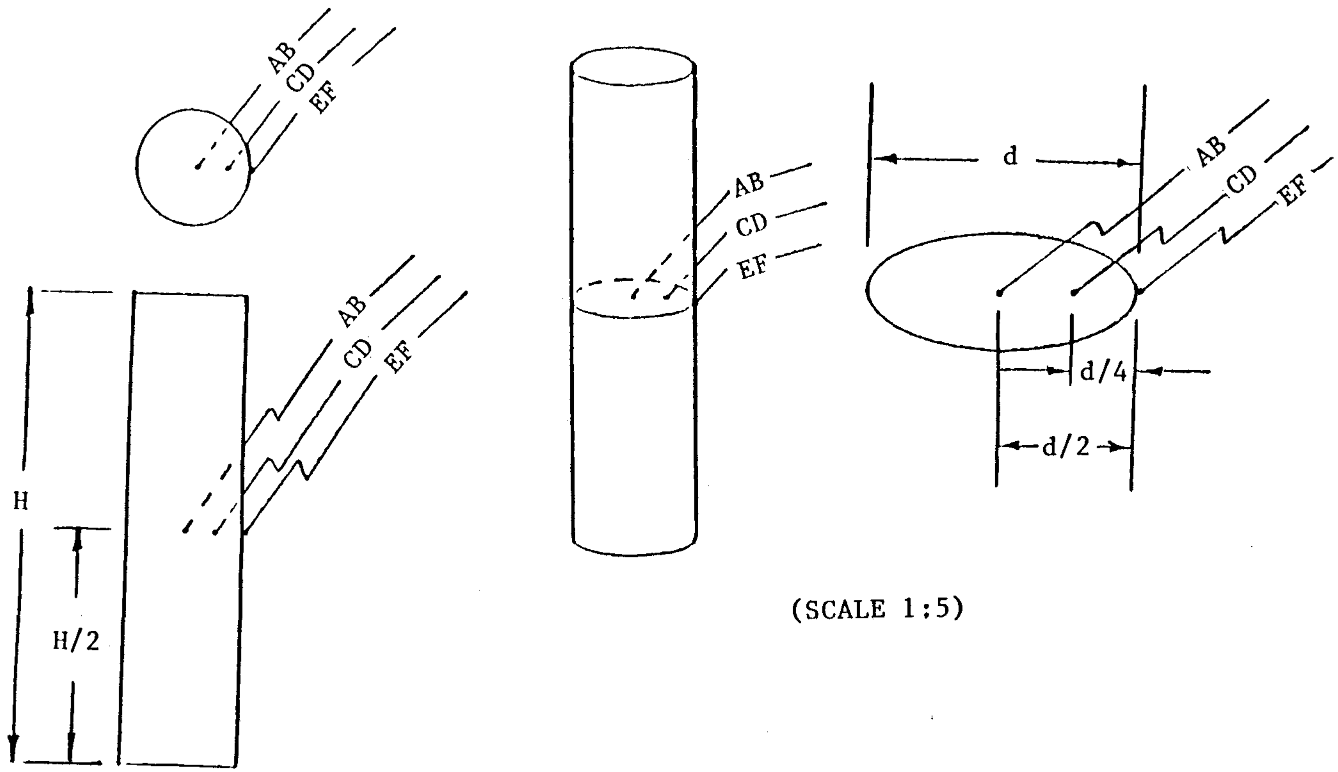

FIGURE 4-1 Thermistor Locations Within The Test Specimen For Temperature Stability Study

which occurred approximately 30 minutes after each temperature change. Figure 4-2 presents the results for one of the tests performed. From the test results it was concluded that monitoring the surface temperature of the ice specimen for 1.5 hours after each temperature change was sufficient time to determine the specimen temperature.

The time required to bring the test systems to thermal equilibrium was also investigated. Three thermistors were placed along the surface of the specimen at the 1/3 points (see Figure 4-3), and a fourth thermistor was placed between the confining pressure cylinder and the environmental chamber approximately 18 inches (46 cm) above the system base (see Figure 4-4). In the case of the cyclic triaxial test system one of the three thermistors used to monitor temperature was freeze bonded to the surface of the ice specimen at the contact point with the lower grip (see thermistor EF on Figure 4-3). The lower grip was found to be the critical point of the test specimen at higher temperatures, as it was always the warmest part of the test specimen. Figure 4-3 and 4-4 show the thermistor positions used during cyclic triaxial testing. The test results revealed that by carefully monitoring the temperature of the environmental chamber outside the confining pressure cylinder, temperature equilibrium could be reached for the specimen in as little as four hours, although six hours was generally required. The method used for changing the temperatures of both test systems was as follows:

(1) As described by Bolander (1980), the temperature was controlled by an environmental chamber and a Versa Therm, model 2156 Proportional Electronic Temperature Controller. The Versa Therm was set to the initial settings for approximately 35 minutes.

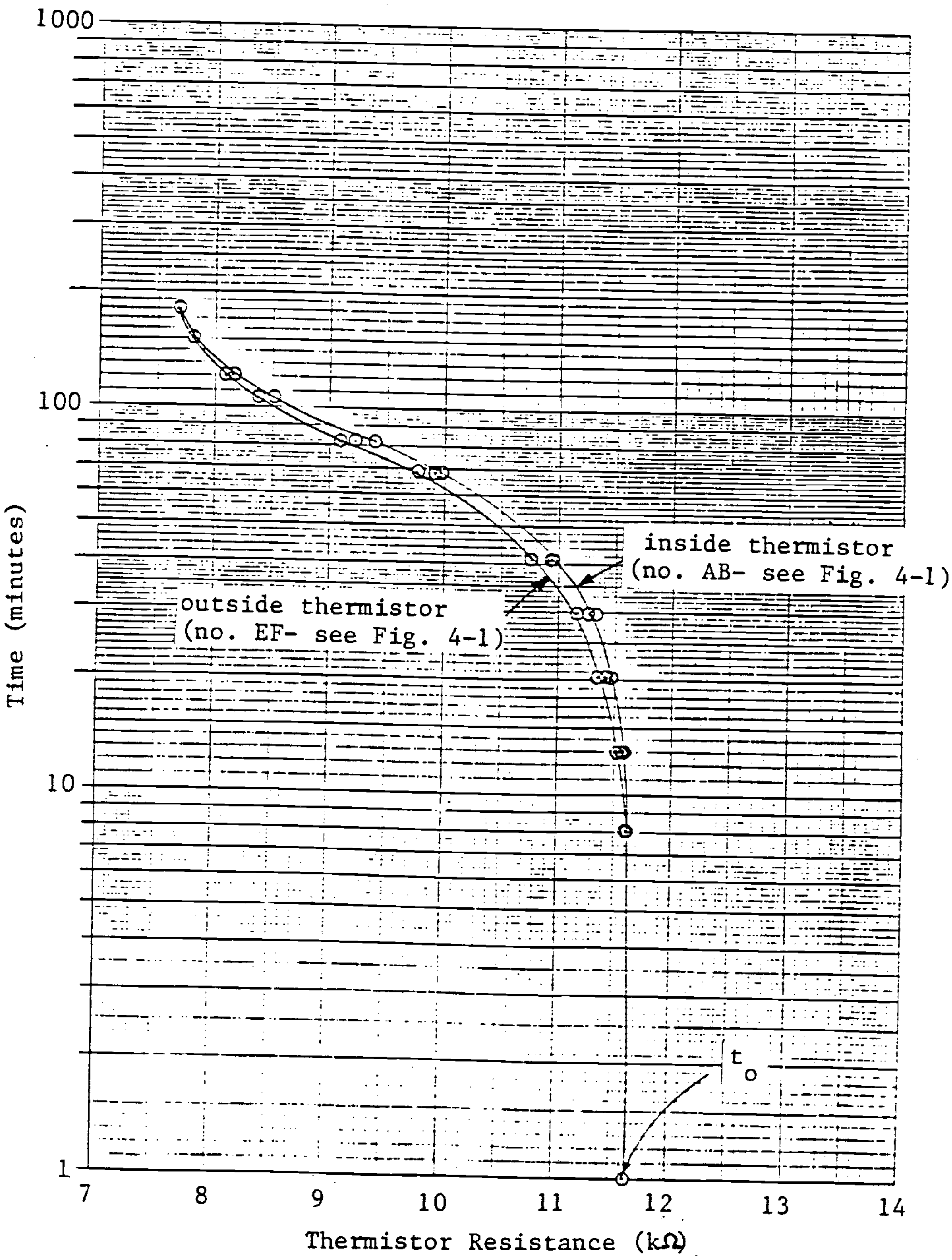

FIGURE 4-2 Time Vs. Thermistor Resistance For Laboratory Prepared Ice Specimen

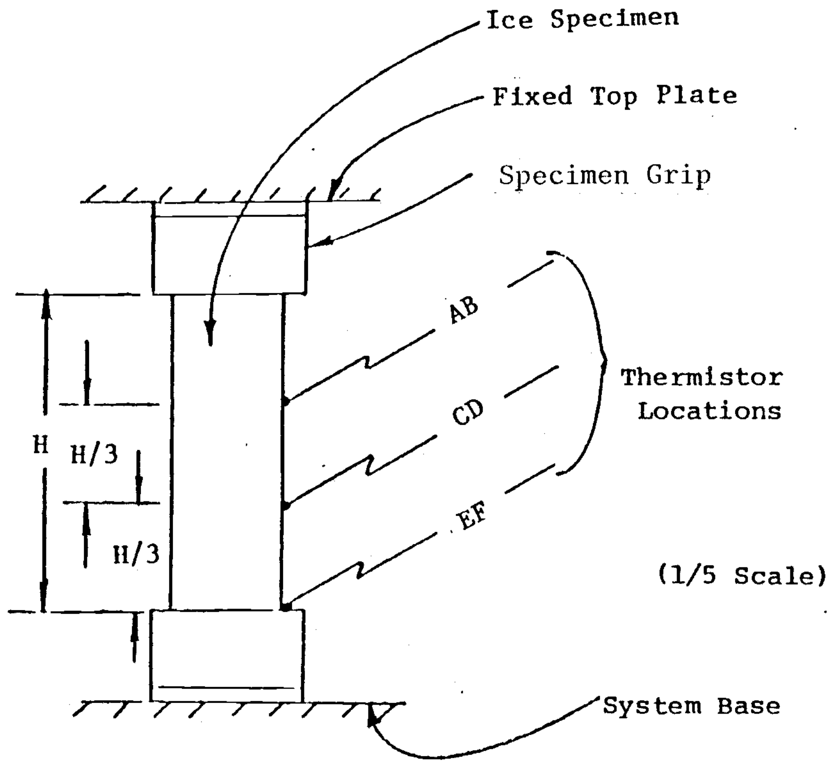

FIGURE 4-3 Location Of Specimen Thermistors For The Cyclic Triaxial Test System

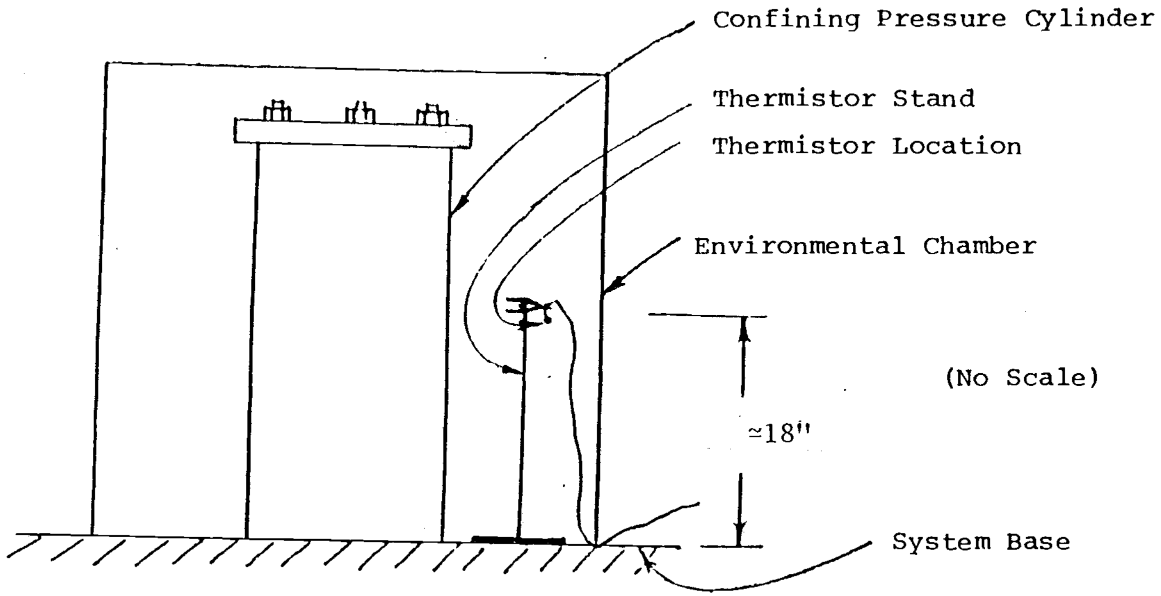

FIGURE 4-4 Location Of The Thermistor Used To Monitor The Temperature Inside The Environmental Chamber And Outside The Confining Pressure Cylinder

(2) After 35 minutes the Versa Therm control settings were adjusted such that the temperature of the thermistor located outside the confining pressure cylinder stabilized to the predetermined temperature desired (i.e., -4°C or -1°C).

(3) The temperature of the specimen was monitored until thermal stability was reached.Stability generally occurred within four to six hours.

4.1.2 Confining Pressure-Time Effects

In the resonant column test system both the dynamic moduli (dynamic Young's modulus and complex shear modulus) and damping ratio were measured as a function of time for each confining pressure change employed in the test program to determine the time required to reach pressure equilibrium. Figure 4-5 shows typical test results obtained. The test results indicated that 20 minutes was sufficient time for pressure effects to reach equilibrium within 98% of the 24 hour results. Pressure time effects were also monitored on the cyclic triaxial test system for all pressures and temperatures used in the test program. The test results confirmed that 20 minutes was sufficient time for pressure equilibrium to be attained. In the testing sequence actually employed during the test program, however, a 30 minute time period was required for data reduction between tests. Section 4.3 outlines the actual testing sequence employed during the test program.

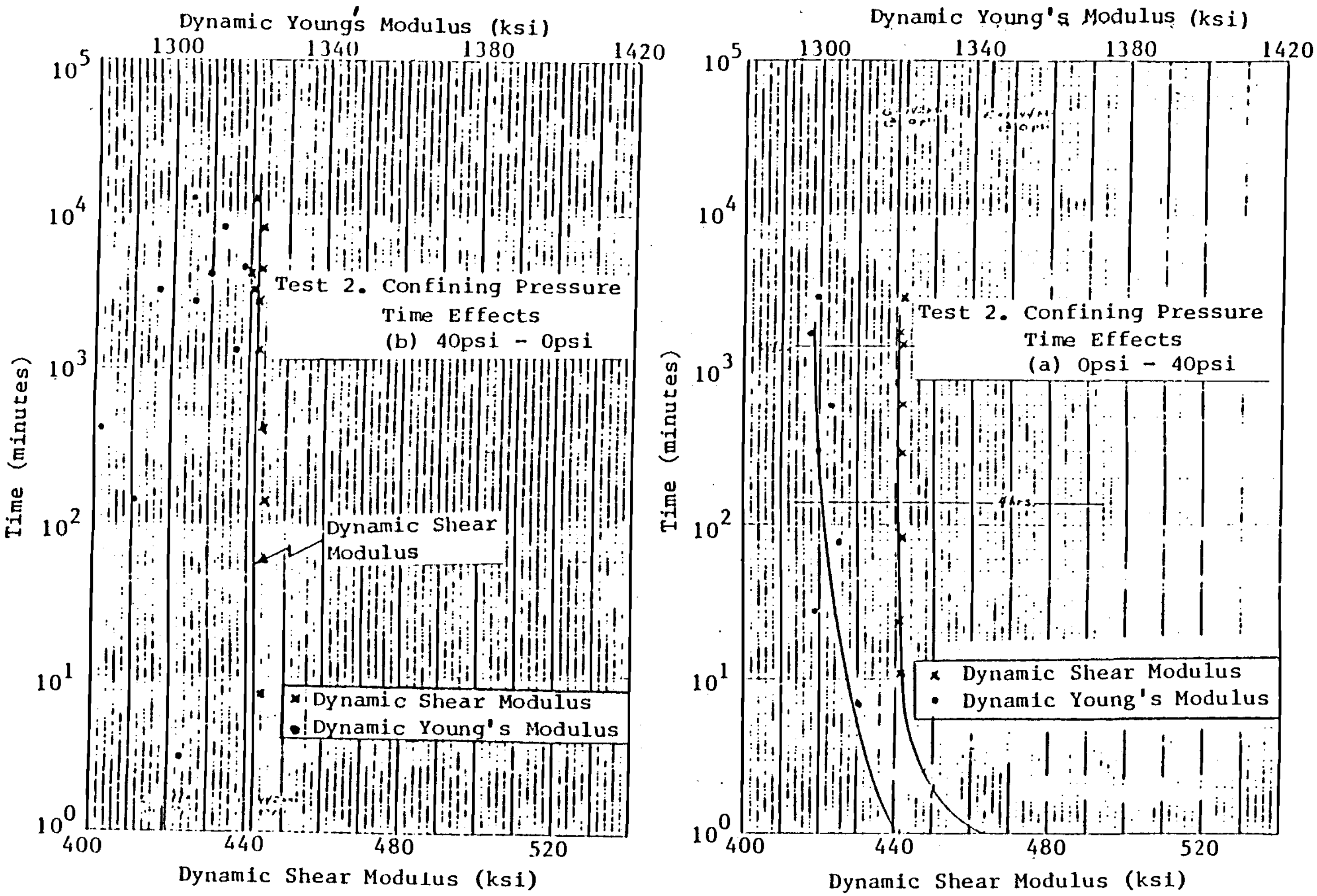

FIGURE 4-5 Confining Pressure Time Effects - Resonant Column Test System

4.1.3 Grip and End Cap Time Effects

After attaching the end caps (resonant column) or grips (cyclic triaxial), the time required for the stabilization of the dynamic properties (dynamic modulus and damping ratio) was determined for the test systems. The method used to determine the time required for stabilization was as follows:

(1) After connecting the end plates or grips the time of attachment was noted.

(2) The dynamic properties were measured at convenient time intervals over a 24 hour period.

Figure 4-6 shows the results obtained for the resonant column test system, while Figure 4-7 shows the results obtained from the cyclic triaxial test system. From Figure 4-6 it can be seen that approximately 4 hours were required after attaching the end caps before resonant column testing could commence. Grip testing was not performed until 24 hours after grip placement for the cyclic triaxial test system, but the results show that 24 hours was sufficient time for stabilization.

4.1.4 Cyclic Triaxial Compression Testing

When specimens are subjected to large strain cyclic triaxial testing, they may fail in tension. To obtain a maximum amount of information from each specimen during the test program, triaxial testing was performed after resonant column testing was complete. In this way all the resonant column test results were obtained before the sample was subjected to large strains. Then, if failure occurred,

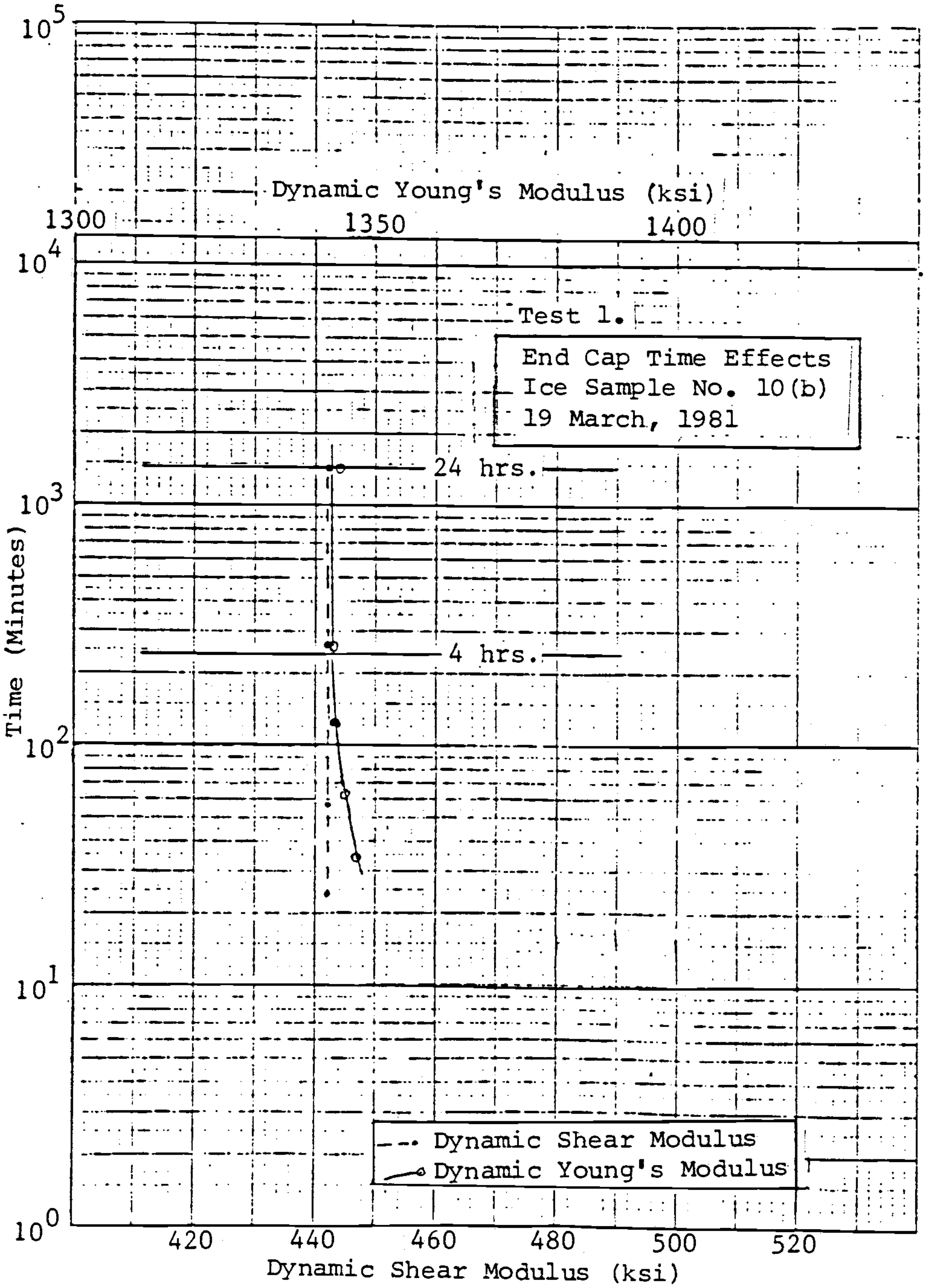

FIGURE 4-6 End Cap Time Effects - Resonant Column Test System

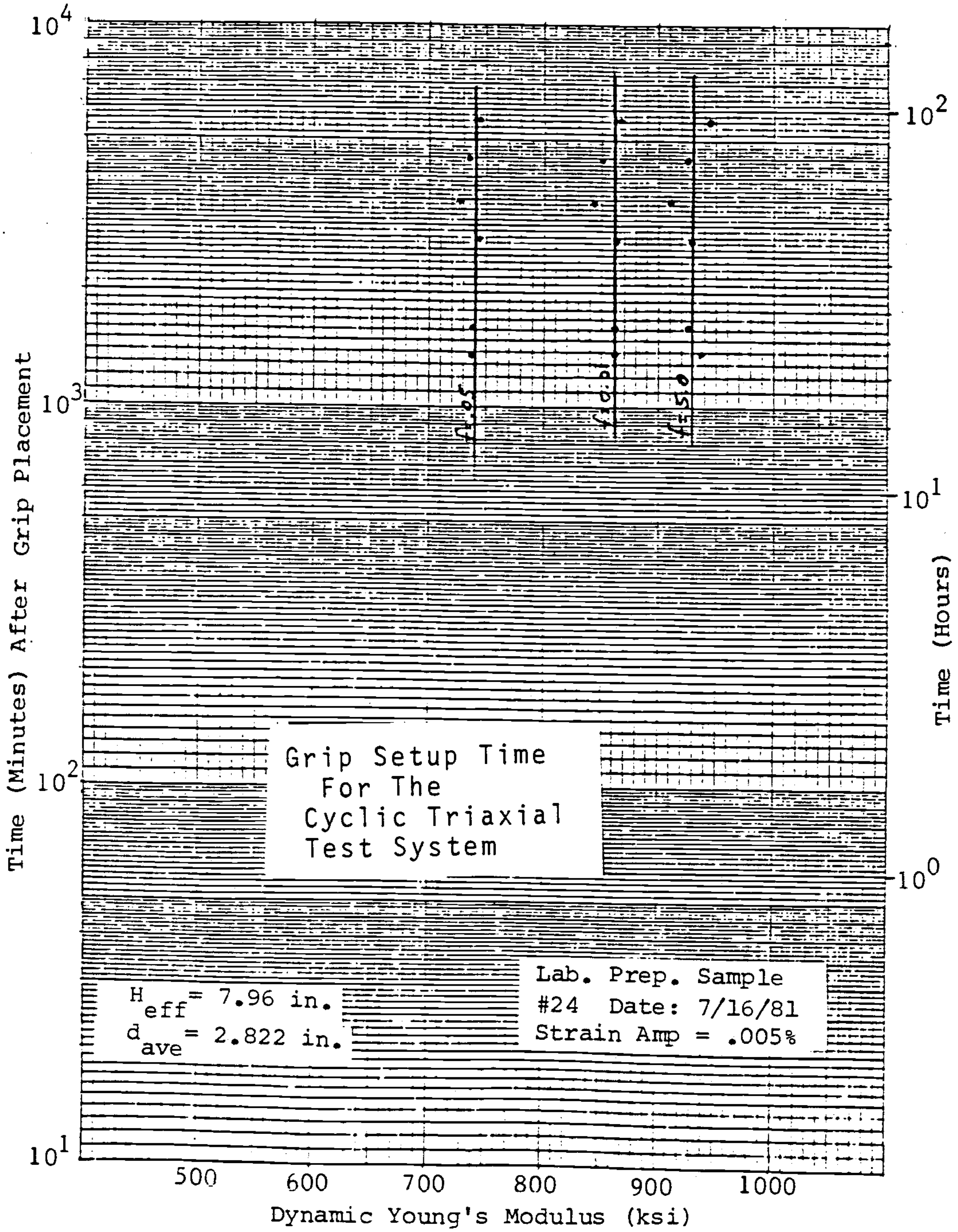

FIGURE 4-7 Grip Setup Time - Cyclic Triaxial Test System

during cyclic triaxial testing, the testing program could be continued on specimens which failed by using a compression testing procedure, if possible. The procedure used to test samples in compression was as follows:

(1) Since most specimens fail near one of the grips, the broken samples were attached to the lathe by the other grip and the broken end of the specimen was turned to a plane surface.

(2) The specimen was then reattached to the cyclic triaxial test system, only the loading platten from the unconfined compressive strength testing system was positioned on top of the specimen in place of the cyclic triaxial test grip.

(3) An initial static load was placed on the specimen which was slightly greater than $\frac{1}{2}\sigma_{(max)}$ as shown on Figure 2-8, so subsequent cyclic loading would always subject the sample to compression loading only.

(4) Cyclic triaxial compression testing was performed.

4.2 Test History

Since cyclic triaxial testing can be destructive, particularly at high strain amplitudes, the resonant column test was always performed first. The cyclic triaxial test history, as previously outlined by Bolander (1980), was altered during this test program, and is given in Section 4.2.2 of this report.

4.2.1 Resonant Column Test History

The resonant column test sequence followed throughout this test program is shown in Figure 4-8. Prior to the test program the specimens were attached to the top cap and base plate by freeze bonding, as outlined by Bolander (1980). The specimens were connected to the resonant column test system and the three thermistors were freeze bonded to the sample. The confining pressure cylinder and environmental chamber were attached and the fourth thermistor, used to monitor the temperature outside the confining pressure cylinder, but within the environmental chamber, was connected to its stand. The specimens were allowed to remain undisturbed for a minimum of four hours to insure the bond between the end caps and specimen was fully developed. Figure 3-5 shows the resonant column test system with a specimen attached, ready for testing. For the first test temperature of -10°C, the Versa Therm was left in the off position. The dynamic properties were determined at 0 psi, 70 psi (4.9 kg/cm^2), 30 psi (2.1 kg/cm^2), and then 0 psi was repeated as a check against pressure disturbance effects. A minimum of 30 minutes was allowed between each pressure change to allow the specimens to reach pressure equilibrium. Once testing was complete for each confining pressure, the temperature was raised to -4°C and the dynamic properties were again determined. The sequence was repeated for -1°C. Finally the temperature was lowered from -1°C to -10°C and the dynamic properties were re-evaluated at 0 psi to verify the test history had not altered the dynamic properties of the specimen. As noted in Section 4.1.2, a minimum of

CONSTANT TEMPERATURE

Longitudinal Mode

→ 0 psi → DV* = 0.5 → DV = 1.5

→ 70 psi → DV = 0.5 → DV = 1.5

→ 30 psi → DV = 0.5 → DV = 1.5

→ 0 psi → DV = 0.5 → DV = 1.5

Torsional Mode

→ CP = 0 psi → DV = 1. → DV = 2.

→ CP = 70 psi → DV = 1. → DV = 2.

→ CP = 30 psi → DV = 1. → DV = 2.

→ CP = 0 psi → DV = 1. → DV = 2.

FIGURE 4-8 Resonant Column Test Sequence For Ice

---

* DV = Drive Volume Setting
(e.g. The Power Output Setting)

four hours was required between each temperature change to insure thermal equilibrium.

4.2.2 Cyclic Triaxial Test History

Due to the potentially destructive nature of the cyclic triaxial test at high strain amplitudes, the cyclic triaxial test was always performed after the resonant column test was completed. Due to failures which occurred early in the test program at high strains and cold temperatures (-10°C), the test sequence (or test history) adapted in this test program was altered from that given by Bolander (1980), as shown in Figure 4-9. The check point tests for -10°C were conducted first at only low and mid strains, followed by a change in temperature to -4°C. Complete testing was performed on the specimen at -4°C, -1°C and finally at -10°C. Most specimens failed in tension before the testing sequence was completed. Whenever a specimen failed, an attempt was made to complete the test sequence using compression testing, whereby the specimen was only subjected to compressive cyclic loading (see Section 4.1.4).

Before a cyclic triaxial test was conducted the specimen and grips had to be attached to the system to insure the test specimen could be subjected to tensile and compressive axial strains. The steps taken to attach the specimen to the test system are as follows:

(1) The specimen was attached to the test system using the procedure outlined in Section 3.4

(2) Three thermistors were freeze bonded to the test specimen; two were located approximately at the 1/3 points of the specimen and

CONSTANT TEMPERATURE

Approximate axial strain = 9.0×10^{-4}%

- → cp = 0 psi → f = 0.05 cps → f = 0.5 cps → f = 5.0 cps
- → cp = 70 psi → f = 0.05 cps → f = 0.5 cps → f = 5.0 cps
- → cp = 30 psi → f = 0.05 cps → f = 0.5 cps → f = 5.0 cps
- → cp = 0 psi → f = 0.05 cps → f = 0.5 cps → f = 5.0 cps

Approximate axial strain = 5.0×10^{-3}%

- → cp = 0 psi → f = 0.05 cps → f = 0.5 cps → f = 5.0 cps
- → cp = 70 psi → f = 0.05 cps → f = 0.5 cps → f = 5.0 cps
- → cp = 30 psi → f = 0.05 cps → f = 0.5 cps → f = 5.0 cps
- → cp = 0 psi → f = 0.05 cps → f = 0.5 cps → f = 5.0 cps

Approximately axial strain = 1.0×10^{-2}%

- → cp = 0 psi → f = 0.05 cps → f = 0.5 cps → f = 5.0 cps
- → cp = 70 psi → f = 0.05 cps → f = 0.5 cps → f = 5.0 cps
- → cp = 30 psi → f = 0.05 cps → f = 0.5 cps → f = 5.0 cps
- → cp = 0 psi → f = 0.05 cps → f = 0.5 cps → f = 5.0 cps

Approximate axial strain = 9.0×10^{-4}%

- → cp = 0 psi → f = 0.05 cps → f = 0.5 cps → f = 5.0 cps

FIGURE 4-9 Cyclic Triaxial Test Sequence For Ice the third thermistor was in contact with the lower grip (see Figure 4-3).

(3) The confining pressure cylinder was attached as outlined by Bolander (1980).

(4) The fourth thermistor was attached to its stand outside the confining pressure cylinder but inside the environmental chamber. (The environmental chamber was not used for the -10°C test.) The sample was allowed to remain undisturbed for a minimum of 24 hours after attachment to the cyclic triaxial test system prior to testing.

Testing was initiated at the -10°C check point, without the environmental chamber. The chamber was placed in position and the temperature was adjusted to -4°C using the procedure outlined in Section 4.1.1. The test history outlined in Figure 4-9 was followed. The temperature was raised to -1°C and the test history was repeated. Finally, the temperature was lowered to ambient room temperature (near -10°C) by turning off the Versa Therm and removing the environmental chamber, and the test history outlined in Figure 4-9 was repeated.

4.3 Ice Specimen Test Program

The chronological schedule for the testing program is shown in Figure 4-10. The schedule allowed two people to perform dynamic testing programs simultaneously. As may be noted from the Figure, each sample took four days to test. During the third day, cyclic triaxial and resonant column testing had to be conducted simultaneously.

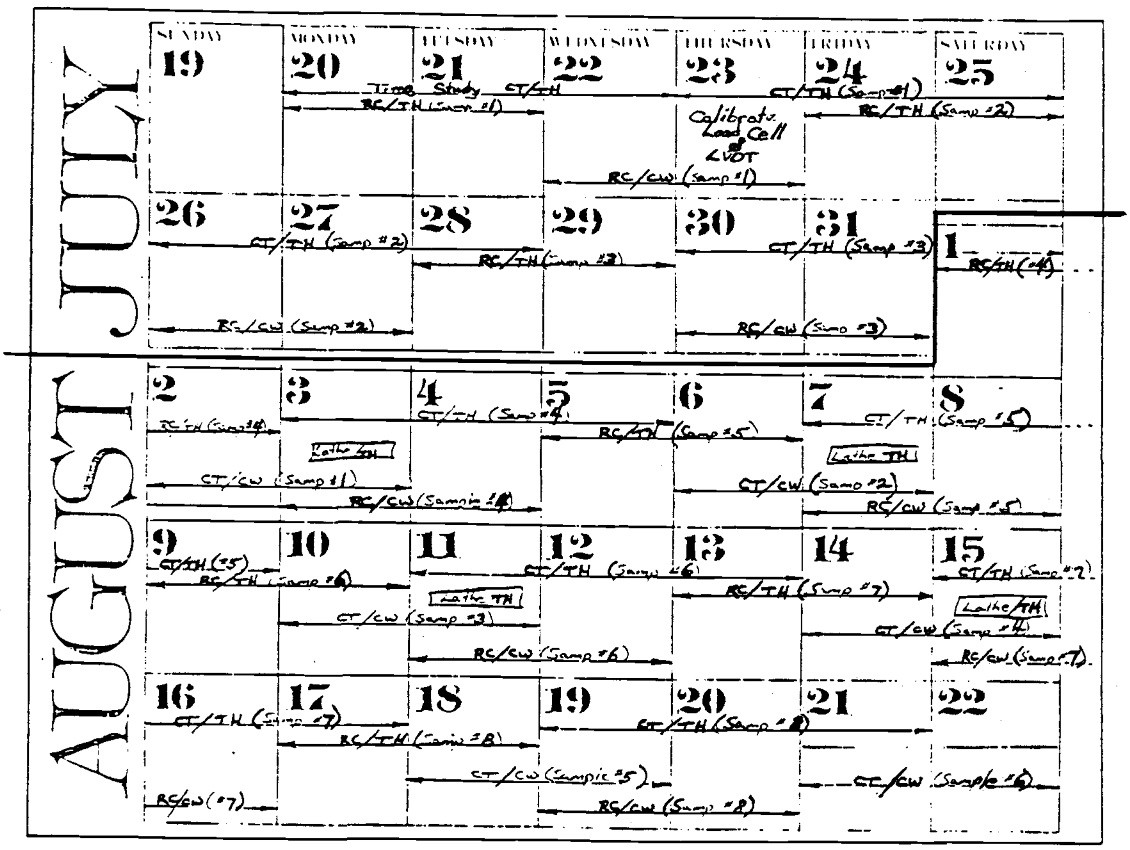

LEGEND

Testing Apparatus:
RC = Resonant Column
CT = Cyclic Triaxial

Researcher Performing Test:
TH = Ted Hammer
CW = Chuck Wilson

FIGURE 4-10 Chronological Schedule For Testing Program

A 30 minute wait between pressure changes was required in order to reduce the cyclic triaxial test data, as well as performing the resonant column tests. The raw data was reduced using a minicomputer, which was interfaced directly with the test systems. A detailed outline of the computer interface with the test systems is given by Bolander (1980).

4.4 Ice Crystal Orientation and Fabric Diagrams

4.4.1 Ice Crystal Orientation

Many methods exist for orienting crystals using a universal stage. The method adopted for this investigation followed the procedure detailed in CRREL Technical Report No. 62 (Langway, Jr., 1958), a summary of which is presented below.

The ice thin section is viewed through two polarizing sheets parallel to the thin section with their polaroids crossed at right angles. The lower sheet (the polarizer) is oriented to transmit light vibrating in the N-S direction relative to the universal stage while the upper polarizing sheet (the analyzer) transmits light vibrating in the E-W direction. The thin section, which is connected to the universal stage below the polarizers can be rotated about a vertical axis (A_1 axis) a N-S axis (A_2 axis) and an E-W axis (A_4 axis). A second vertical axis is available by which the thin section can be rotated together with the first vertical axis (A_1) and its azimuth scale. This axis is referred to as the outer vertical axis (A_4 axis).

Figure 4-11 is a sketch of the rotation axes of the universal stage in the rest position. The orientation of each crystal is determined as follows (after Langway, Jr., 1958):

(1) Set the horizontal axes (A_2 and A_4) at zero readings (see Figure 4-11).

(2) Select a grain for measurement and rotate the A_1 axis to extinction.

(3) Test the extinction by rotation on A_2. If the grain departs from extinction, return the A_2 to zero and rotate A_1 by 90° to alternate extinction and retest A_2 for extinction.

(4) Depress A_4 by 15° to 20° (to illuminate the crystal), and then rotate A_2 to extinction.

(5) Return A_4 to zero, then rotate A_5 by 45°. If the grain remains dark, the optical axis coincides with the line of site. If the grain illuminates the optical axis is normal to the line of site and A_2.

In addition to the following steps outlined above, there are two special orientation cases that commonly occur, which are:

(1) When in its initial position, a crystal remains dark for all positions of A_1 and

(2) When step 3 gives extinction in both A_1 positions.

Details of crystal orientation determination for these two special cases, together with expanded details on the normal procedure for crystal orientation determination are given in CRREL Technical Report No. 62 (Langway Jr., 1958).

For this test program, the orientation of the ice crystals in thin sections were measured and plotted on fabric diagrams for six

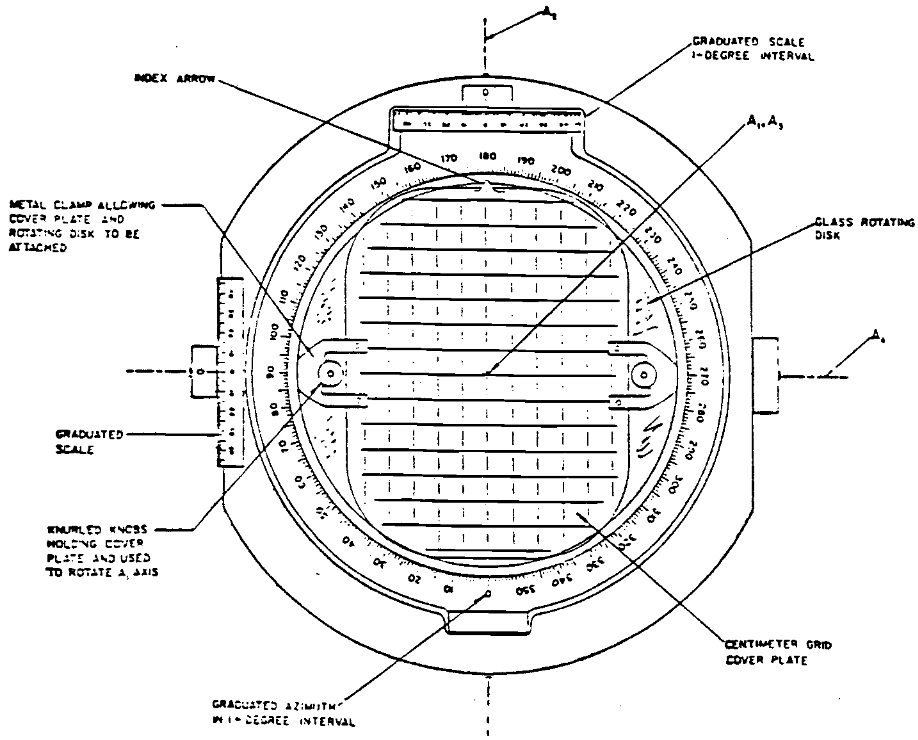

FIGURE 4-11 Plan view of the rotation axes of universal stage at the rest position.

FIGURE 4-11 Plan View Of The Rotation Axes Of Universal Stage At The Rest Position

(after Langway Jr., 1958)

specimens. All measurements were adjusted for refractive index differences between ice and air using Snell's law and an empirical correction developed by Langway, Jr. (1958) to obtain corrected orientations.

Details of the corrections and procedures are given in CRREL Technical Report No. 62. The fabric diagrams are included in Appendix B for all thin sections prepared in the test program. Photographs of each thin section, as observed through the polarizing sheets, were also taken and the photographs are presented in Appendix B. Details of fabric diagram construction follow.

4.4.2 Fabric Diagrams

Fabric diagrams are graphical representations in which the orientations of the optical axes of individual crystals within a sample are plotted to determine if a sample has a preferred crystal orientation (i.e., if the sample is anisotropic). The orientation of each crystal is plotted on a Schmidt equal-area net. The Schmidt net is a graph constructed such that equal areas on the net correspond to equal areas on the spherical projection from which the net was constructed. Figure 4-12 is a copy of a Schmidt equal-area net.

To form a fabric diagram, the orientation of the C-axis of the ice crystals within an ice thin section are plotted on a Schmidt net by the following procedure:

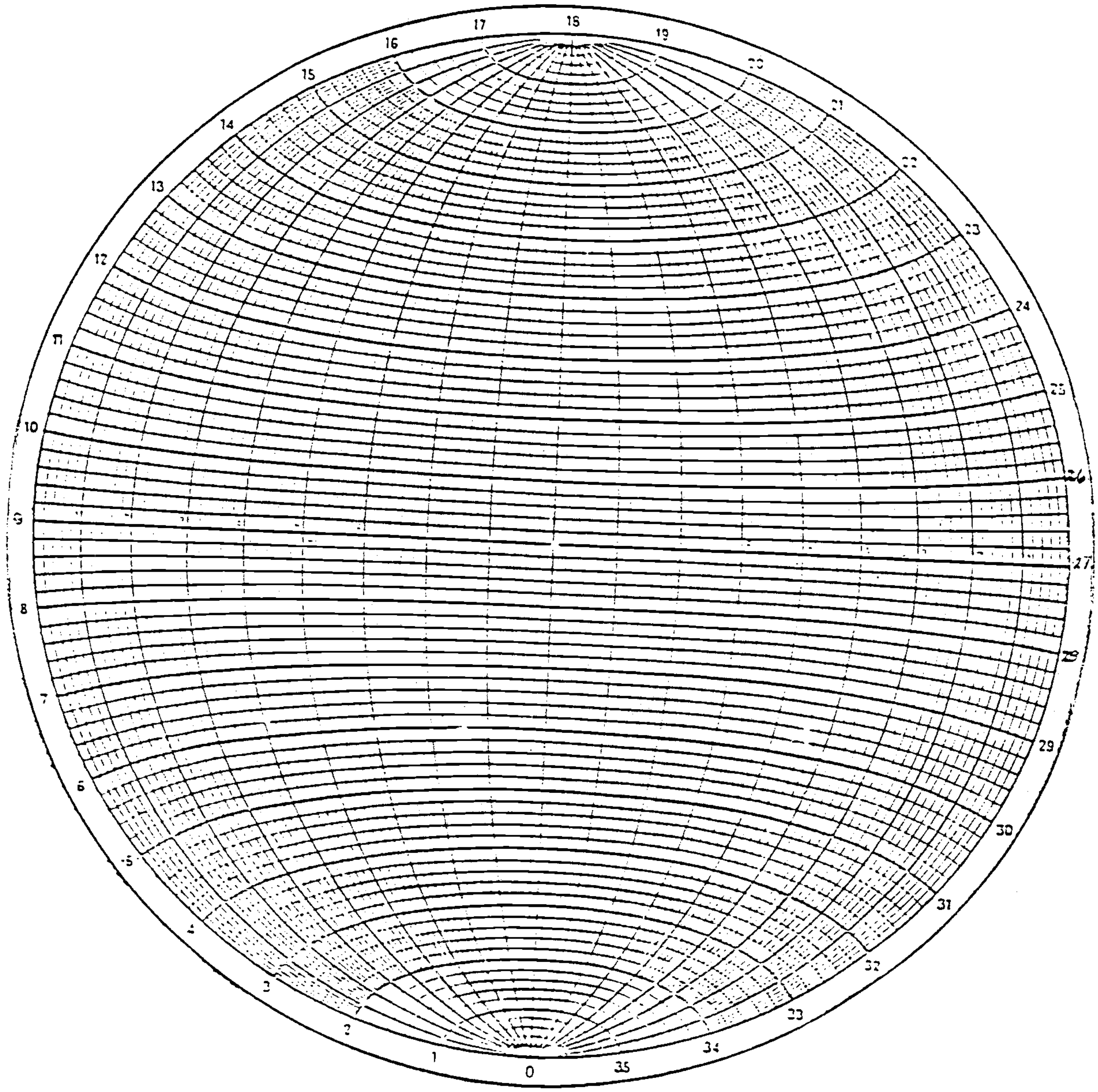

FIGURE 4-12 Schmidt Equal Area Net

(after Langway Jr., 1958)

(1) A piece of tracing paper with a reference arrow is placed over the Schmidt net, such that the arrow corresponds to the 0 azimuth of the net (bottom edge of net).

(2) A_1 is located by rotating the tracing paper about the center to the correct azimuth (perimeter value on the graph).

(3) A_2 is plotted on the E-W diameter of the net.

(4) After all points have been plotted the points are counted using a centimeter grid (part of the universal stage) and a 1% counter. The 1% counter is made of clear acetate to the specification shown on Figure 4-13, and is used to form preferred orientation contours. Contours were not developed for this test program, as they are not a requirement for determining if samples are isotropic. The interpretation of fabric diagrams is presented in the next section.

A detailed description of the construction of fabric diagrams may be found in CRREL Technical Report No. 62. Appendix B contains a copy of the fabric diagrams developed during this test program.

4.4.3 Interpretation of Fabric Diagrams

The orientation of the optical axes of individual ice crystals within a sample become a fabric diagram when plotted on a Schmidt net. This fabric diagram represents graphically the orientation of individual crystals relative to a fixed reference. The Schmidt net is a graph constructed such that all equal areas on the net are representative of equal areas on a sphere from which the Schmidt net was derived and all crystal orientations plotted on the net represent a direction the crystal would point to in space (or on the sphere). As an

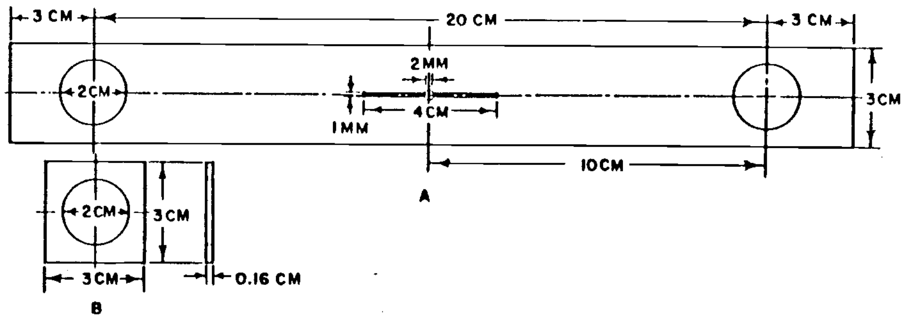

FIGURE 4-13 Specifications For 1% Counters For Schmidt Equal Area Net. For Use With A Standard 20-cm Diameter Net. Counters May Be Made Of 2mm Thick Plastic.

A - Periphery Counter

B - Interior Counter

(after Langway Jr., 1958)

example, if all the crystals of a sample were oriented in a single direction their projected points on a Schmidt net would plot at a single point. If the crystals were completely randomly oriented (isotropic), on the other hand, their projected points would plot uniformly across the Schmidt net, lying at approximately equal distances from each other indicating no preferred orientation.

5. PRESENTATION AND INTERPRETATION OF DYNAMIC PROPERTY TEST RESULTS

5.1 Variations Observed in Naturally Frozen Ice Samples

All samples tested in the program may be described as dirty brown bubbly ice with silt lenses. Using the ice classification designation outlined by Pihlainen and Johnson (1963), all samples would be termed Cloudy Ice since they were predominantly sound, non-pervious ice and were opaque due to entrained air bubbles and silt particles. The samples were classified as high density ice with measured densities ranging between 56.0 pcf (.898 gm/cc) to 56.3 pcf (.902 gm/cc), and an average density of 56.2 pcf (.901 gm/cc). The samples were obtained from the USA CRREL permafrost tunnel near Fairbanks, and were extracted from wedge ice (Bolander, 1980). Crystallographic mapping of the ice crystals revealed that the samples were anisotropic. Appendix B presents the crystallography results for the six samples which were mapped onto a Schmidt net. Visual inspection revealed that the samples were non-homogeneous, with silt lenses clearly observed, which were most pronounced in the specimens taken at a 45° orientation. The non-homogeneous nature of the 45° samples lead to inconsistent test results and premature failure along the silt lenses during the test program. It is believed the test results obtained from the 45° oriented test specimens were not representative of the dynamic properties of ice, as the dynamic properties of the silt lenses were measured simultaneously.

Density was not considered a factor contributing to the variations in dynamic properties since all samples were of approximately the same density (within 0.3 pcf or .005 gm/cc). Anisotropy, temperature, confining pressure, strain amplitude and frequency of loading were considered as factors contributing to variations in dynamic properties during the test program.

All data collected during the test program was initially plotted as a function of temperature and the results are presented in Appendix A. The plotting of data as a function of temperature was necessary to allow test results to be interpreted at constant temperatures, since during the test program the temperature varied from specimen to specimen, due to both the variation in ambient cold room temperature and the time limits imposed by the test schedule (see Figure 4-10). The coldest test temperature (approximately -10°C) was performed at the ambient coldroom temperature. For the other test temperatures of -4°C and -1°C, an environmental chamber was used for temperature control as outlined in Section 4.1. Even though the temperature of the test specimen could be brought close to the test temperature desired, the time limitations imposed by the test schedule resulted in small temperature variations. The maximum variations observed during the test program are shown in Table 5-1. The variations in test temperature for the majority of the tests were generally much closer to the desired test temperature than indicated by Table 5-1.

5.2 Resonant Column Test Results

Inspection of the resonant column test results revealed that, for the test conditions utilized, confining pressure and strain amplitude had little effect on the dynamic properties. This is shown on Figures

Table 5-1: Temperature Variations Observed During Test Program

Temperature Desired (°C)	Temperature Range Observed (°C)
-10	-7.4 to - 11.9
-4	-2.3 to - 5.8
-1	-0.85 to - 2.2

5-1 through 5-4 where the test results have been plotted combining all confining pressures and all strain amplitudes. An inspection of the results indicates the maximum variation in dynamic Young's and shear modulus was 25% and 40%, respectively. Larger variations were observed in damping ratio for some tests, but most of the test results showed little variance, and no correlation with confining pressure was observed. The resonant column test results given in Figures 5-1 through 5-4 present the results as follows:

(1) Figure 5-1 presents dynamic Young's modulus vs. temperature for all confining pressures.

(2) Figure 5-2 presents dynamic shear modulus vs. temperature for all confining pressures.

(3) Figure 5-3 presents damping ratio vs. temperature for the longitudinal mode of vibration.

(4) Figure 5-4 presents damping ratio vs. temperature for the torsional mode of vibration.

Appendix A presents the results plotted for each confining pressure and strain amplitude. The resonant column test results showed no correlation with the dynamic properties and either confining pressure or strain amplitude. When comparing test results for vertical core samples with test results for horizontal core samples at constant temperature, Figures 5-1 and 5-2 reveal a maximum variation of dynamic moduli of approximately 10%. Greater variation in test results (25% on Figure 5-1 and 40% on Figure 5-2) was observed for the 45° orientation core samples. These samples were non-homogeneous in nature.

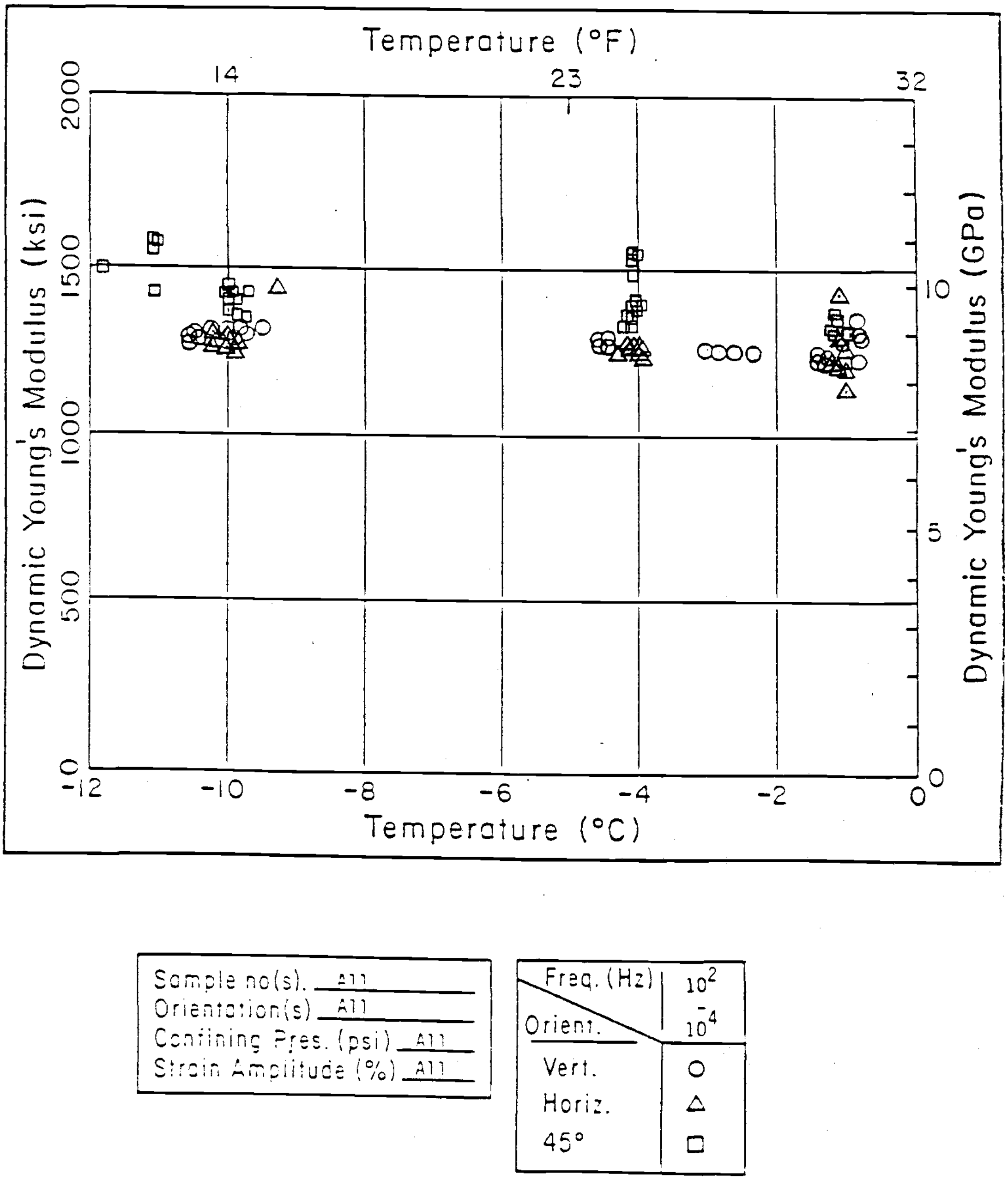

FIGURE 5-1 Resonant Column Test Results - Dynamic Young's Modulus Vs. Temperature

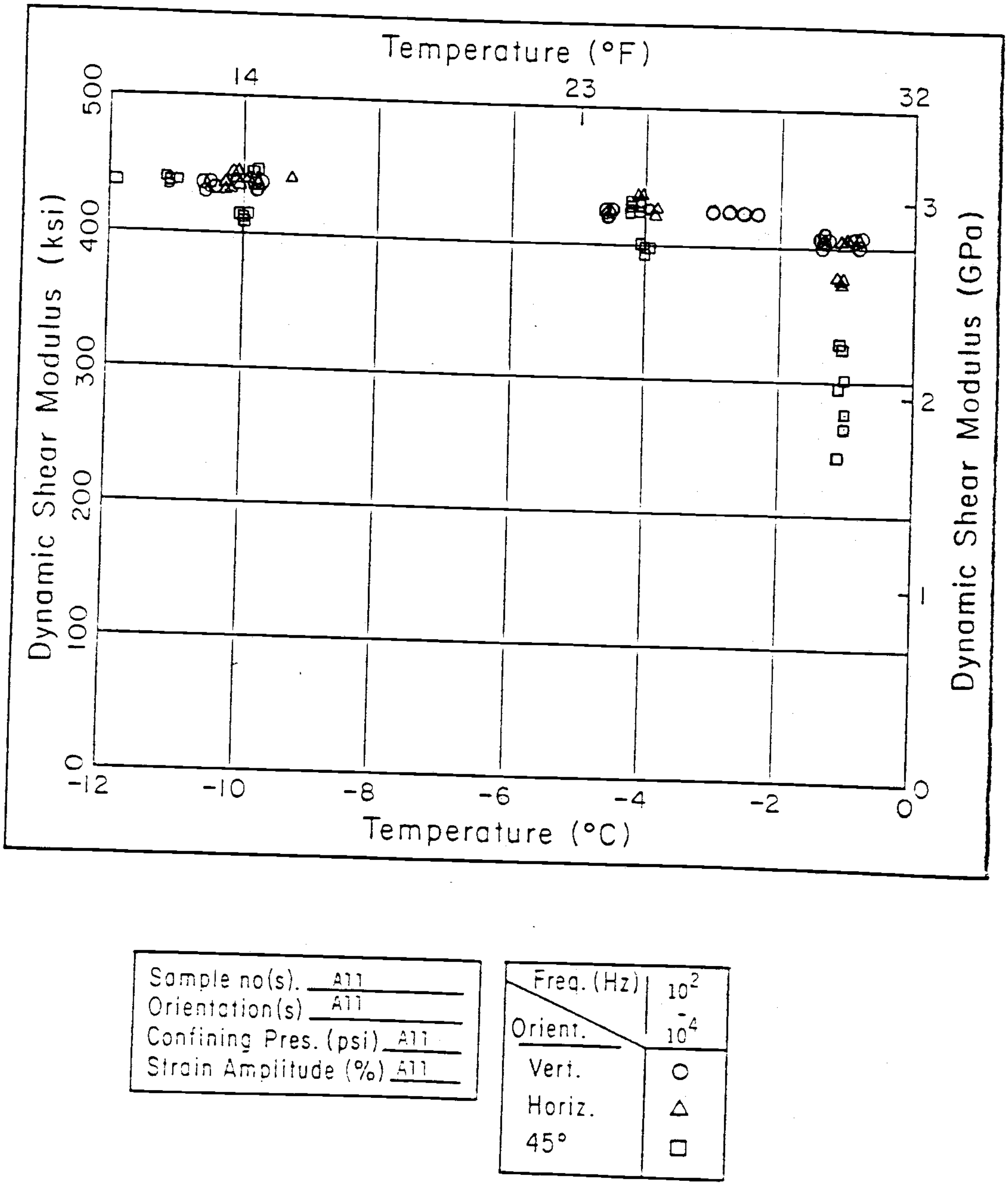

FIGURE 5-2 Resonant Column Test Results - Dynamic Shear Vs. Temperature

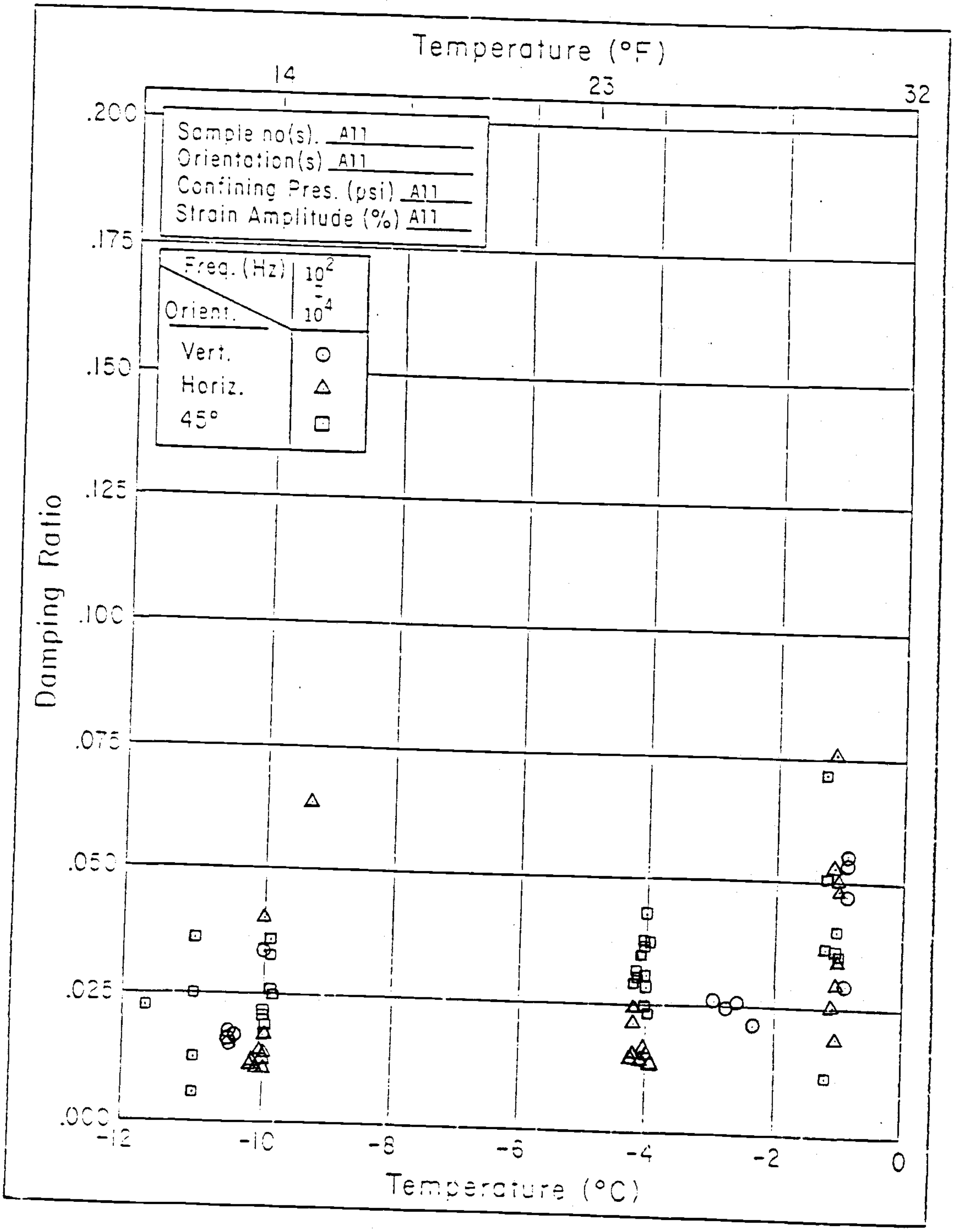

FIGURE 5-3 Resonant Column Test Results - Damping Ratio Vs. Temperature For Longitudinal Mode Of Vibration

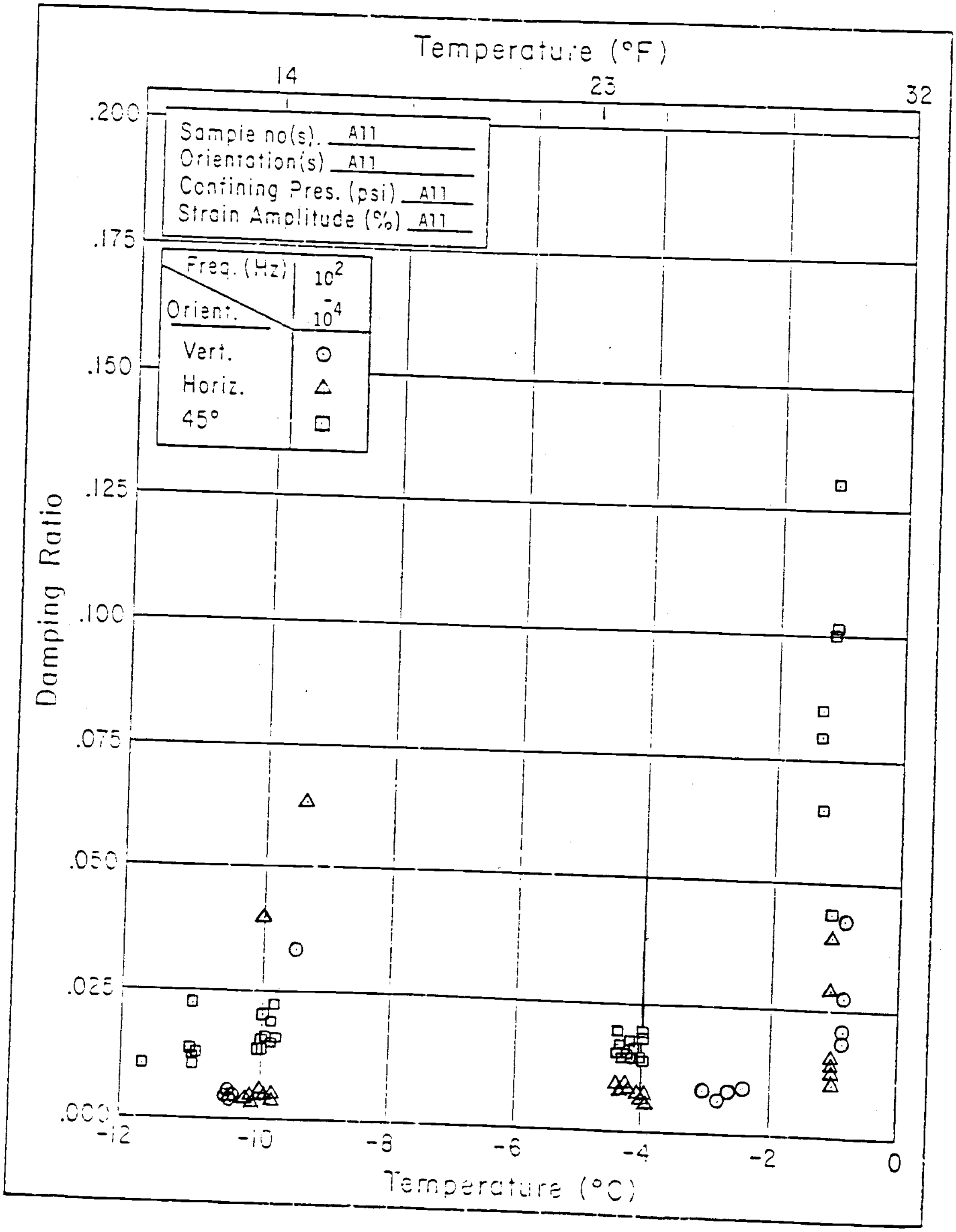

FIGURE 5-4 Resonant Column Test Results - Damping Ratio Vs. Temperature For Torsional Mode Of Vibration

The damping ratio test results revealed a large amount of variation at constant temperature (see Figures 5-3 and 5-4). Inspection of Figures 5-3 and 5-4 reveal the largest variation was observed for the 45° orientation samples and at the warmest test temperature (-1°C).

5.3 Cyclic Triaxial Test Results

The results of the cyclic triaxial test program showed much larger variations in dynamic properties for the parameters investigated (i.e., temperature, frequency, strain amplitude, sample orientation) than those observed during resonant column testing. To provide easy observation of the effects of the different parameters, the results have been put in tabular form, separating the results into groups of samples with similar core orientation. Tables 5-2 through 5-4 present average test results adjusted to normalized temperatures of -10°C, -4°C and -1°C. The results shown in the tables are different from those anticipated, and an interpretation of these results is given in Section 5.5. From the tabulated results, Figures 5-5 through 5-28 were constructed, which present the data as follows:

(1) Figures 5-5 through 5-10 present all of the test results as a function of temperature, at three strain amplitudes (approximately .0009%, .005% and .01%). No attempt was made to distinguish between different orientations and confining pressures as all the results generally fell within a relatively narrow band. Each Figure also shows the arithmetic mean of all values obtained.

(2) Figures 5-11 through 5-16 present all of the test results as a function of $\log_{10}$ frequency (Hz) for three temperatures (-10°C, -4°C

Table 5.2 - Dynamic Properties - Cyclic Triaxial Test Results. Vertical Orientation

Sample No(s) 78 and 65
Confining Pres. (psi) All

Temp (°C)	Nominal Strain Amp (%)	Frequency (Hz)	E_d (ksi)	D (ratio)
-10	.0009	0.05	1240	.125
		0.5	1300	.112
		5.0	1470	.09
	.005	0.05	1470	.070
		0.5	1200	.065
		5.0	1310	.060
	.01	0.05	850	.062
		0.5	990	.08
		5.0	1040	.15
-4	.0009	0.05	1400	.107
		0.5	1550	.102
		5.0	1710	.095
	.005	0.05	970	.10
		0.5	1160	.085
		5.0	1300	.083
	.01	0.05	850	.098
		0.5	970	.062
		5.0	1030	.053
-1	.0009	0.05	1260	.118
		0.5	1450	.112
		5.0	1500	.110
	.005	0.05	740	.105
		0.5	960	.09
		5.0	1110	.086
	.01	0.05	750	.112
		0.5	830	.072
		5.0	900	.073

Table 5.3 - Dynamic Properties - Cyclic Triaxial Test Results
Horizontal Orientation

Sample No(s) 72 and 73
Confining Pres. (psi) All

Temp (°C)	Nominal Strain Amp (%)	Frequency (Hz)	E_d (ksi)	D (ratio)
-10	.0009	0.05	1180	.128
		0.5	1410	.102
		5.0	1510	.092
	.005	0.05	840	.128
		0.5	950	.084
		5.0	1050	.06
	.01	0.05	730	.135
		0.5	850	.075
		5.0	940	.05
-4	.0009	0.05	1360	.147
		0.5	1510	.116
		5.0	1670	.1
	.005	0.05	840	.151
		0.5	1000	.1
		5.0	1100	.08
	.01	0.05	750	.149
		0.5	960	.08
		5.0	1010	.06
-1	.0009	0.05	1170	.152
		0.5	1420	.12
		5.0	1560	.108
	.005	0.05	670	.16
		0.5	890	.107
		5.0	1000	.088
	.01	0.05	640	.15
		0.5	850	.08
		5.0	910	.062

Table 5.4 - Dynamic Properties - Cyclic Triaxial Test Results.
45 Degree Orientation

Sample No(s) 71,69,70 and 75*
Confining Pres. (psi) All

Temp (°C)	Nominal Strain Amp (%)	Frequency (Hz)	E_d (ksi)	D (ratio)
-10	.0009	0.05	1420	.1
		0.5	1500	.088
		5.0	1600	.083
	.005	0.05	970	.111
		0.5	1100	.08
		5.0	1200	.05
	.01	0.05	600	.123
		0.5	700	.085
		5.0	770	.075
-4	.0009	0.05	1380	.11
		0.5	1470	.09
		5.0	1690	.083
	.005	0.05	930	.125
		0.5	1060	.094
		5.0	1160	.068
	.01	0.05	830	.12
		0.5	850	.084
		5.0	1000	.085
-1	.0009	0.05	1000	.11
		0.5	1200	.09
		5.0	1450	.078
	.005	0.05	760	.12
		0.5	900	.08
		5.0	960	.06
	.01	0.05	670	.137
		0.5	700	.085
		5.0	850	.065

* Sample #75 was rejected due to the poor condition of the sample.

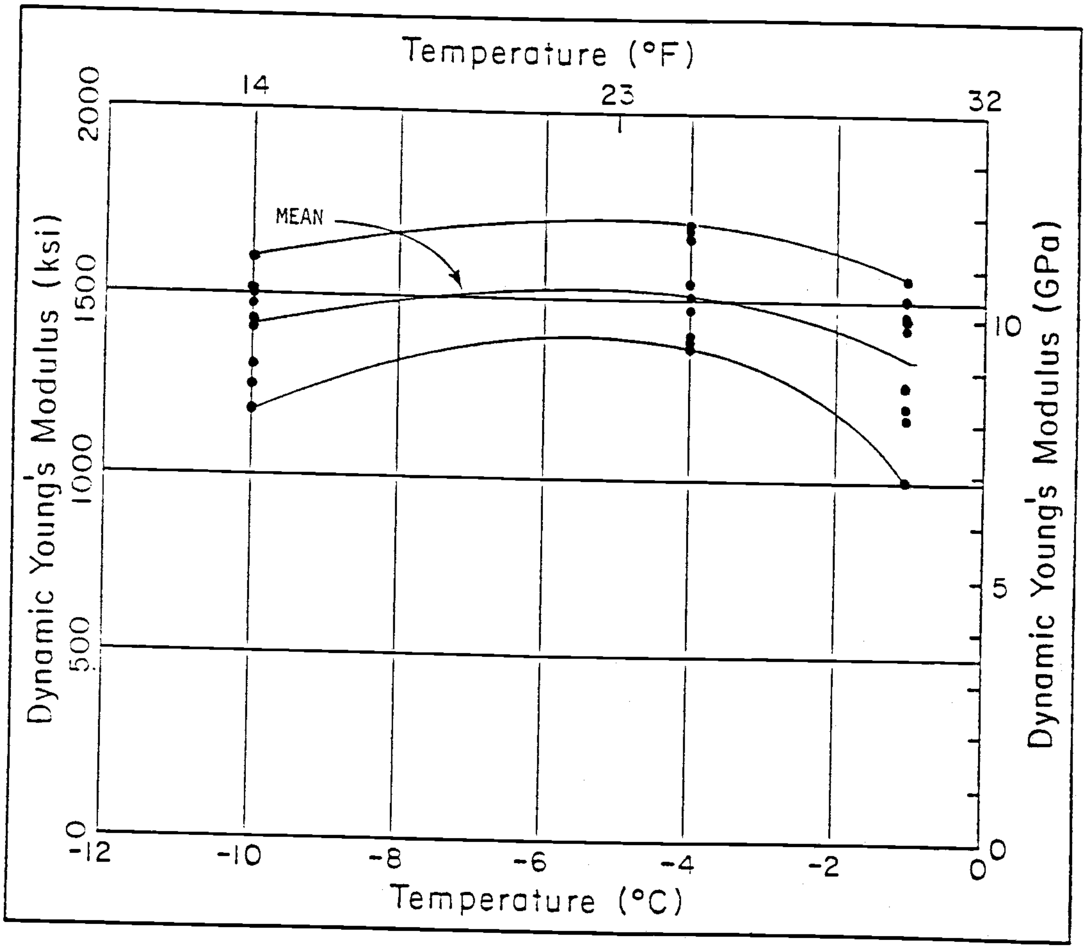

Sample no(s). All
Orientation(s) All
Confining Pres. (psi) All
Strain Amplitude (%) .0009

FIGURE 5-5 Cyclic Triaxial Test Results - Dynamic Young's Modulus Vs. Temperature For Strain Amplitude Of 0.0009%

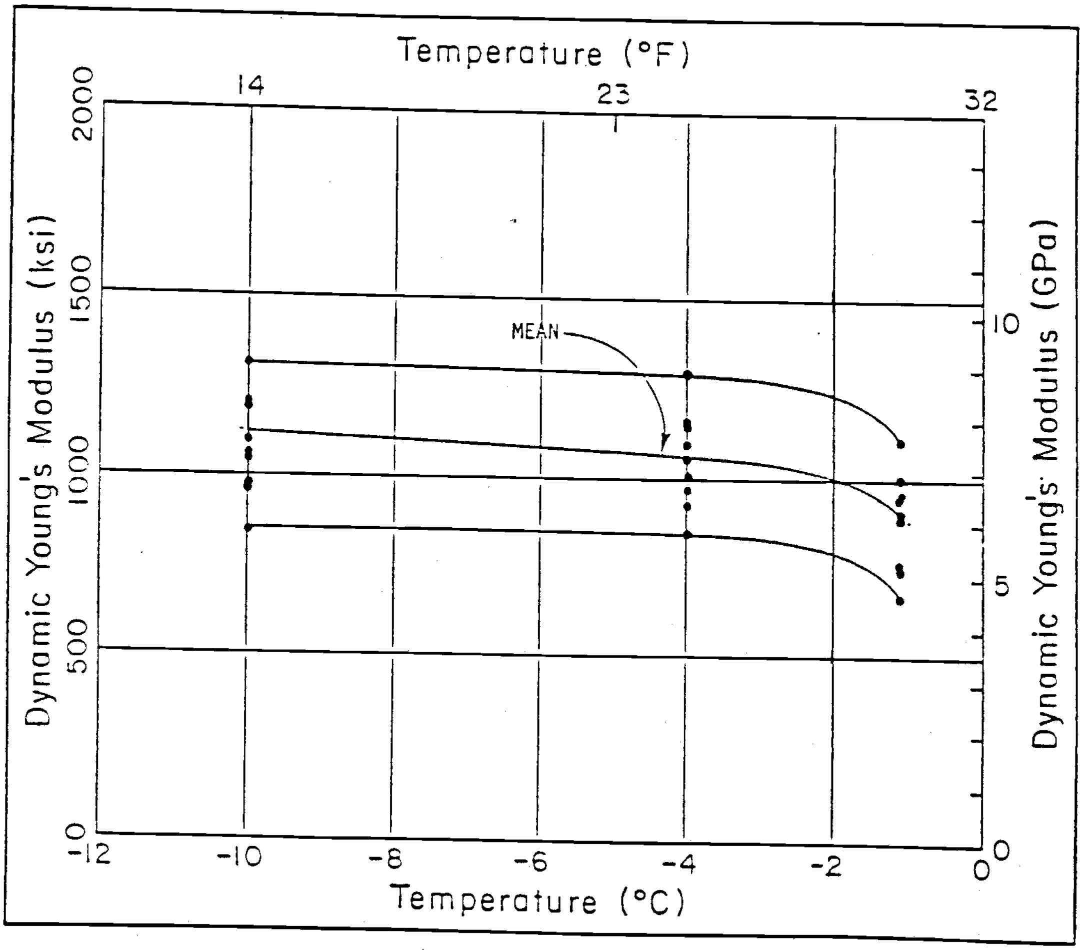

Sample no(s).	All
Orientation(s)	All
Confining Pres. (psi)	All
Strain Amplitude (%)	.005

FIGURE 5-6 Cyclic Triaxail Test Results - Dynamic Young's Modulus Vs. Temperature For Strain Amplitude Of 0.005%

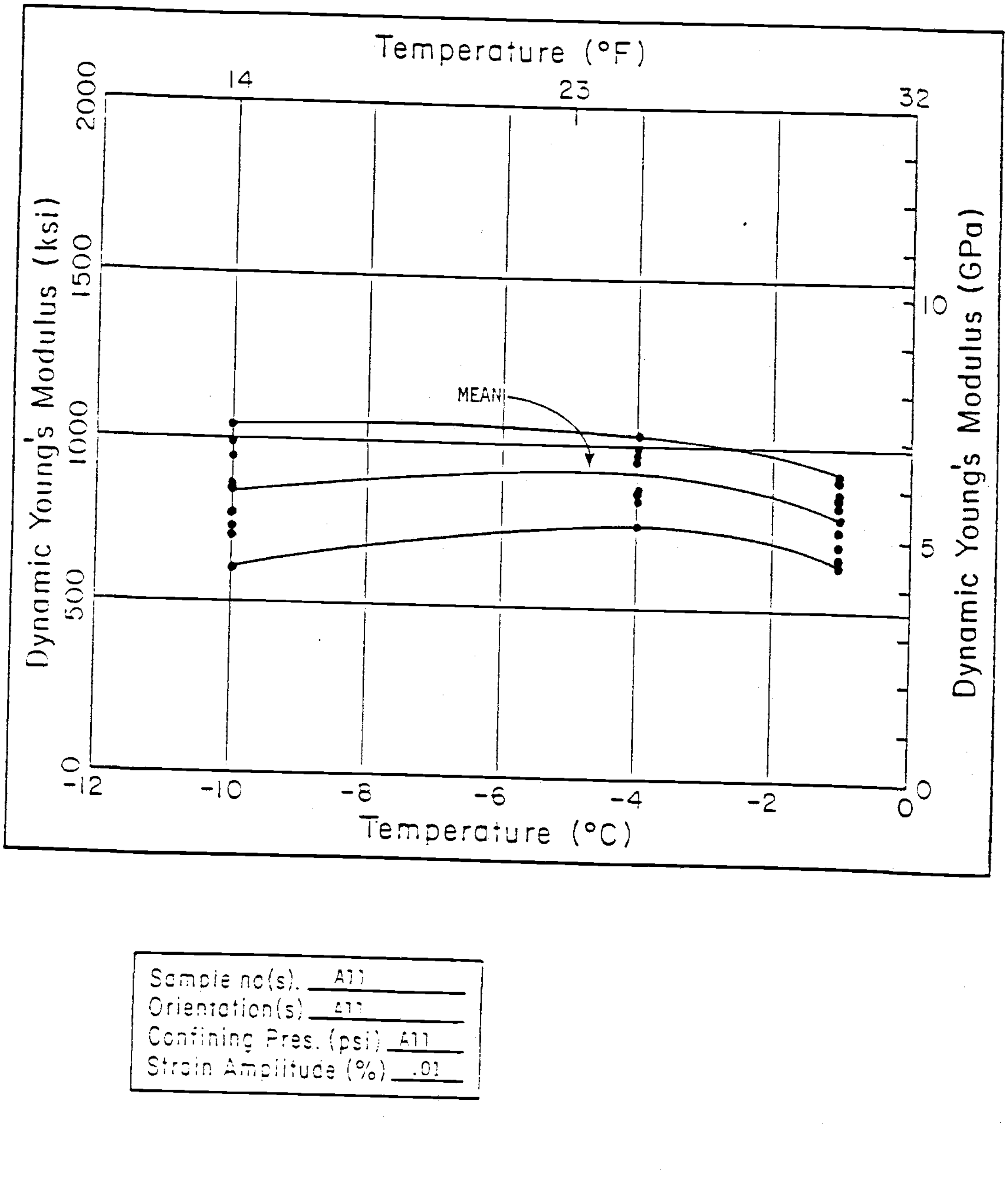

FIGURE 5-7 Cyclic Triaxial Test Results - Dynamic Young's Modulus Vs. Temperature For Strain Amplitude Of 0.01%

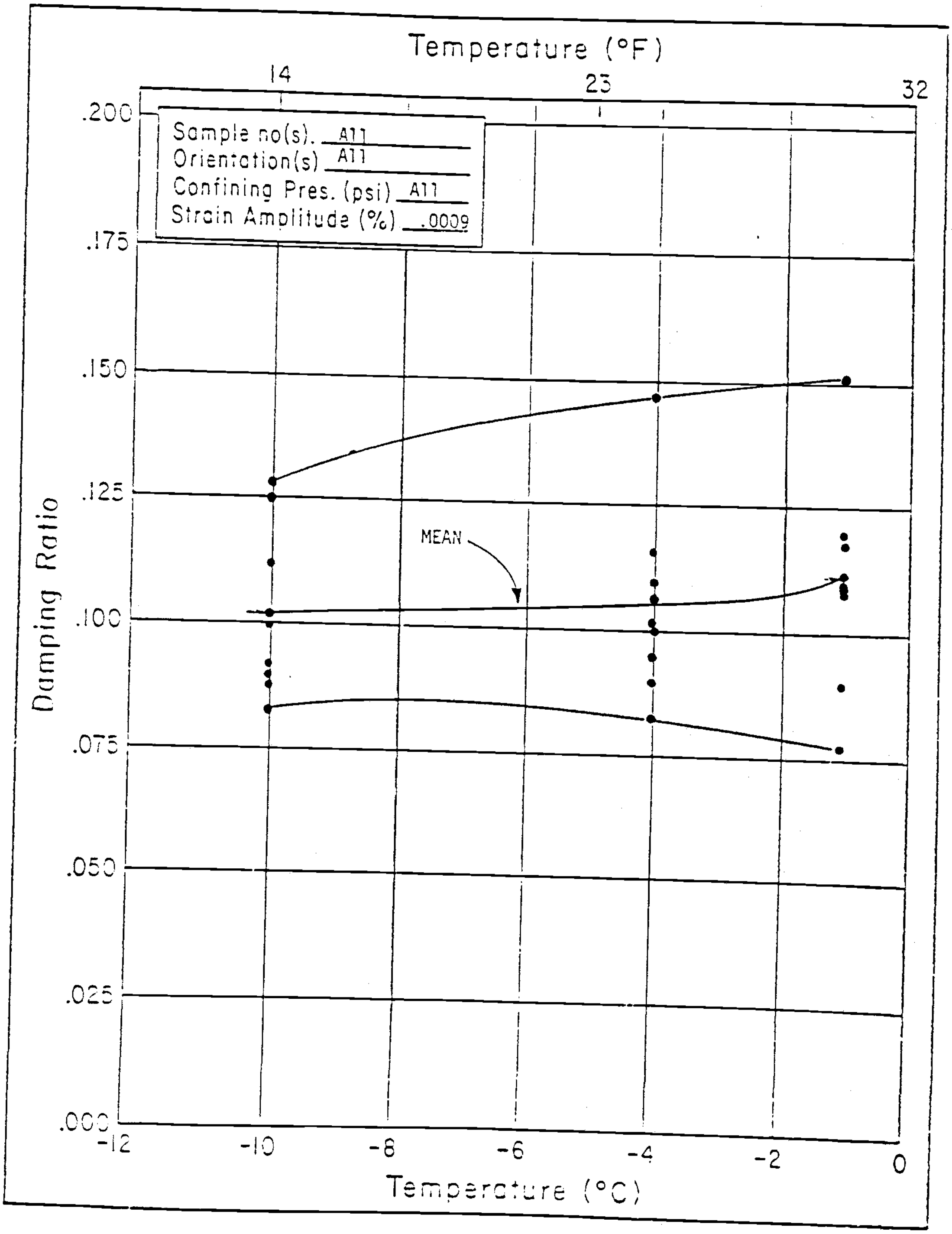

FIGURE 5-8 Cyclic Triaxial Test Results - Damping Ratio Vs. Temperature For Strain Amplitude of 0.0009%

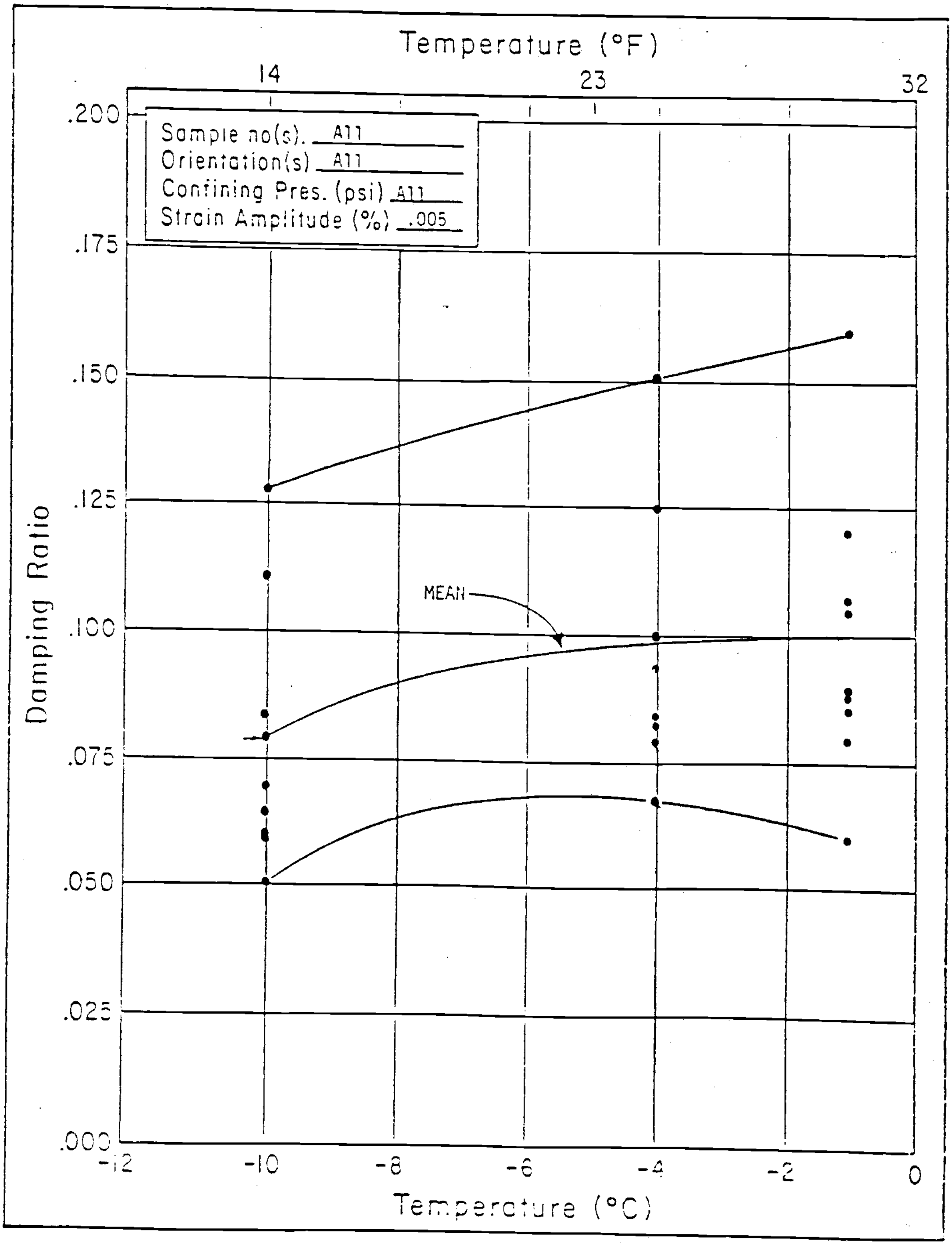

FIGURE 5-9 Cyclic Triaxial Test Results - Damping Ratio Vs. Temperature For Strain Amplitude Of 0.005%

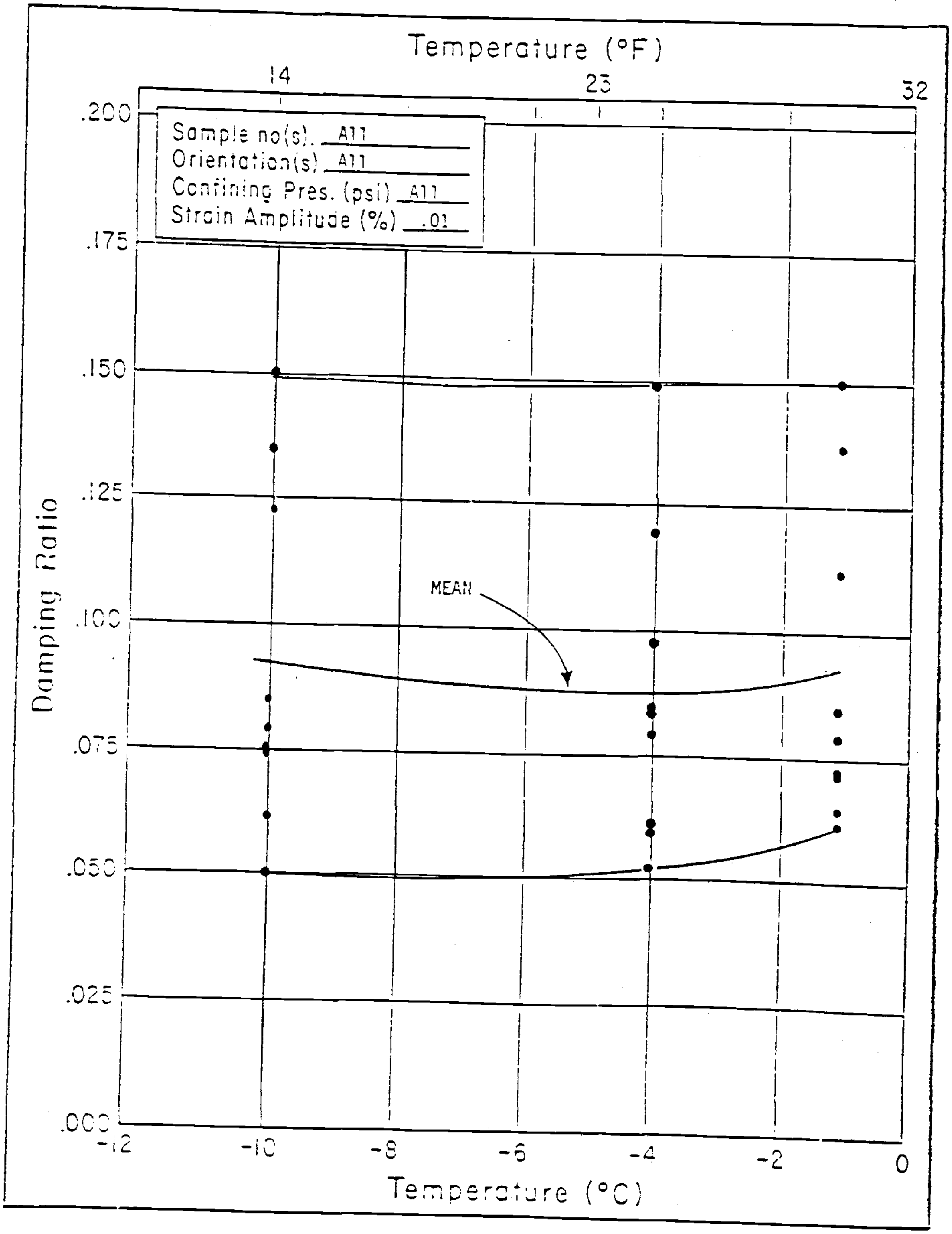

FIGURE 5-10 Cyclic Triaxial Test Results - Damping Ratio Vs. Temperature For Strain Amplitude Of 0.01%

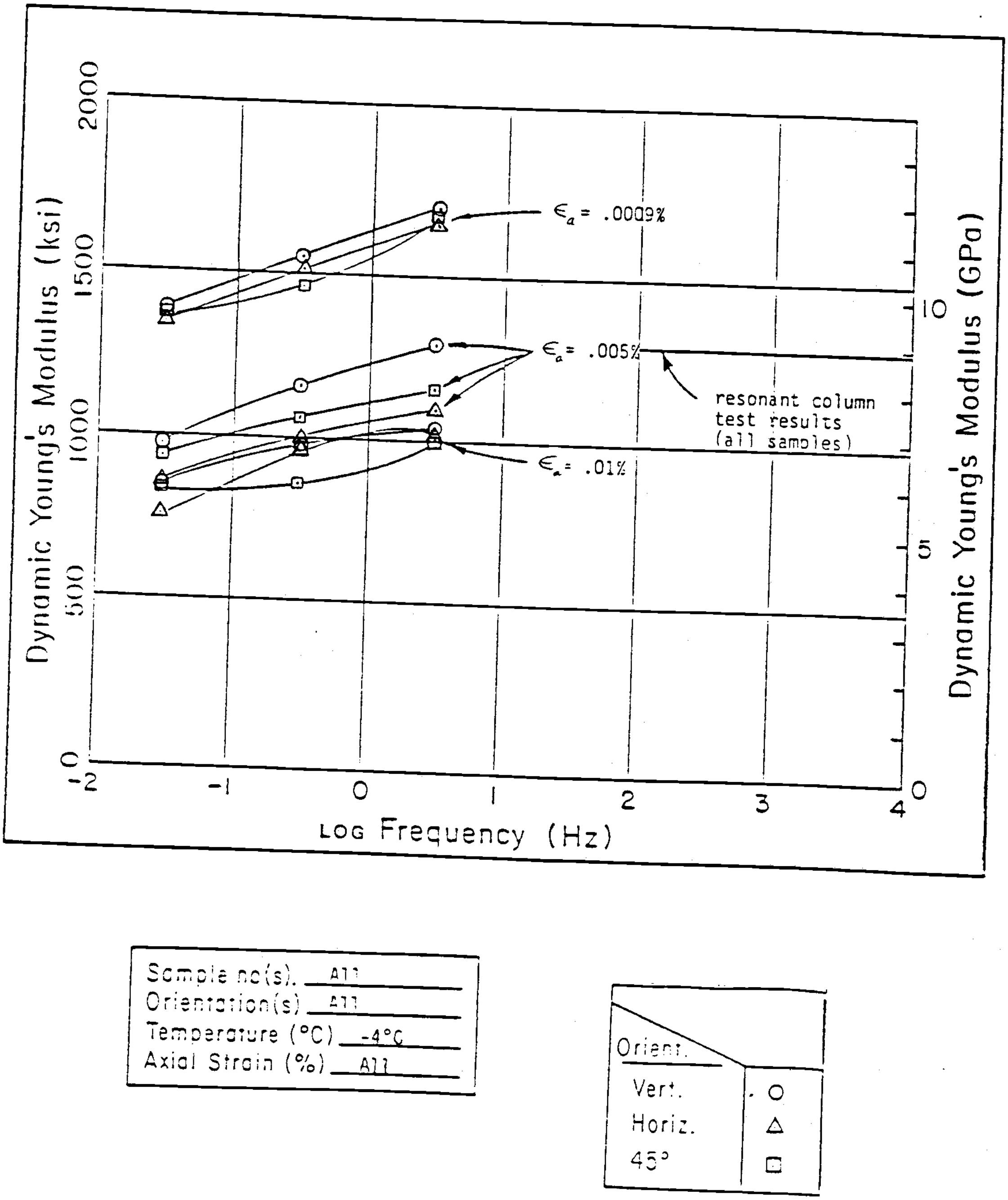

FIGURE 5-11 Cyclic Triaxial And Resonant Column Test Results - Dynamic Young's Modulus Vs. Frequency For Temperature Of -4^{0}C

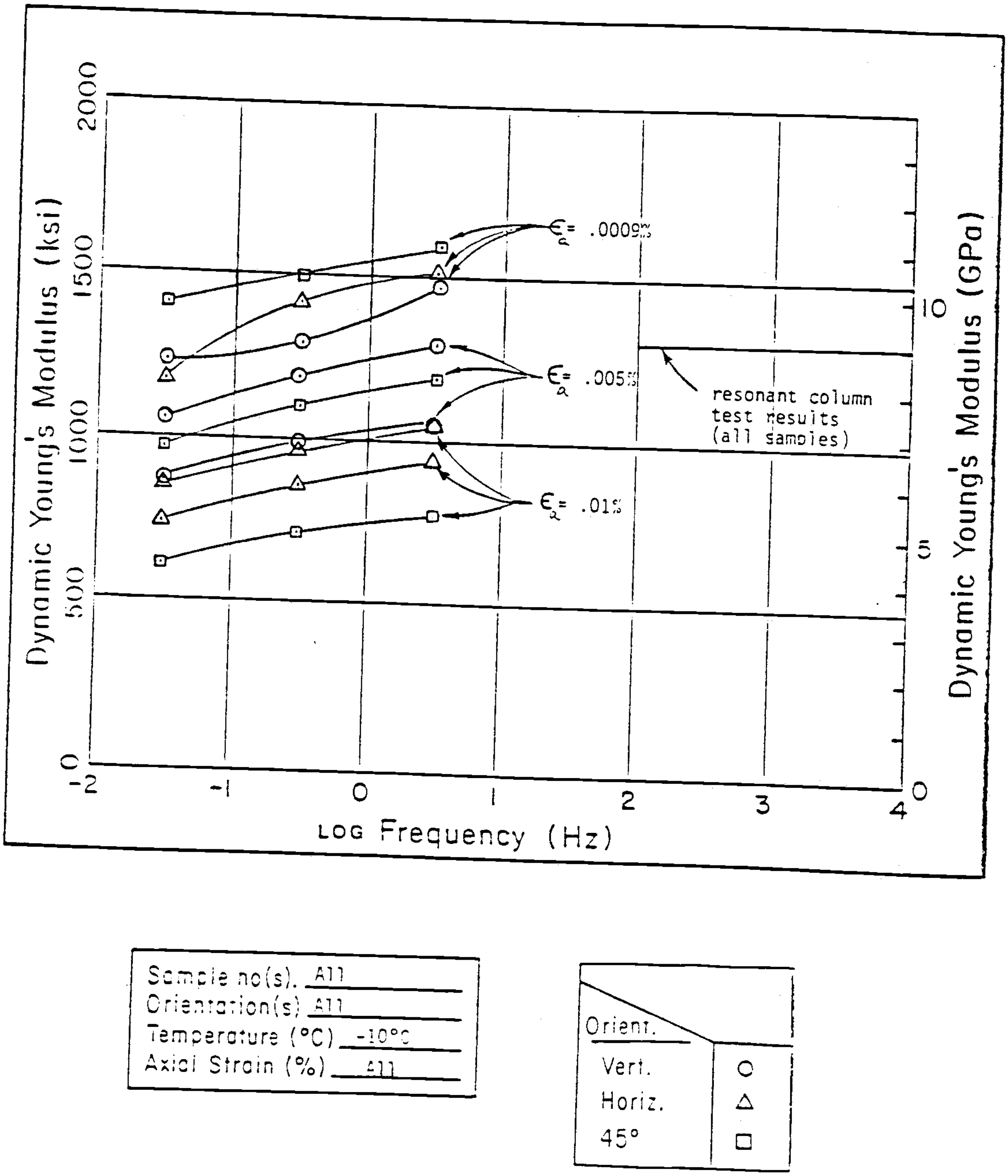

FIGURE 5-12 Cyclic Triaxial And Resonant Column Test Results - Dynamic Young's Modulus Vs. Frequency For Temperature Of -10°C

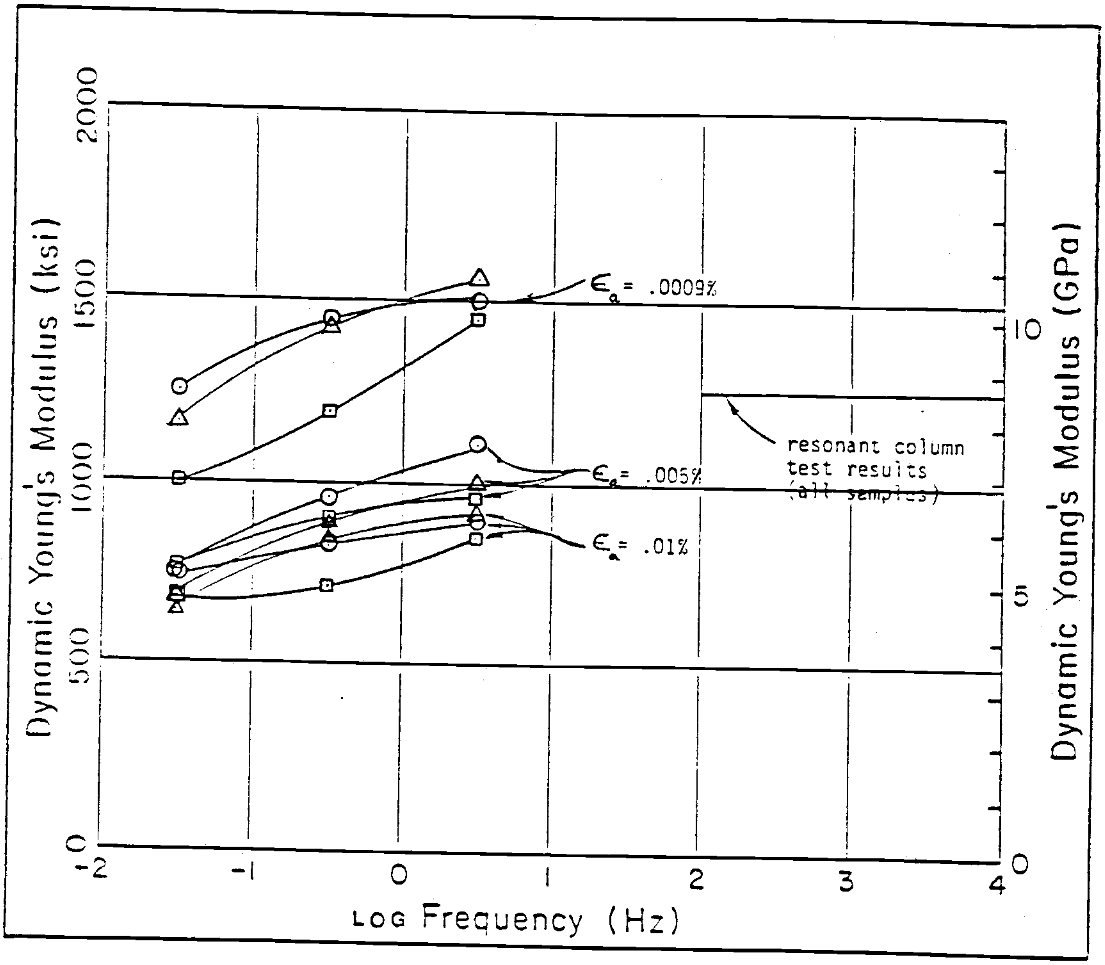

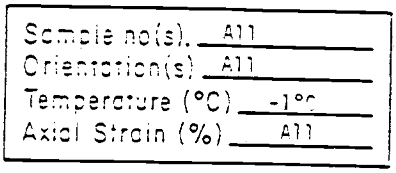

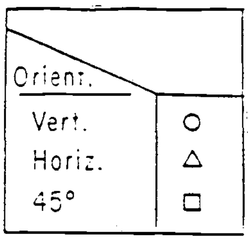

FIGURE 5-13 Cyclic Triaxial And Resonant Column Test Results - Dynamic Young's Modulus Vs. Frequency For Temperature Of -1°C

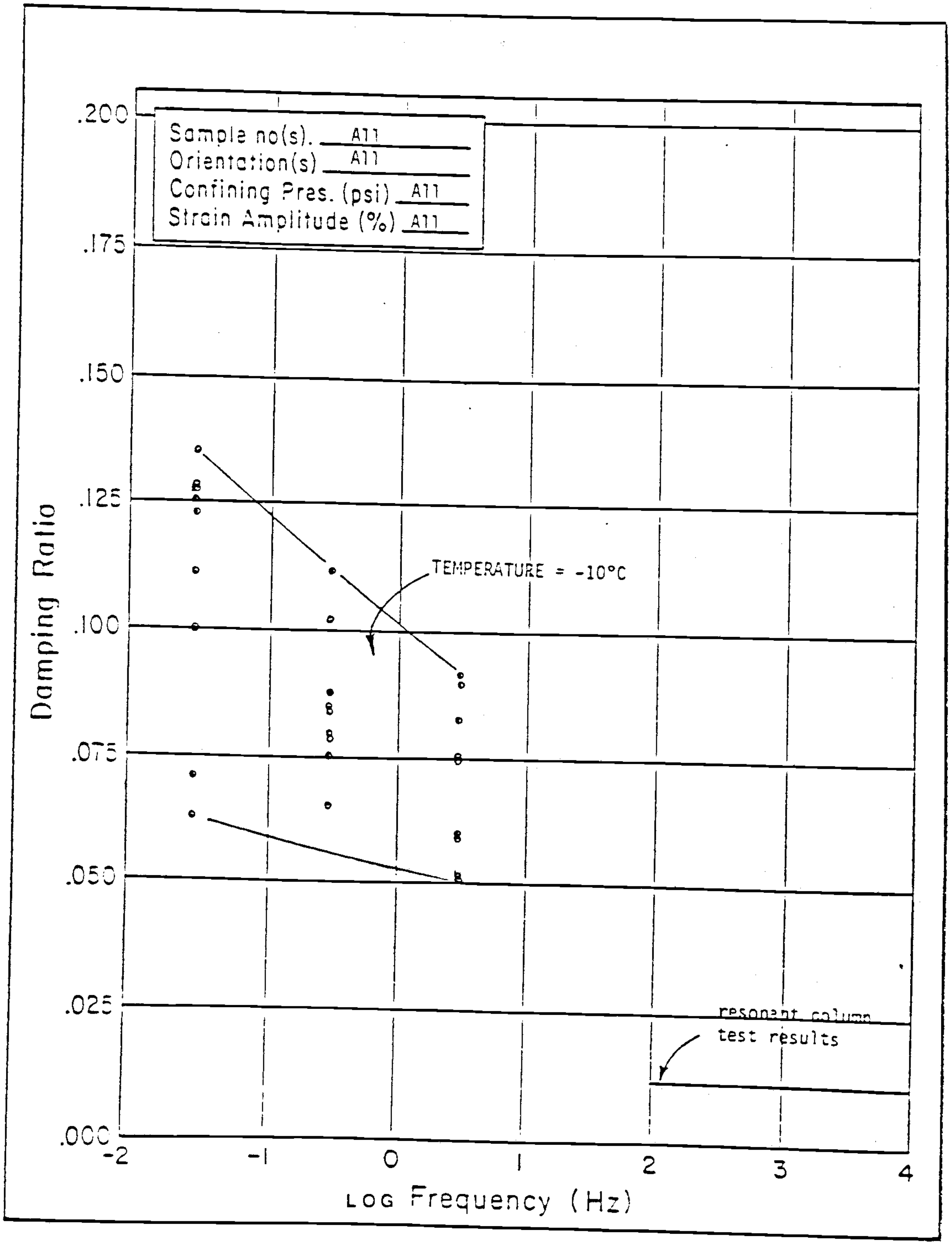

FIGURE 5-14 Cyclic Triaxial And Resonant Test Results - Damping Ratio Vs. Frequency For Temperature of -10°C

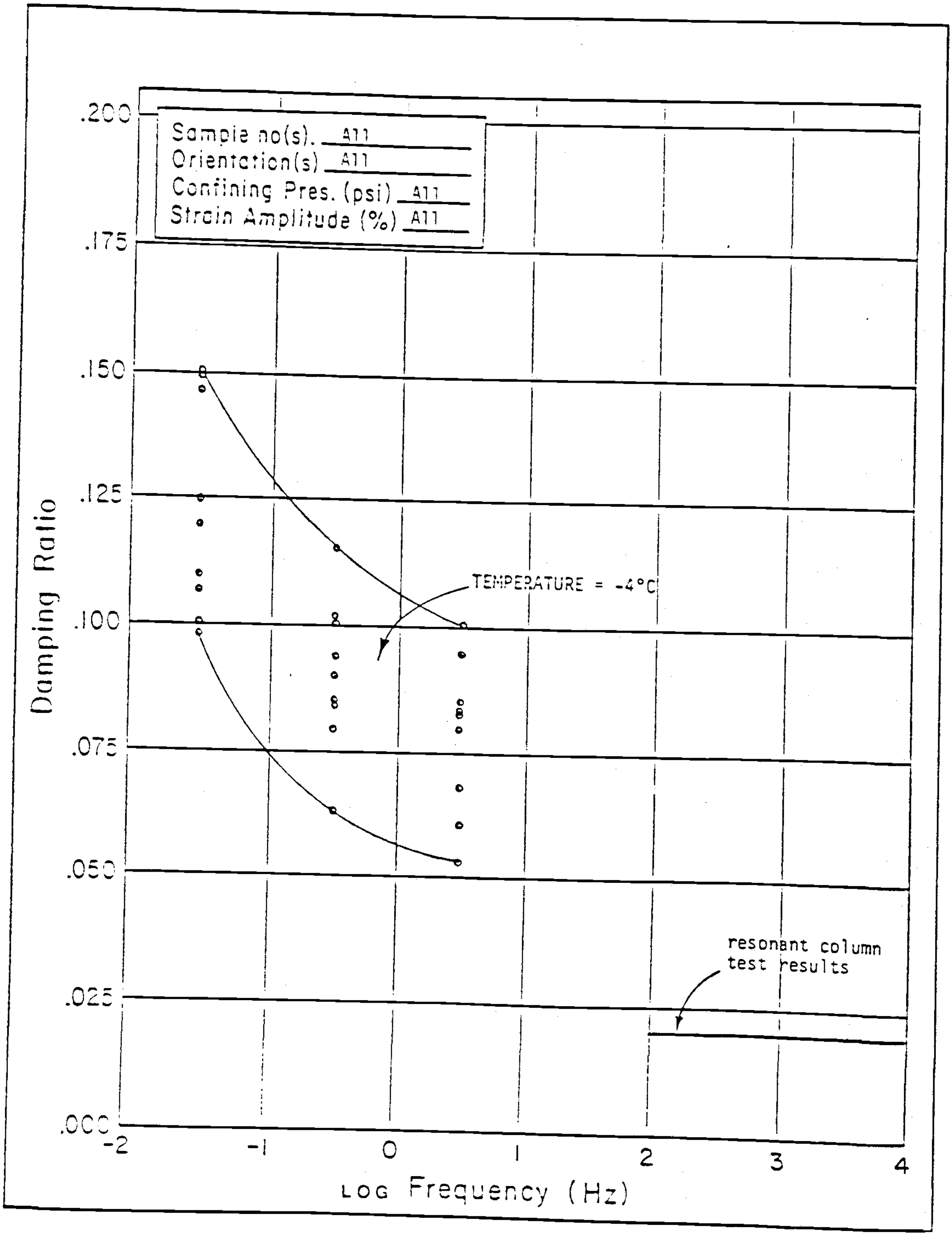

FIGURE 5-15 Cyclic Triaxial And Resonant Column Test Results - Damping Ratio Vs. Frequency For Temperature of -4°C

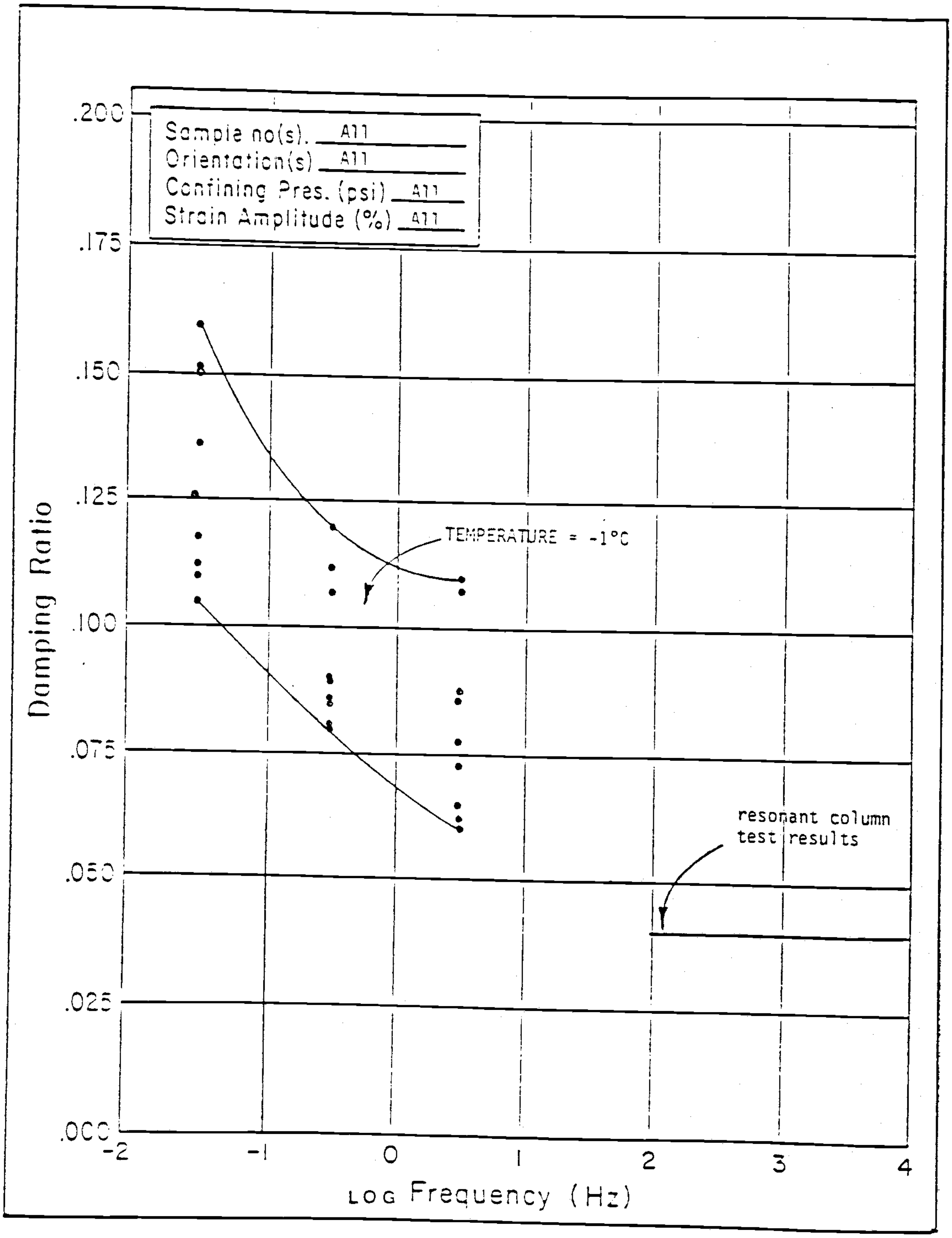

FIGURE 5-16 Cyclic Triaxial And Resonant Column Test Results - Damping Ratio Vs. Frequency For Temperature Of -1°C

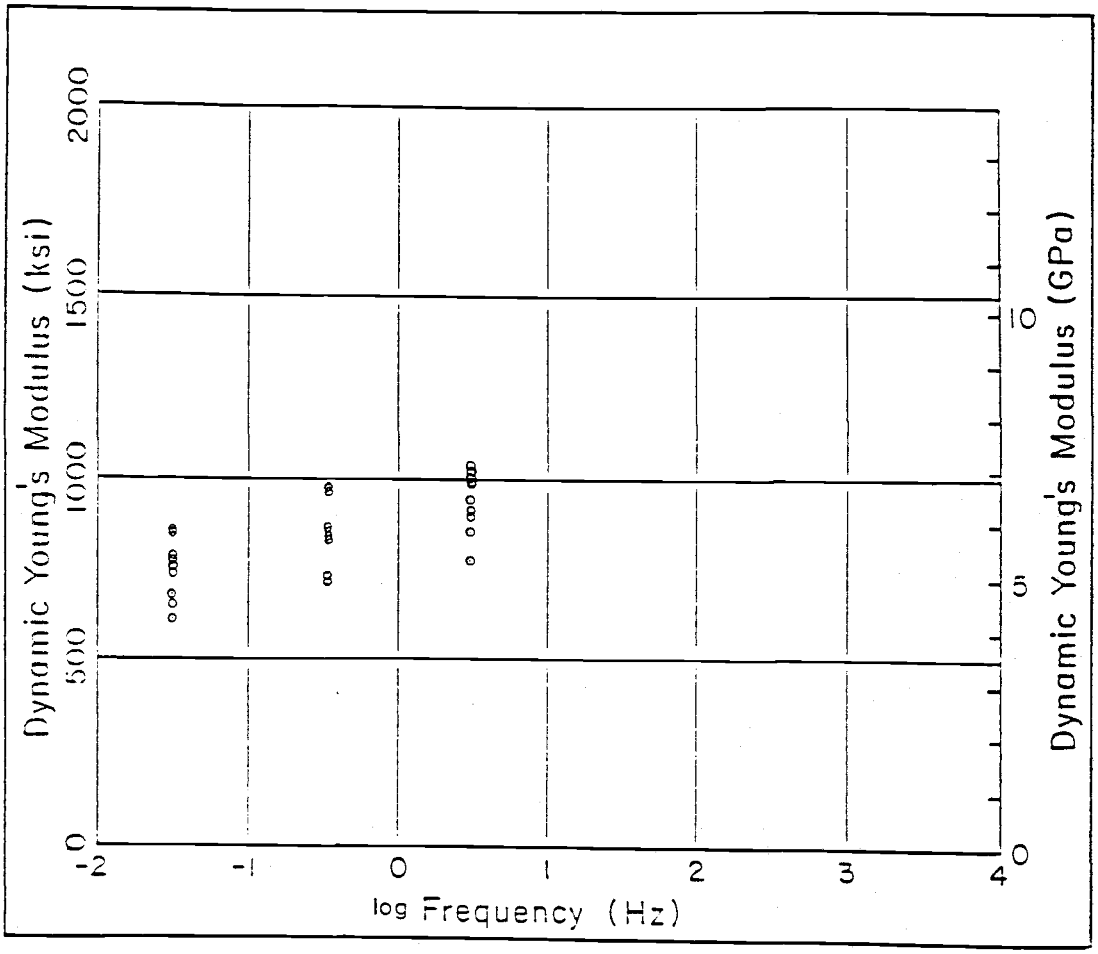

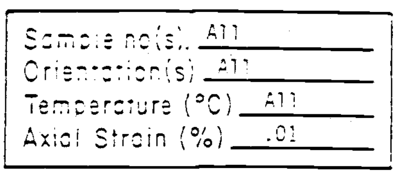

FIGURE 5-17 Cyclic Triaxial And Resonant Column Test Results - Dynamic Young's Modulus Vs. Frequency For Strain Amplitude Of 0.01%

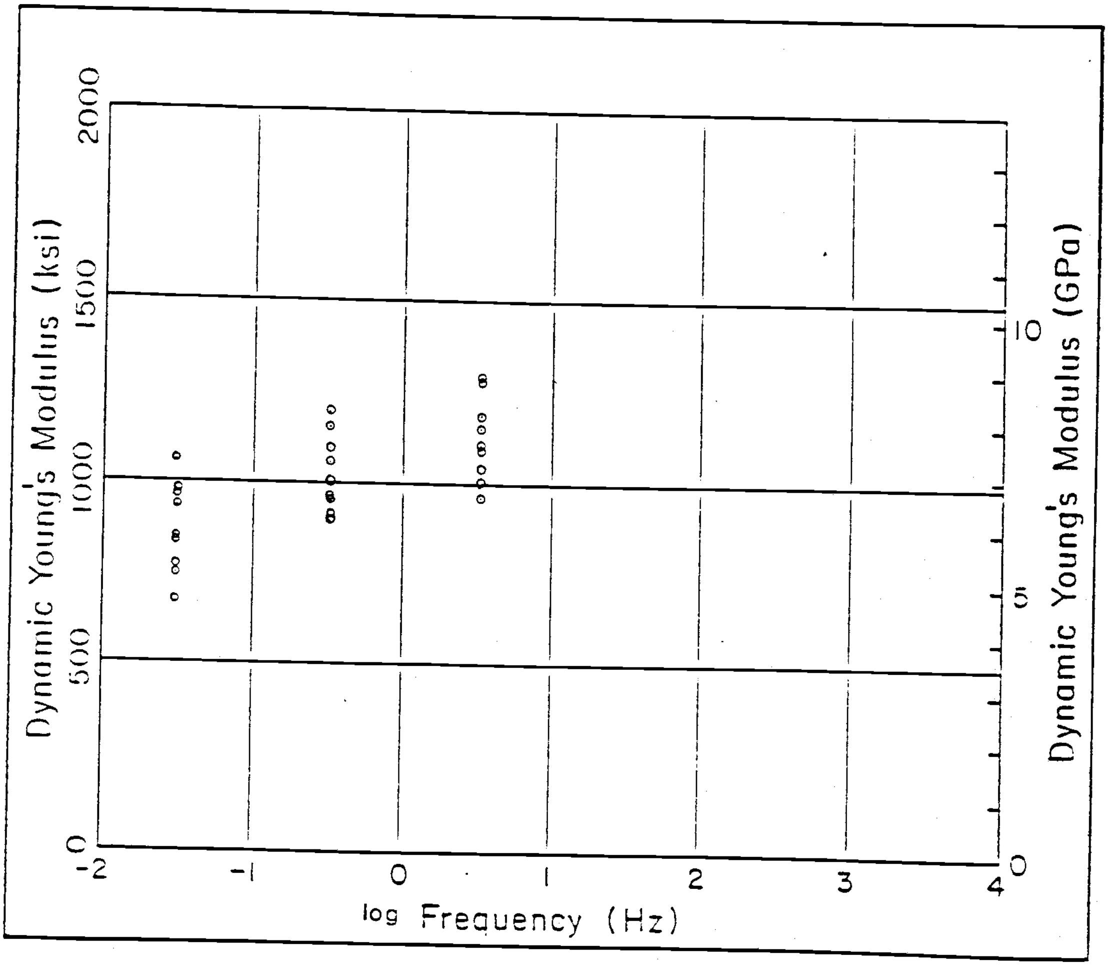

Sample no(s). All
Orientation(s) All
Temperature (°C) All
Axial Strain (%) .005

FIGURE 5-18 Cyclic Triaxial Test Results - Dynamic Young's Modulus Vs. Frequency For Strain Amplitude of 0.005%

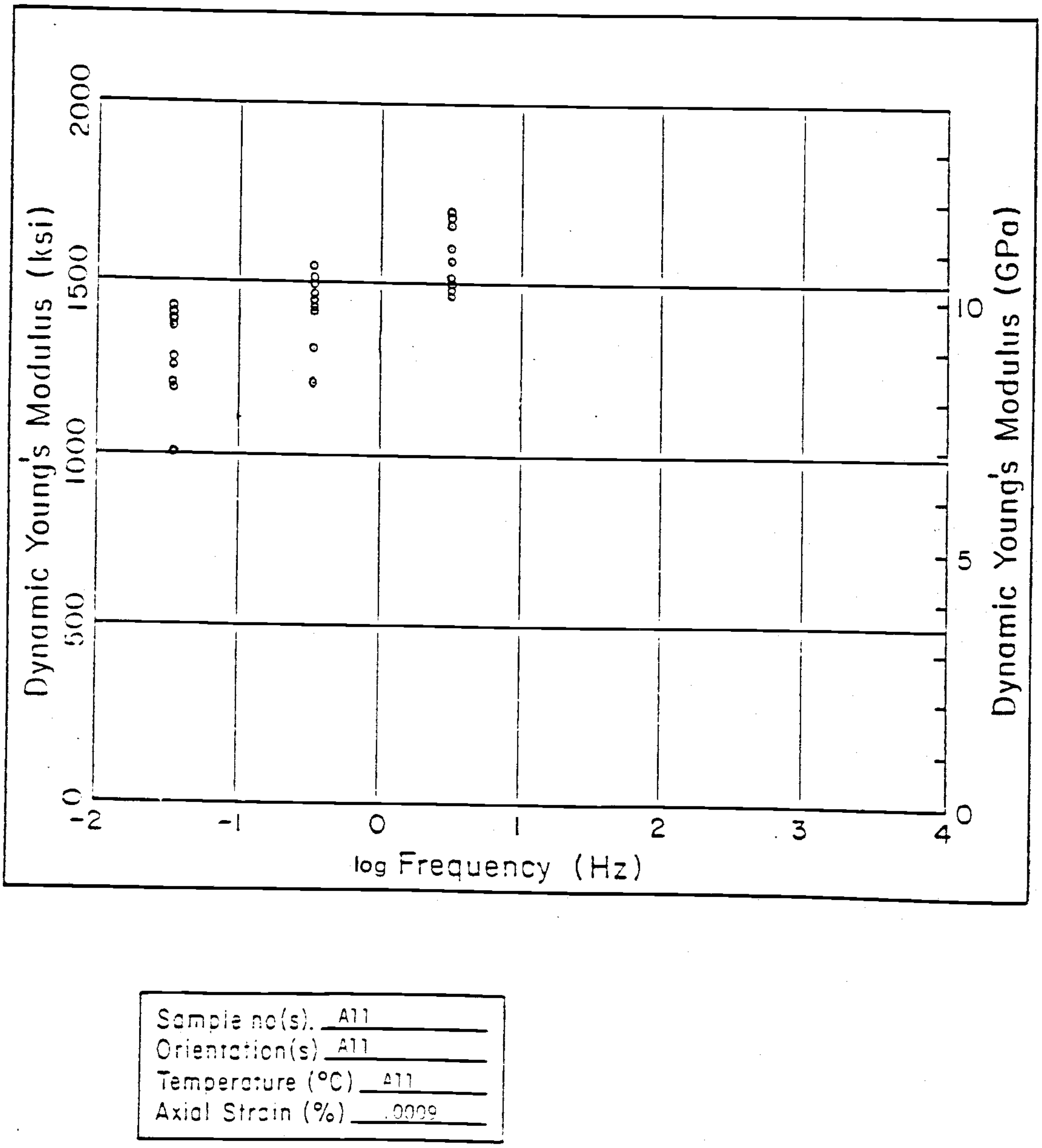

FIGURE 5-19 Cyclic Triaxial Test Results - Dynamic Young's Modulus Vs. Frequency For Strain Amplitude of 0.0009%

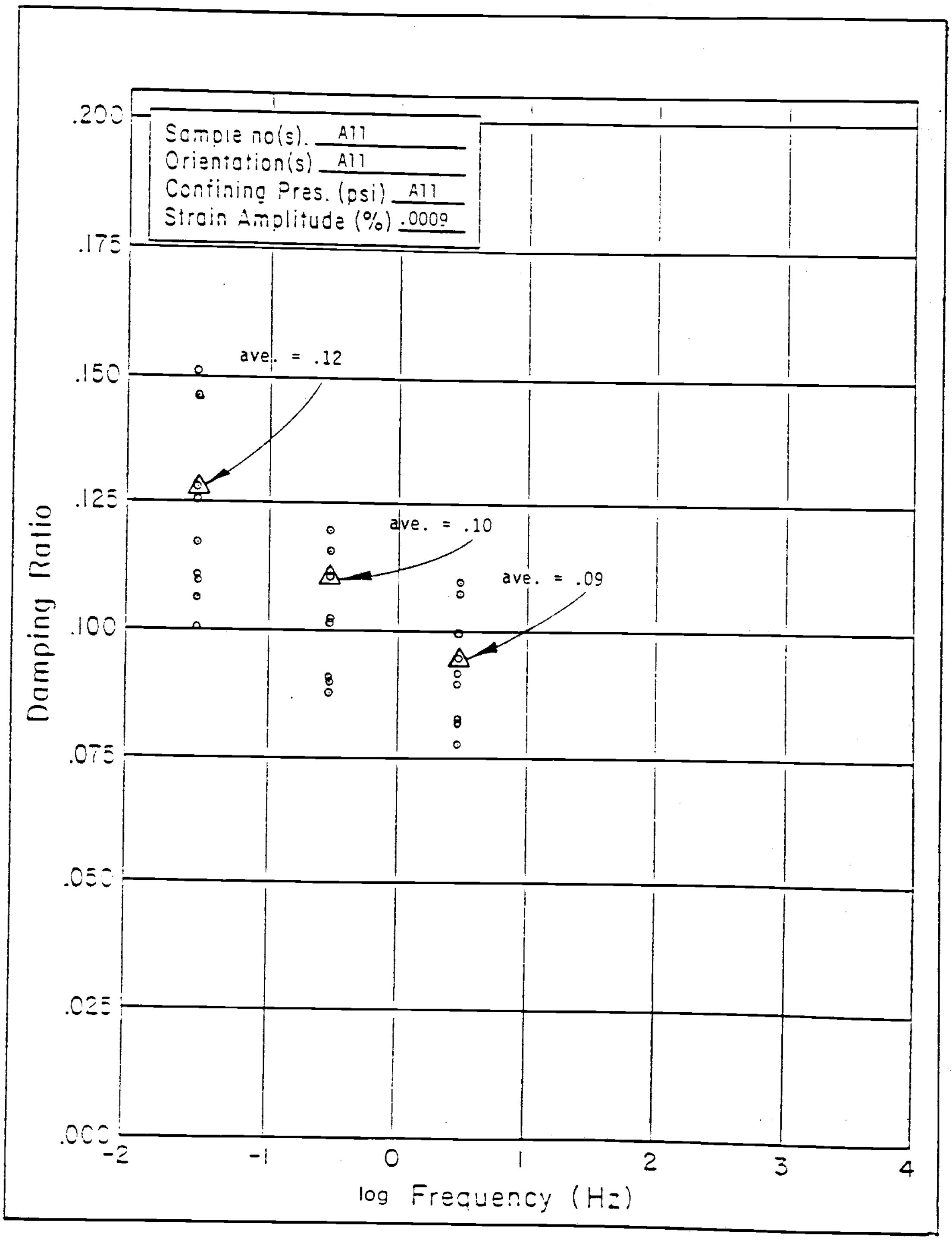

FIGURE 5-20 Cyclic Triaxial Test Results - Damping Ratio Vs. Frequency For Strain Amplitude of 0.0009%

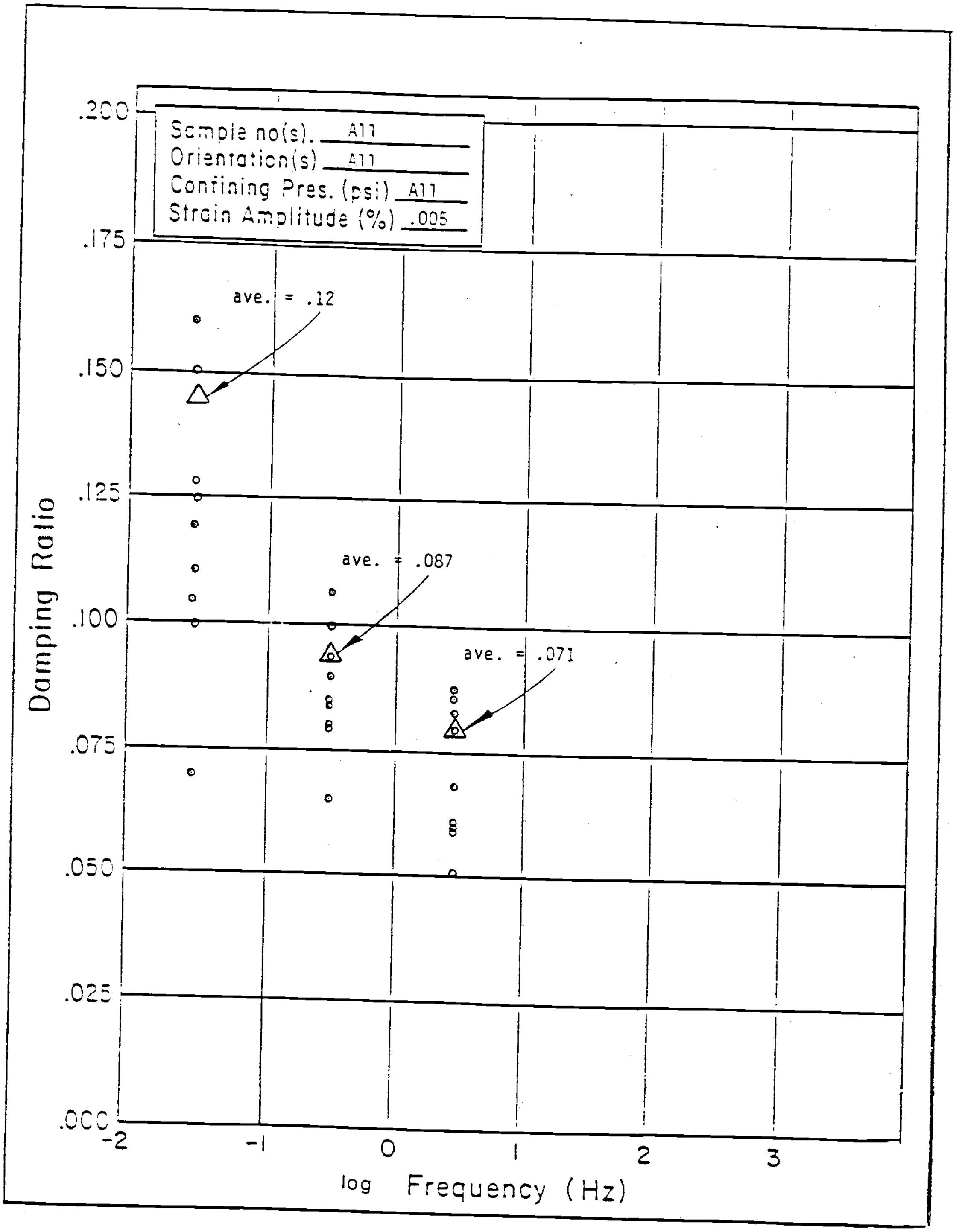

FIGURE 5-21 Cyclic Triaxial Test Results - Damping Ratio
Vs. Frequency For Strain Amplitude of 0.005%

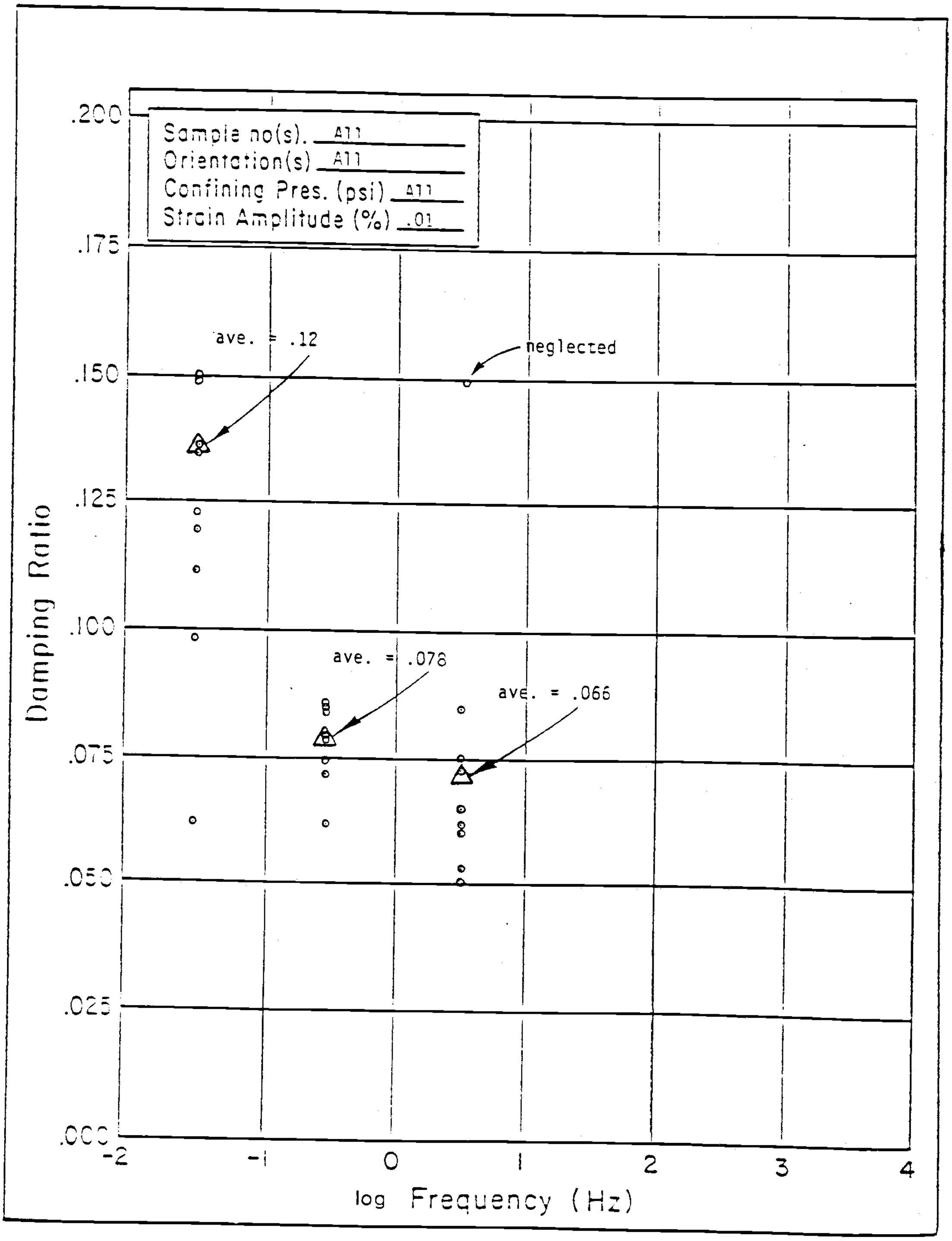

FIGURE 5-22 Cyclic Triaxial Test Results - Damping Ratio Vs. Frequency For Strain Amplitude of 0.01%

and -1°C). Due to the trends revealed for dynamic Young's modulus, both orientation and strain amplitude are shown separately on Figures 5-11 through 5-13. No trends were evident for the damping ratio, however, so all results are presented without distinguishing between different orientations and strain amplitudes.

(3) Figures 5-17 through 5-22 present all of the test results plotted as a function of $\log_{10}$ frequency (Hz) at three strain amplitudes (.0009%, .005% and .01%).

(4) Figures 5-23 through 5-28 present dynamic properties vs. axial strain ($\log_{10}$ percent) at three temperatures (-10°C, -4°C and -1°C). Mean value relationships are shown where applicable.

5.4 Summary of Test Results

The results of the resonant column test program may be summarized as follows:

Values of dynamic Young's modulus for ice ranging in density from 56.1 psf ± 0.1 (0.90gm/cc ± .002), temperatures from -1°C to -10°C, confining pressures from 0 to 70 psi (0 to 5kg/cm^2) and strain amplitudes of 10^{-6}% to 10^{-3}%, were from 1207 to 1582 ksi (8.3 to 10.9 GPa) or a 24% variation over the range of test parameters considered. The damping ratios associated with longitudinal excitation ranged from .005 to .08. Values of dynamic shear modulus for ice ranging in density, temperature, confining pressure and strain amplitude equivalent to those for dynamic Young's modulus, were from 228 to 448 ksi (1.6 to 3.1 GPa) or a 49% variation over the test parameters considered. The damping ratio associated with torsional excitation ranged

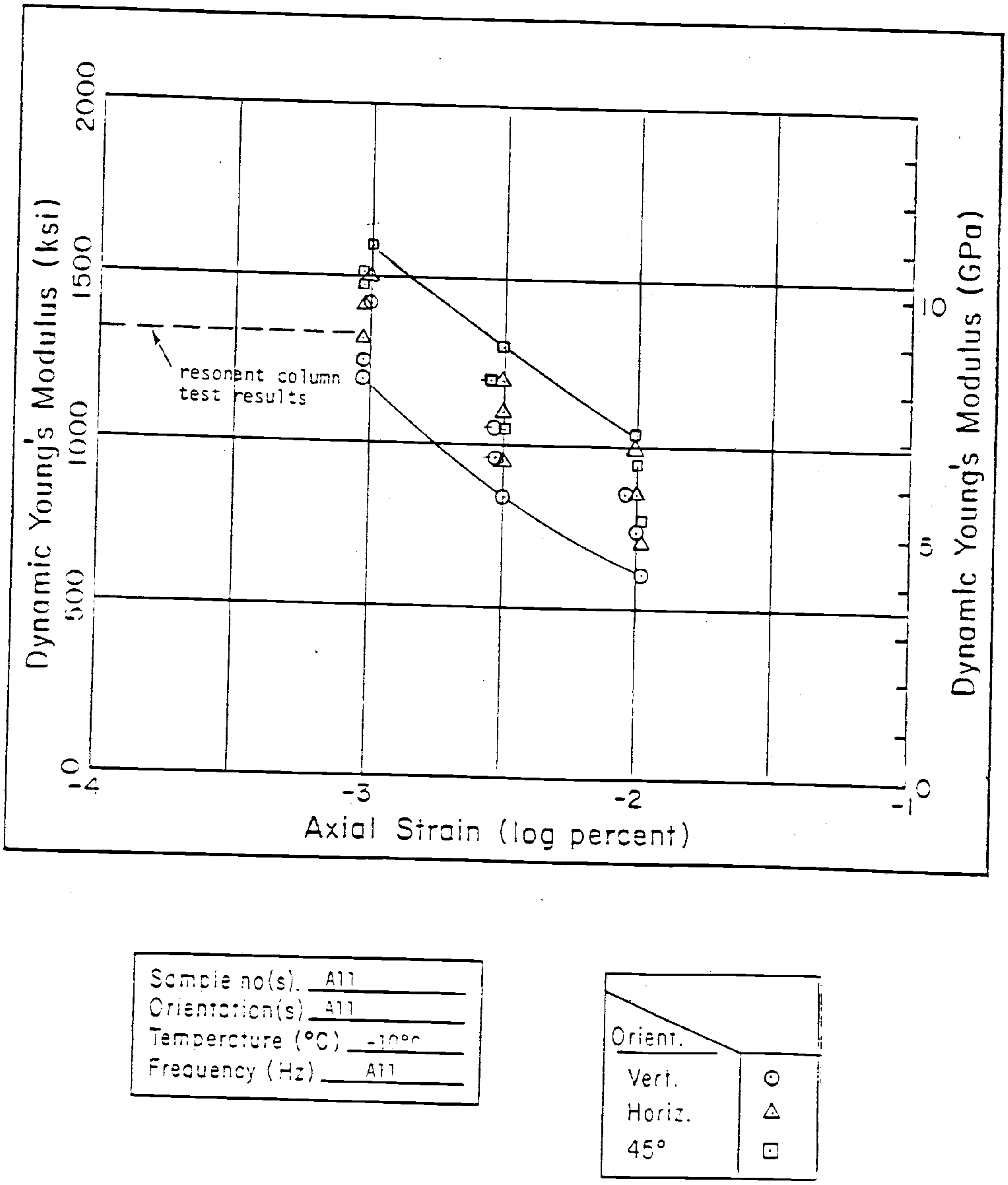

FIGURE 5-23 Cyclic Triaxial And Resonant Column Test Results - Dynamic Young's Modulus Vs. Axial Strain For Temperature Of -10°C

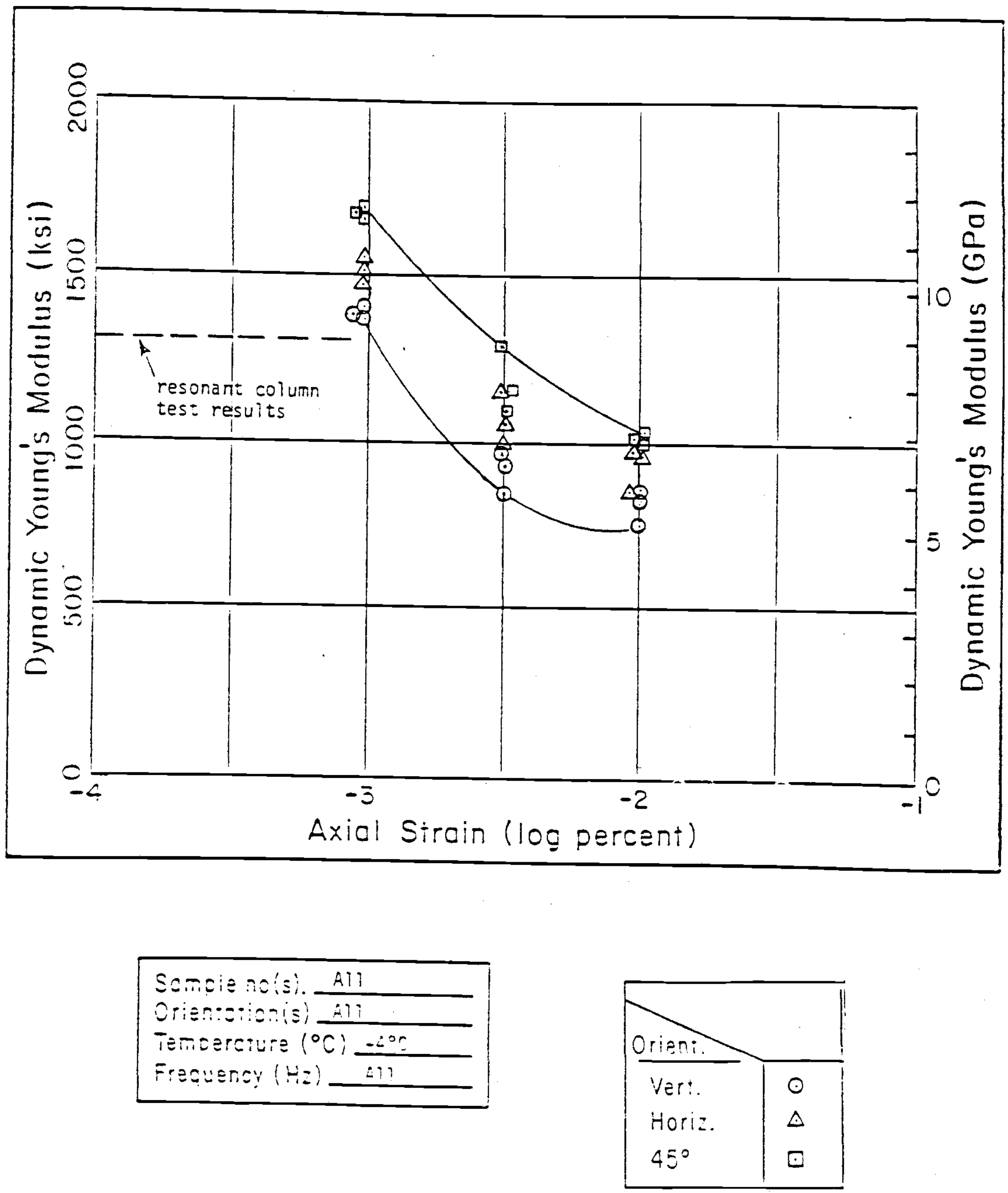

FIGURE 5-24 Cyclic Triaxial And Resonant Column Test Results - Dynamic Young's Modulus Vs. Axial Strain For Temperature Of -4°C

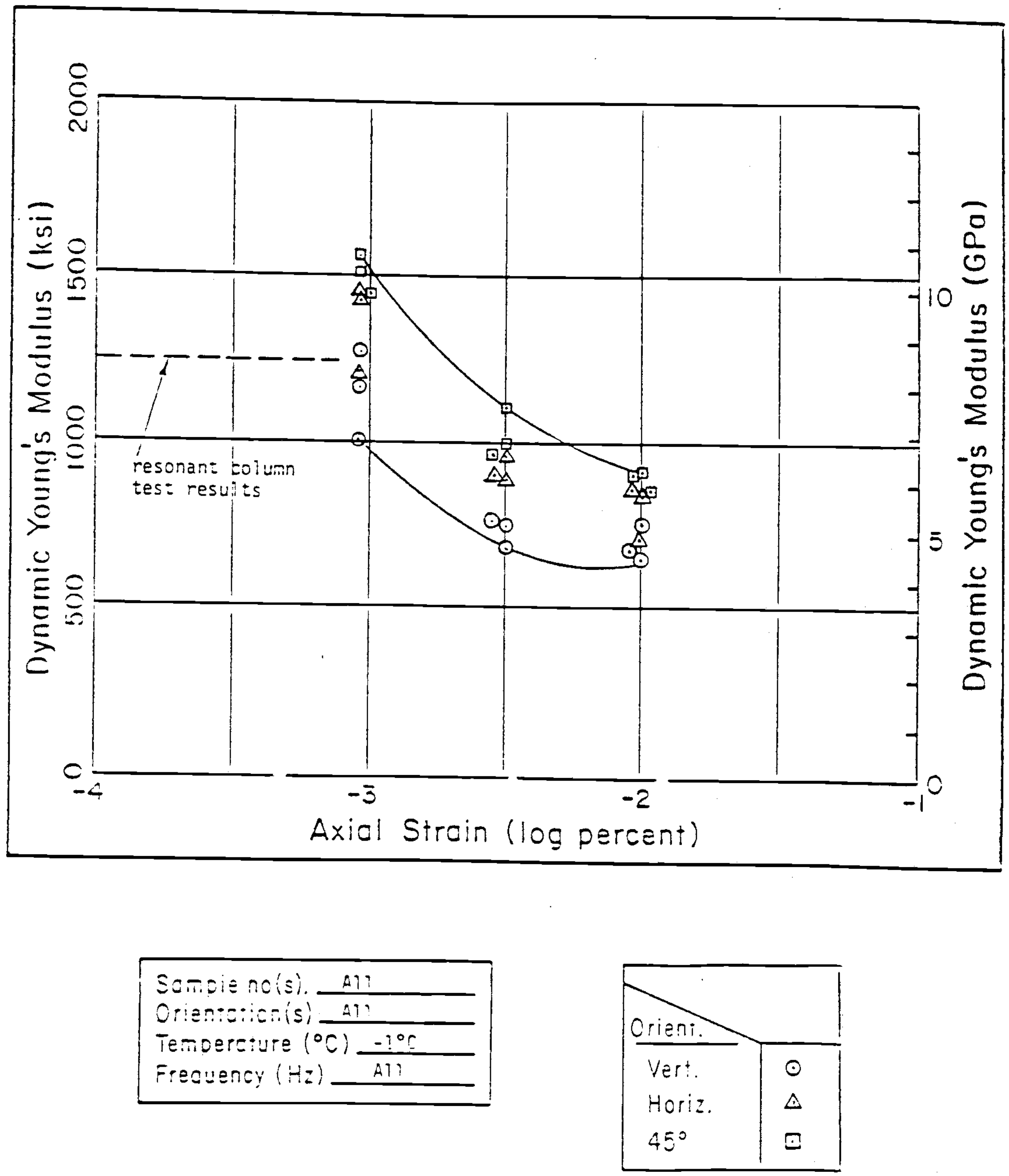

FIGURE 5-25 Cyclic Triaxial And Resonant Column Test Results - Dynamic Young's Modulus Vs. Axial Strain For Temperature Of -1°C

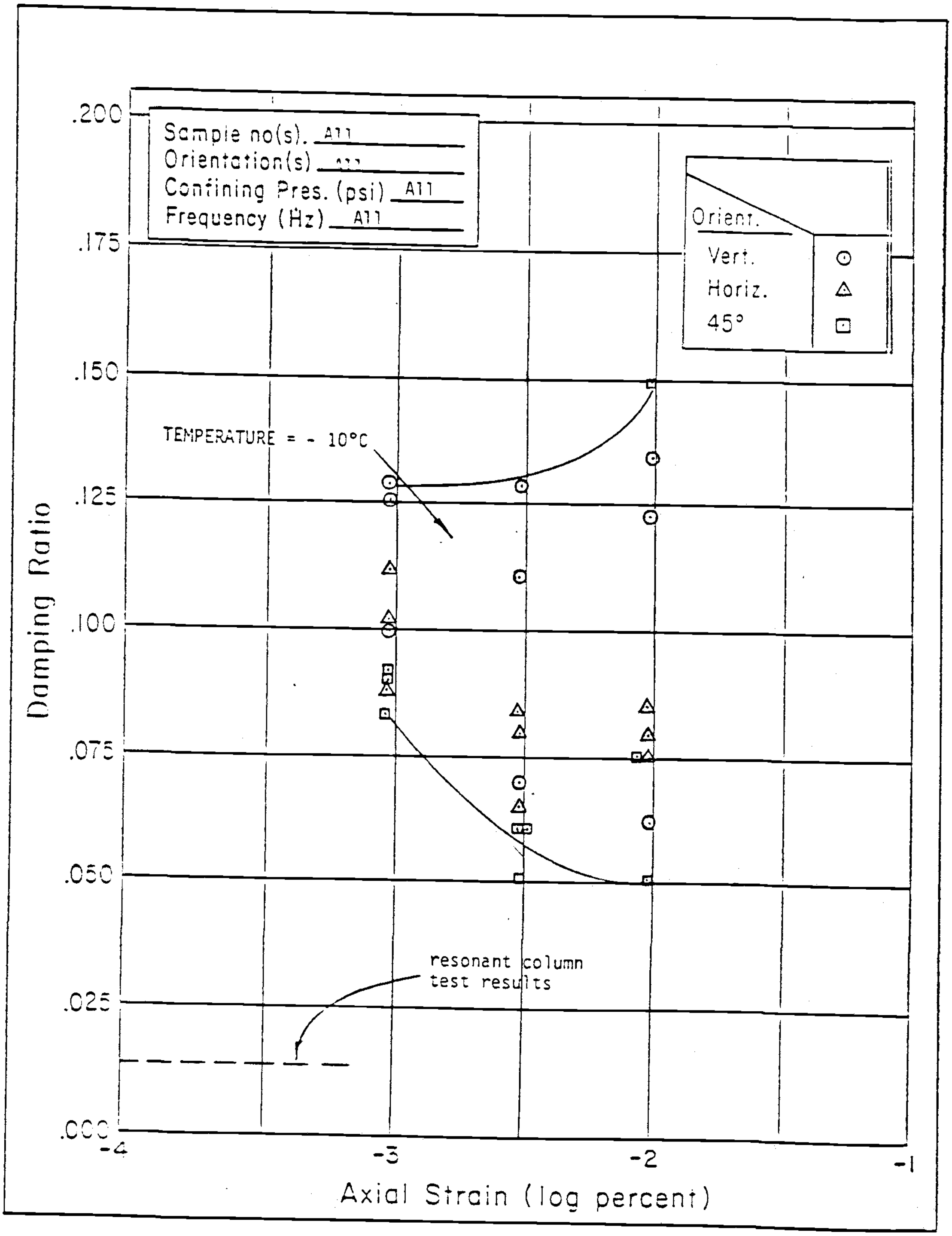

FIGURE 5-26 Cyclic Triaxial And Resonant Column Test Results - Damping Ratio Vs. Axial Strain For Temperature Of -10°C

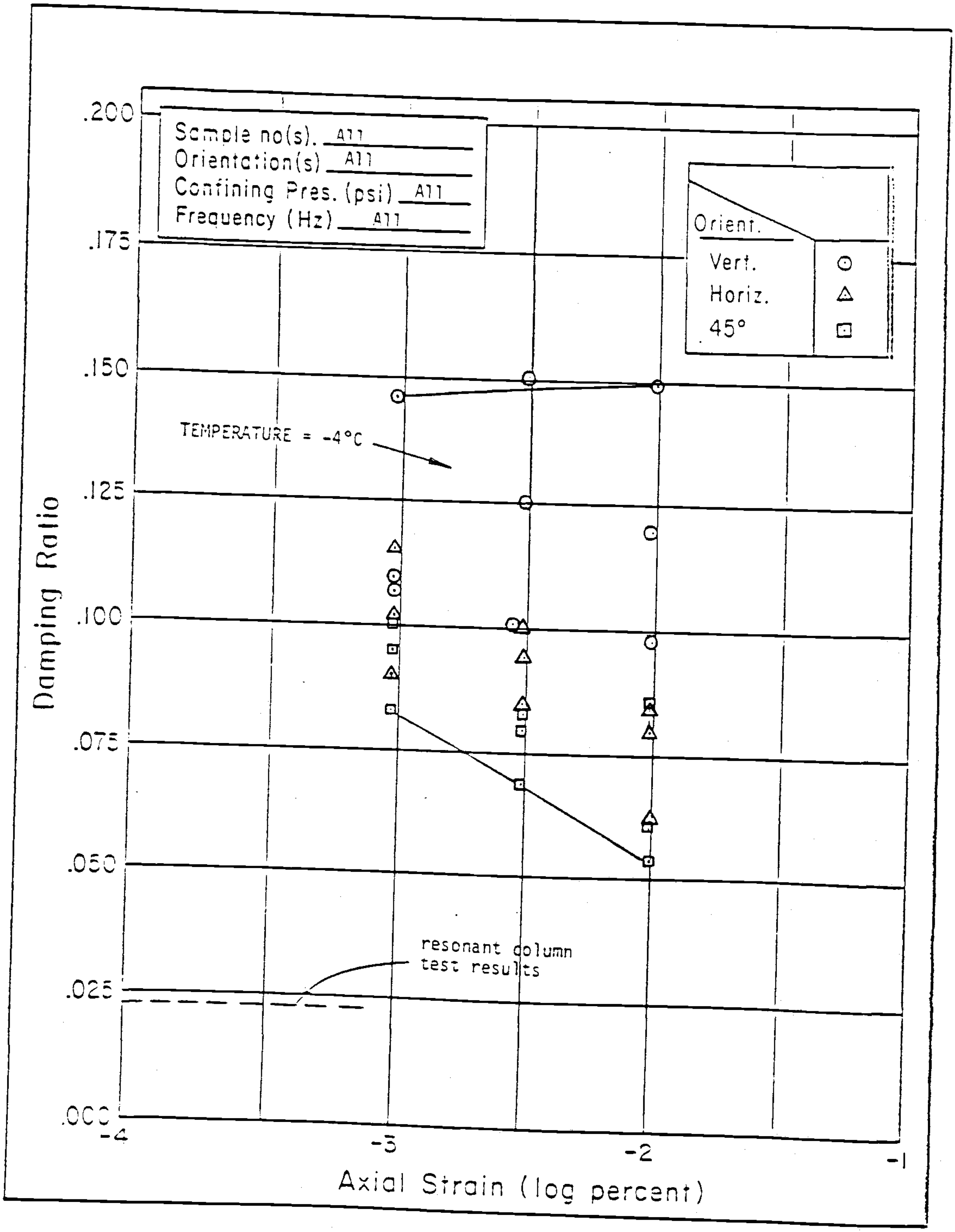

FIGURE 5-27 Cyclic Triaxial And Resonant Column Test Results - Damping Ratio Vs. Axial Strain For Temperature of -4°C

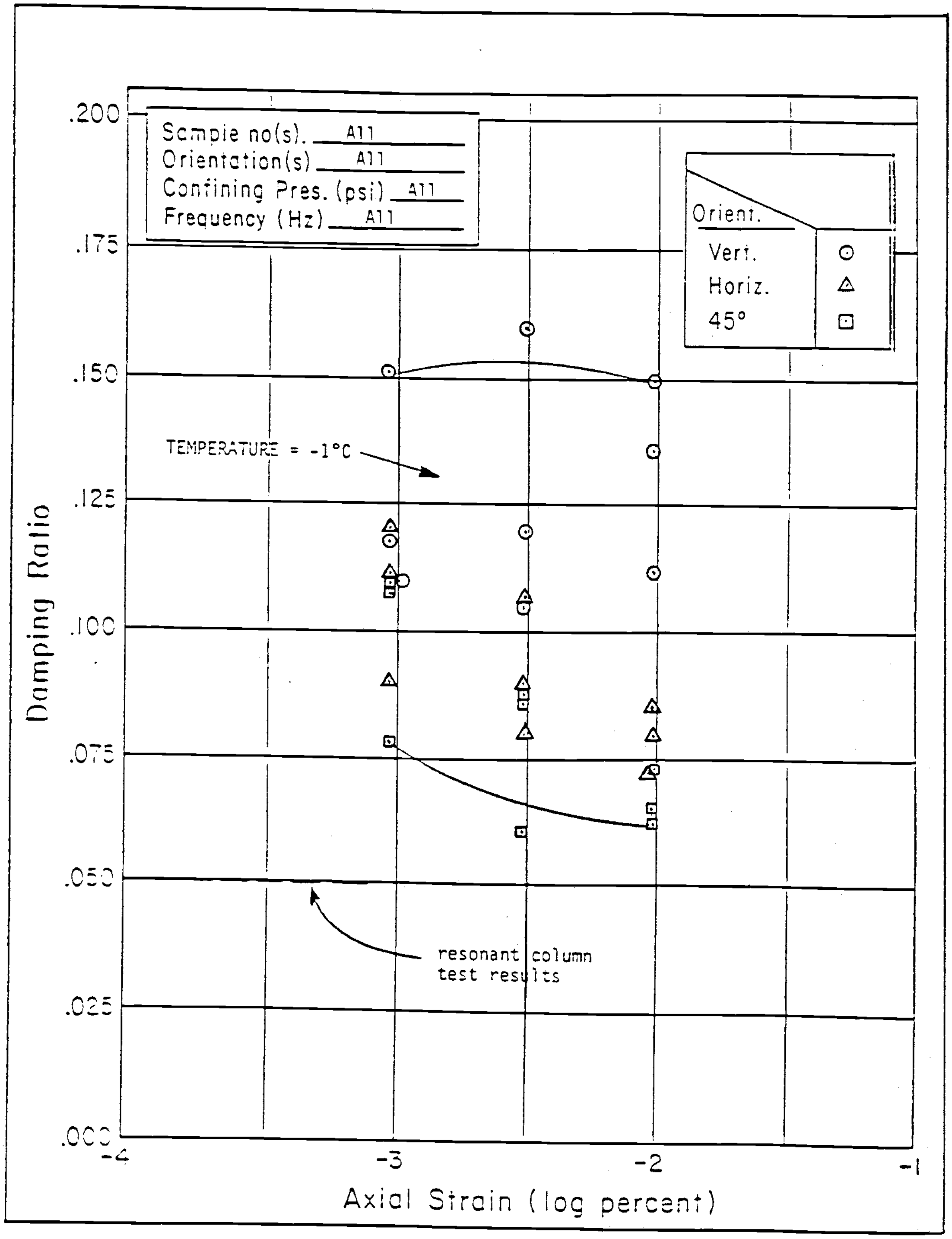

FIGURE 5-28 Cyclic Triaxial And Resonant Column Test Results - Damping Ratio Vs. Axial Strain For Temperature Of -1°C

from .004 to .13.

The cyclic triaxial test results may be summarized as follows:

(1) Dynamic Young's modulus increases with increased frequency over the range of frequencies considered (.05 Hz to 5.0 Hz). The increase is approximately 18% with a range of 13% to 33% for all temperatures and strain amplitudes considered. The greatest variations were observed at the warmest temperatures (-1°C).

(2) The damping ratio decreases with an increase in frequency over the range of frequencies considered (.05 Hz to 5.0 Hz). The decrease is approximately 27% with a range of 3% to 59% for all temperatures and strain amplitudes considered. No correlation with temperature was observed.

(3) Dynamic Young's modulus decreases with increased strain amplitude over the range of strain amplitudes considered (.0009% to .01%). The decrease is approximately 38% with a range of 31% to 58% for all temperatures and frequencies considered.

(4) The damping ratio decreases with increased strain amplitude over the range of strain amplitudes considered (.0009% to .01%). The average decrease is 10%, but the data is scattered with a range of -67% to 50%. (The negative sign indicates that the damping ratio increased by 67% rather than decreased with an increase in strain amplitude for one of the tests.)

(5) In general, the combination of higher test frequency and increased strain amplitude caused a greater variation in damping ratio. Apparently, the frequency of loading and the stain amplitude have a synergetic effect with respect to damping ratio stability.

(6) Dynamic Young's modulus decreases with increased temperature

over the range of test temperatures considered (-10°C to -1°C). Temperature has an insignificant effect between -10°C and -4°C, though, showing no effect to a slight increase in the value of dynamic Young's modulus (see Figures 5-4, 5-5 and 5-6). Between -4°C and -1°C dynamic Young's modulus decreased by approximately 13%.

(7) The damping ratio increases with an increase in temperature over the range of test temperatures measured (-10°C to -1°C). The damping ratio increases by an average of 10% (see Figures 5-8, 5-9 and 5-10).

(8) Core orientation does not appear to have a significant effect on the dynamic properties of the naturally frozen ice tested in the research program. Variations observed between vertical and horizontal core orientations were generally less than the variation observed within a given orientation.

(9) Since most samples failed during cyclic triaxial testing, few unconfined compressive strength test results were obtained. The few unconfined compressive strength test results which were obtained showed strength values to be much less than anticipated. It was felt the high strain amplitude testing performed prior to the unconfined compressive strength tests had likely reduced the strength of the specimens through microcracking, fatigue or some other mechanism (Haynes, 1973; Mellor and Cole, 1981). Therefore, no correlation with dynamic properties was made and the results are not presented herein.

5.5 Interpretation of Test Results

5.5.1 Resonant Column

Dynamic Young's moduli were not significantly affected by any test variable other than temperature when measured over the frequencies and strain amplitudes associated with resonant column testing. Referring to Figure 5-1, it can be seen that no significant difference in dynamic Young's modulus is associated with crystal or core orientation. In general, the change in dynamic Young's modulus between horizontal and vertical specimens was less than about 3%. The scatter observed for the cores oriented at 45° may be attributed to the non-homogeneous nature of the samples. Silt lenses, which were found to be continuous across these samples, undoubtedly had an influence on the dynamic properties (see Figure 5-1). Although silt lenses were present in horizontal and vertical core samples as well, they were not continuous across the samples and, therefore, had a lesser influence on the dynamic properties. Similarly, the dynamic shear moduli were not influenced significantly by any of the parameters investigated other than temperature (see Figure 5-2). Again, the scatter observed for the ice specimens associated with cores oriented at 45° is due to the non-homogeneous nature of these samples.

The damping ratios measured are shown on Figure 5-3 and 5-4. The test results show more scatter than observed for moduli, but are generally good. The maximum variation in test results was approximately 60% from the mean value with most results showing far less scatter. The largest scatter in damping ratio was observed for tests conducted at the warmest temperature (approximately -1°C).

The value of the damping ratio associated with the longitudinal mode of vibration was approximately 60% greater than the damping ratio value associated with the torsional mode of vibration.

From the resonant column data collected during the test program, preliminary design curves were developed to obtain dynamic properties from simple index properties of naturally frozen ice. Appendix C presents design curves for obtaining dynamic properties under resonant column loading conditions.

5.5.2 Cyclic Triaxial

The cyclic triaxial test results, as summarized in Tables 5-2, 5-3 and 5-4 showed much greater variation in dynamic properties for the parameters investigated. In general, dynamic Young's modulus (E_d) decreased as the test temperature increased when all other test parameters remained constant. An exception was noted for the smallest strain amplitude (.0009%) tests, where an increase was observed in E_d between -10 and -4°. This anomaly is attributed to the fact that the test equipment was being utilized at the lower end of its strain amplitude capabilities. At -4°C it is believed some component of the test system other than the sample may have contributed to the modulus measured. Possibly a portion of the antitilt device was rubbing against the frame (resisting movement) during the test sequence. A similar phenomenon was noted for the damping ratio (D).

In general, as the frequency of loading increased, E_d increased and D decreased. As the strain amplitude increased the value of E_d

and D decreased. Exceptions were noted which were felt to be variances associated with experimental error.

From the test results it is evident that strain amplitude has the most significant affect on dynamic Young's modulus for the range of strain amplitudes considered in the test program (.0009% to .01%), but frequency of loading and temperature also have a significant affect on dynamic Young's modulus.

The damping ratio was found to be most significantly influenced by the frequency of loading, but was also influenced by the temperature and strain amplitude (see Figures 5-5 through 5-28).

Design curves were developed from the cyclic triaxial data collected for predicting dynamic properties of naturally frozen ice, based on simple physical properties (see Appendix C).

The resonant column and cyclic triaxial test results shown in Figures 5-11 through 5-15 show lower measured moduli for resonant column testing than under low frequency, high strain amplitude cyclic triaxial testing. It is believed this apparent discrepancy can be attributed to creep time effects occurring for the cyclic triaxial test system.

N.K. Sinha (1978) proposed a model to explain creep effects on measured moduli in terms of stress, temperature, grain size, and time of measurement after loading. The modulus decreases rapidly with time due to creep under certain combinations of grain size, temperature and stress level (a 25% decrease and measured modulus may occur in as little as .01 seconds after load application). Although not specifically considered during this research program, it believed the moduli measured may have been influenced by time of measurement under certain combinations of stress, loading frequency and temperature.

6. CONCLUSIONS AND RECOMMENDATIONS

6.1 Conclusions

Chapter 5 provided a summary of test results for the eight naturally occurring wedge ice samples tested. The results were presented for each test system employed (cyclic triaxial and resonant column) and trends and similarities were described. When all the data collected (cyclic triaxial and resonant column) for the samples tested is compared collectively, certain conclusions can be drawn, which are as follows:

(1) Dynamic moduli increased with increased frequency of loading and strain amplitude, but showed a decrease with ascending temperature. Frequency of loading and strain amplitude had a greater influence on moduli than temperature, over the range of test parameters considered. The trends were more pronounced for the cyclic triaxial test results than for the resonant column test results.

(2) In general, the damping ratio decreased with increased frequency of loading and strain amplitude but showed an increase with increased temperature. The trends were more pronounced for the cyclic triaxial test results than for the resonant column test results.

(3) Little variation was observed in dynamic properties as a function of sample core orientations. Therefore, for the naturally occurring ice tested, the dynamic properties were not significantly influenced by the direction in which they were measured. It should be noted variations were observed for the samples cored at an orientation of 45°, but those variations were attributed to the non-homogeneous

nature of the samples rather than their anisotropy.

(4) The location, quantity and characteristics of silt lenses can significantly affect the dynamic properties of naturally occurring ice. It is assumed other impurities would also affect the dynamic properties.

(5) Greater variation was observed in damping ratio than in moduli for the test variables considered.

(6) No conclusions can be made regarding the relationship between unconfined compressive strength and dynamic properties. This is due to the large number of samples which failed during testing before the test history was complete.

(7) From the data collected during this test program, design curves were developed for obtaining dynamic properties from simple index properties of naturally frozen ice. Since only a limited number of samples were tested from only one site, these design curves should be considered very preliminary. The design curves are presented in Appendix C.

6.2 Recommendations

In the interest of continuing the present research program as well as refining the knowledge gained by this study, the following recommendations should be considered:

(1) A similar test program should be conducted on naturally occurring ice obtained from different sites and geologic conditions. All ice samples tested in this test program came from the same approximate location, as previously noted.

(2) For the purpose of eventually defining a relatively simple laboratory test to determine dynamic properties of ice, alternative test equipment should be developed which correlates with dynamic properties obtained from the cyclic triaxial test system. Also, if the need for sample grips could be eliminated through correlative studies using compressive cyclic loading, the task of determining dynamic properties would be made easier.

(3) As noted previously, the study of creep effects were not considered in this research program. However, it is believed the inconsistencies noted between cyclic triaxial and resonant column test results (see Figures 5-11 through 5-13) may be attributed to the fact that time related creep caused a reduction in the measured dynamic properties for the cyclic triaxial test system. It is recommended that future studies be directed towards quantifying creep effects in terms of Sinha's (1978) proposed creep laws.

BIBLIOGRAPHY

1. Baker, T.H.W., "Transportation, Preparation, and Sample Storage of Frozen Soil Samples for Laboratory Testing", Paper presented at the ASTM Symposium on the Preparation of Specimens for Laboratory Testing - The Effects on Test Results, held the 22nd to 27th of June, 1975, National Research Council of Canada, Division of Building Research, Ottawa, Canada, May, 1975.

2. Bolander, L.W., "Test Equipment and Procedures to Evaluate Dynamic Properties of Naturally Frozen Soil", M.S. Project Report Oregon State University, Corvallis, Oregon, 1980.

3. Chung, Y.C., and Tyler, R.L., "Evaluation of Free-Free and Free-Fixed Resonant Column Testing Devices", Report No. R-S-79-1, Tennessee Valley Authority, Singleton Materials Engineering Laboratory, Knoxville, Tennessee, 1979.

4. Glen, J.W., "The Physics of Ice", Monograph 11-C2b, U.S. Army CRREL, Hanover, New Hampshire, 1974.

5. Glen, J.W., "The Mechanics of Ice", Monograph 11-C2b, U.S. Army CRREL, Hanover, New Hampshire, 1974.

6. Haynes, F.D., "Tensile Strength of Ice Under Triaxial Stresses", Research Report 312, U.S. Army CRREL, Hanover, New Hampshire, 1973.

7. Idriss, I.M., and Seed, H.B., "Seismic Response of Horizontal Soil Layers", Journal of the Soil Mechanics and Foundation Division, ASCE, Vol. 94, No. SM4, 1968.

8. Kaplar, C.W., "Laboratory Determination of Dynamic Moduli of Frozen Soils and of Ice", Research Report 163, U.S. Army CRREL, Hanover, New Hampshire, 1981.

9. Langway, C.C. Jr., "Ice Fabrics and The Universal Stage", Technical Report 62, U.S. Army CRREL, Hanover, New Hampshire, 1958.

10. Law, K.T., "Design of a Loading Platen for Testing Ice and Frozen Soil", Canadian Geotechnical Journal, Vol, 14, No. 2, May 1977.

11. Lysmer, J., Takekazu, U., Seed, H.G. and Hwant, R., "LUSH - A Computer Program for Complex Response Analysis of Soil-Structure Systems", Report No. EERC 74-4, Earthquake Engineering Research Center, University of California, Berkeley, California, 1974.

12. Mellor, M., and Cole, D., "Cyclic Loading and Fatigue in Ice", Cold Regions Science and Technology, (1981) 41-53, Elsevier Scientific Publishing Co., 1981.

13. O'Brian, J.J., and O'Brian, M.W., "How to Run a Lathe", South Bend Lathe Works, South Bend, Indiana, 1942.

14. Petrie, G., "How to Find the Dynamic Properties of Frozen Soils", unpublished notes, 1980.

15. Pihlainen, J.A., and Johnston, G.H., "Guide to a Field Description of Permafrost for Engineering Purposes", Technical Memorandum 79, National Research Council of Canada, Ottawa, Canada, 1963.

16. Seed, H.B., Lysmer, J., and Hwang, R., "Soil-Structure Interaction Analysis for Evaluating Seismic Response", National Science Foundation, Report No. EERC 74-6, Earthquake Engineering Research Center, University of California, Berkeley, California, 1974.

17. Sinha, N.K., "Rheology of Columnar-Grained Ice", National Research Council of Canada, DBR Paper No. 838, Division of Building Research.

18. Sinha, N.K., Short-Term Rheology of Polycrystalline Ice", National Council of Canada, DBR Paper No. 789, Division of Building Research.

19. Stevens, H.W., "Measurement of the Complex Moduli and Damping of Soils Under Dynamic Loads", Technical Report 173, U.S. Army CRREL, Hanover, New Hampshire, 1966.

20. Stevens. H.W., "Operator's Manual-Vibratory Dynamic Test for Frozen Soils", Internal Report 384, U.S. Army CRREL, Hanover, New Hampshire, 1974.

21. Stevens, H.W., "The Response of Frozen Soils to Vibratory Loads", Technical Report 265, U.S. Army CRREL, Hanover, New Hampshire., 1975.

22. Streeter, V.L., Wylie, E.B., and Richart Jr., F.E., "Soil Motion Computations by Characteristics Method", Journal of the Geotechnical Engineering Division, ASCE, Vol. 100, No. ET-3, Proceedings Paper 10410, 1974, pp. 247-263.

23. Vinson, T.S., and Chaichanavong, T., "Dynamic Properties of Ice and Frozen Clay Under Cyclic Triaxial Loading Conditions", Report No. MSU-CE-76-4, Vol. 1, Division of Engineering Research, Michigan State University, East Lansing, Michigan, 1976.

34. Vinson, T.S., "Dynamic Properties of Frozen Soils Under Simulated Earthquake Conditions", Proceedings of the 3rd International Conference on Permafrost, 1978.

35. Vinson, T.S., "Response of Frozen Ground to Dynamic Loading", Chapter 9, Geotechnical Engineering for Cold Regions, McGraw-Hill Inc., 1978.

36. Woods, R.D., "Measurement of Dynamic Soil Properties", from Proceedings of the American Society of Civil Engineers GED Specialty Conference on Earthquake Engineering and Soil Dynamics, Pasadena, California, 1978.

37. Wilson, C.W., "Dynamic Properties of Naturally Frozen Fairbanks Silt", M.S. Thesis, Oregon State University, Corvallis, Oregon, 1982.

APPENDICES

APPENDIX A

DYNAMIC PROPERTY LABORATORY TEST DATA

Test temperature had the greatest measured influence on dynamic properties, especially at the warmer test temperatures (e.g., when samples were near the melting point). Both time and equipment limitations created a situation where exact temperature control was impractical if not impossible to attain. Therefore, in order to normalize the test data for interpretation purposes, all test data was plotted initially as a function of temperature. In this way test results could be interpolated at three constant temperatures, which were -10°C, -4°C and -1°C. Appendix A presents all test data plotted as a function of temperature

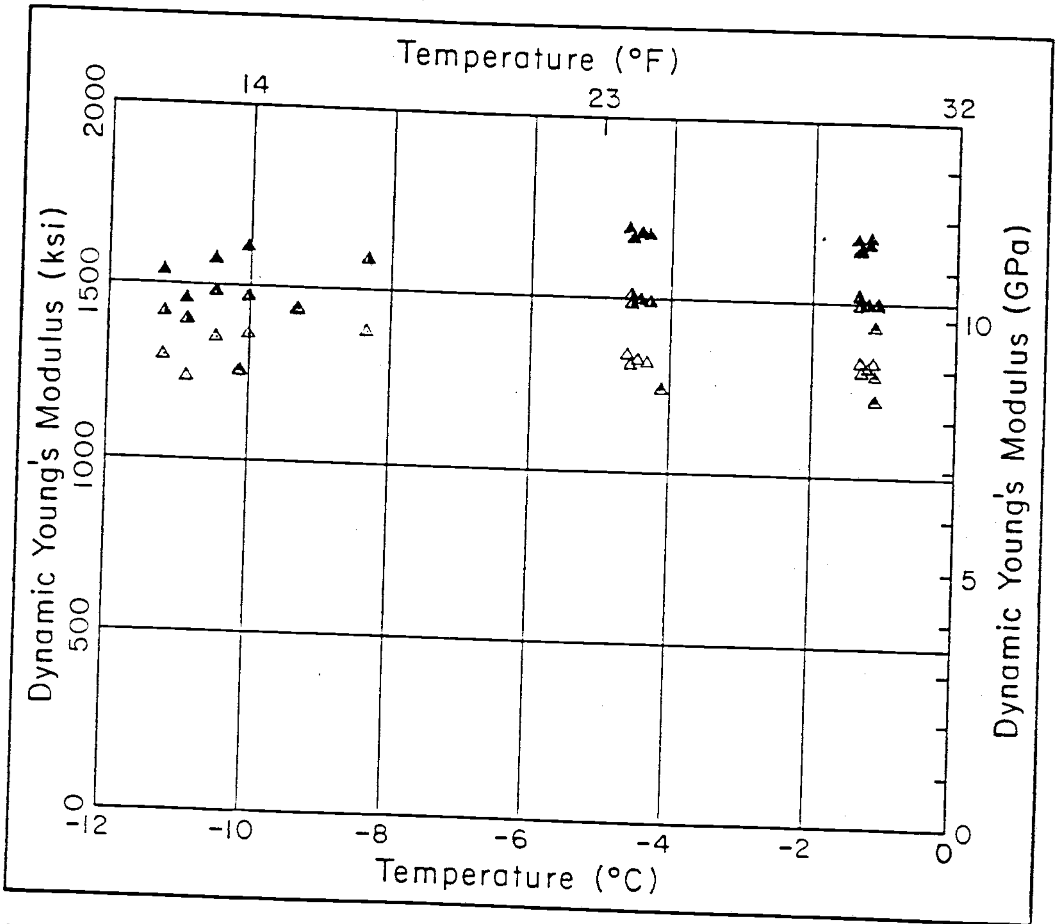

FIGURE A-1 Dynamic Young's Modulus vs. Temperature

Sample no(s). 72
Orientation(s) Horizontal
Confining Pres. (psi) All
Strain Amplitude (%) .0009

Orient. \ Freq. (Hz)	.05	0.5	5.0
Vert.	○	◐	●
Horiz.	△	◭	▲
45°	□	◧	■

▲ Resonant column test results

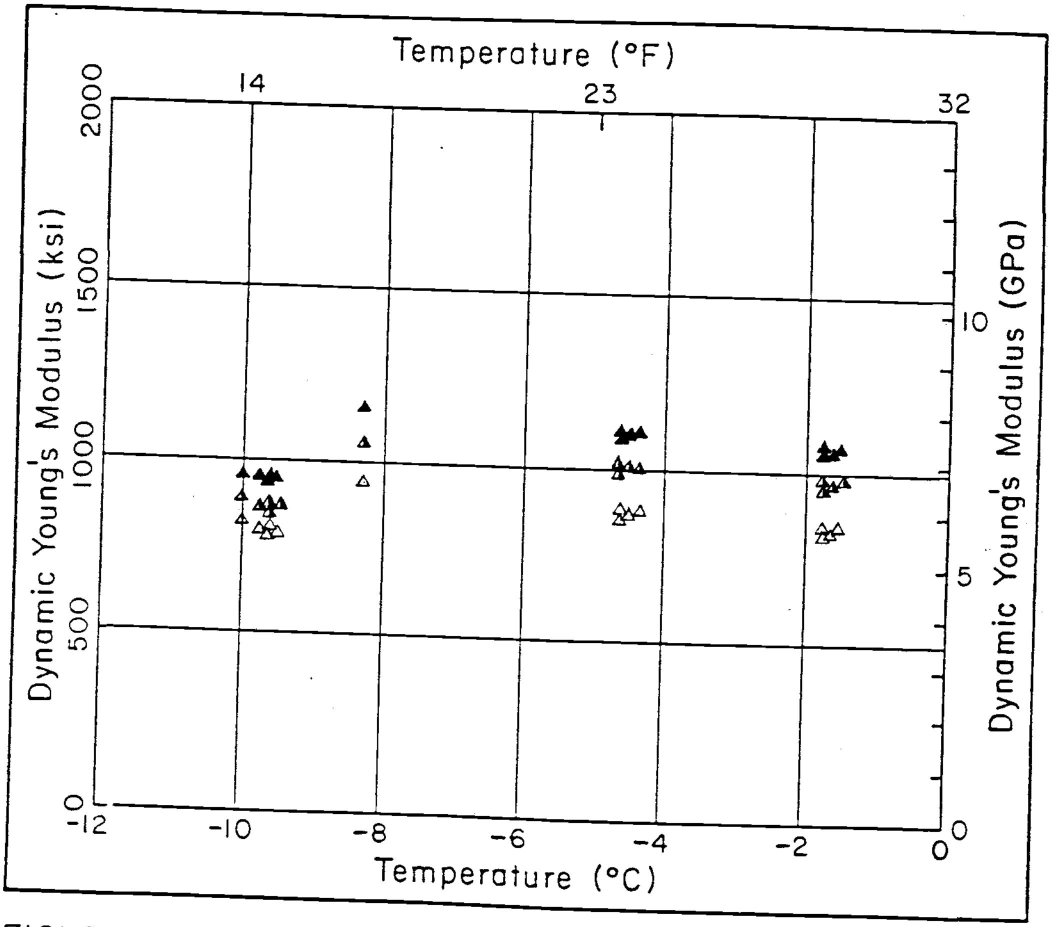

FIGURE A-2 Dynamic Young's Modulus vs. Temperature

Sample no(s). 72
Orientation(s) Horizontal
Confining Pres. (psi) All
Strain Amplitude (%) .005

Freq. (Hz) / Orient.	.05	0.5	5.0
Vert.	○	◑	●
Horiz.	△	◭	▲
45°	□	◨	■

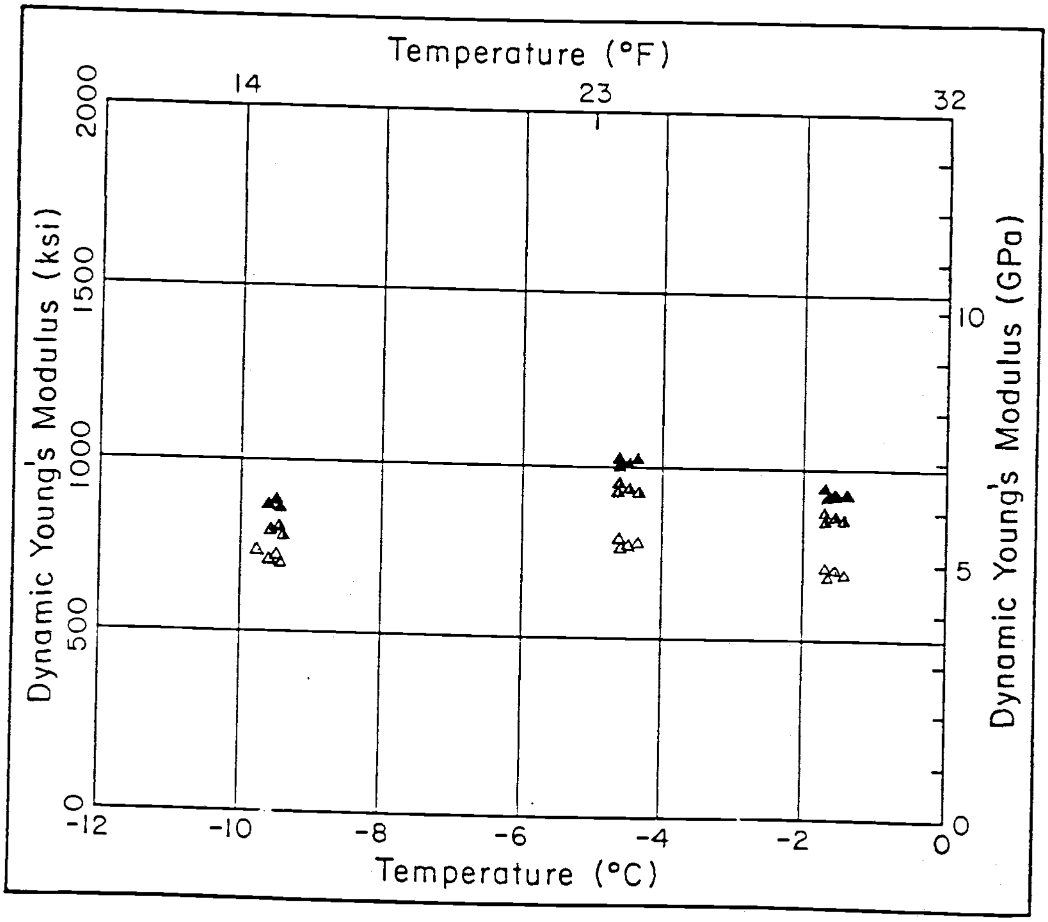

FIGURE A-3 Dynamic Young's Modulus vs. Temperature

Sample no(s). 72
Orientation(s) Horizontal
Confining Pres. (psi) All
Strain Amplitude (%) .01

Orient. \ Freq. (Hz)	.05	0.5	5.0
Vert.	○	◑	●
Horiz.	△	◭	▲
45°	□	◨	■

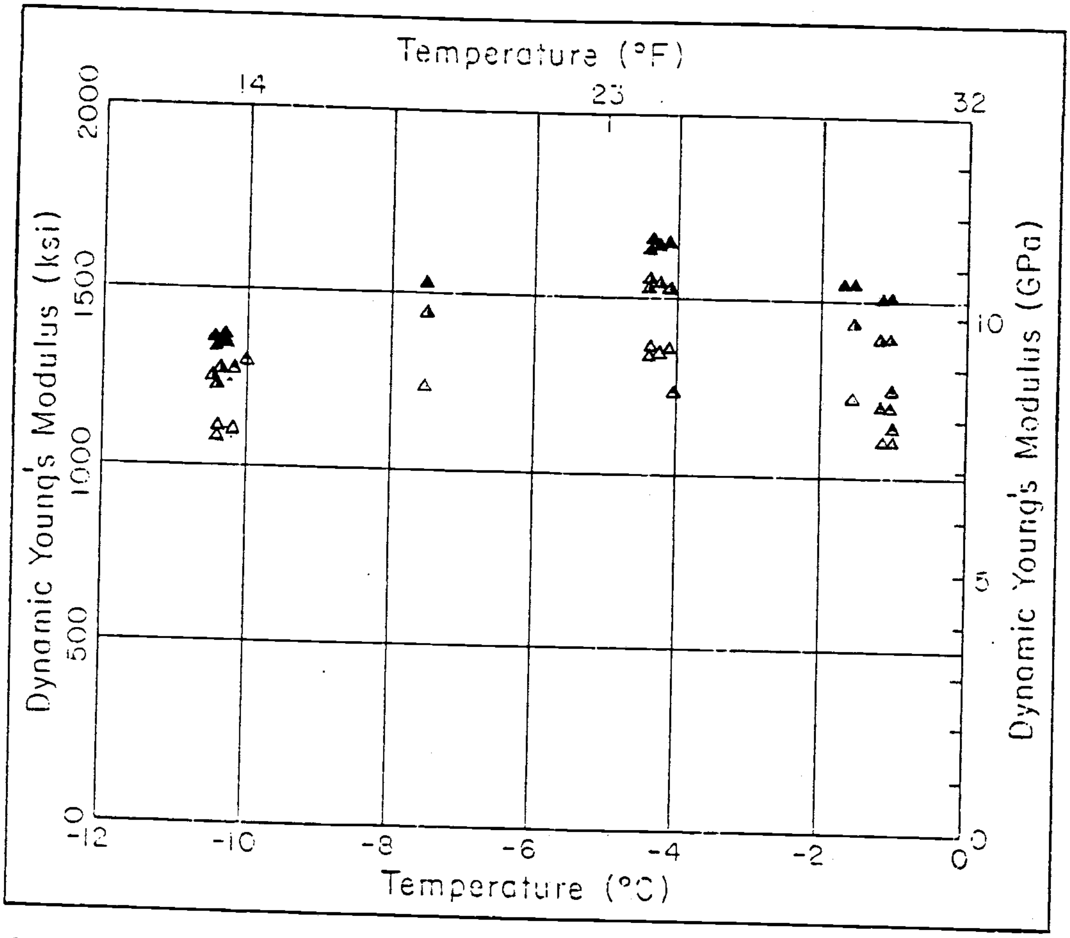

FIGURE A-4 Dynamic Young's Modulus vs. Temperature

Sample no(s). 73
Orientation(s) Horizontal
Confining Pres. (psi) All
Strain Amplitude (%) .0009

Freq. (Hz) / Orient.	.05	0.5	5.0
Vert.	○	◐	●
Horiz.	△	◭	▲
45°	□	◧	■

▲ Resonant column test results

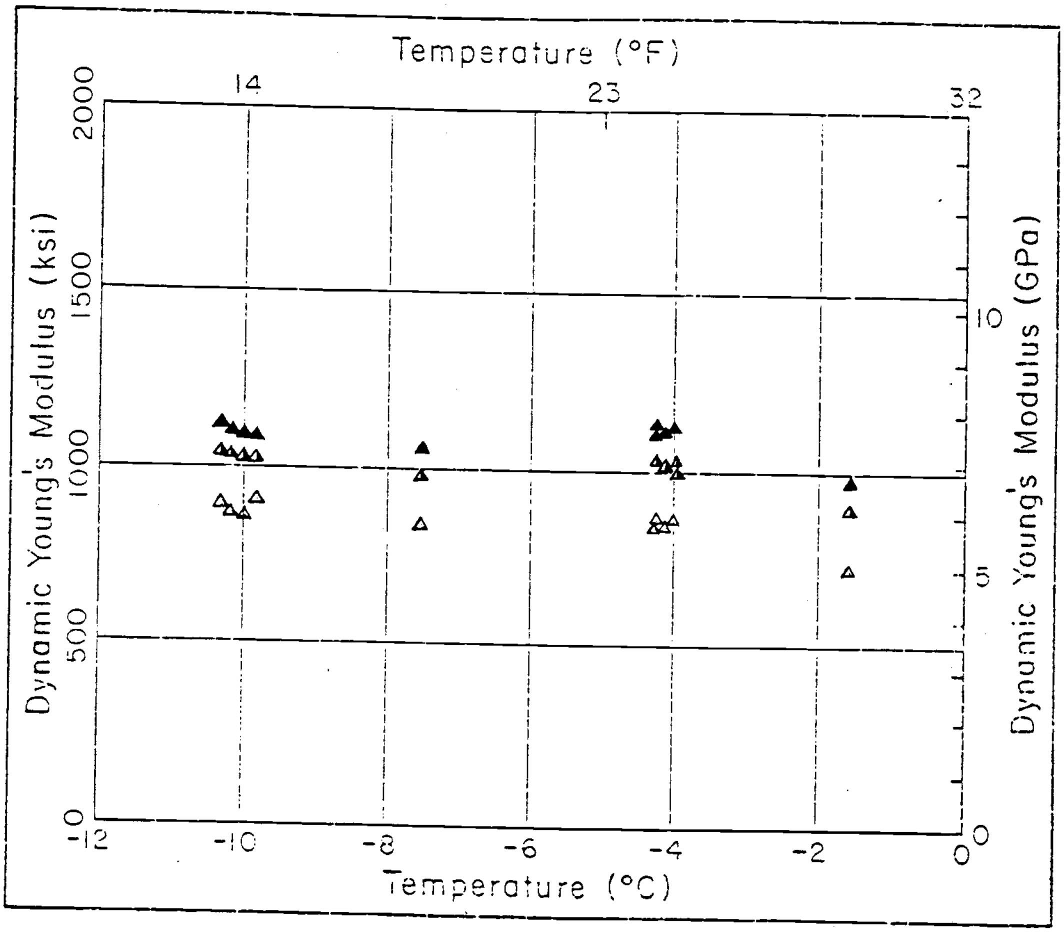

FIGURE A-5 Dynamic Young's Modulus vs. Temperature

Sample no(s). 73
Orientation(s) Horizontal
Confining Pres. (psi) All
Strain Amplitude (%) .005

Freq. (Hz) / Orient.	.05	0.5	5.0
Vert.	○	◑	●
Horiz.	△	◭	▲
45°	□	◧	■

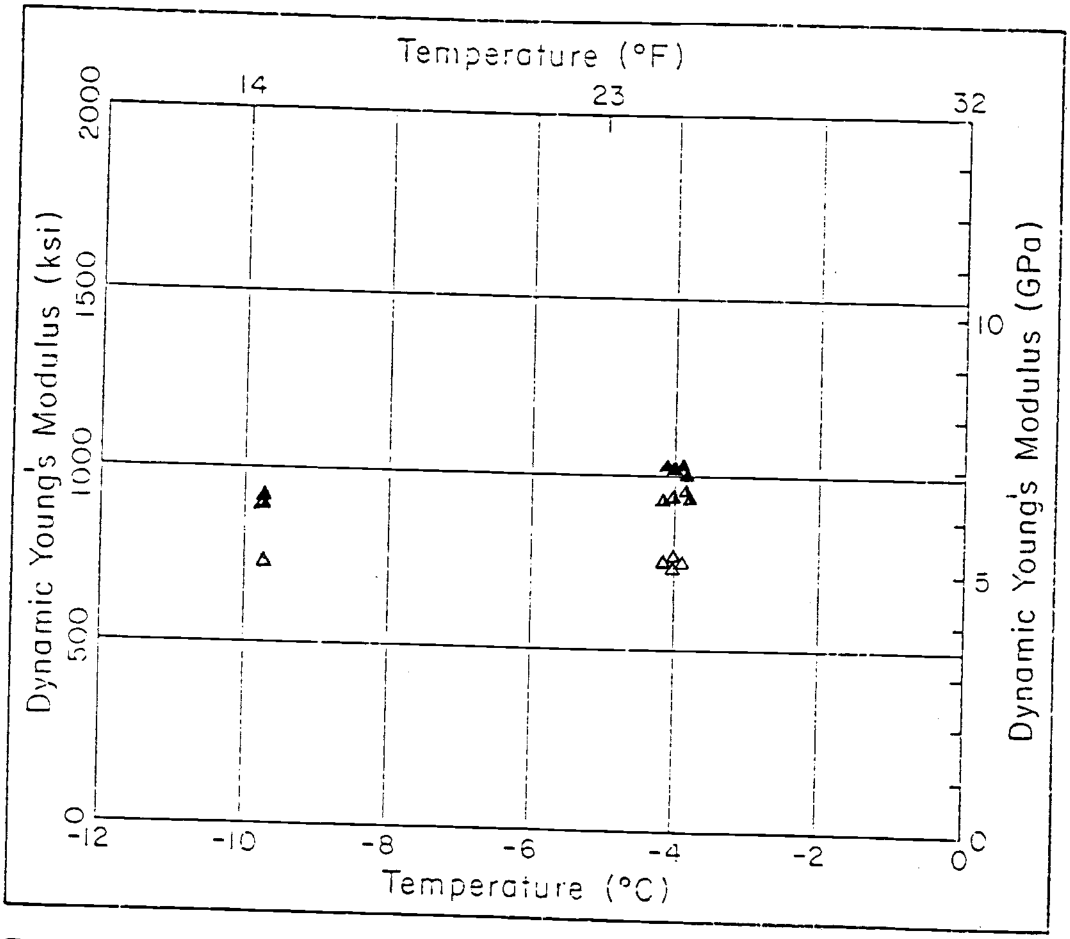

FIGURE A-6 Dynamic Young's Modulus vs. Temperature

Sample no(s).	73
Orientation(s)	Horizontal
Confining Pres. (psi)	All
Strain Amplitude (%)	.01

Freq. (Hz) / Orient.	.05	0.5	5.0
Vert.	○	◑	●
Horiz.	△	◭	▲
45°	□	◨	■

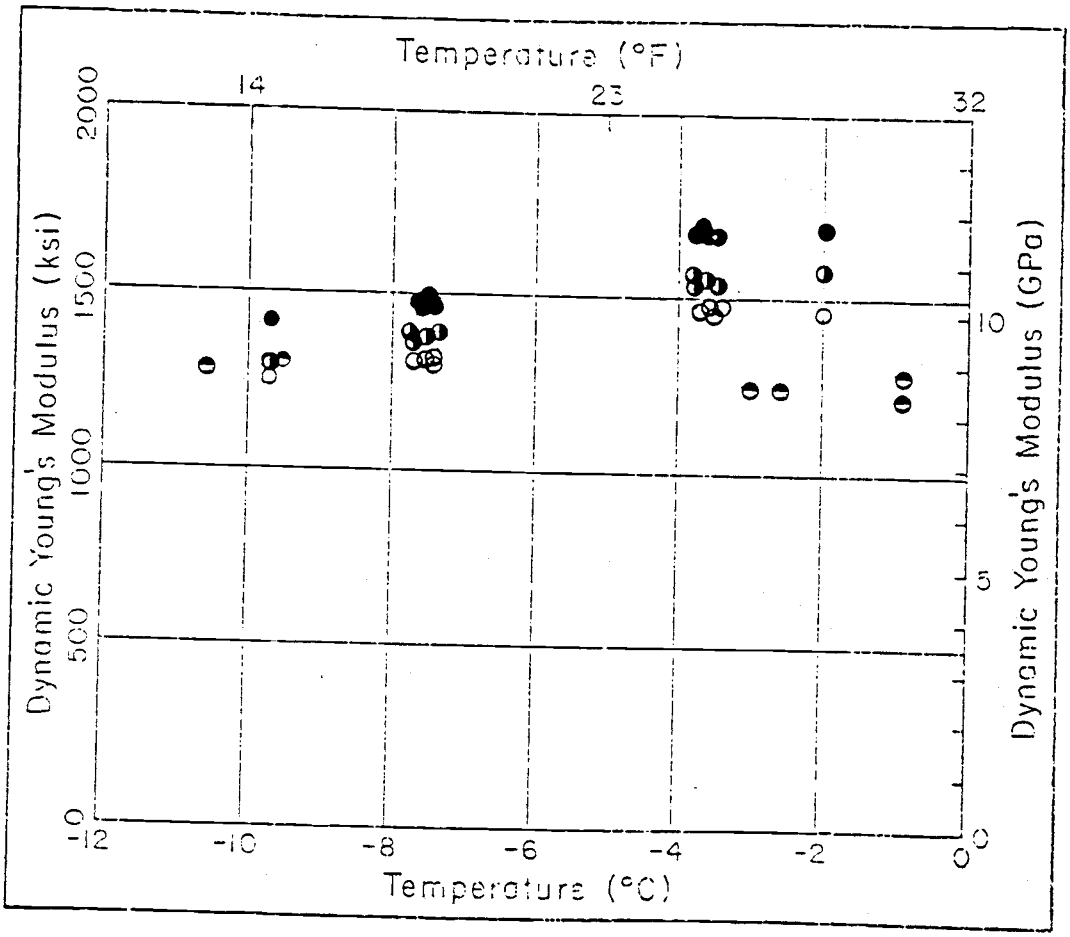

FIGURE A-7 Dynamic Young's Modulus vs. Temperature

Sample no(s).	78
Orientation(s)	Vertical
Confining Pres. (psi)	All
Strain Amplitude (%)	.0009

Freq. (Hz) / Orient.	.05	0.5	5.0
Vert.	○	◑	●
Horiz.	△	◭	▲
45°	□	◨	■

⊖ Resonant column test results

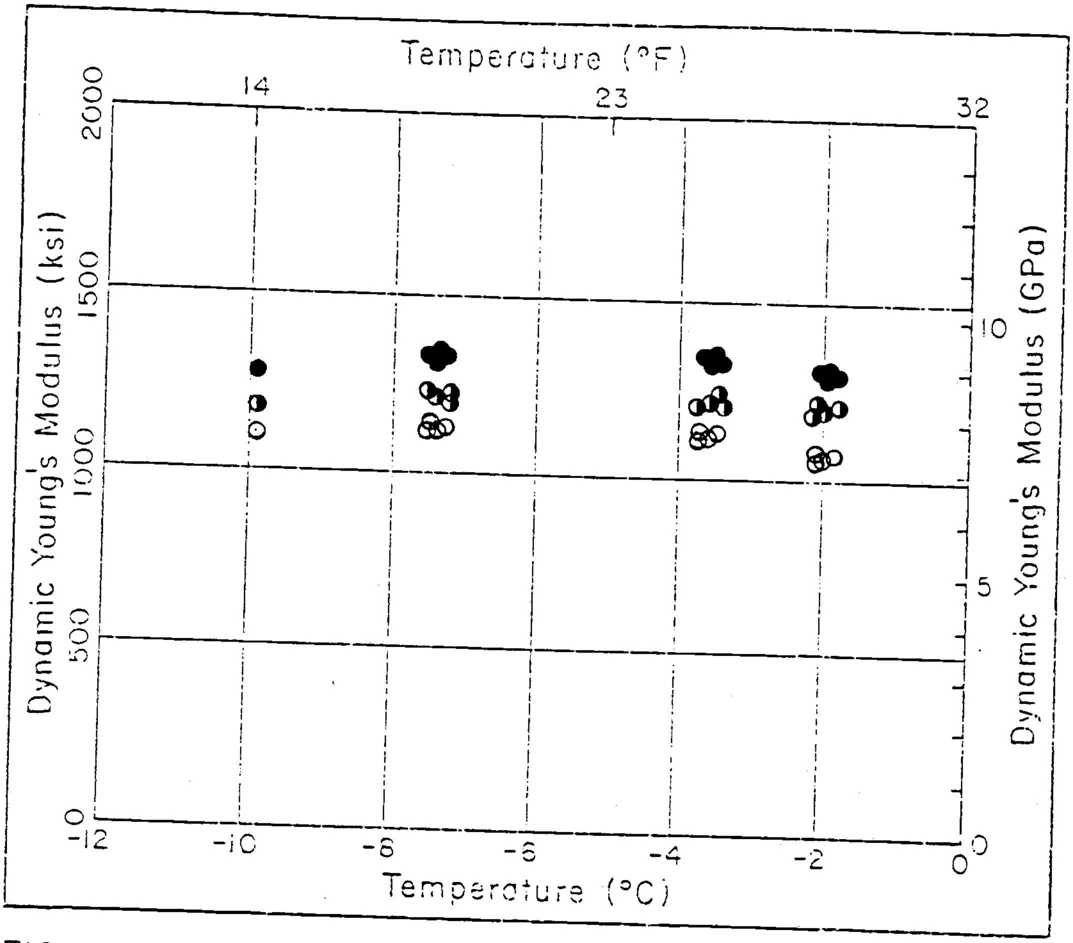

FIGURE A-8 Dynamic Young's Modulus vs. Temperature

Sample no(s). 78
Orientation(s) Vertical
Confining Pres. (psi) All
Strain Amplitude (%) .005

Freq. (Hz) / Orient.	.05	0.5	5.0
Vert.	○	◑	●
Horiz.	△	◭	▲
45°	□	◧	■

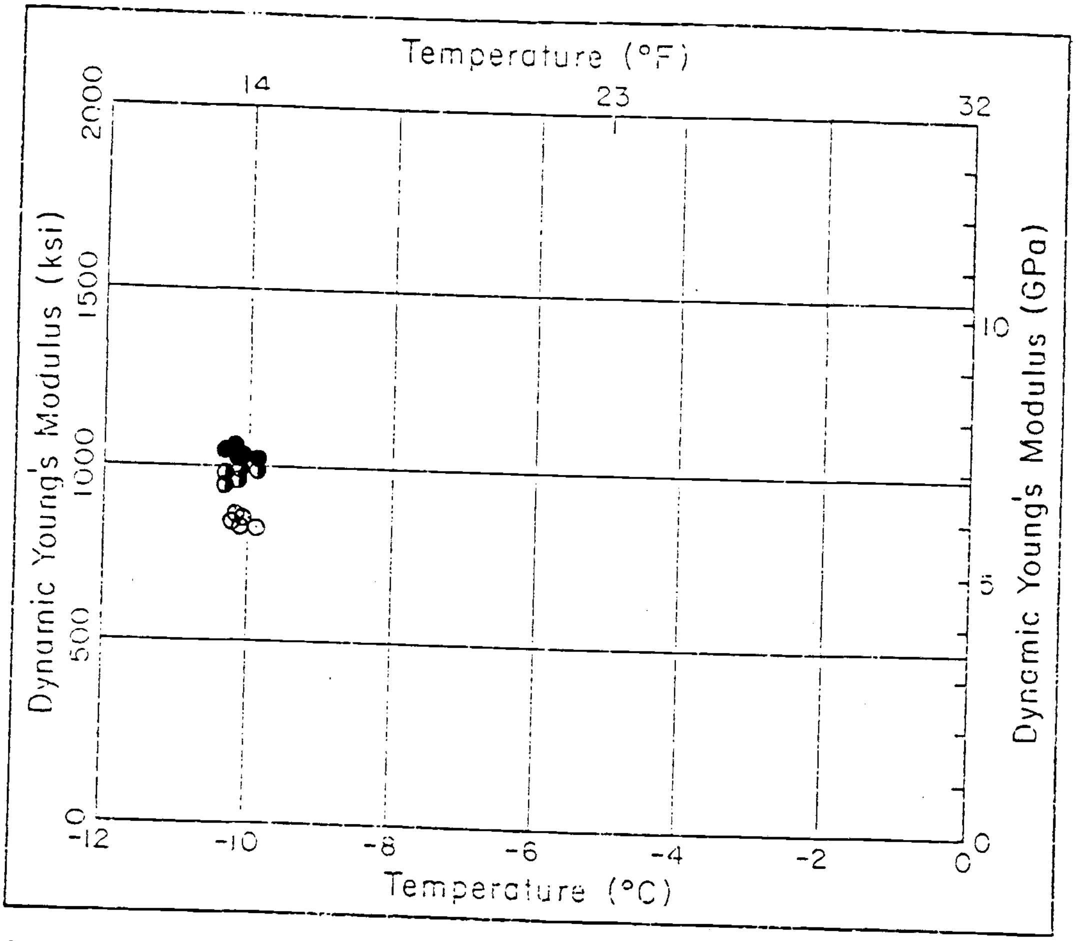

FIGURE A-9 Dynamic Young's Modulus vs. Temperature

Sample no(s). 78
Orientation(s) Vertical
Confining Pres. (psi) All
Strain Amplitude (%) .01

Freq. (Hz) / Orient.	.05	0.5	5.0
Vert.	○	◑	●
Horiz.	△	◭	▲
45°	□	◧	■

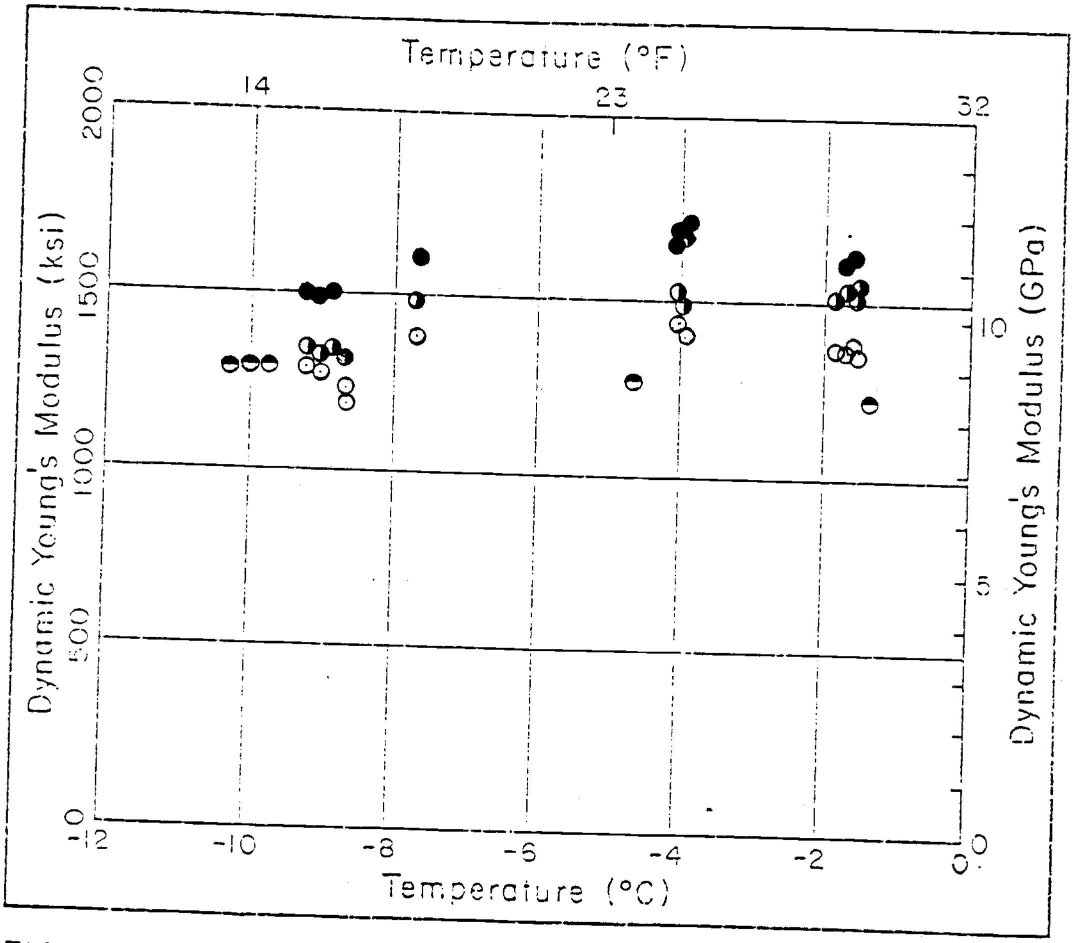

FIGURE A-10 Dynamic Young's Modulus vs. Temperature

Sample no(s). 65
Orientation(s) Vertical
Confining Pres. (psi) All
Strain Amplitude (%) .0009

Freq. (Hz) / Orient.	.05	0.5	5.0
Vert.	○	◑	●
Horiz.	△	▲	▲
45°	□	◧	■

⊖ Resonant column test results

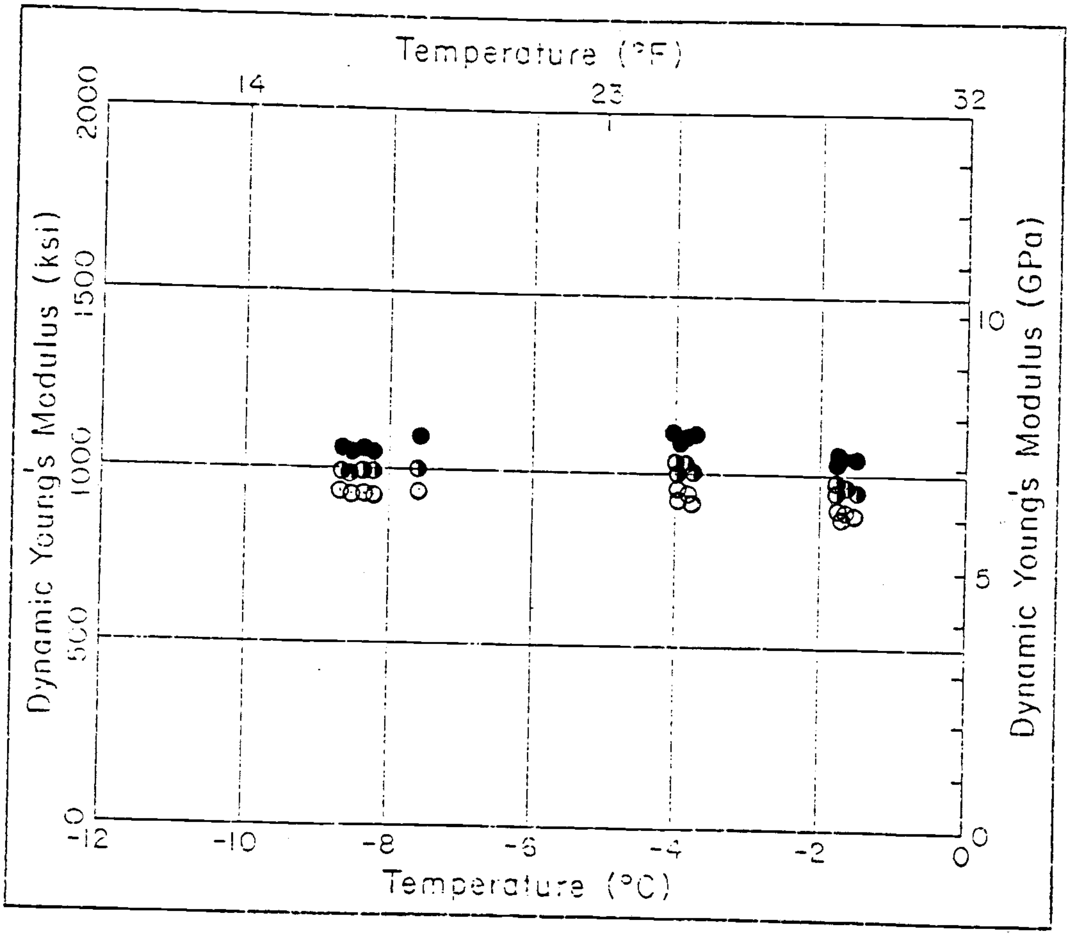

FIGURE A-11 Dynamic Young's Modulus vs. Temperature

Sample no(s). 65
Orientation(s) Vertical
Confining Pres. (psi) All
Strain Amplitude (%) .005

Freq. (Hz) / Orient.	.05	0.5	5.0
Vert.	⊙	◑	●
Horiz.	△	▲	▲
45°	⊡	◧	■

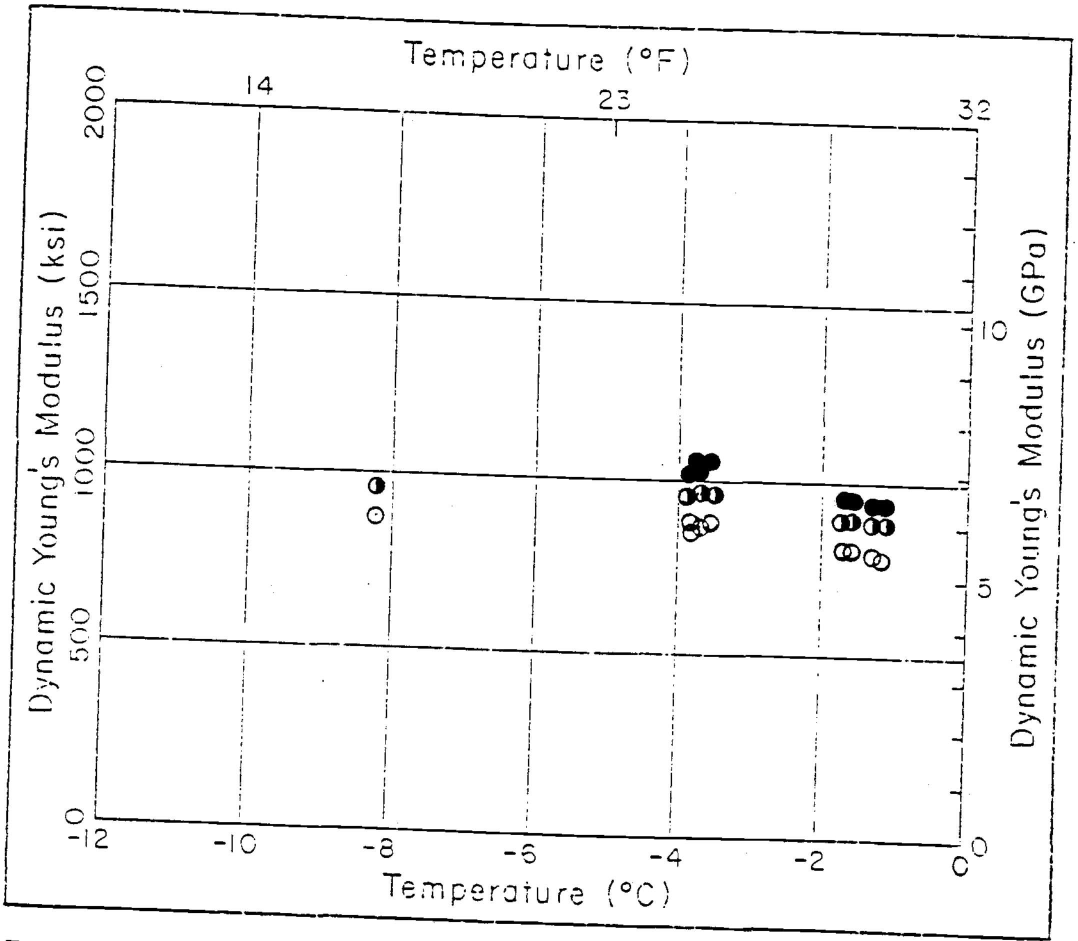

FIGURE A-12 Dynamic Young's Modulus vs. Temperature

Sample no(s). 65
Orientation(s) Vertical
Confining Pres. (psi) All
Strain Amplitude (%) .01

Freq. (Hz) / Orient.	.05	0.5	5.0
Vert.	○	◑	●
Horiz.	△	◭	▲
45°	□	◧	■

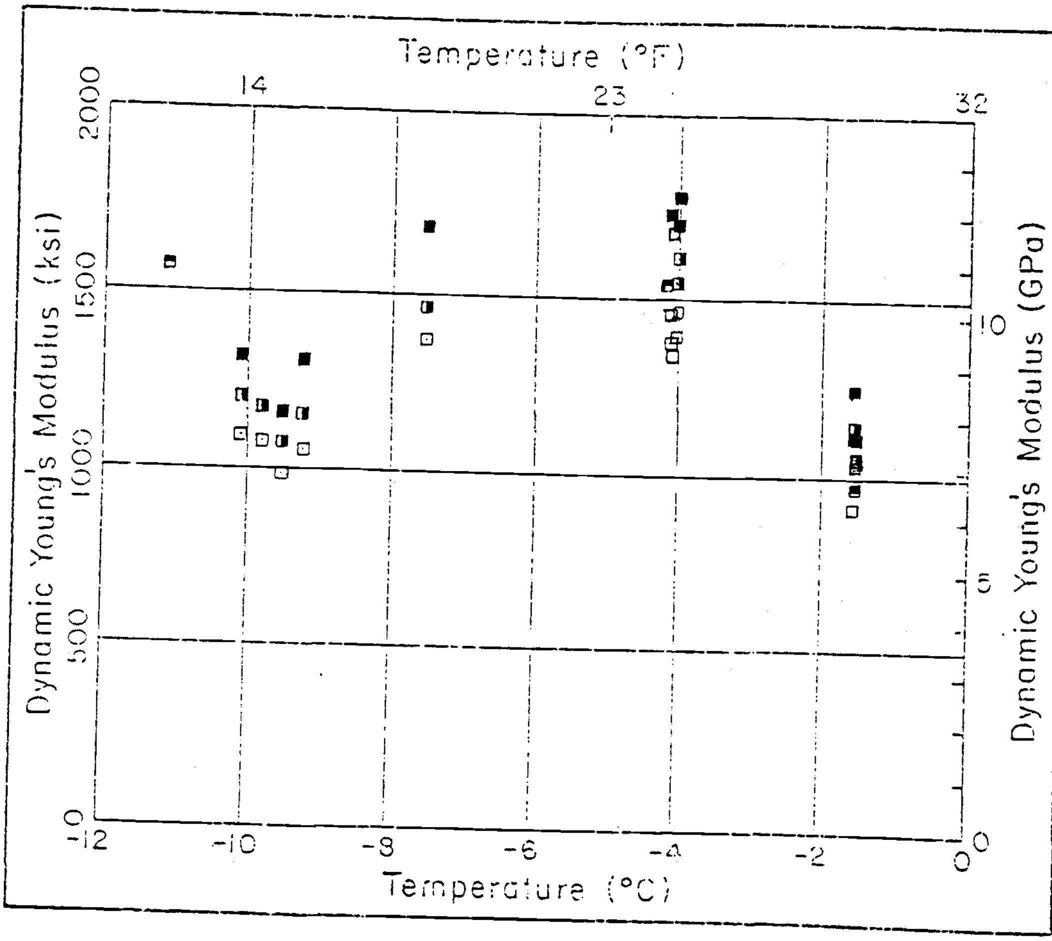

FIGURE A-13 Dynamic Young's Modulus vs. Temperature

Sample no(s). 69
Orientation(s) 45°
Confining Prss. (psi) All
Strain Amplitude (%) .0009

Freq. (Hz) / Orient.	.05	0.5	5.0
Vert.	○	◑	●
Horiz.	△	▲	▲
45°	□	◧	■

■ Resonant column test results

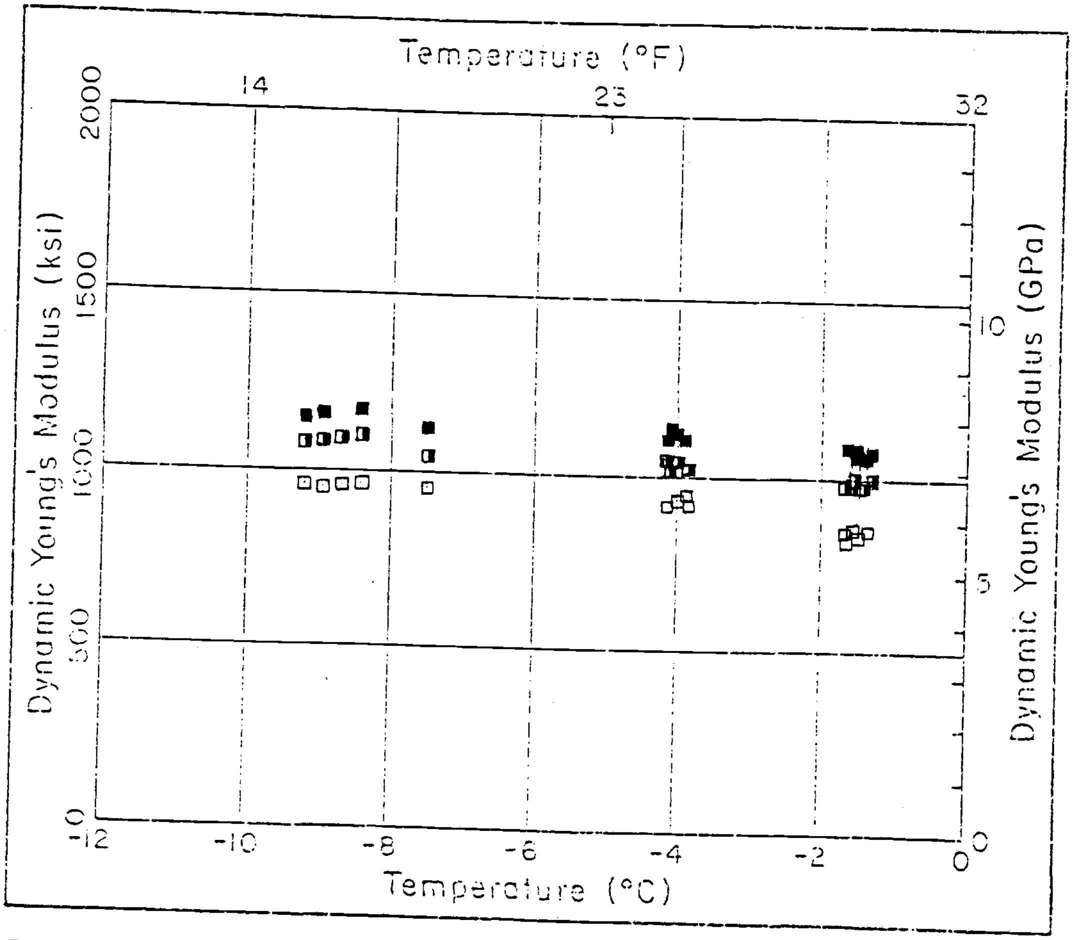

FIGURE A-14 Dynamic Young's Modulus vs. Temperature

Sample no(s). 69
Orientation(s) 45°
Confining Pres. (psi) All
Strain Amplitude (%) .005

Freq. (Hz) / Orient.	.05	0.5	5.0
Vert.	○	◑	●
Horiz.	△	◭	▲
45°	□	◧	■

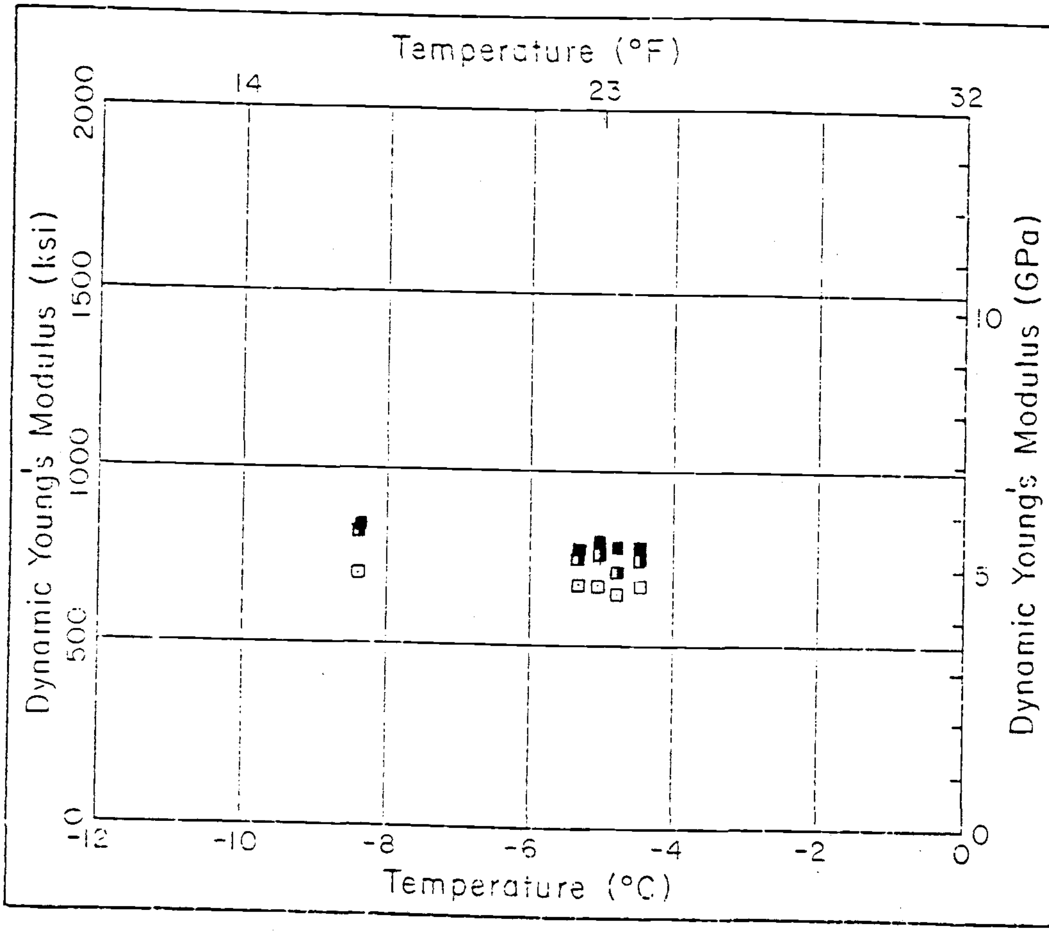

FIGURE A-15 Dynamic Young's Modulus vs. Temperature

Sample no(s). 69
Orientation(s) 45°
Confining Pres. (psi) All
Strain Amplitude (%) .01

Freq. (Hz) / Orient.	.05	0.5	5.0
Vert.	○	◑	●
Horiz.	△	◭	▲
45°	□	◧	■

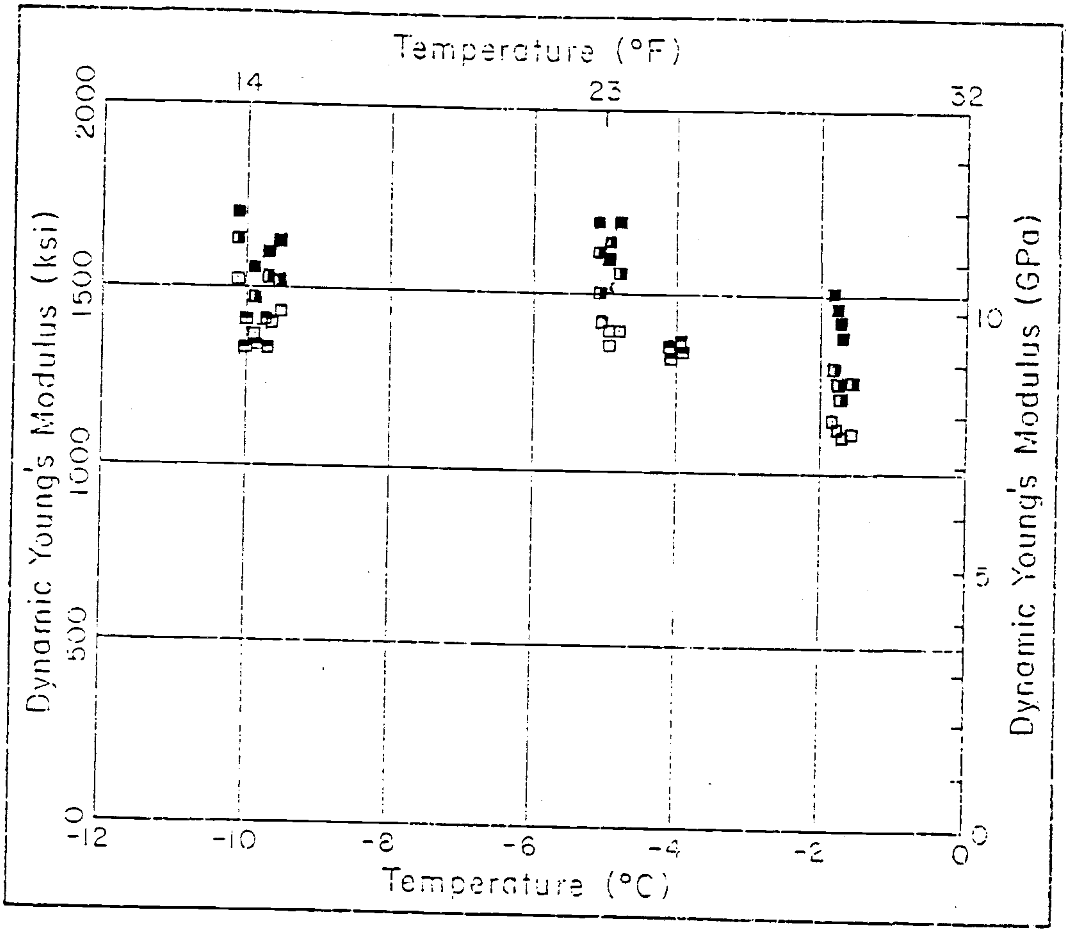

FIGURE A-16 Dynamic Young's Modulus vs. Temperature

Sample no(s).	70
Orientation(s)	45°
Confining Pres. (psi)	All
Strain Amplitude (%)	.0009

Freq. (Hz) / Orient.	.05	0.5	5.0
Vert.	○	◑	●
Horiz.	△	▲	▲
45°	□	◨	■

▭ Resonant column test results

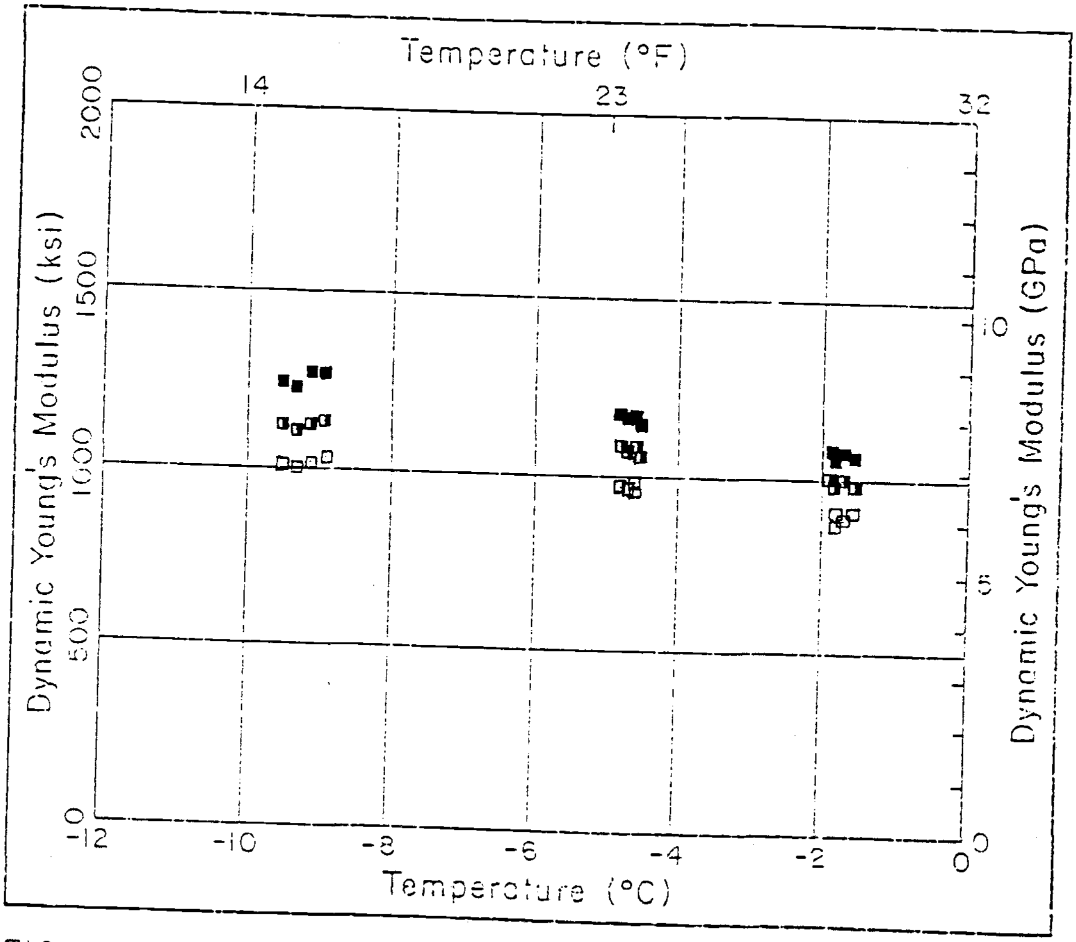

FIGURE A-17 Dynamic Young's Modulus vs. Temperature.

Sample no(s). 70
Orientation(s) 45°
Confining Pres. (psi) All
Strain Amplitude (%) .005

Freq. (Hz) / Orient.	.05	0.5	5.0
Vert.	○	◑	●
Horiz.	△	◭	▲
45°	□	◧	■

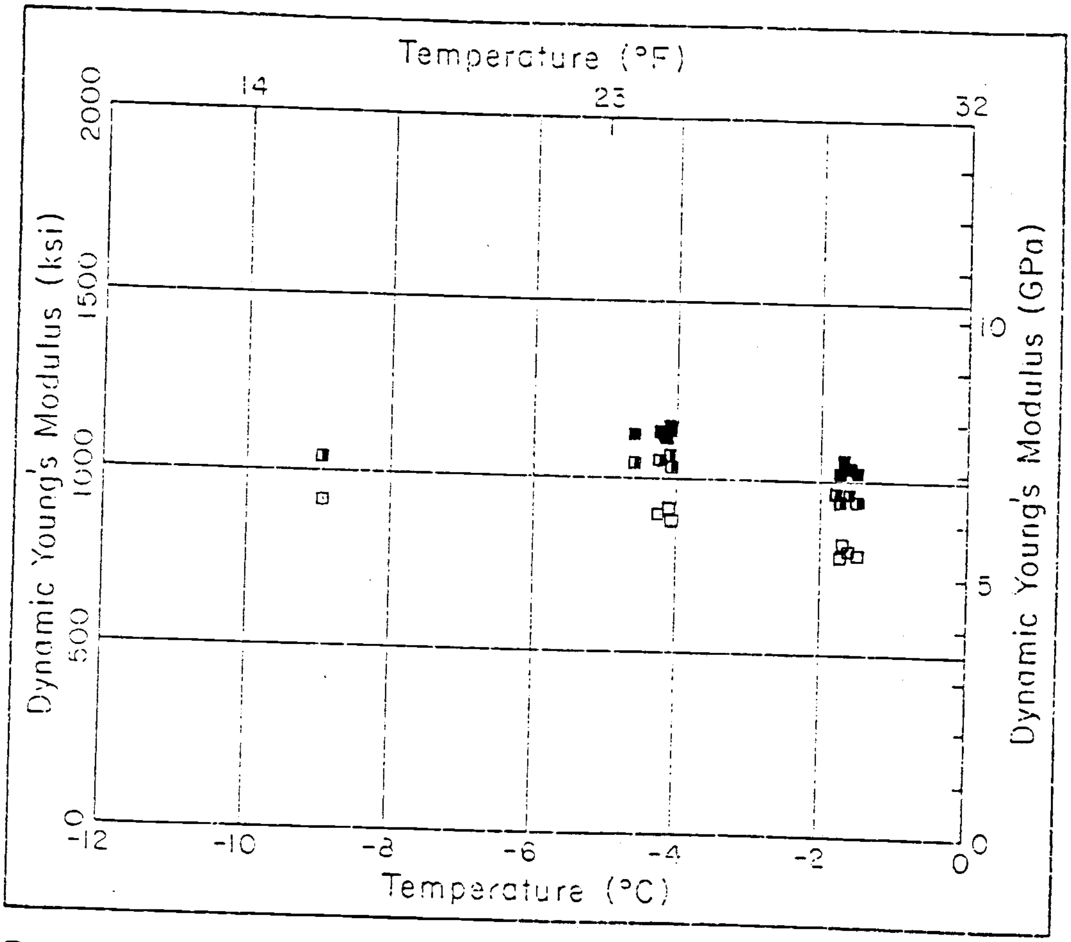

FIGURE A-18 Dynamic Young's Modulus vs. Temperature

Sample no(s). 70
Orientation(s) 45°
Confining Pres. (psi) All
Strain Amplitude (%) .01

Freq. (Hz) / Orient.	.05	0.5	5.0
Vert.	○	◑	●
Horiz.	△	◭	▲
45°	□	◧	■

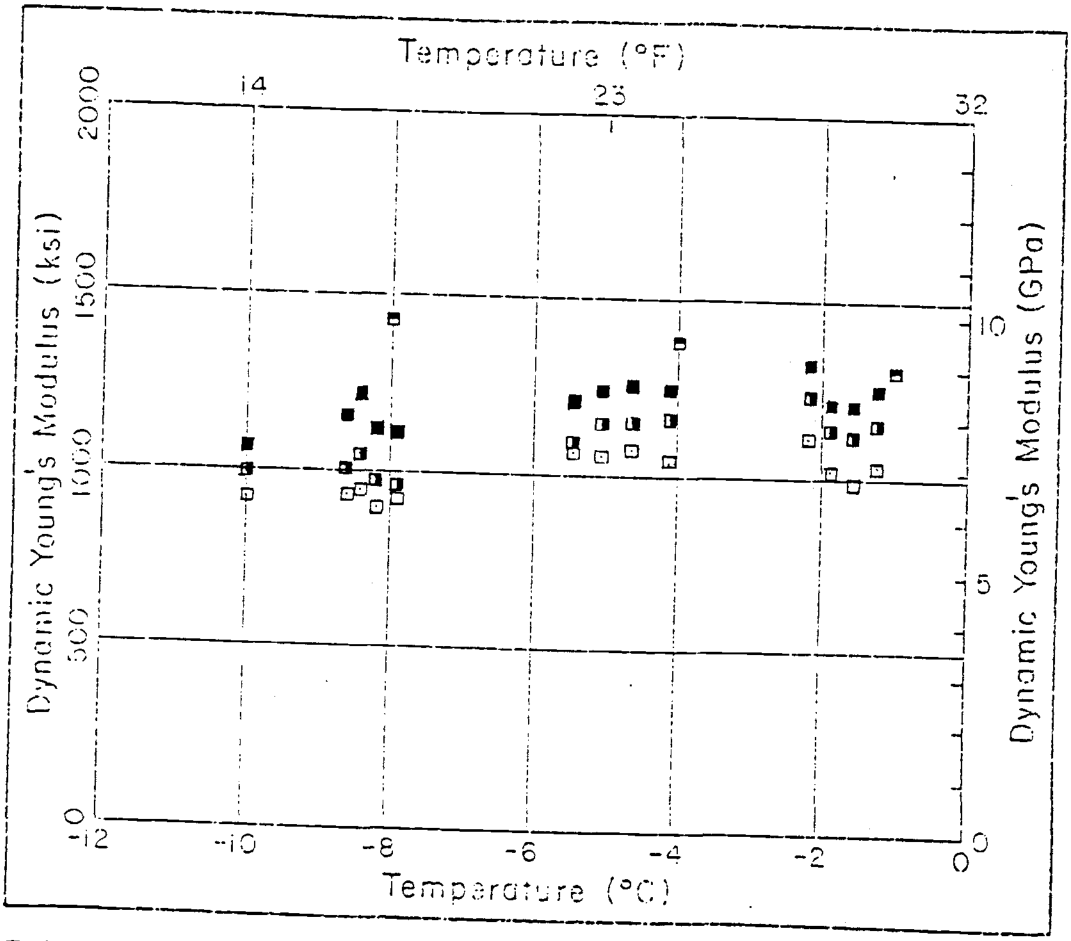

FIGURE A-19 Dynamic Young's Modulus vs. Temperature

Sample no(s). 71
Orientation(s) 45°
Confining Pres. (psi) All
Strain Amplitude (%) .0009

Freq. (Hz) / Orient.	.05	0.5	5.0
Vert.	○	◑	●
Horiz.	△	◭	▲
45°	□	◨	■

■ Resonant column test results

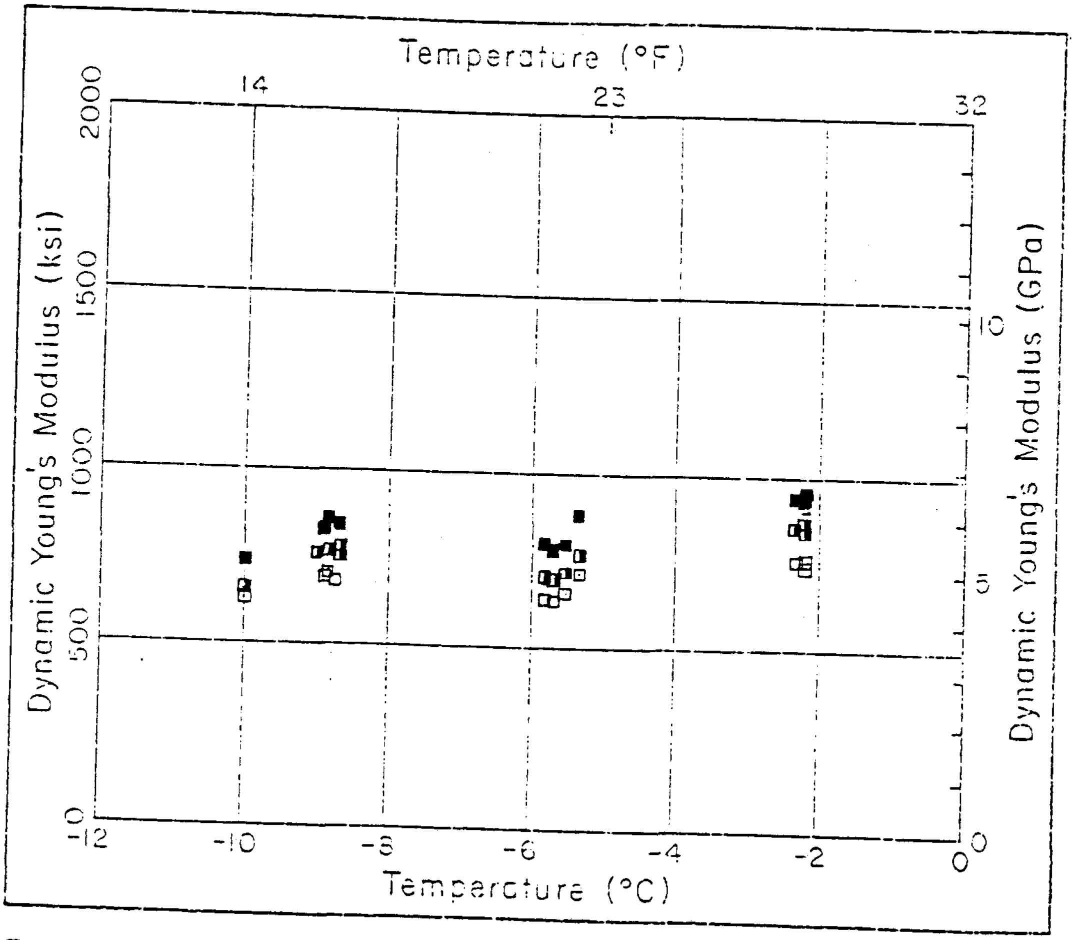

FIGURE A-20 Dynamic Young's Modulus vs. Temperature

Sample no(s). 71
Orientation(s) 45°
Confining Pres. (psi) All
Strain Amplitude (%) .005

Freq. (Hz) / Orient.	.05	0.5	5.0
Vert.	○	◑	●
Horiz.	△	▲	▲
45°	□	◨	■

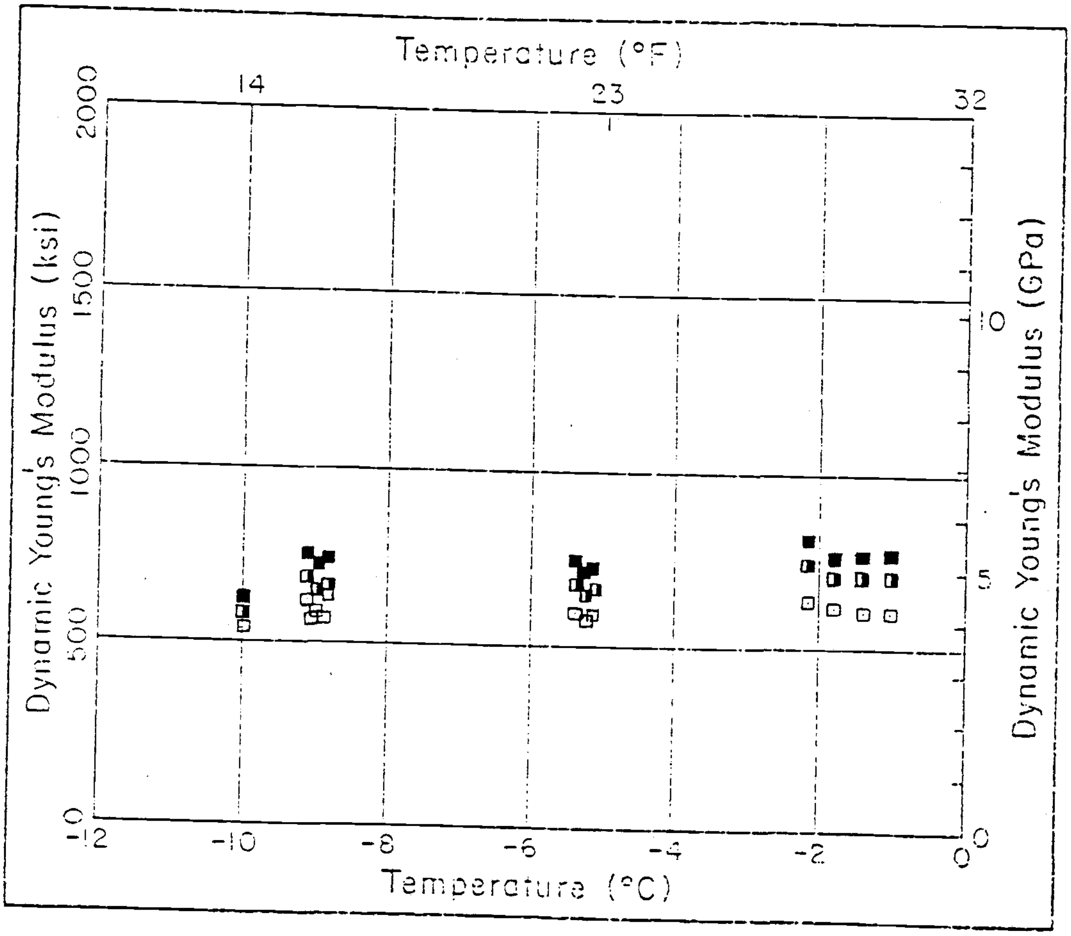

FIGURE A-21 Dynamic Young's Modulus vs. Temperature

Sample no(s). 71
Orientation(s) 45°
Confining Pres. (psi) All
Strain Amplitude (%) .01

Freq. (Hz) / Orient.	.05	0.5	5.0
Vert.	○	◐	●
Horiz.	△	◭	▲
45°	□	◧	■

KEY: Interpretation of Damping ratio curves which follow (Figures A-22 through A-42)

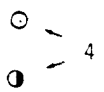

The number indicates that the point represents several points (from 2 to 4) which have been averaged and are represented by a single point.

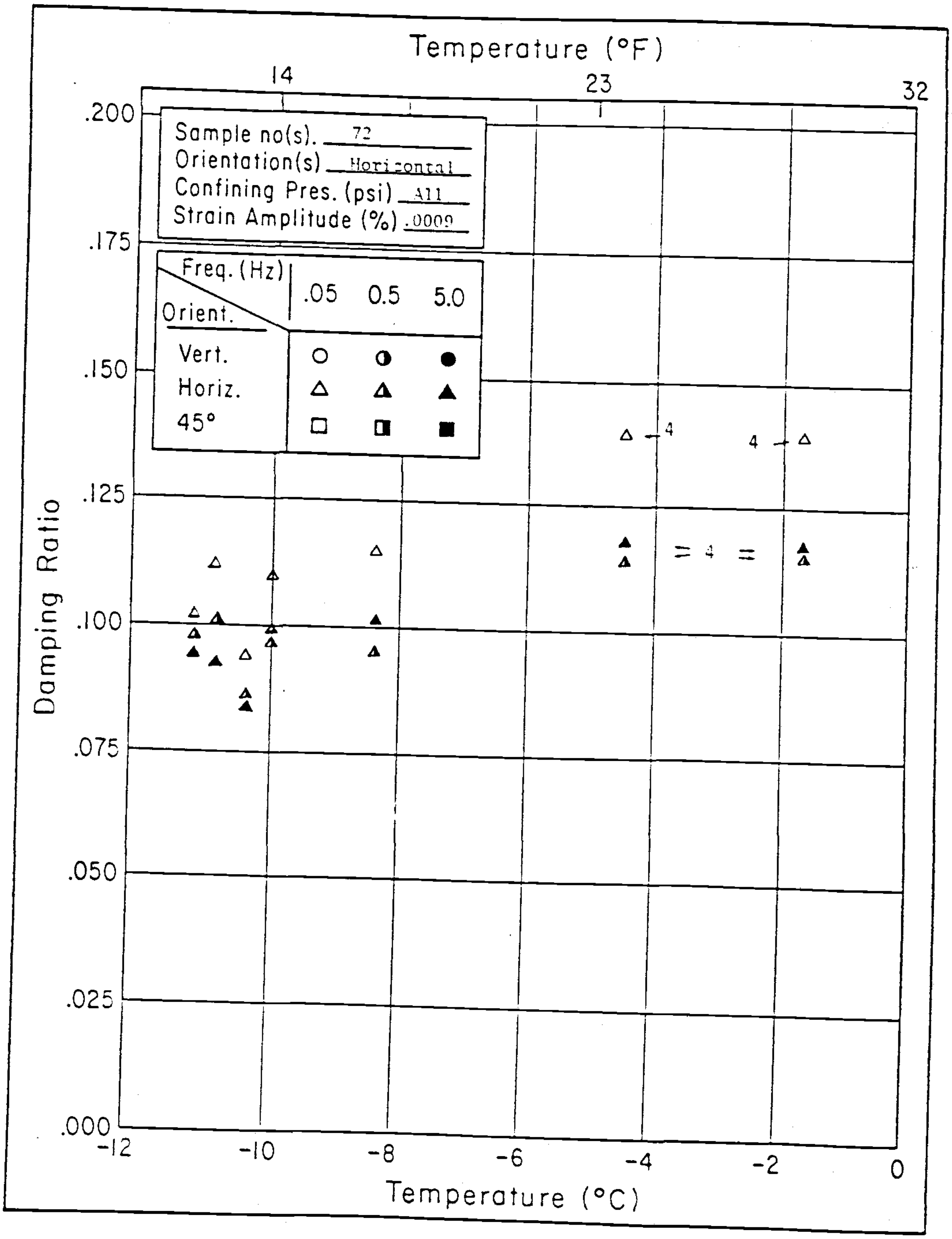

FIGURE A-22 Damping Ratio versus Temperature

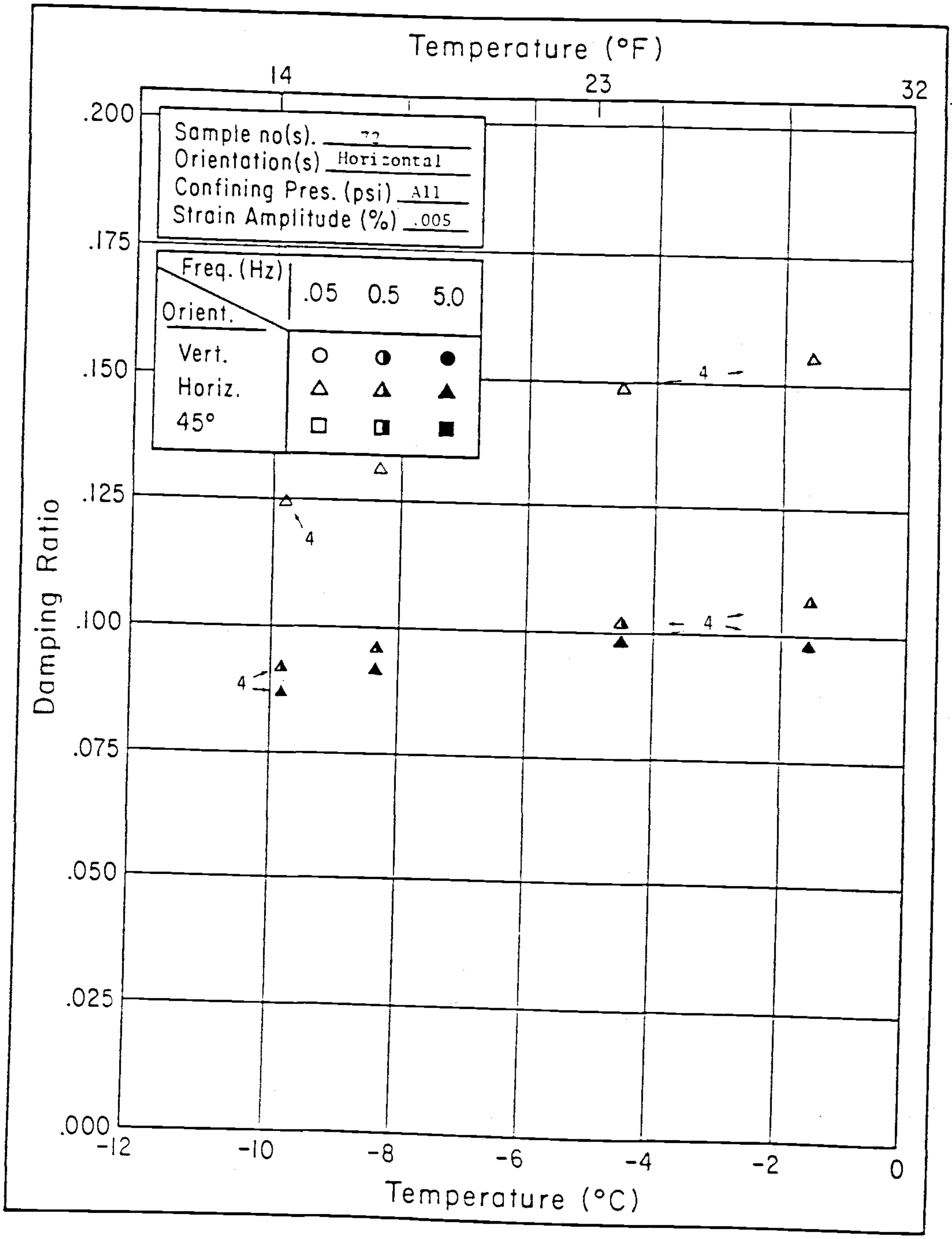

FIGURE A-23 Damping Ratio versus Temperature

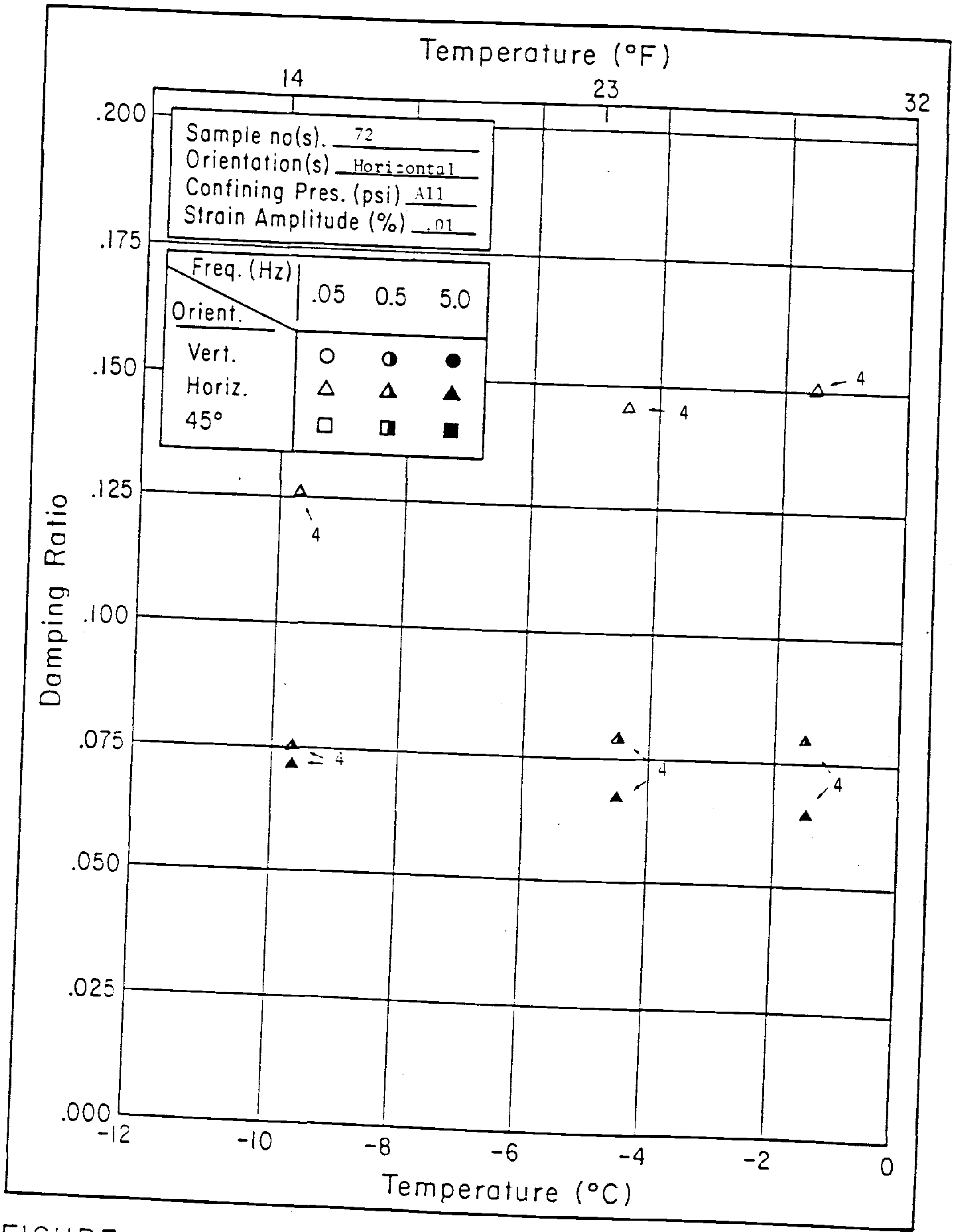

FIGURE A-24 Damping Ratio versus Temperature

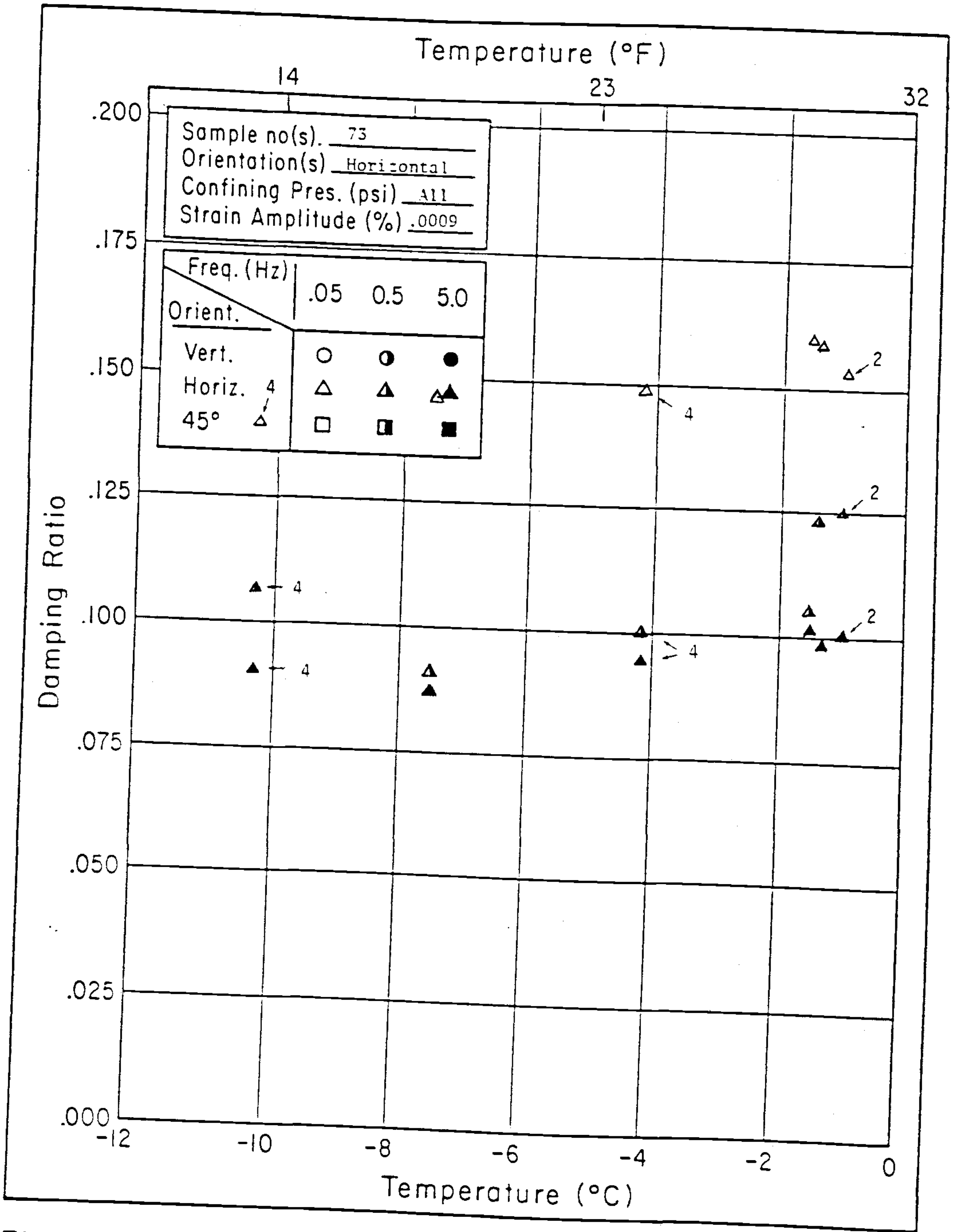

FIGURE A-25 Damping Ratio versus Temperature

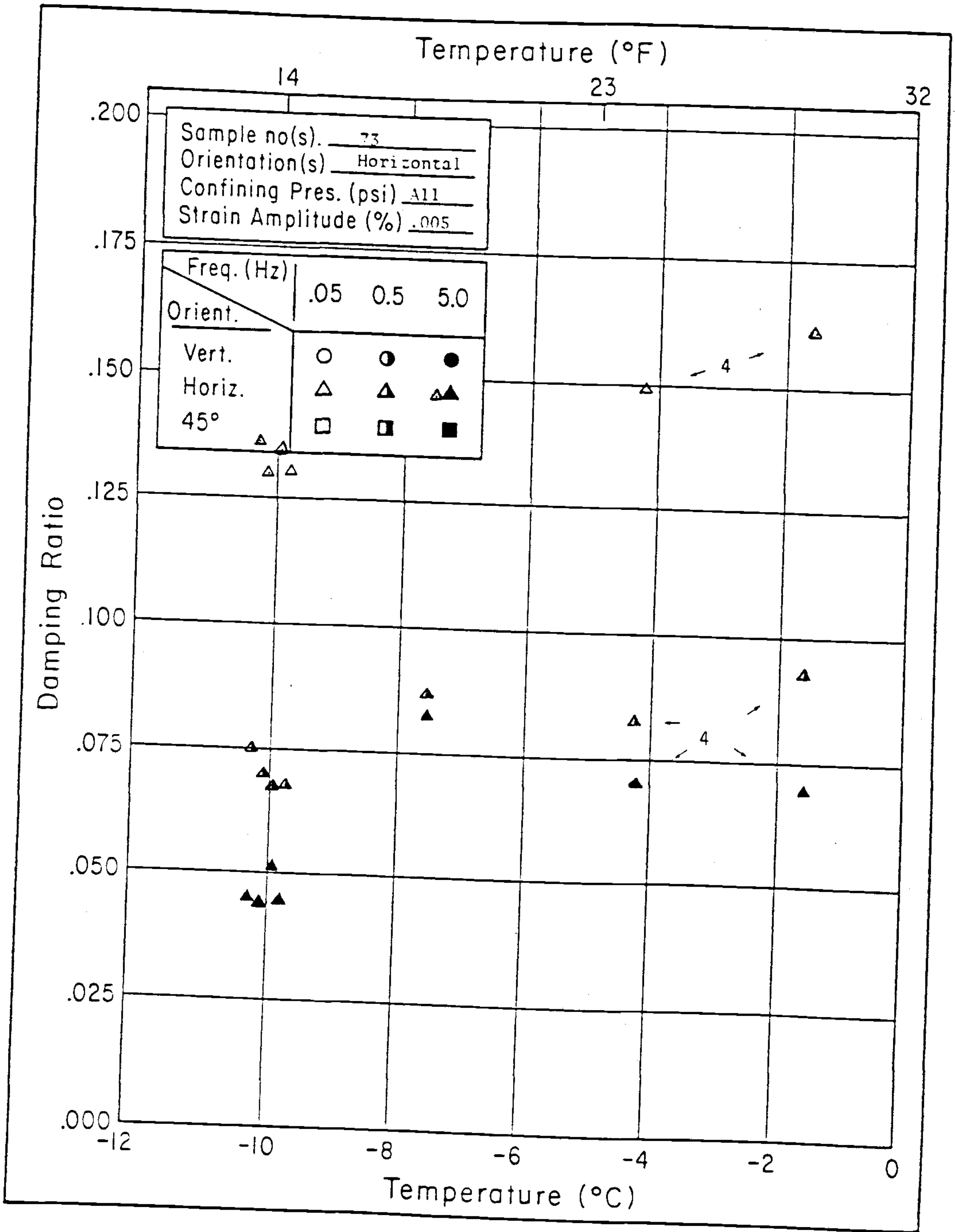

FIGURE A-26 Damping Ratio versus Temperature

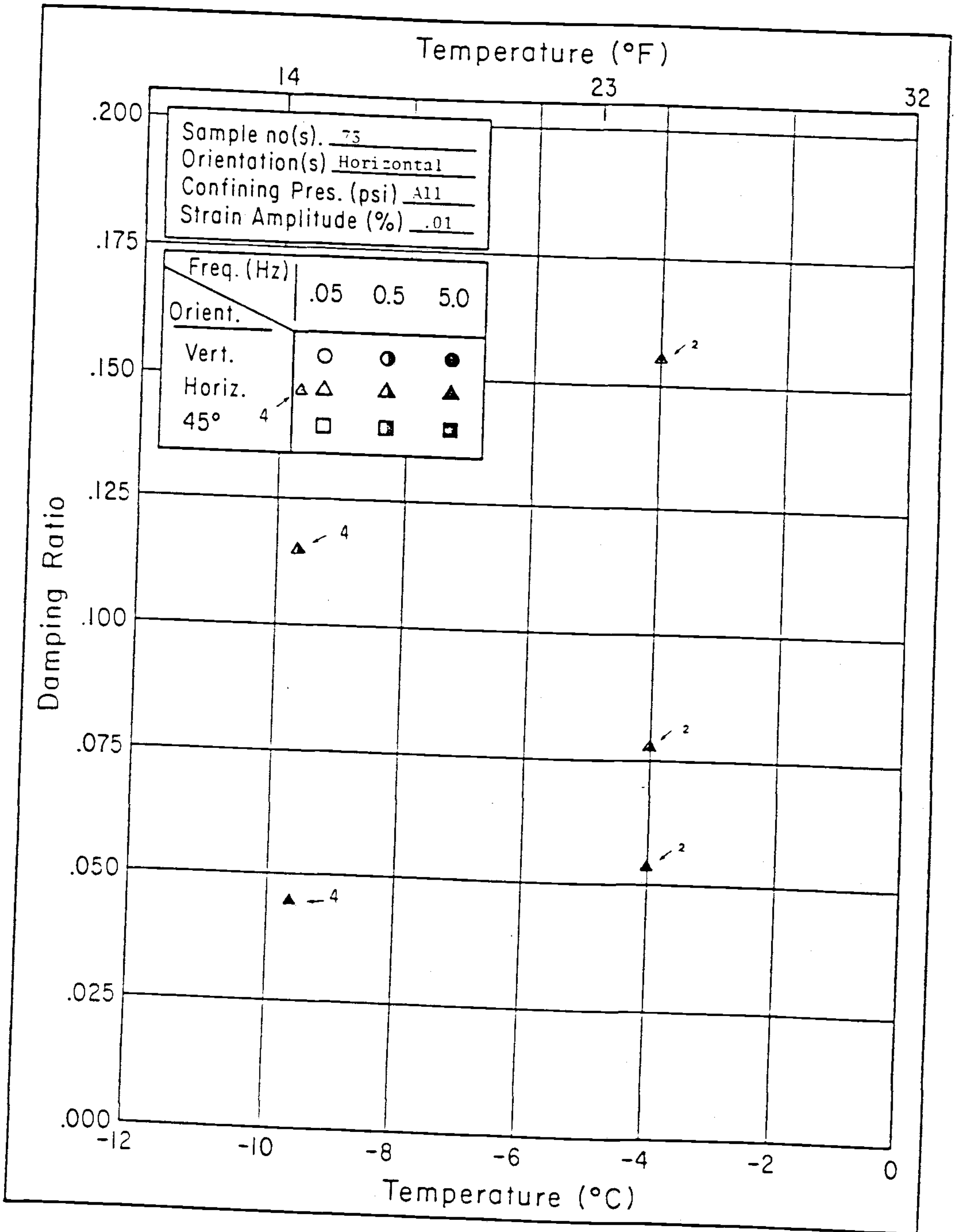

FIGURE A-27 Damping Ratio versus Temperature

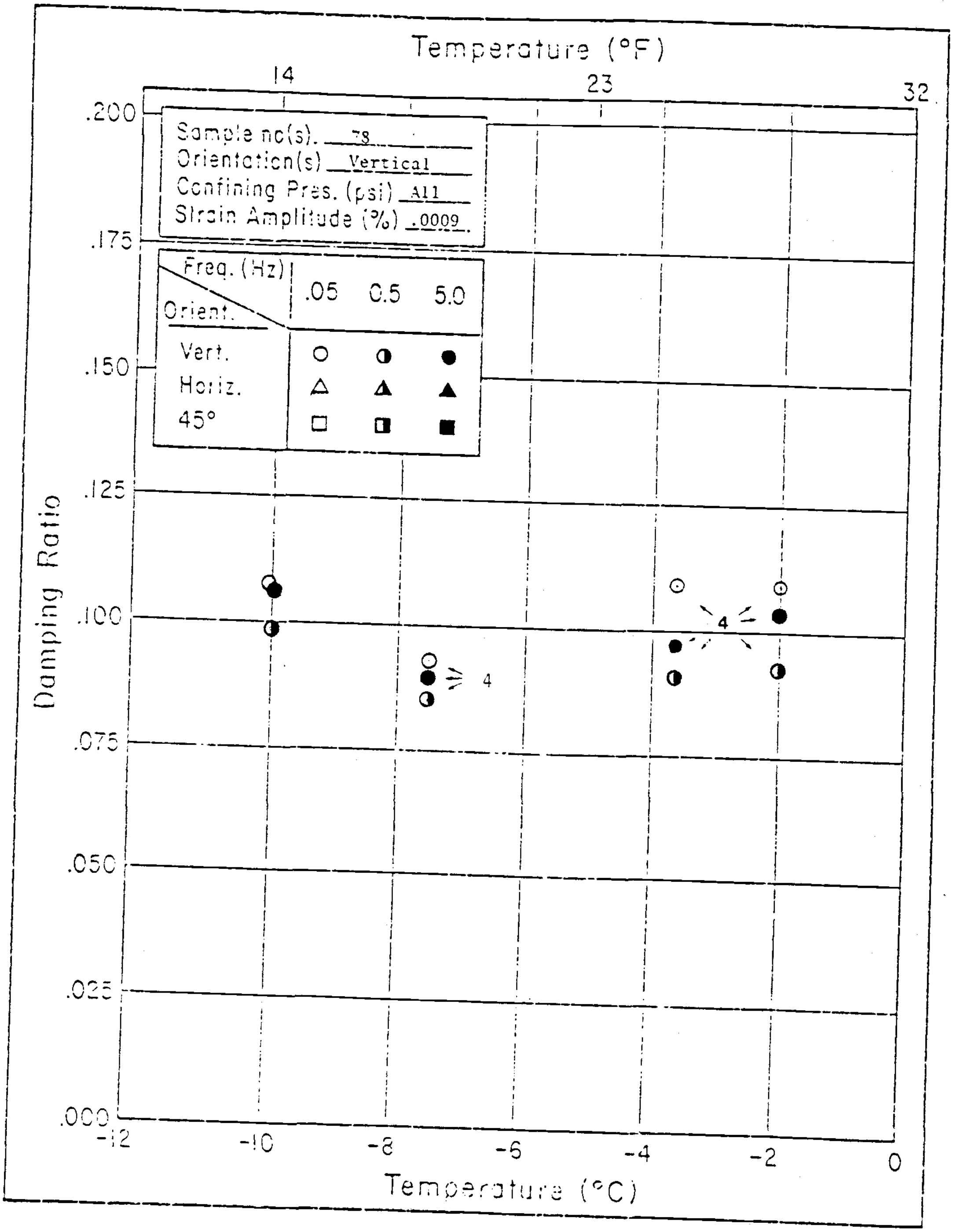

FIGURE A-28 Damping Ratio versus Temperature

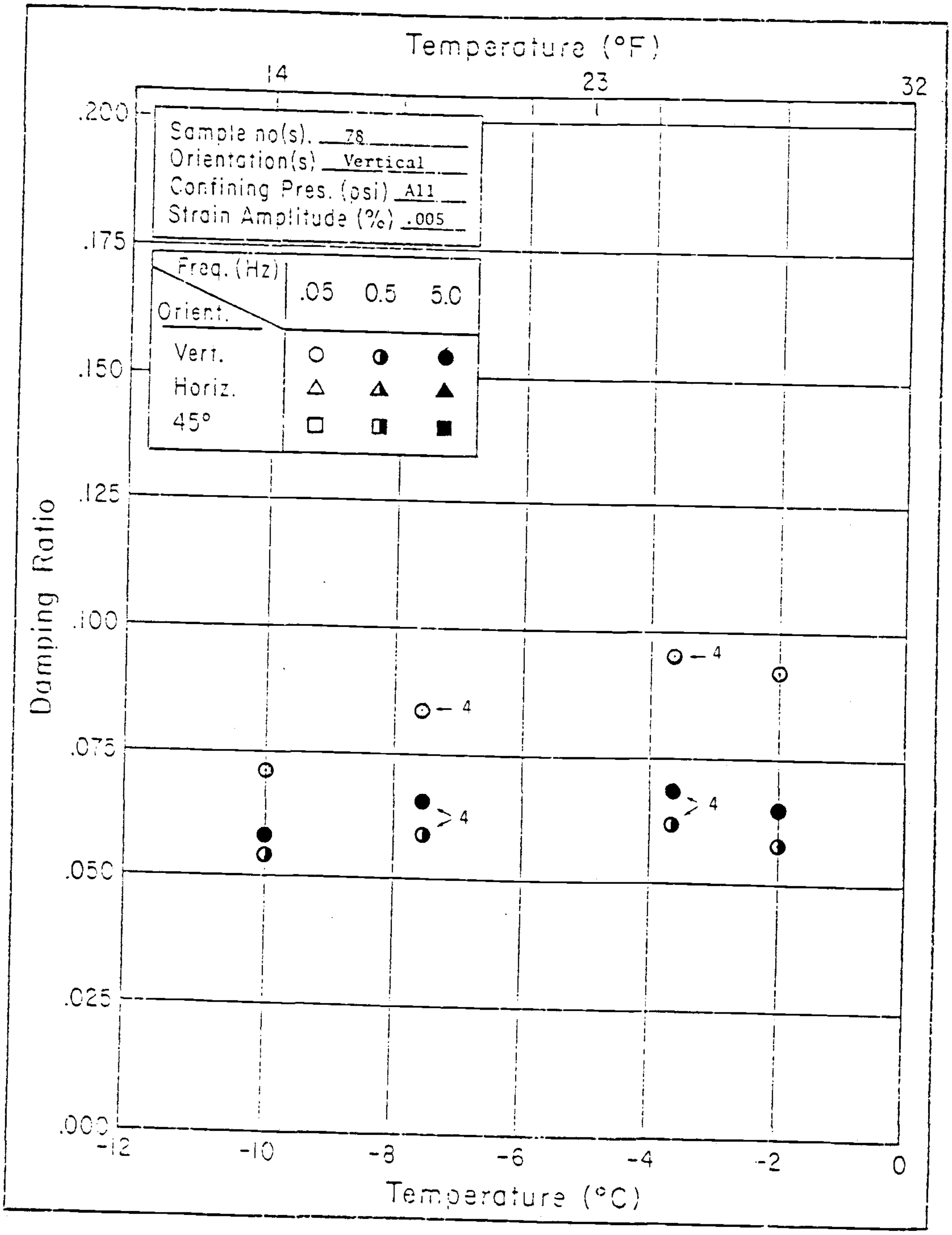

FIGURE A-29 Damping Ratio versus Temperature

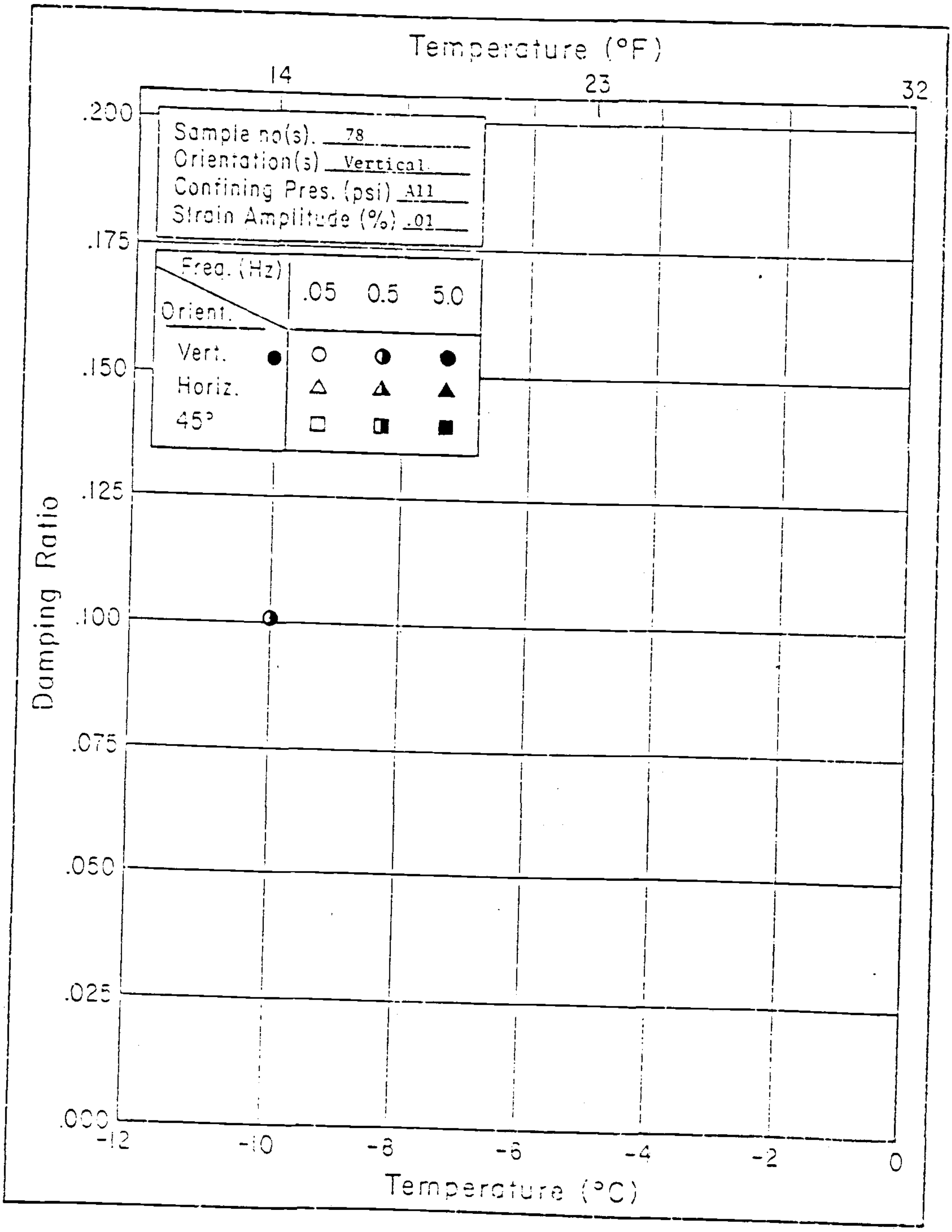

FIGURE A-30 Damping Ratio versus Temperature

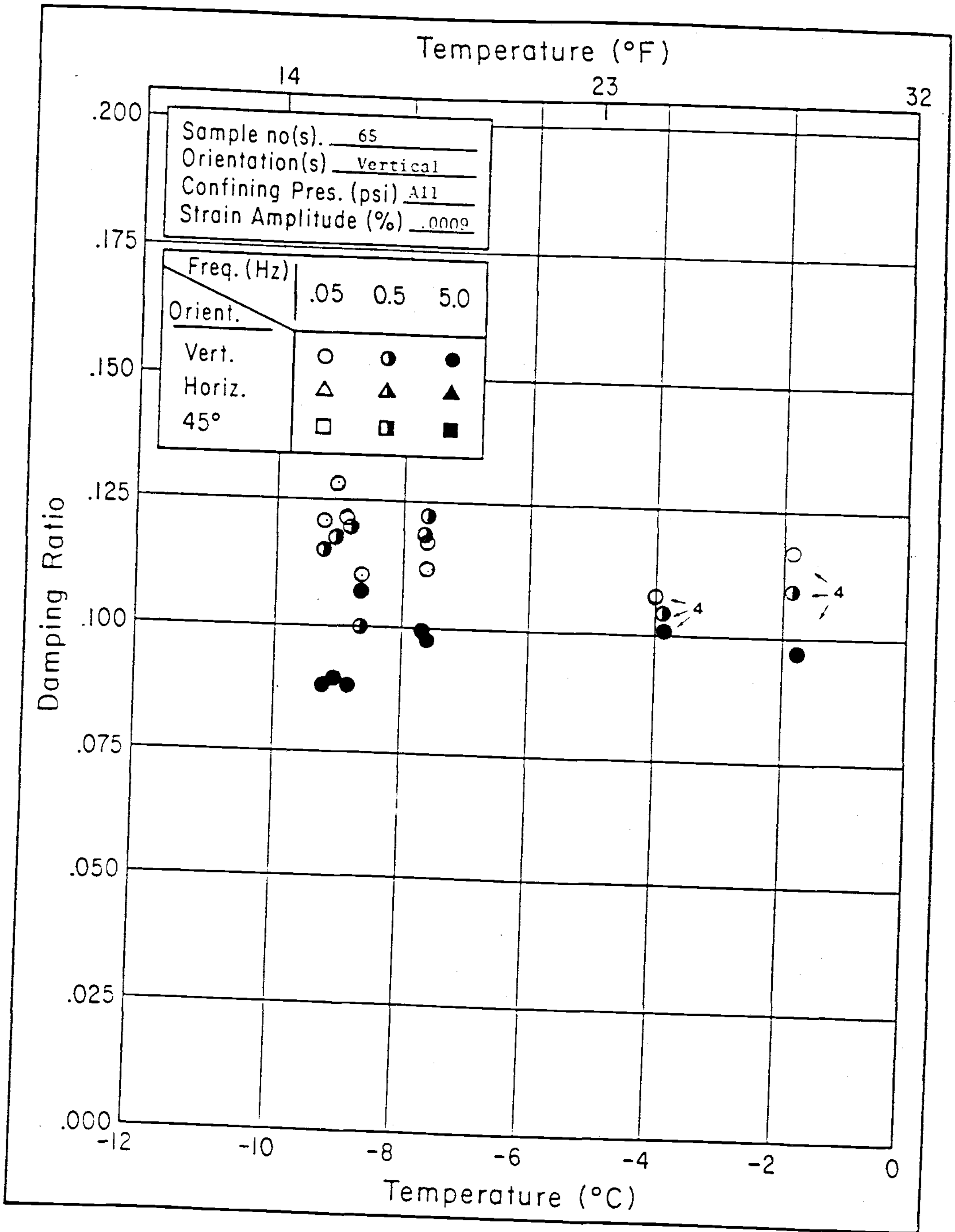

FIGURE A-31 Damping Ratio versus Temperature

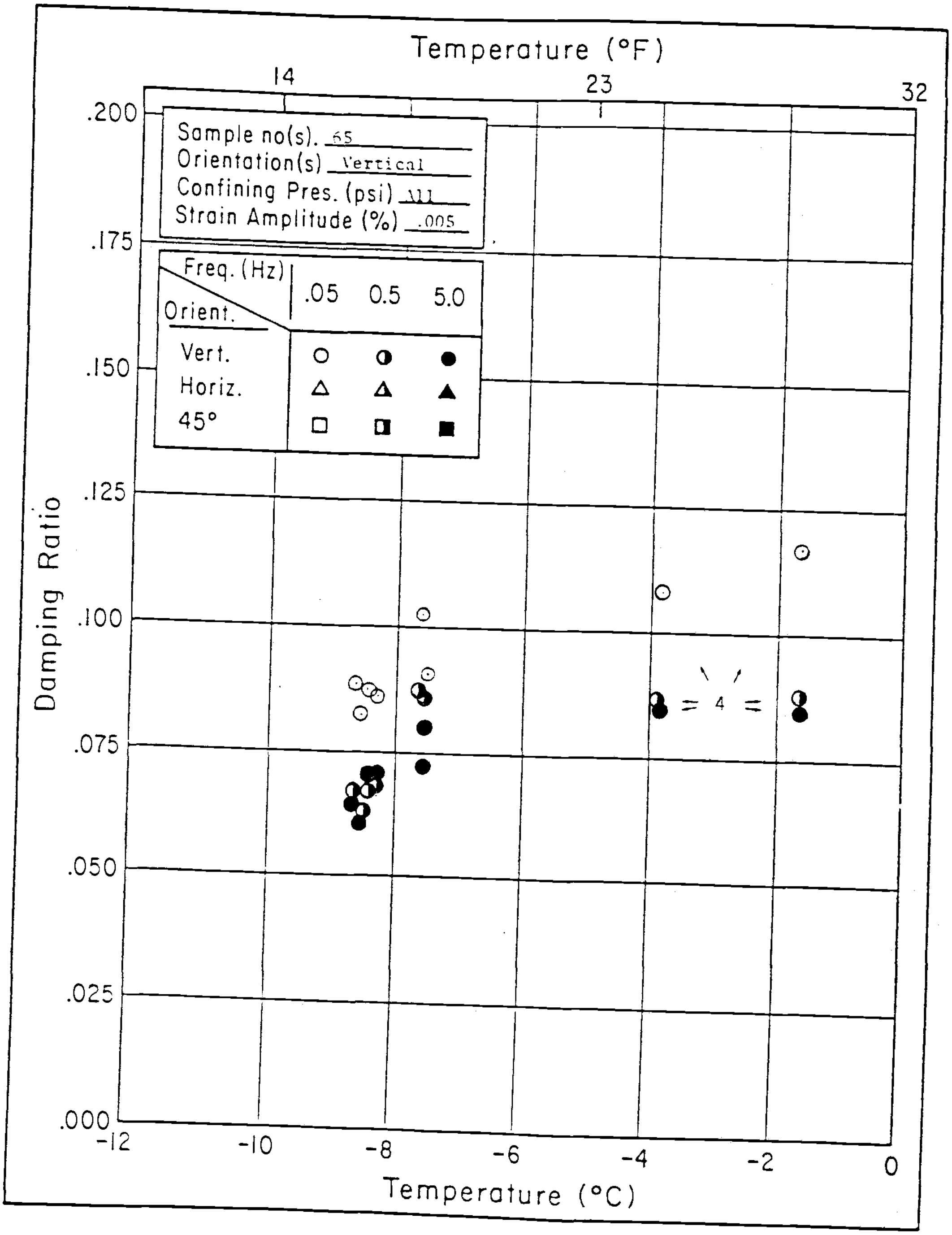

FIGURE A-32 Damping Ratio versus Temperature

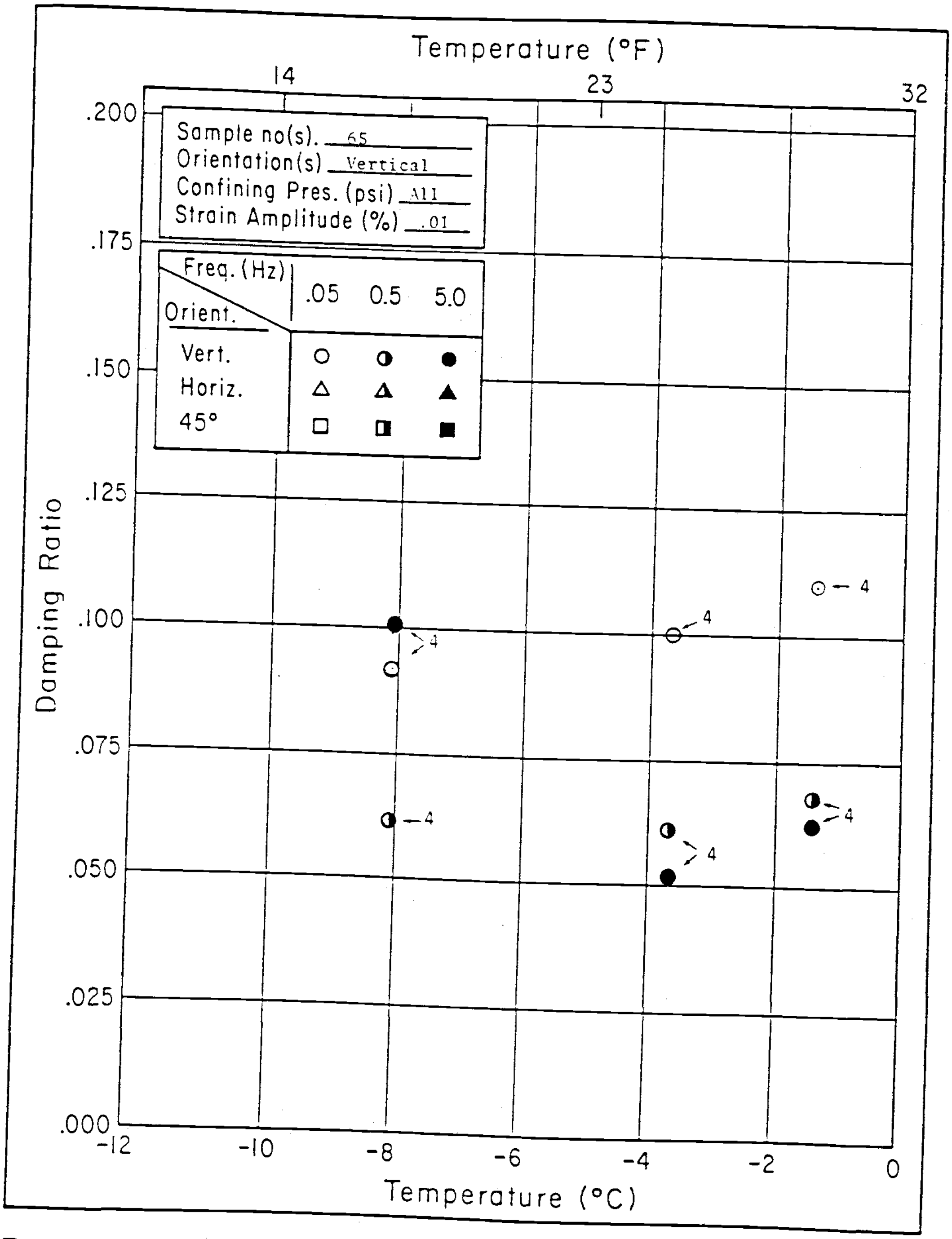

FIGURE A-33 Damping Ratio versus Temperature

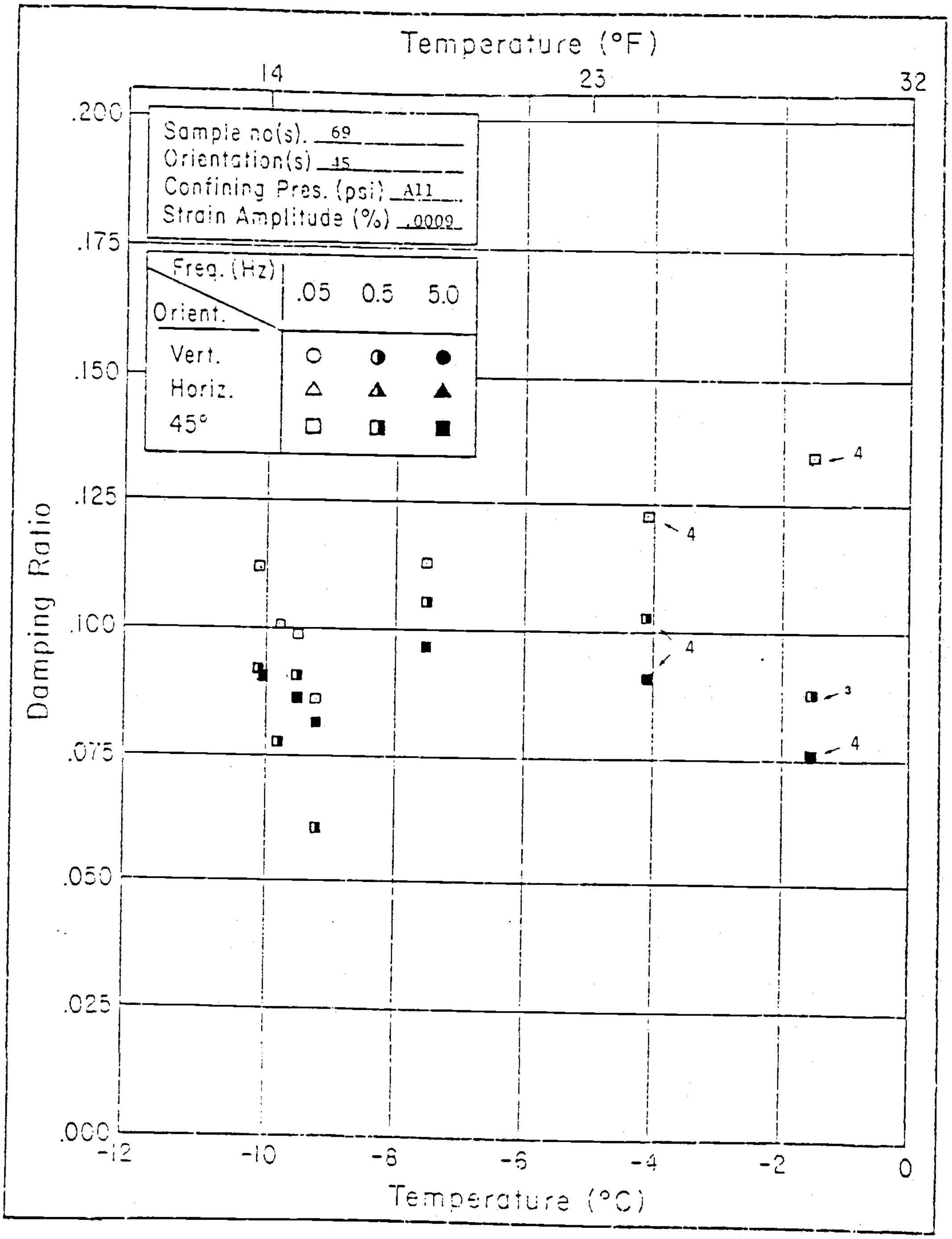

FIGURE A-34 Damping Ratio versus Temperature

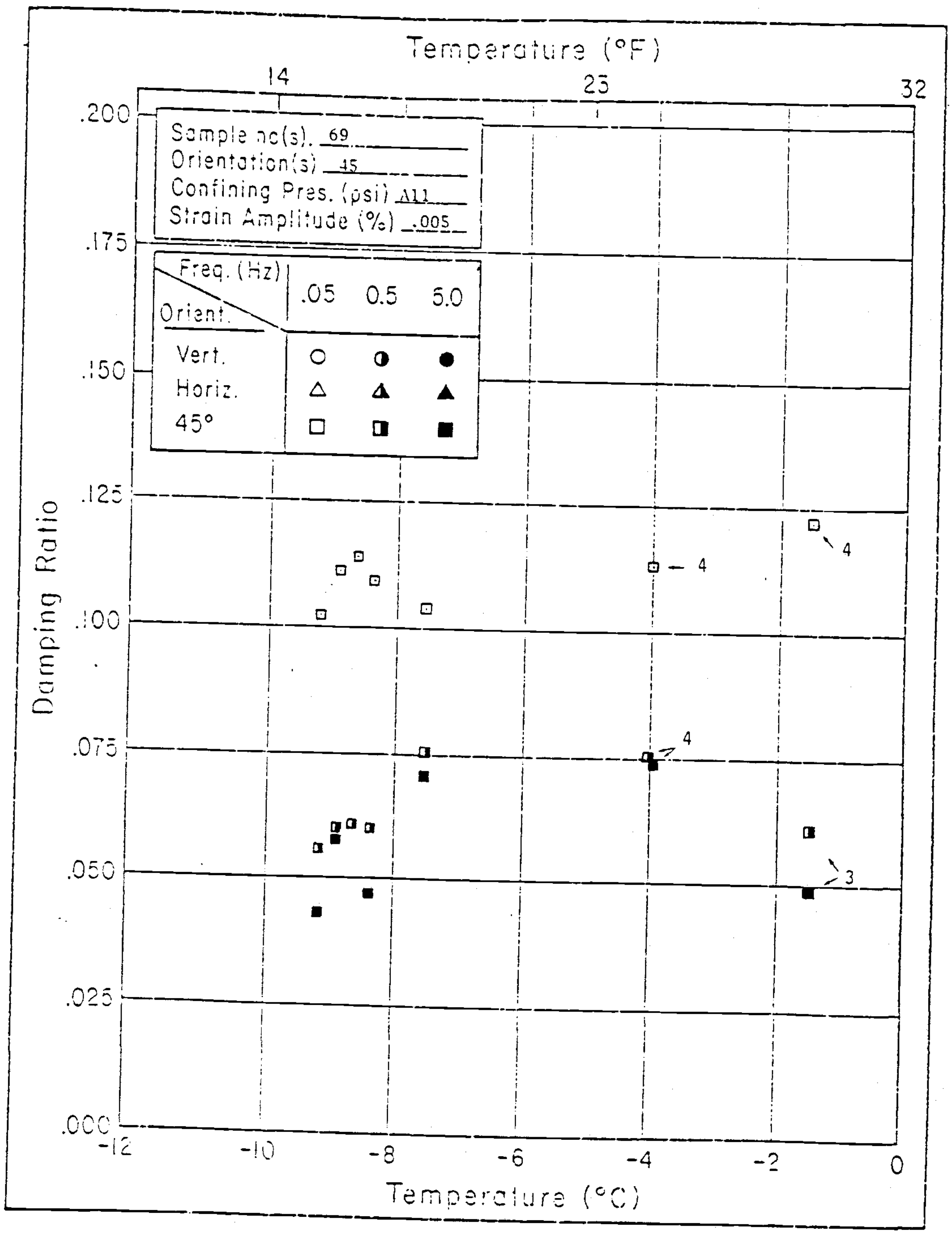

FIGURE A-35 Damping Ratio versus Temperature

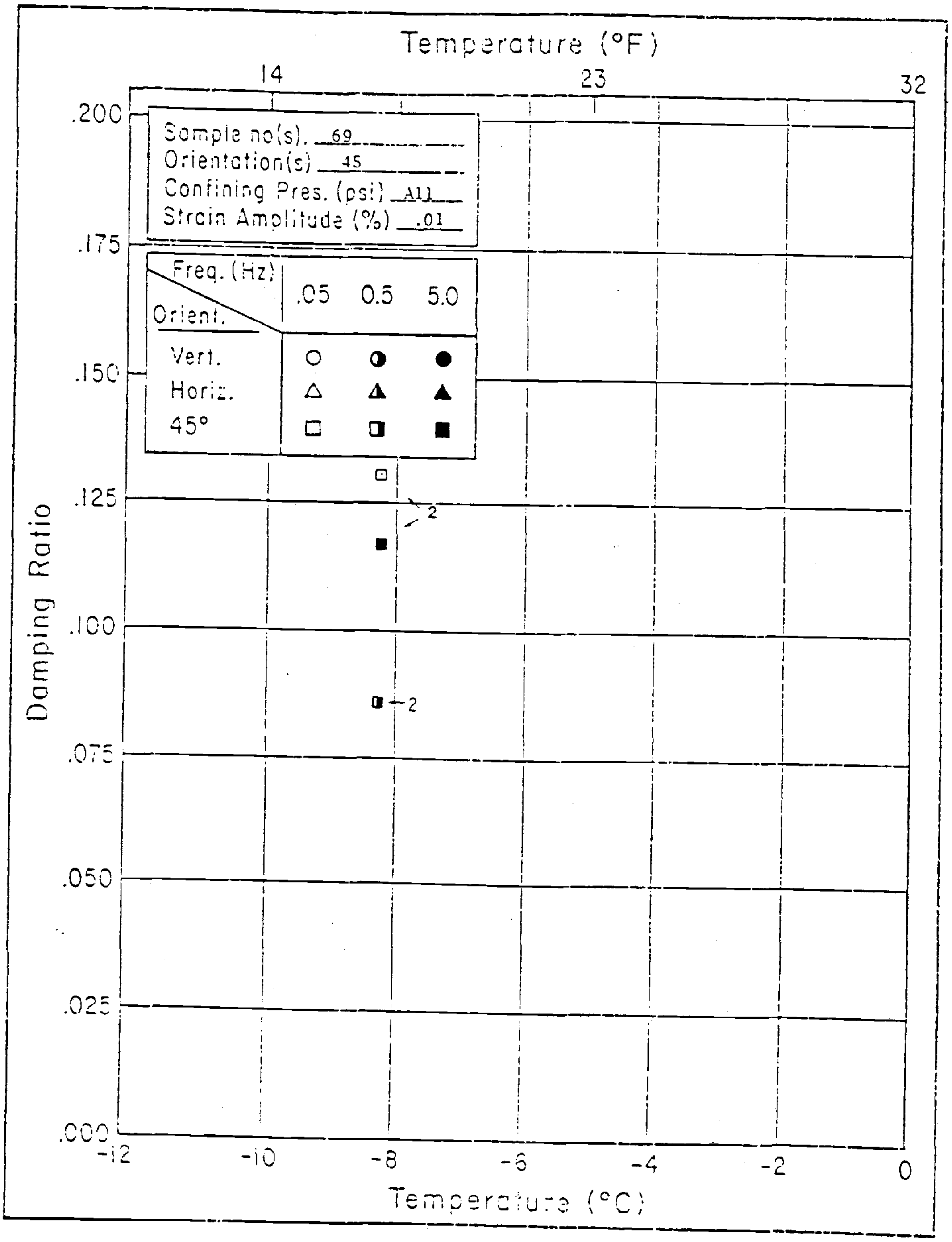

FIGURE A-36 Damping Ratio versus Temperature

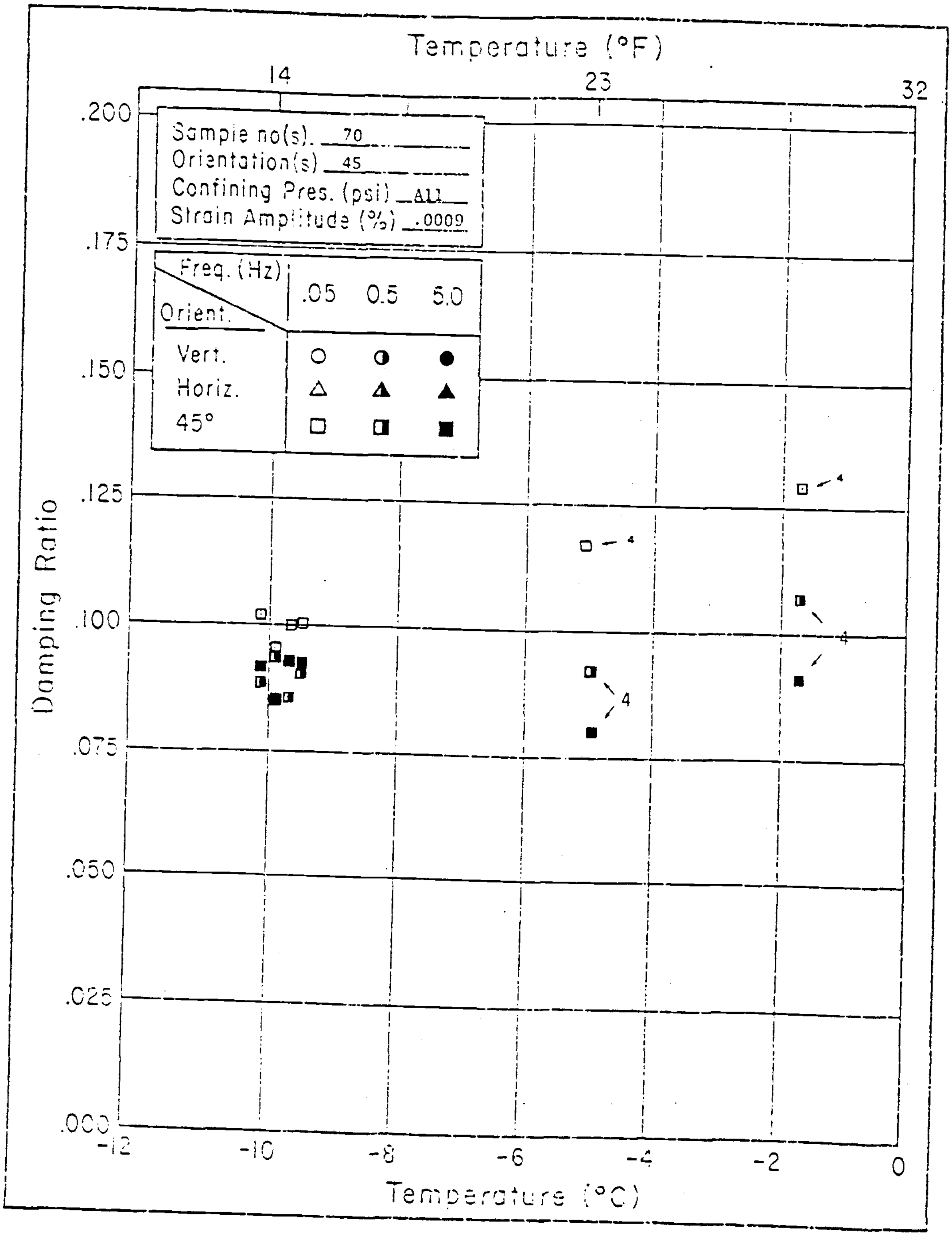

FIGURE A-37 Damping Ratio versus Temperature

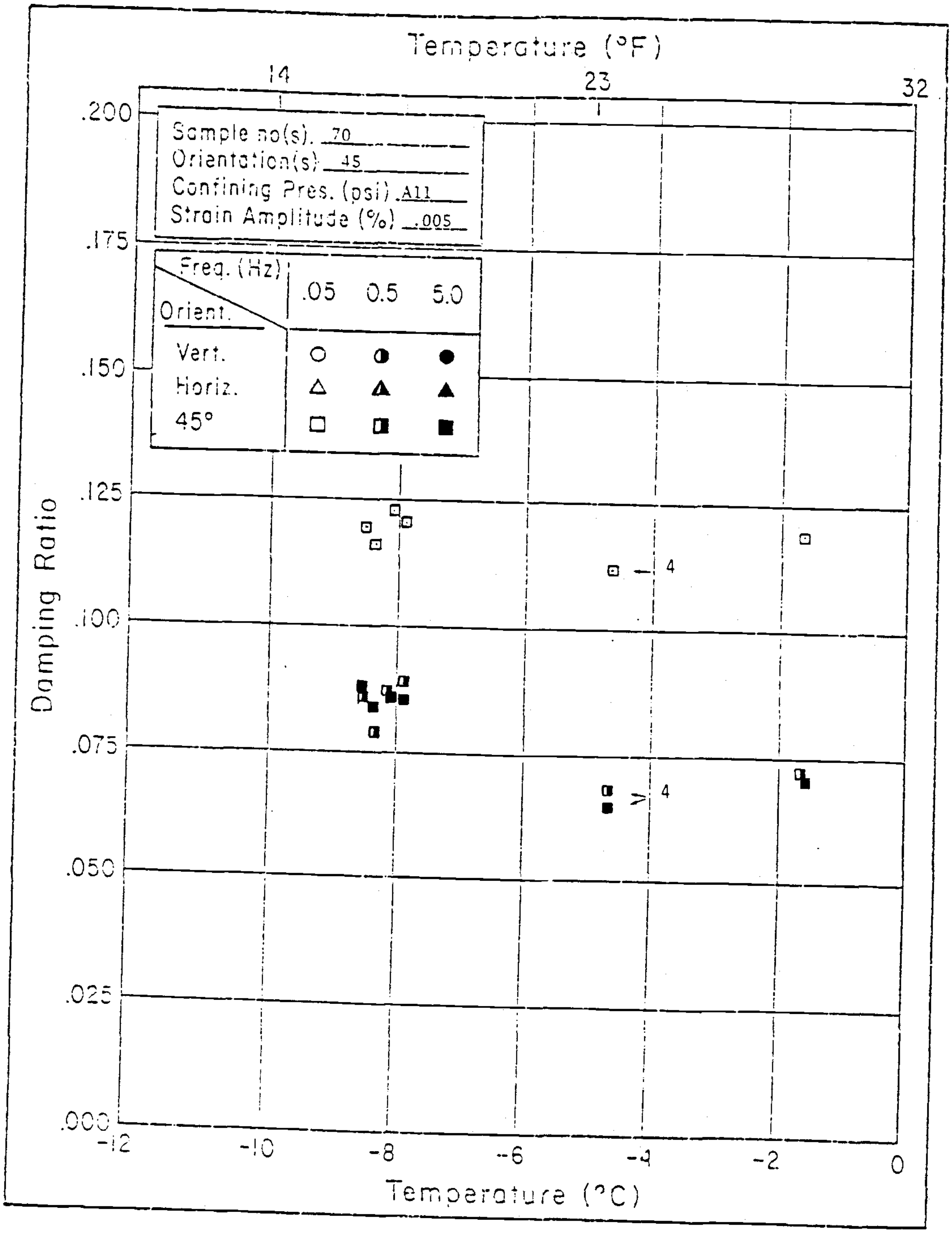

FIGURE A-38 Damping Ratio versus Temperature

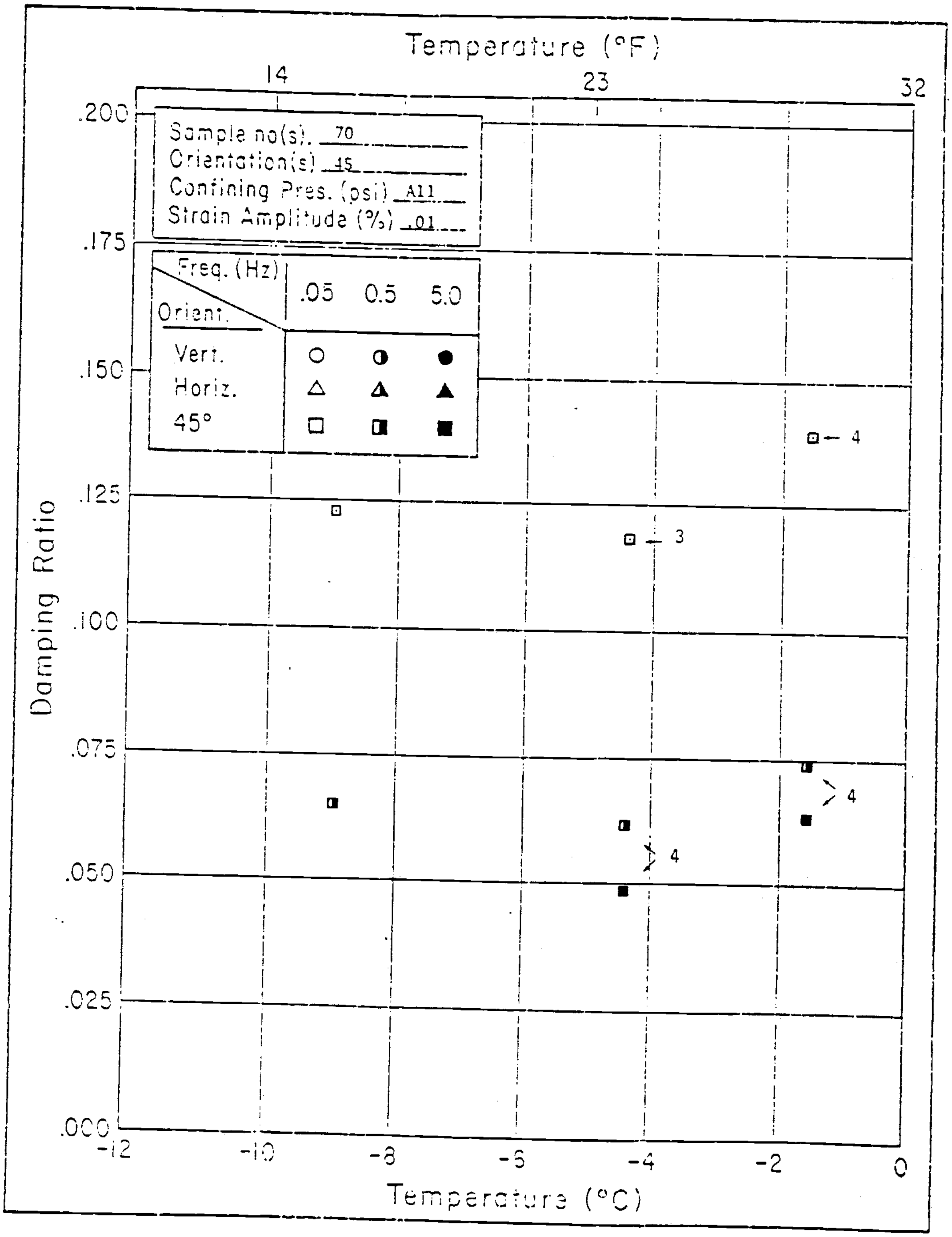

FIGURE A-39 Damping Ratio versus Temperature

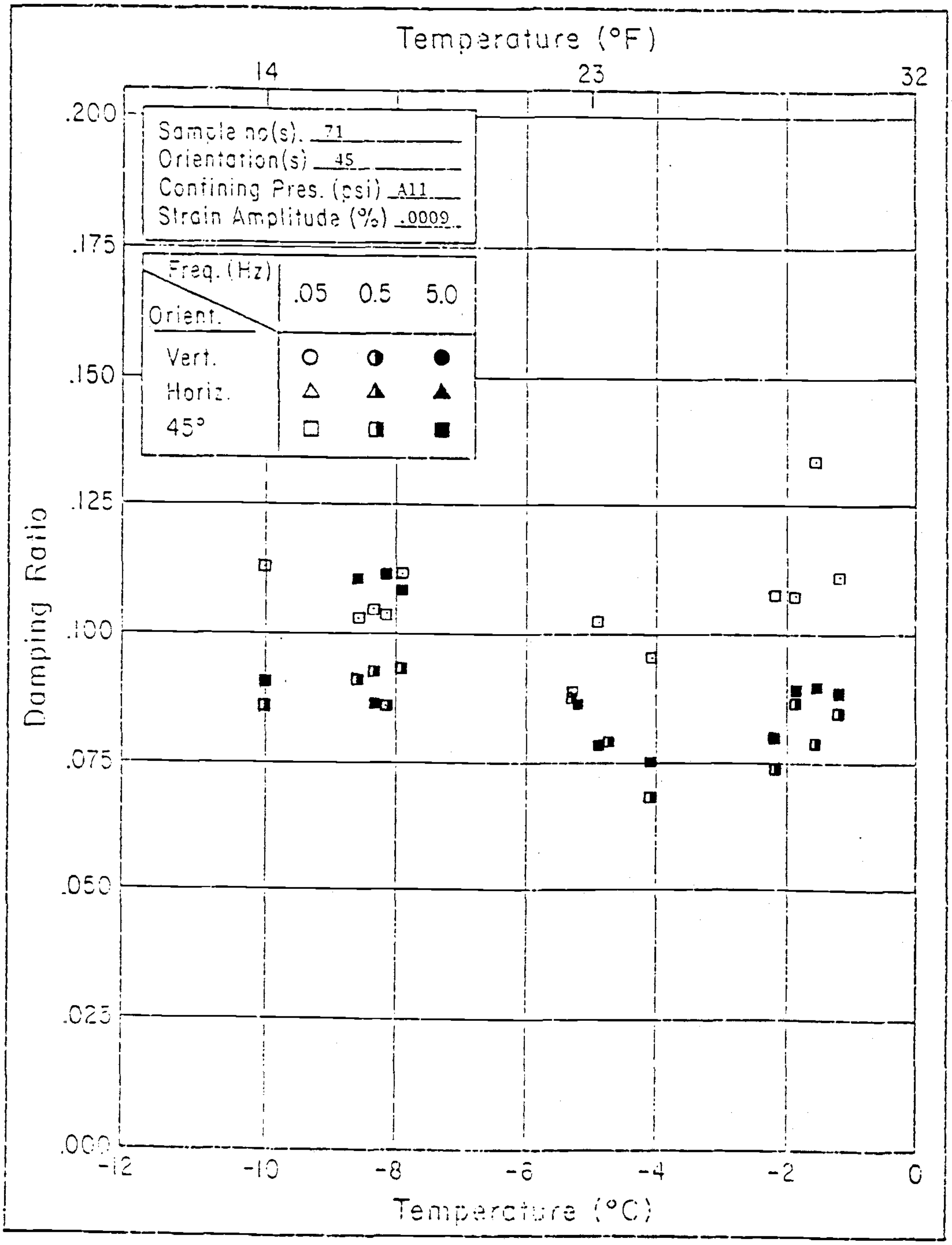

FIGURE A-40 Damping Ratio versus Temperature

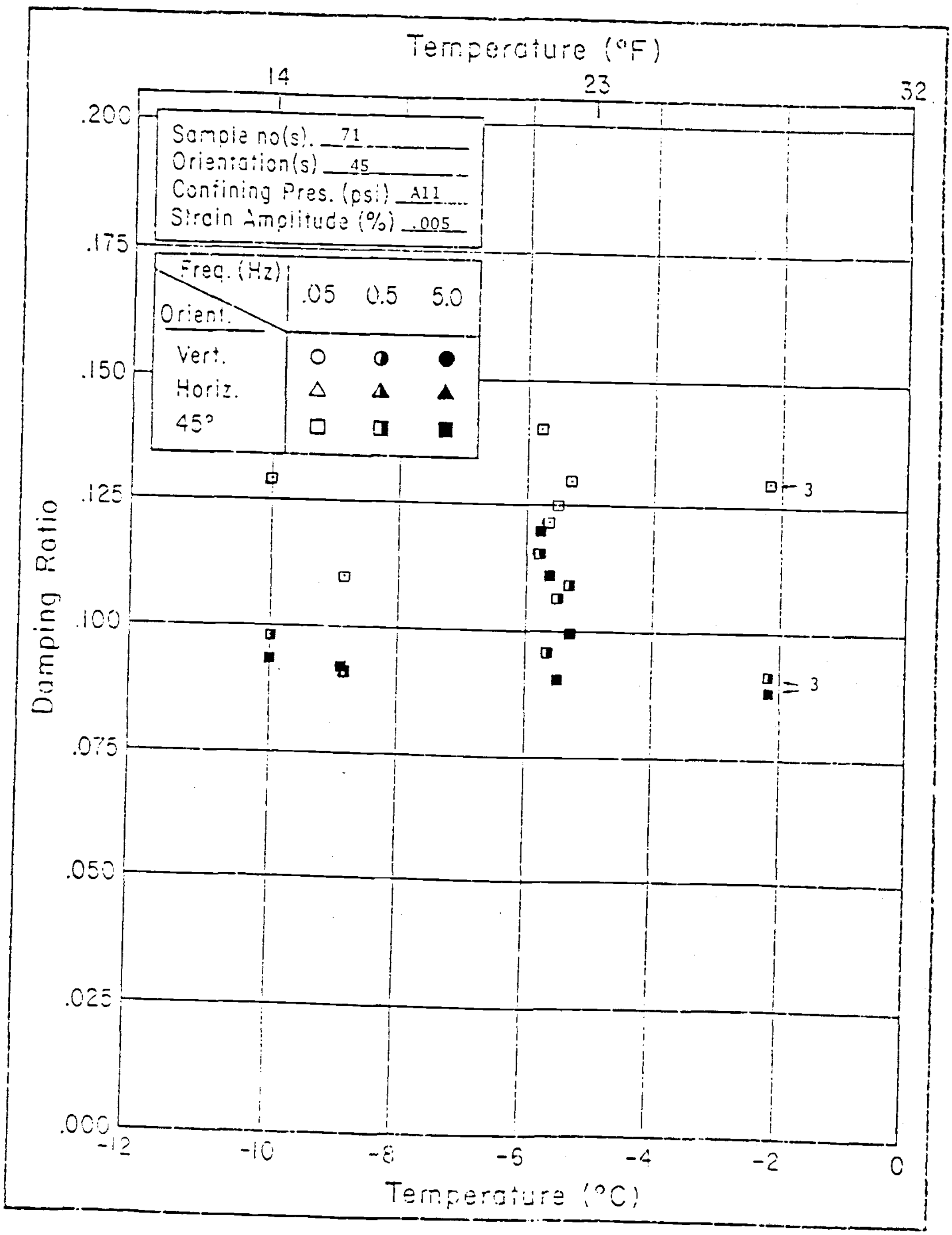

FIGURE A-41 Damping Ratio versus Temperature

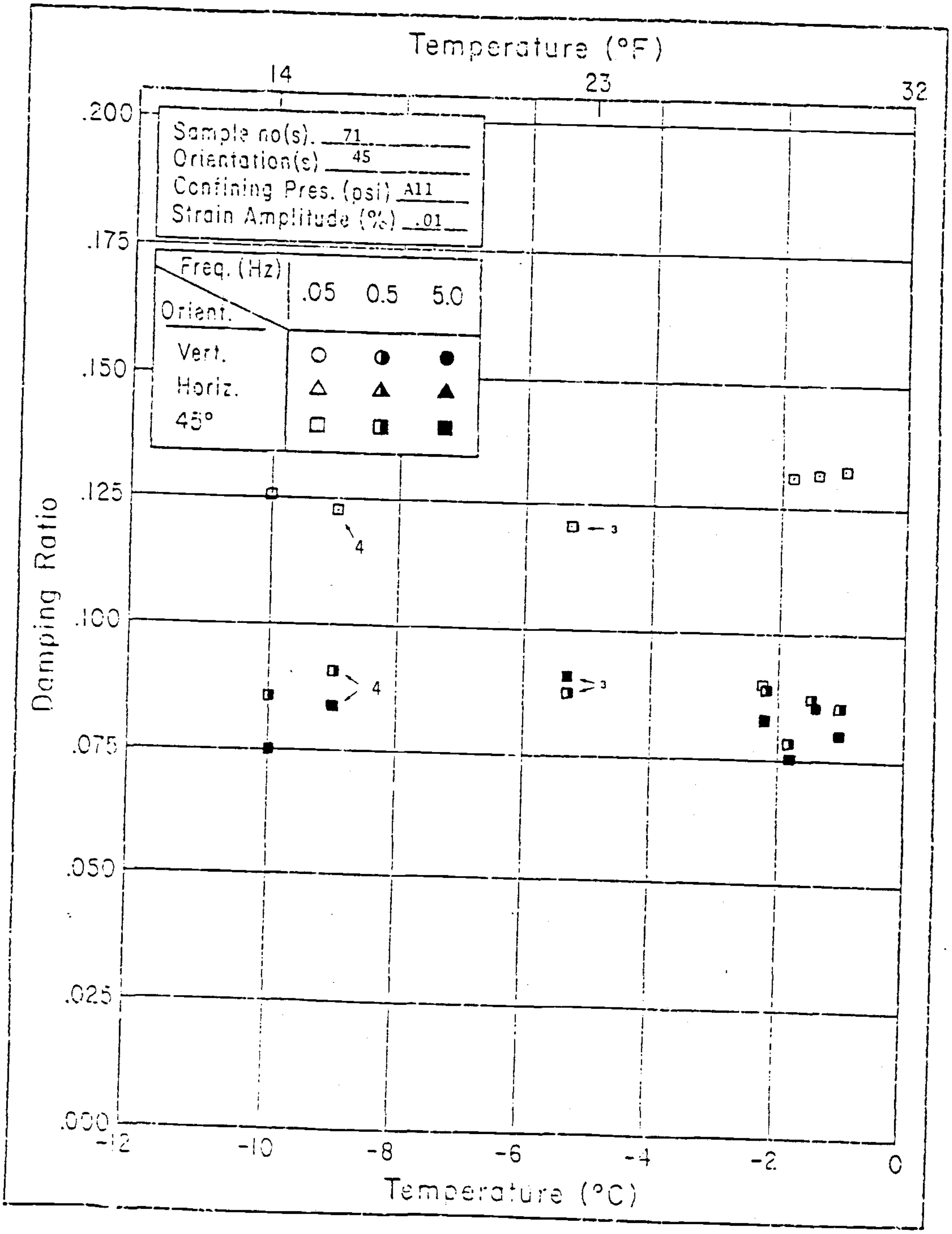

FIGURE A-42 Damping Ratio versus Temperature

APPENDIX B

ICE CRYSTALLOGRAPHY TEST DATA AND FABRIC DIAGRAMS

Ice thin sections were prepared for each ice specimen and ice crystal orientations were measured using a universal stage. From the ice crystal orientation data, ice fabric diagrams were constructed to determine if the ice samples were anisotropic. The fabric diagrams are presented in Appendix B together with a photograph of each thin section viewed through the polarizing sheets while the thin section was attached to the universal stage.

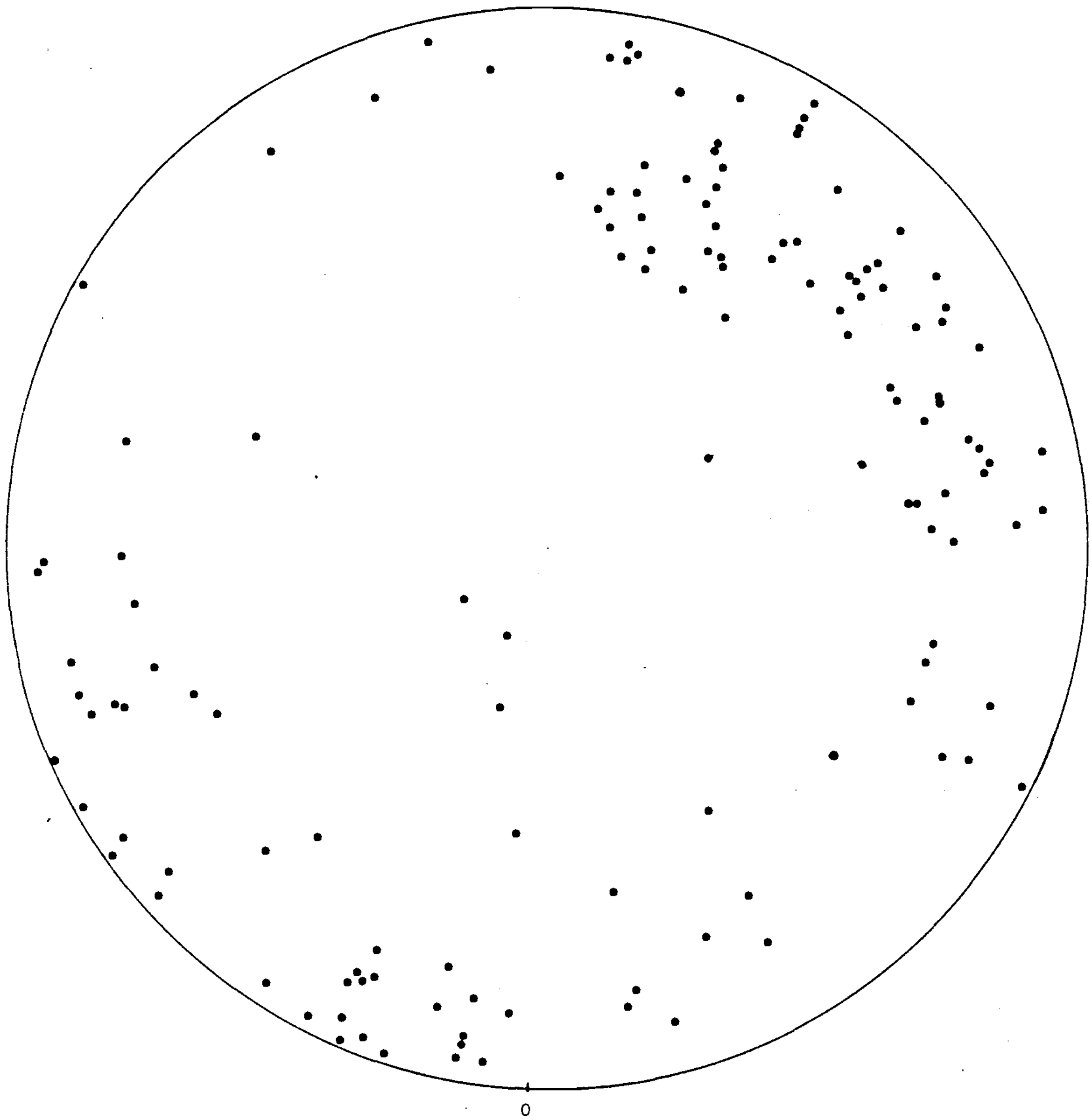

FIGURE B-1 Fabric Diagram For Sample No.65

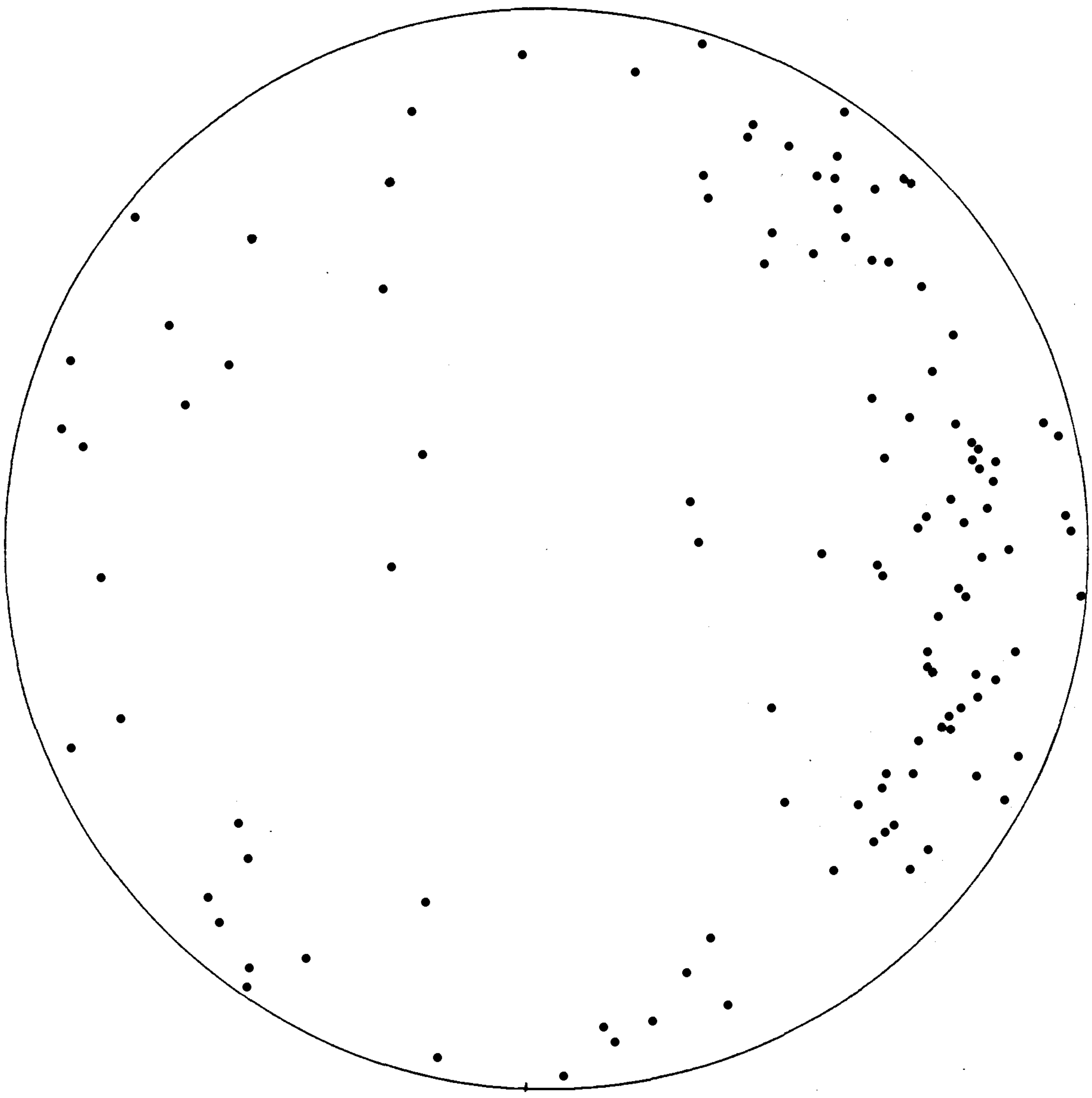

FIGURE B-2 Fabric Diagram For Sample No.71

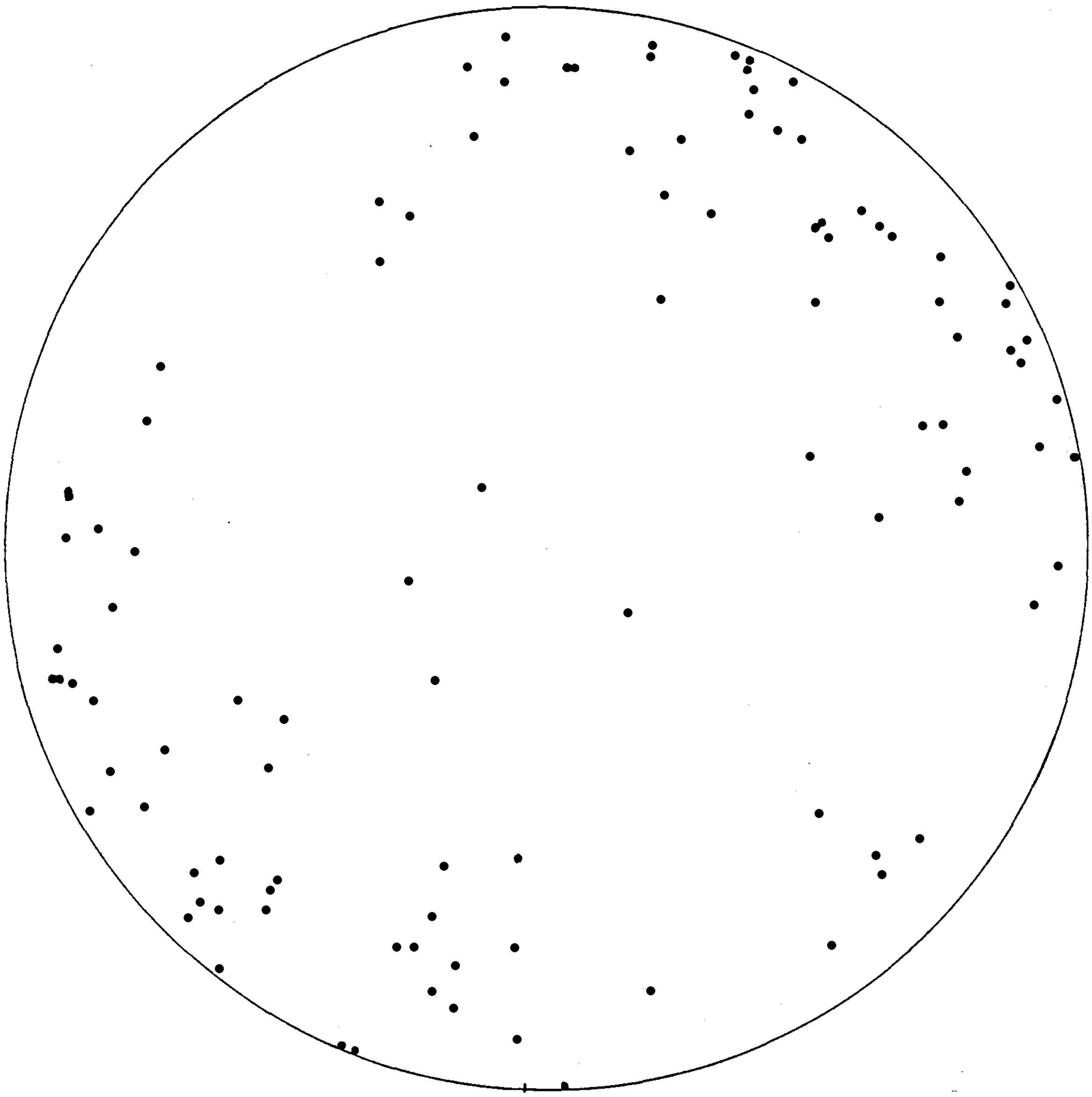

FIGURE B-3 Fabric Diagram For Sample No.72

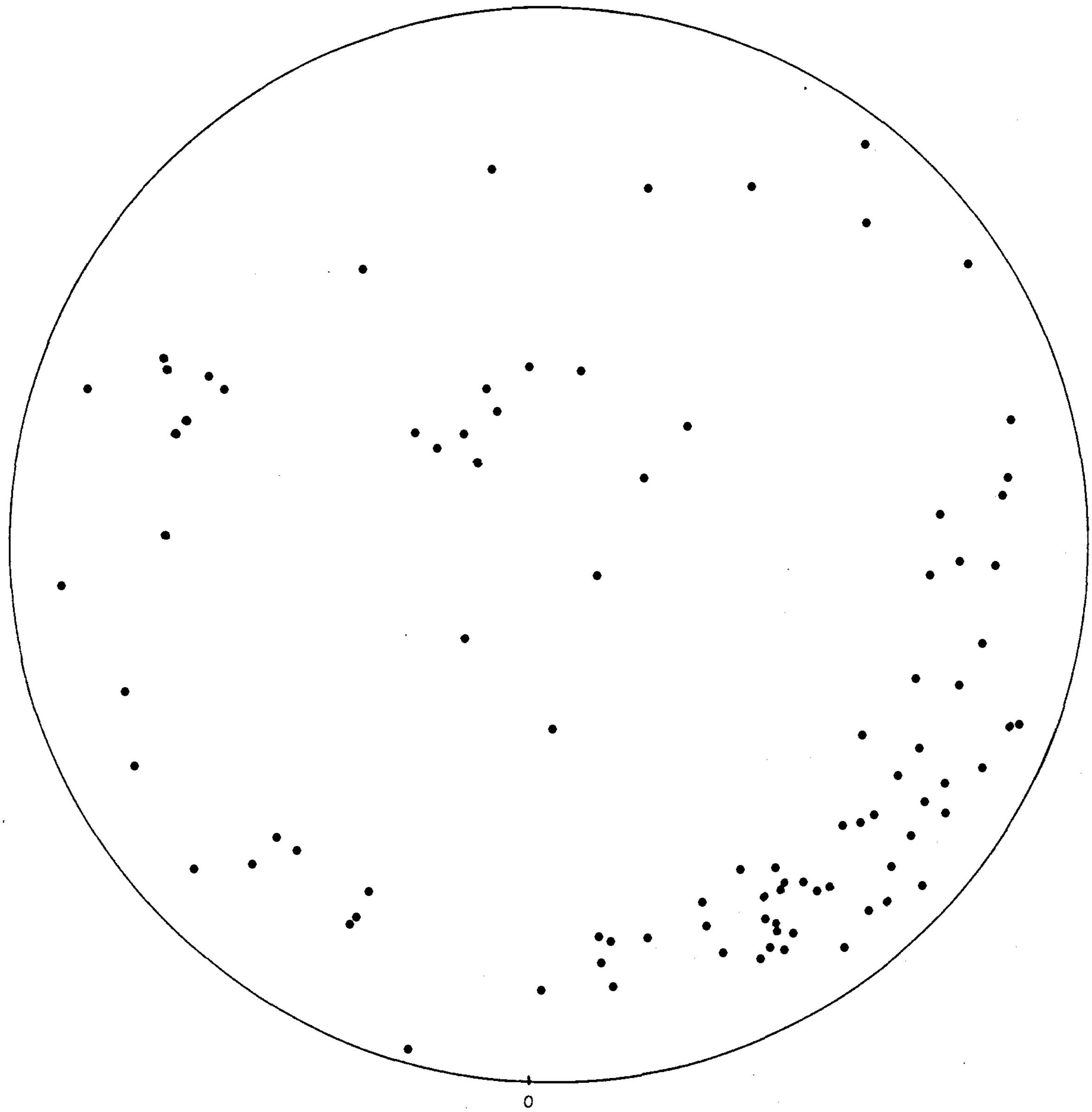

FIGURE B-4 Fabric Diagram For Sample No. 73

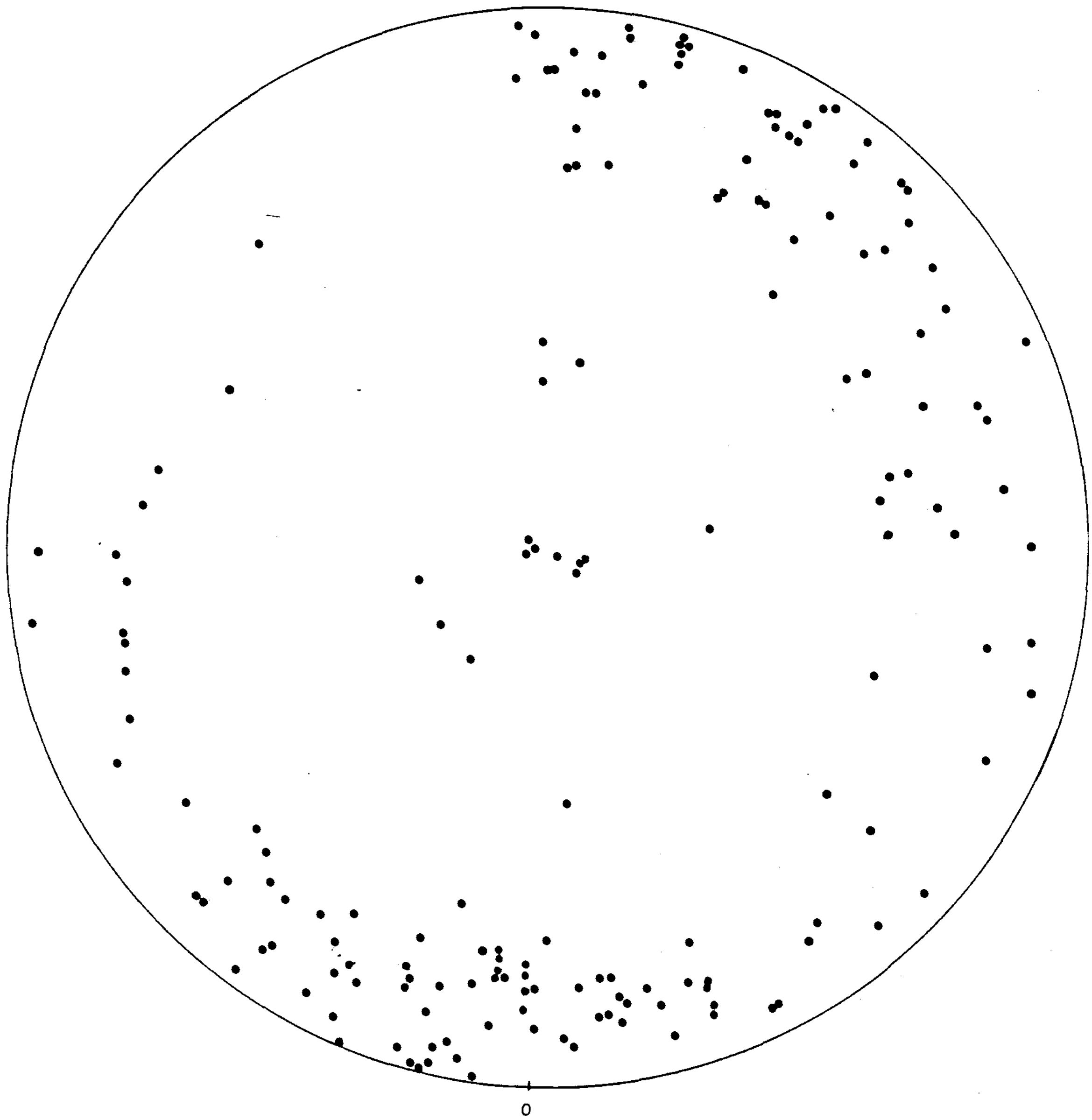

FIGURE B-5 Fabric Diagram For Sample No.75

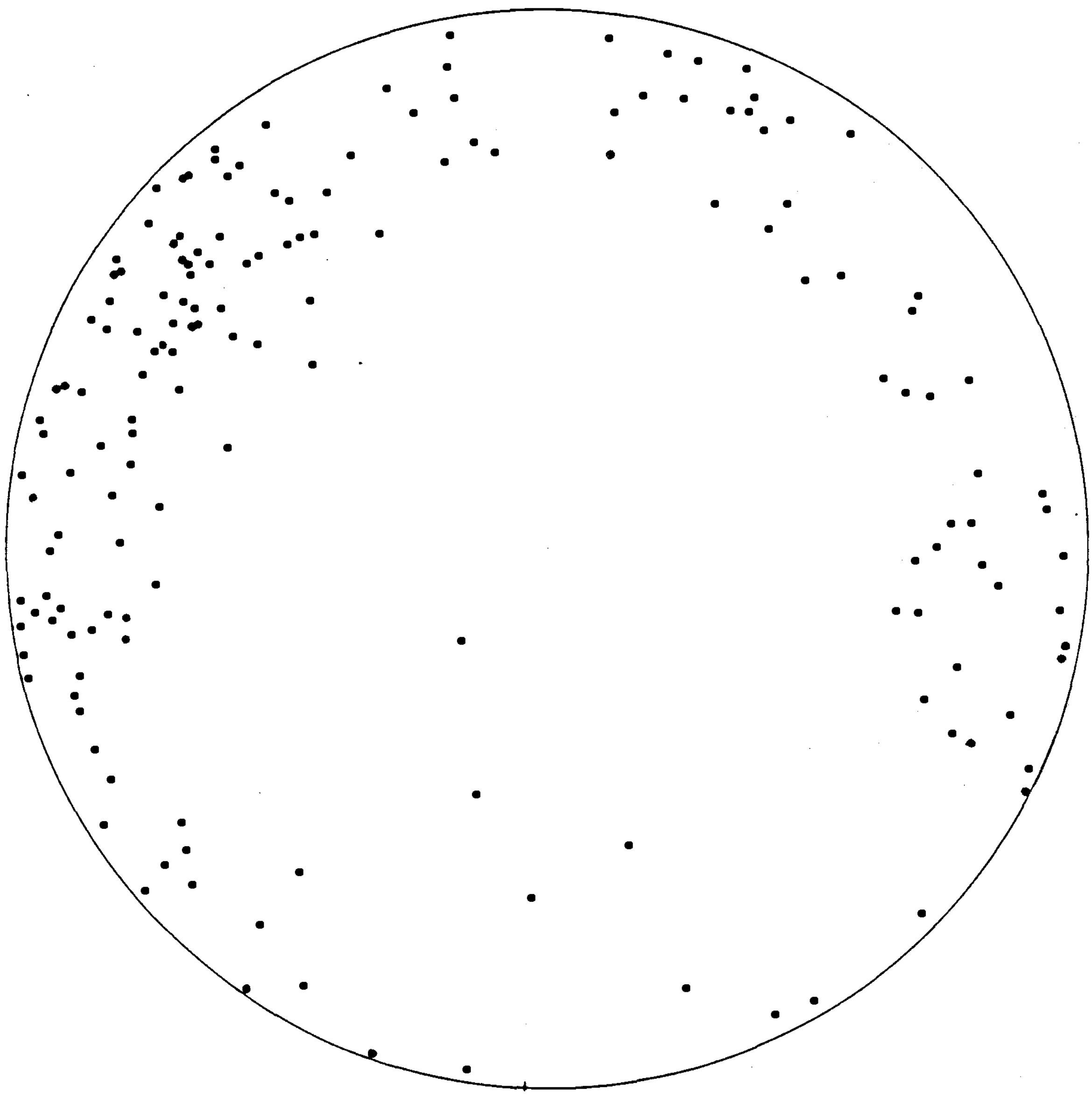

FIGURE B-6 Fabric Diagram For Sample No.78

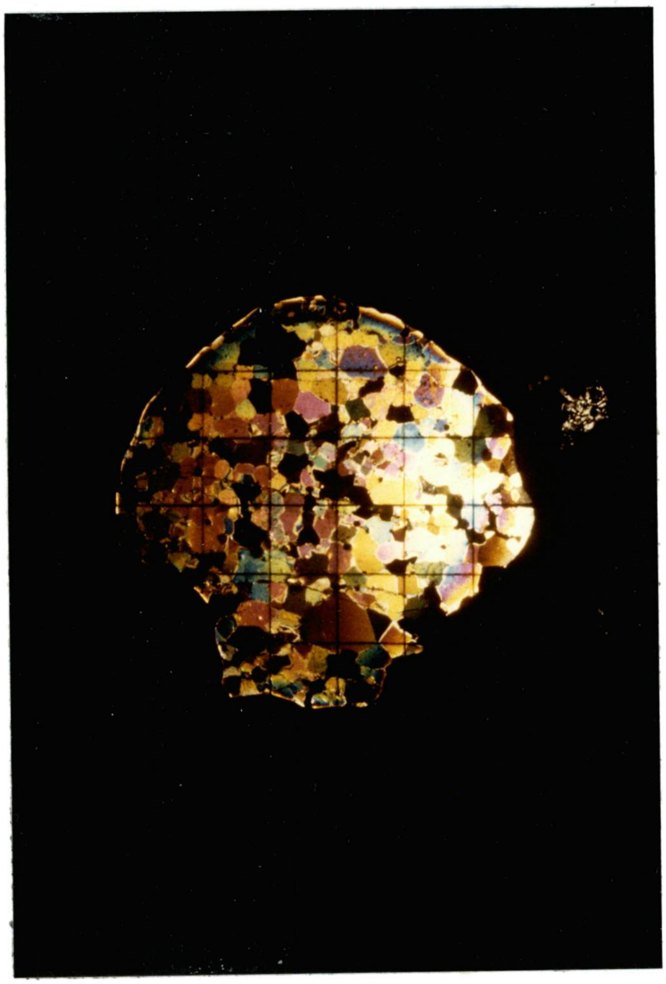

FIGURE B-7 Thin Section Photograph Of Sample No.65

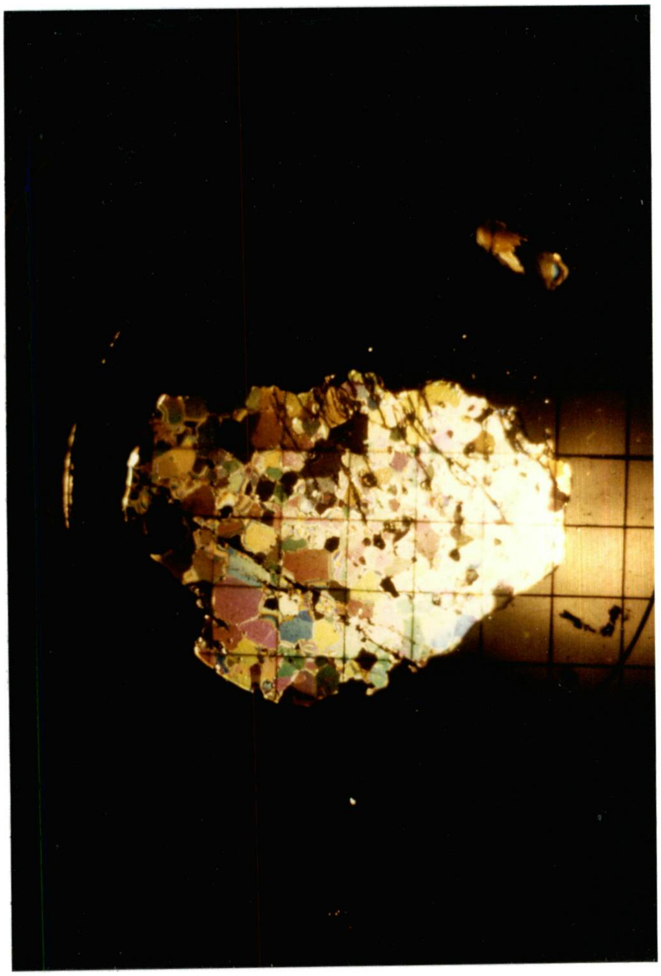

FIGURE B-8 Thin Section Photograph Of Sample No.71

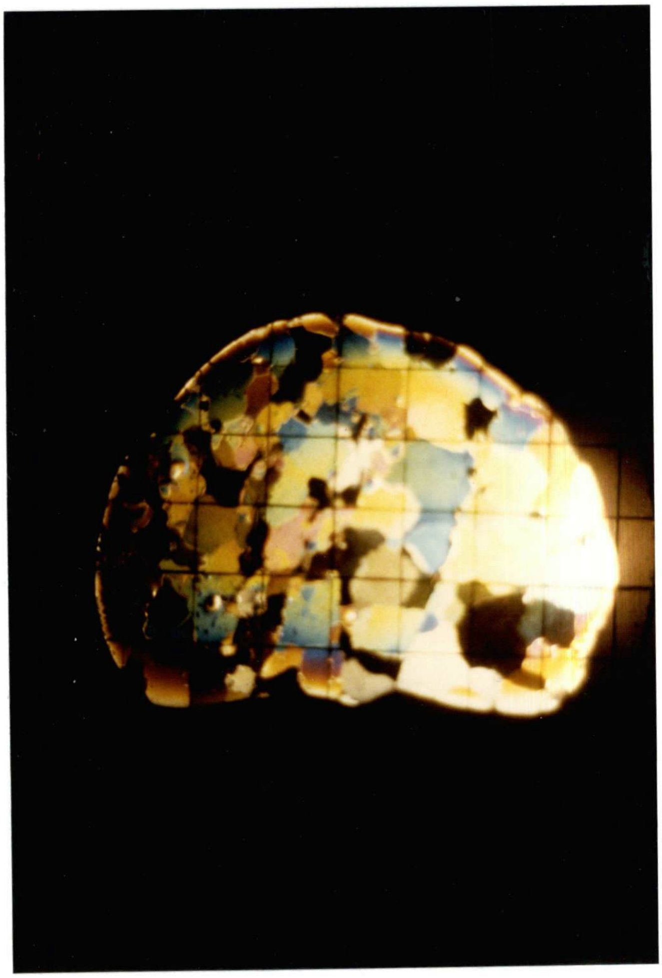

FIGURE B-9 Thin Section Photograph Of Sample No.72

FIGURE B-10 Thin Section Photograph Of Sample No.73

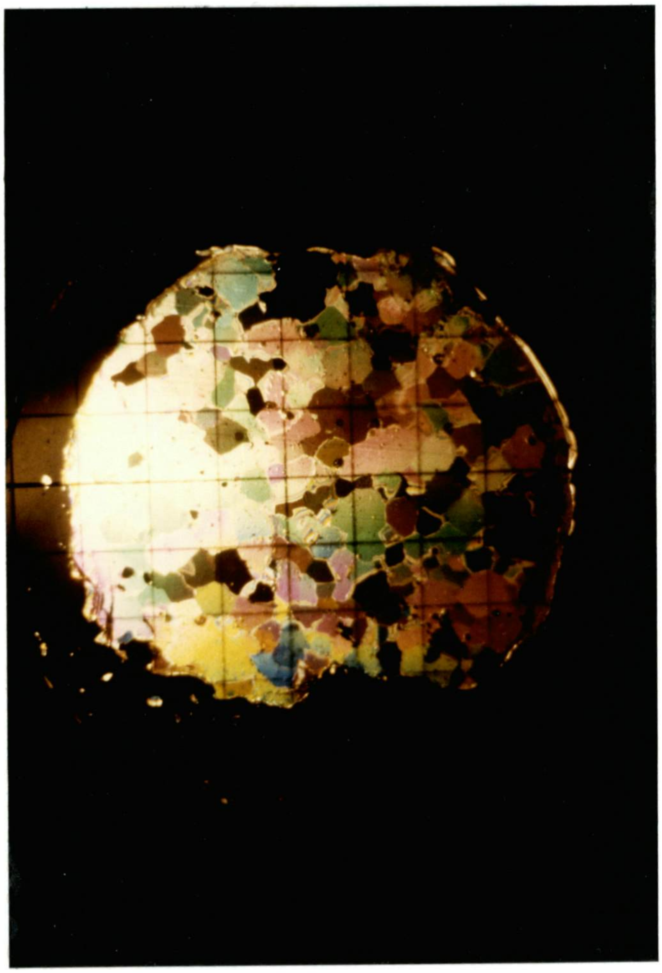

FIGURE B-11 Thin Section Photograph Of Sample No.75

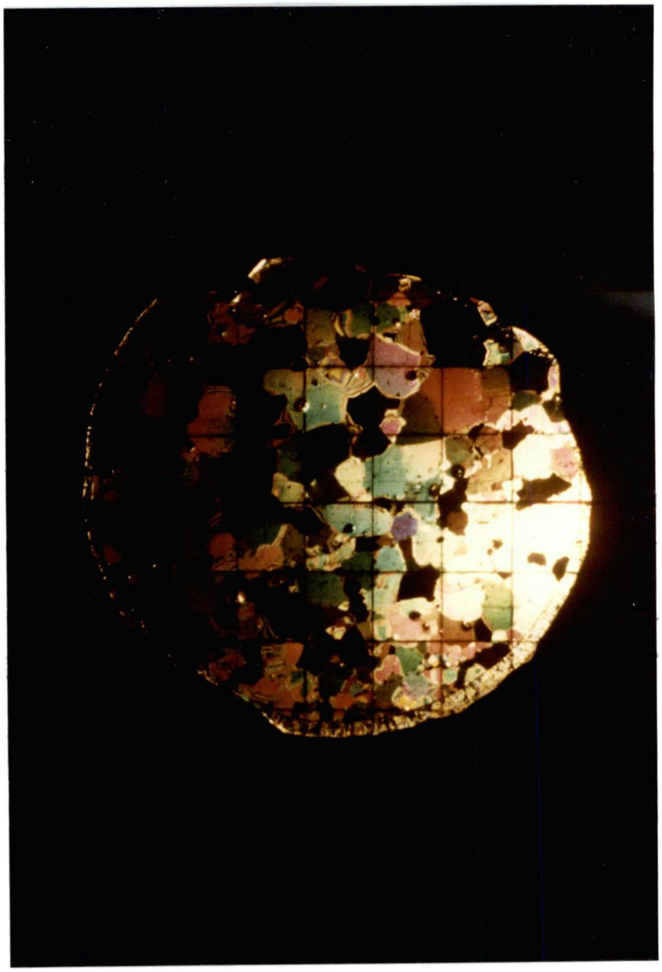

FIGURE B-12 Thin Section Photograph Of Sample No.78

APPENDIX C

DESIGN CURVES FOR DYNAMIC PROPERTIES OF NATURALLY FROZEN ICE

C.1 Design Curves for Field Loading Conditions Similar to Resonant Column Test Conditions

Ice specimens were tested in the resonant column device at varying temperatures and confining pressures over a limited range of low strain amplitudes (see Figure 2-6). The specimens were obtained from core samples of naturally frozen anisotropic ice and were tested at different core orientations (vertical, horizontal and at 45°). Of the variables considered, only temperature had a significant affect on the dynamic properties measured. Since the resonant column test results were influenced only by temperature, separate design curves were developed for use when strain amplitudes and frequencies commensurate with resonant column loading conditions are anticipated under field conditions. Design curves are presented in Figures C-1 through C-3. The resonant column test results were also combined with the cyclic triaxial test results to construct design curves for more general loading conditions.

For the situation where only resonant column loading conditions exist (e.g., high frequency, low strain amplitude loading), Figures C-1 through C-3 can be used as follows to obtain dynamic properties:

(1) With a knowledge of the temperature of the ice, Figure C-1 is entered to obtain a value of dynamic Young's modulus.

(2) Similarly, with the temperature known, Figure C-2 is entered to obtain a dynamic shear modulus.

(3) Finally, Figure C-3 is entered to obtain a damping ratio. Figures C-1 through C-3 are only applicable under resonant column loading conditions. Most engineering problems would require the use of the general design curves described in the next section.

C.2 Design Curves for General Dynamic Loading Conditions

Ice specimens were tested in the cyclic triaxial device at varying temperatures, confining pressures, frequencies and strain amplitudes. All four parameters (temperature, confining pressure, frequency and strain amplitude) were found to influence the dynamic properties during cyclic triaxial testing.

Figures C-4 through C-11 were developed as design curves for the solution of engineering problems involving dynamic properties. The design curves are intended for use as follows:

(1) With a knowledge of the temperature and strain amplitude of the ice for which dynamic properties are desired, Figure C-4 is entered to obtain a value of dynamic Young's modulus.

(2) With the value of modulus obtained for Figure C-4, Figure C-5 is entered as a check curve incorporating the anticipated frequency of loading.

(3) Figure C-6 is entered as a second check curve to verify the anticipated strain amplitudes.

(4) Finally, Figure C-7 is entered to obtain a refined dynamic Young's modulus.

(5) Figure C-4 is rechecked with the results of step 5.

For a value of damping ratio, Figures C-8 through C-11 are entered as per Figures C-4 through C-7 above.

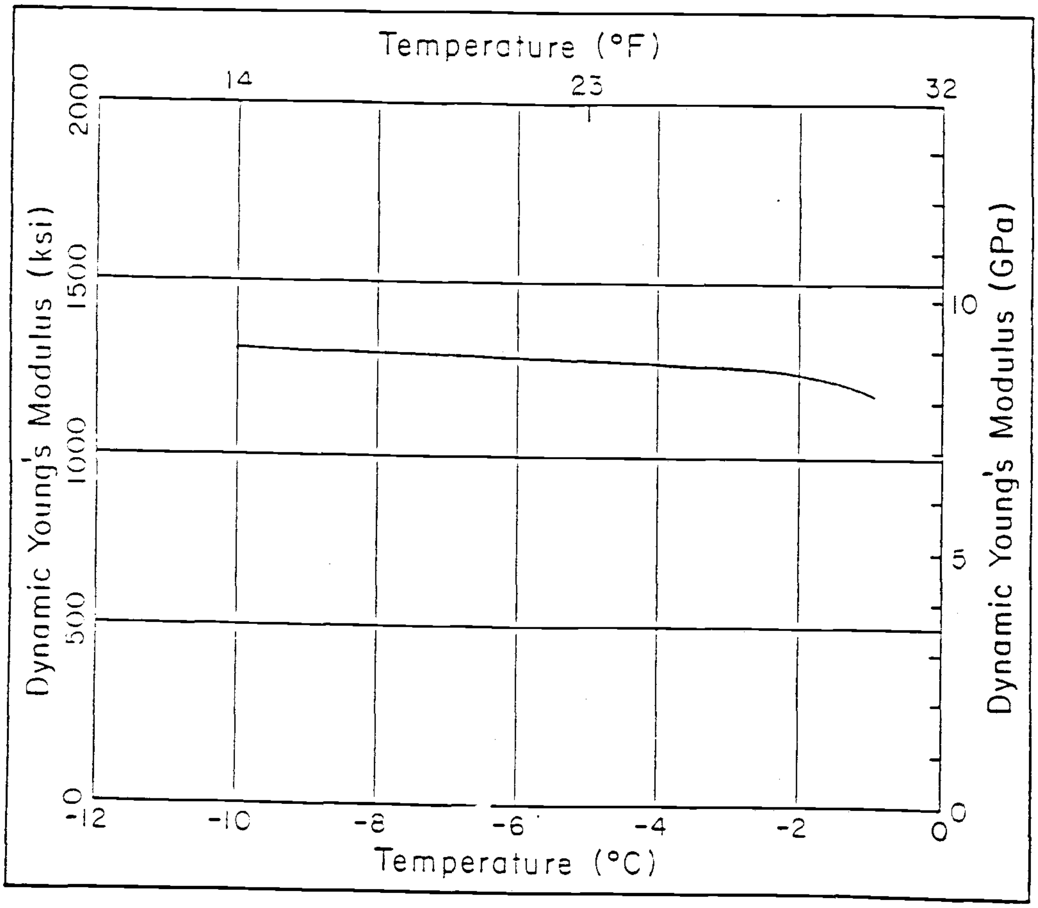

Figure C-1

Design Curve For Determining Dynamic Young's Modulus (Resonant Column Only)

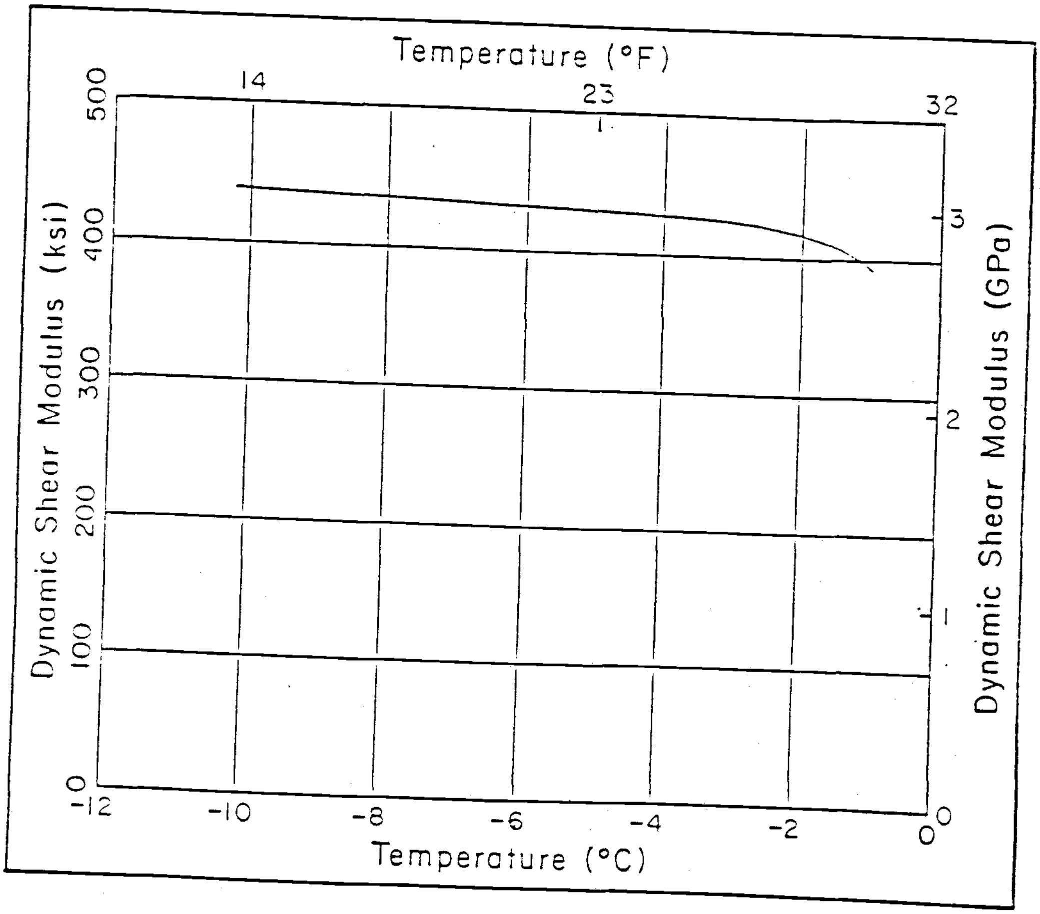

Figure C-2

Design Curve For Determining Dynamic Shear Modulus (Resonant Column Only)

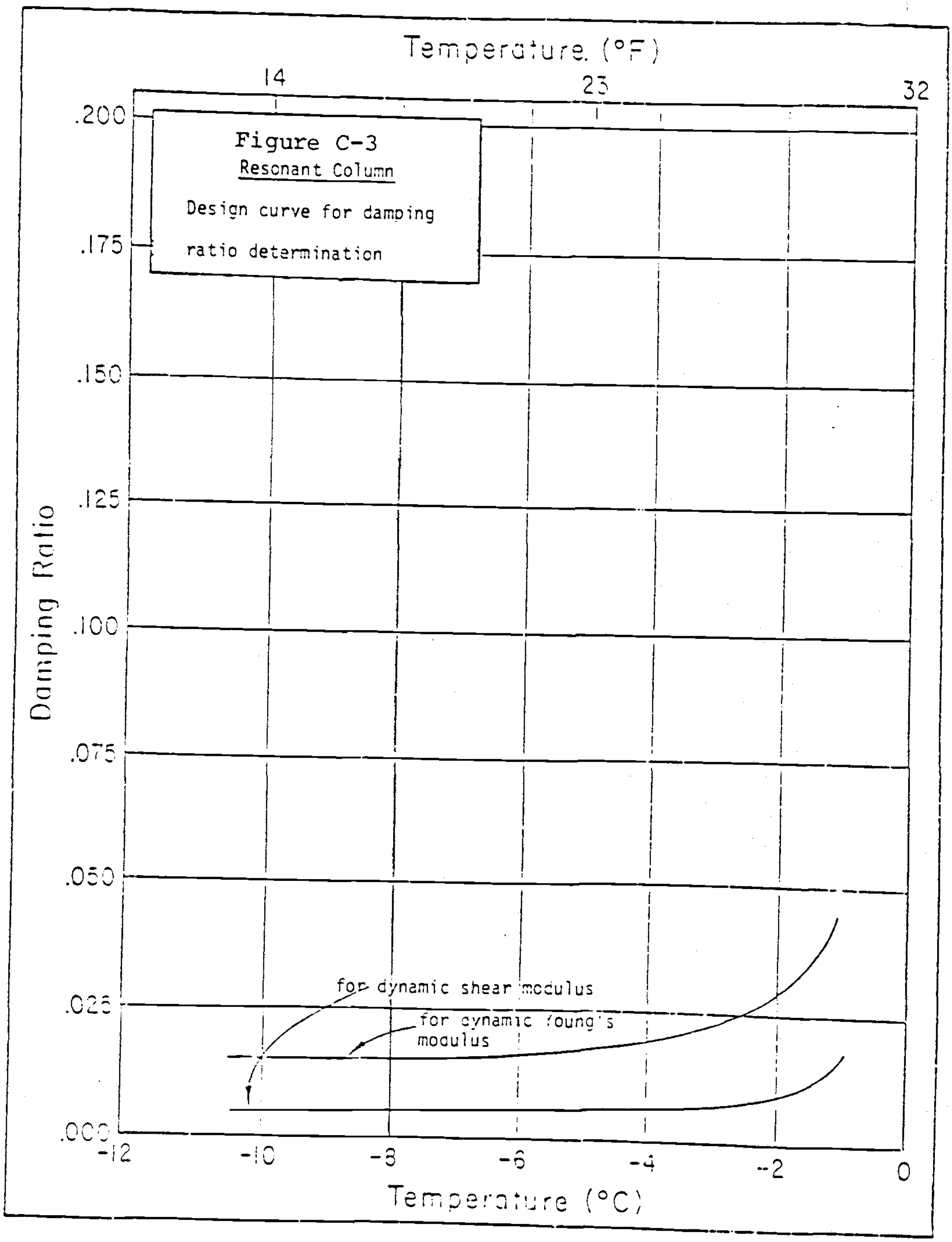
Temperature (°F)
14
23
32
.200
.175
.150
.125
.100
.075
.050
.025
.000
Damping Ratio
Figure C-3
Resonant Column
Design curve for damping ratio determination
for dynamic shear modulus
for dynamic Young's modulus
-12
-10
-8
-6
-4
-2
0
Temperature (°C)

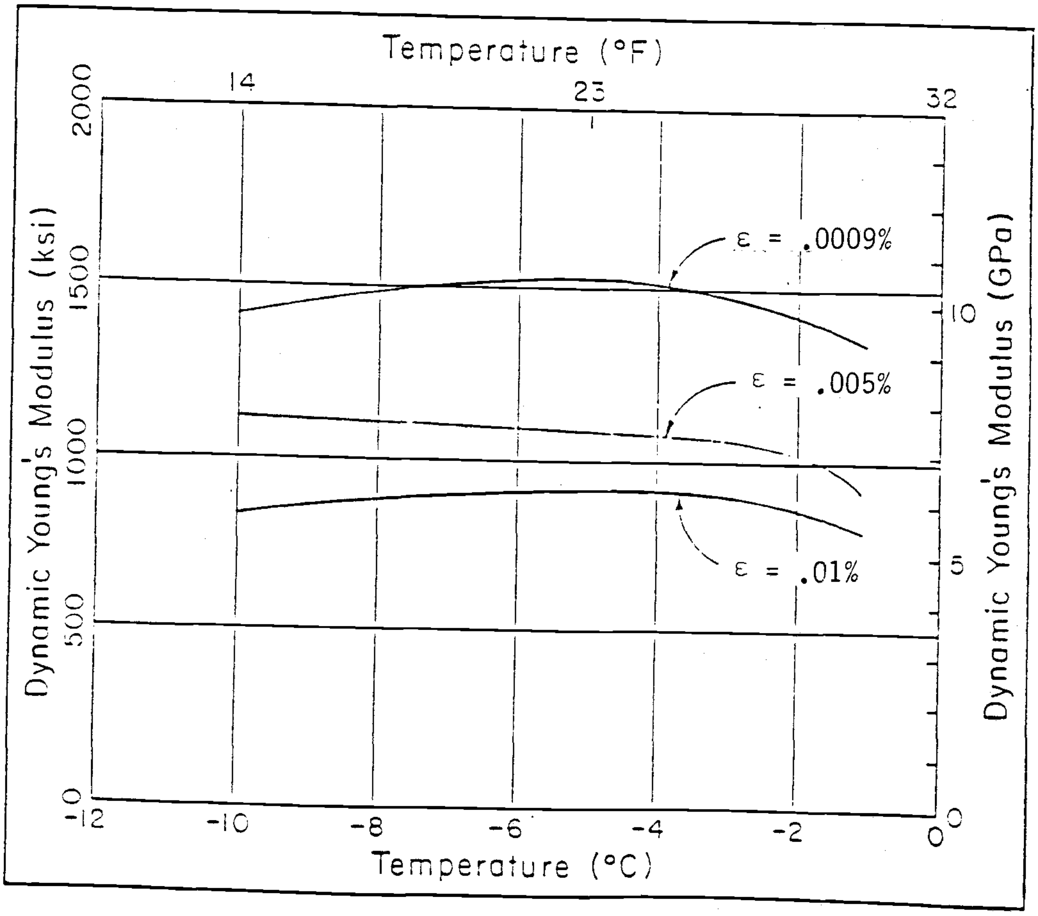

Figure C-4

Cyclic Triaxial

Design curve #1 for dynamic Young's modulus determination

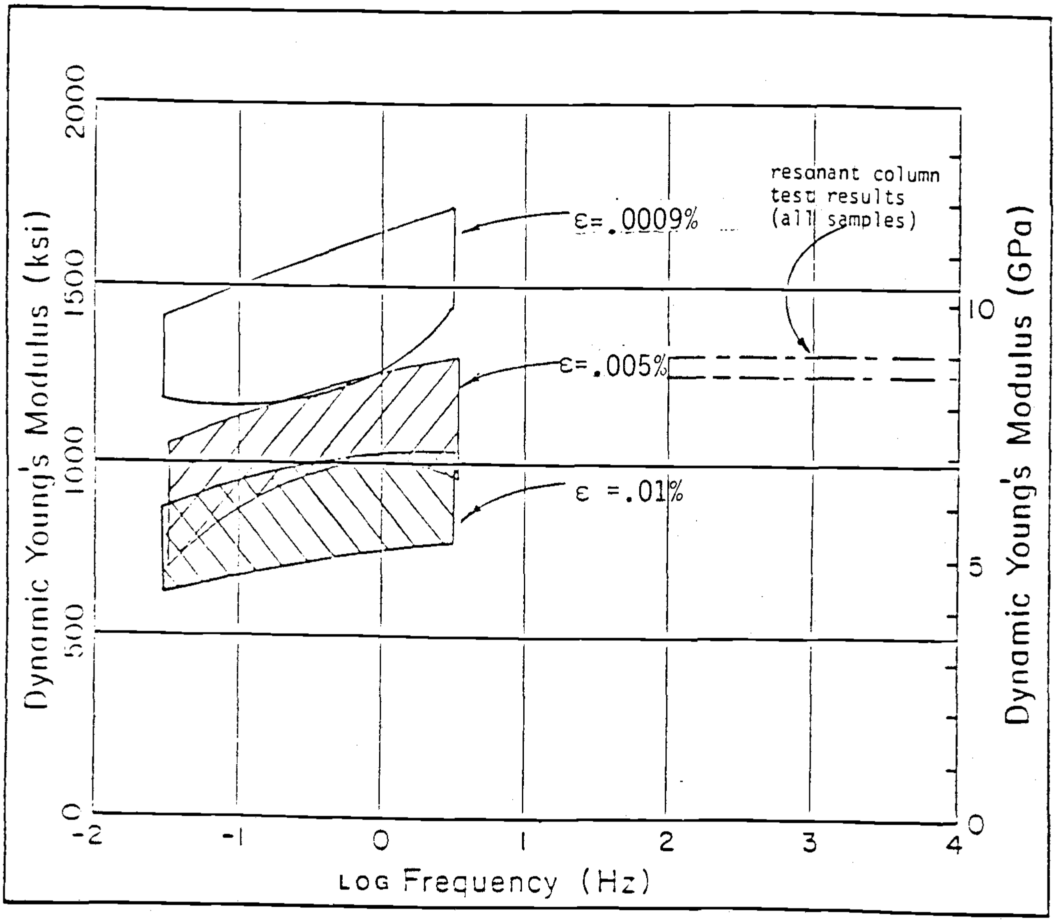

Figure C-5

Design curve #2, summary envelopes for dynamic Young's modulus determination

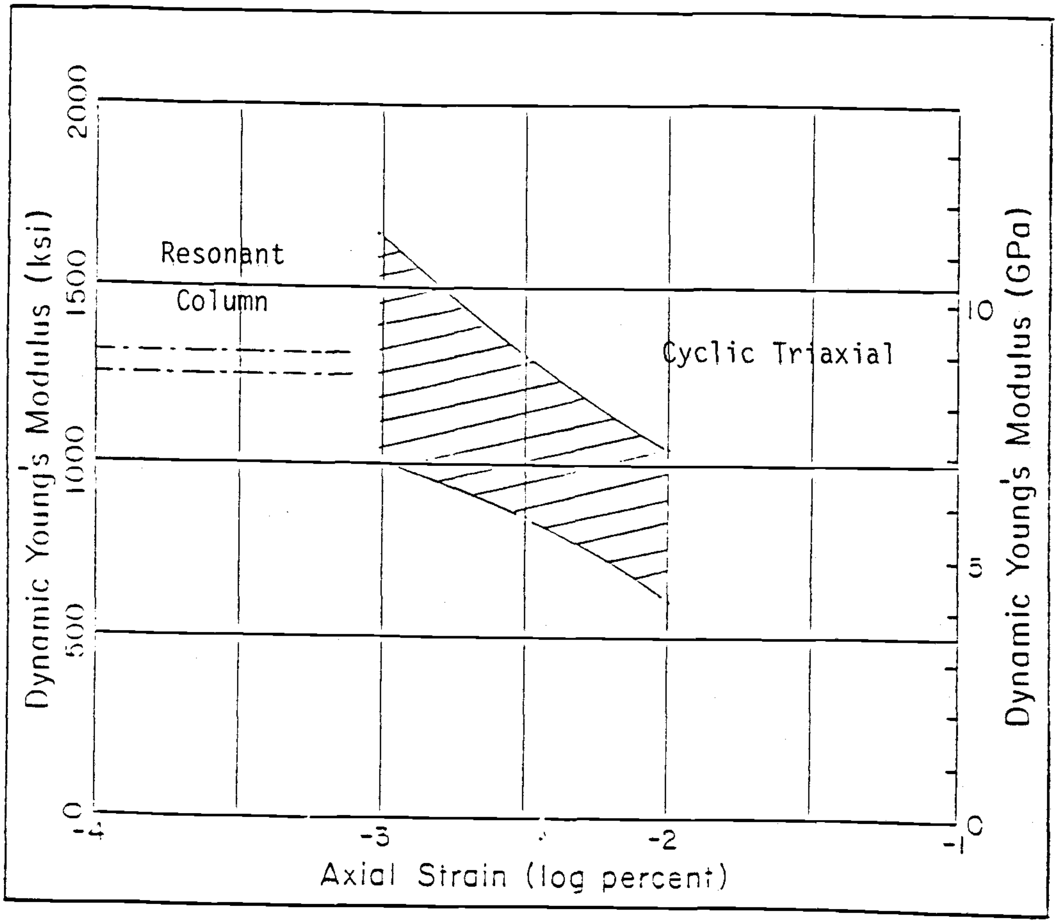

Figure C-6

Design curve #3 for dynamic Young's modulus determination

(check curve)

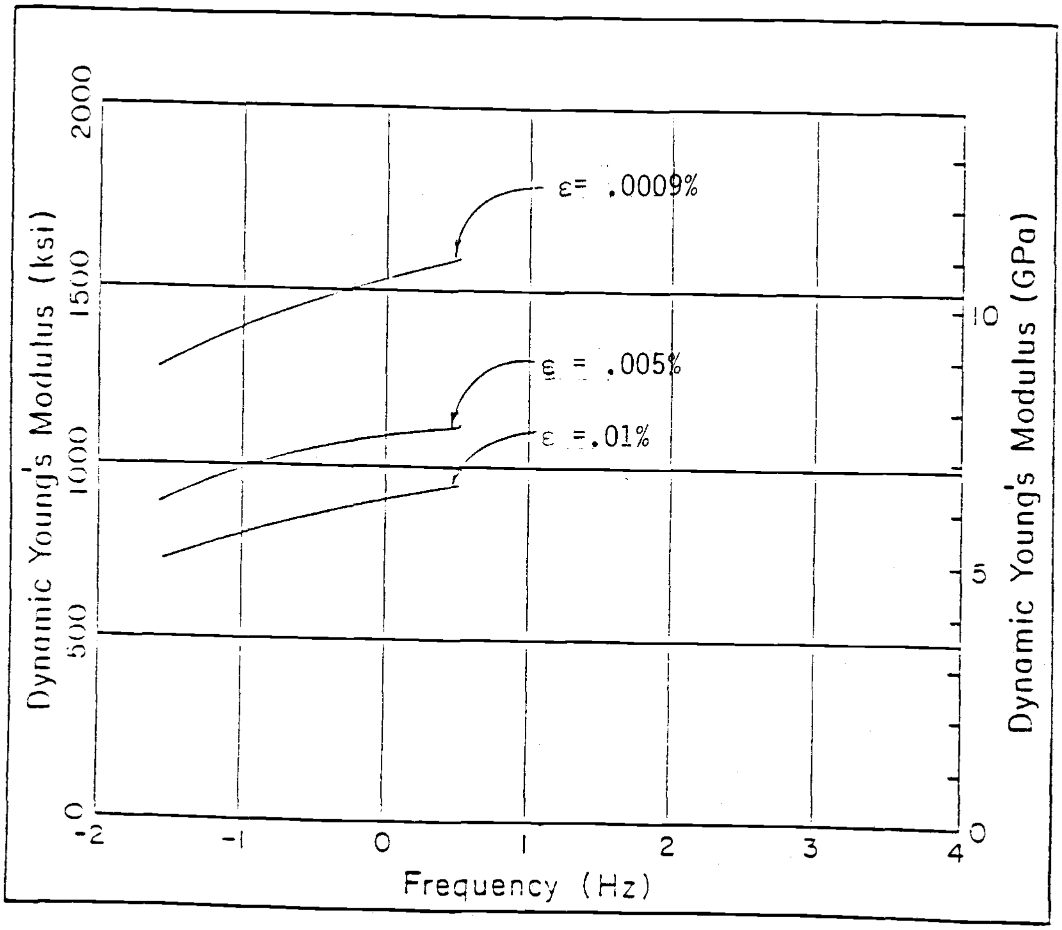

Figure C-7

Cyclic Triaxial

Design curve #4 for dynamic Young's modulus determination

(check curve)

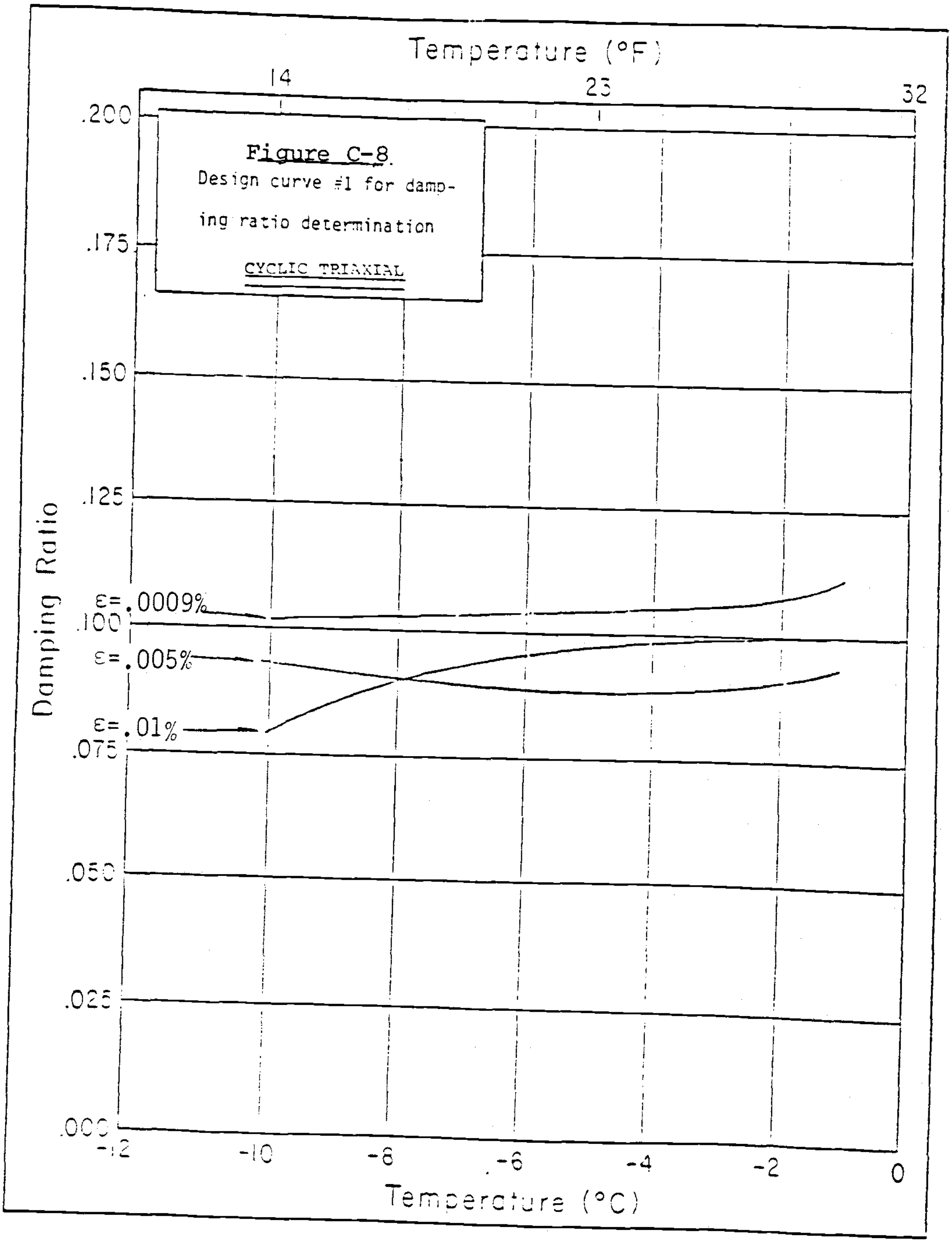

Figure C-8

Design curve #1 for damping ratio determination

CYCLIC TRIAXIAL

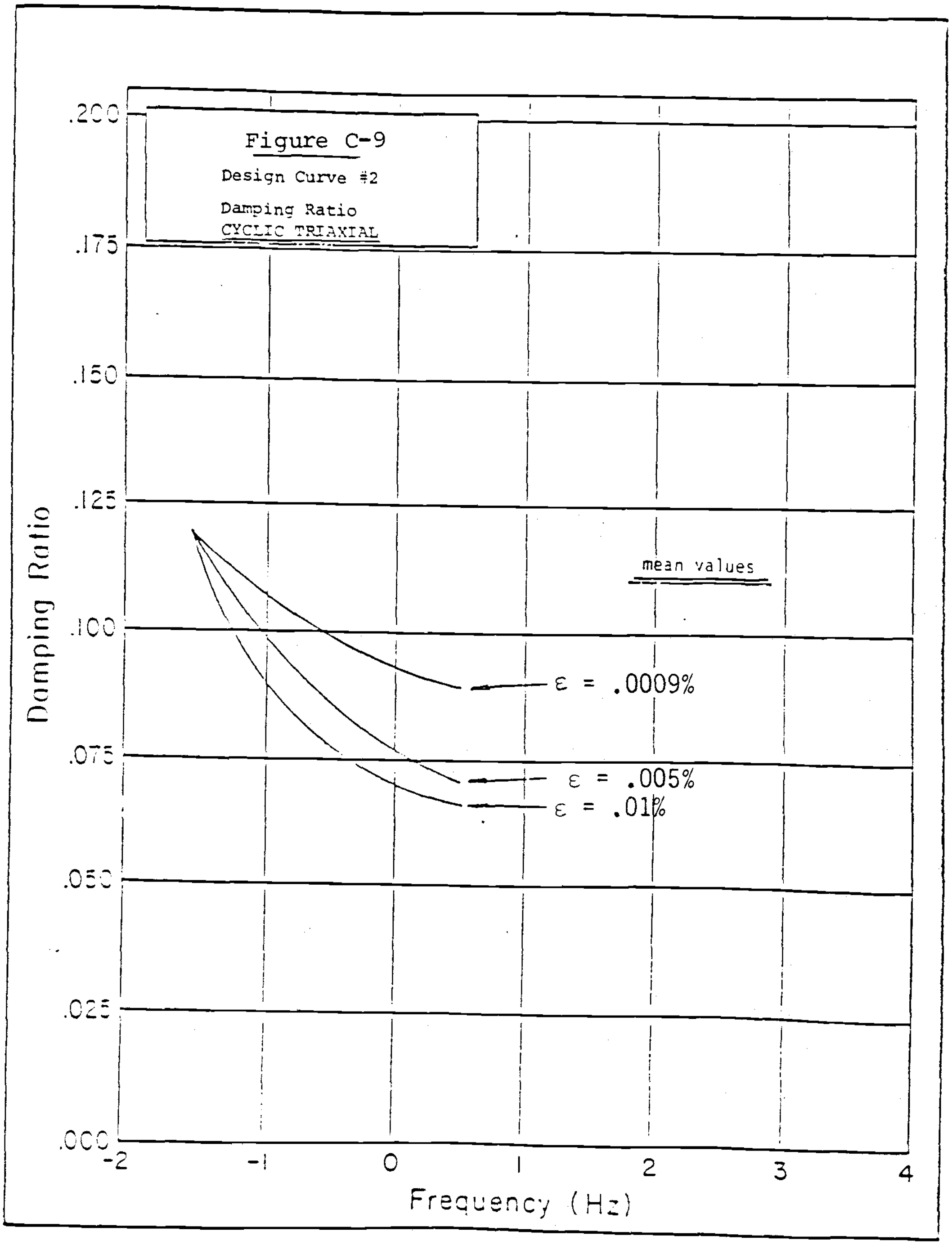

Figure C-9
Design Curve #2
Damping Ratio
CYCLIC TRIAXIAL
mean values
ε = .0009%
ε = .005%
ε = .01%
Damping Ratio
.200
.175
.150
.125
.100
.075
.050
.025
.000
-2
-1
0
1
2
3
4
Frequency (Hz)

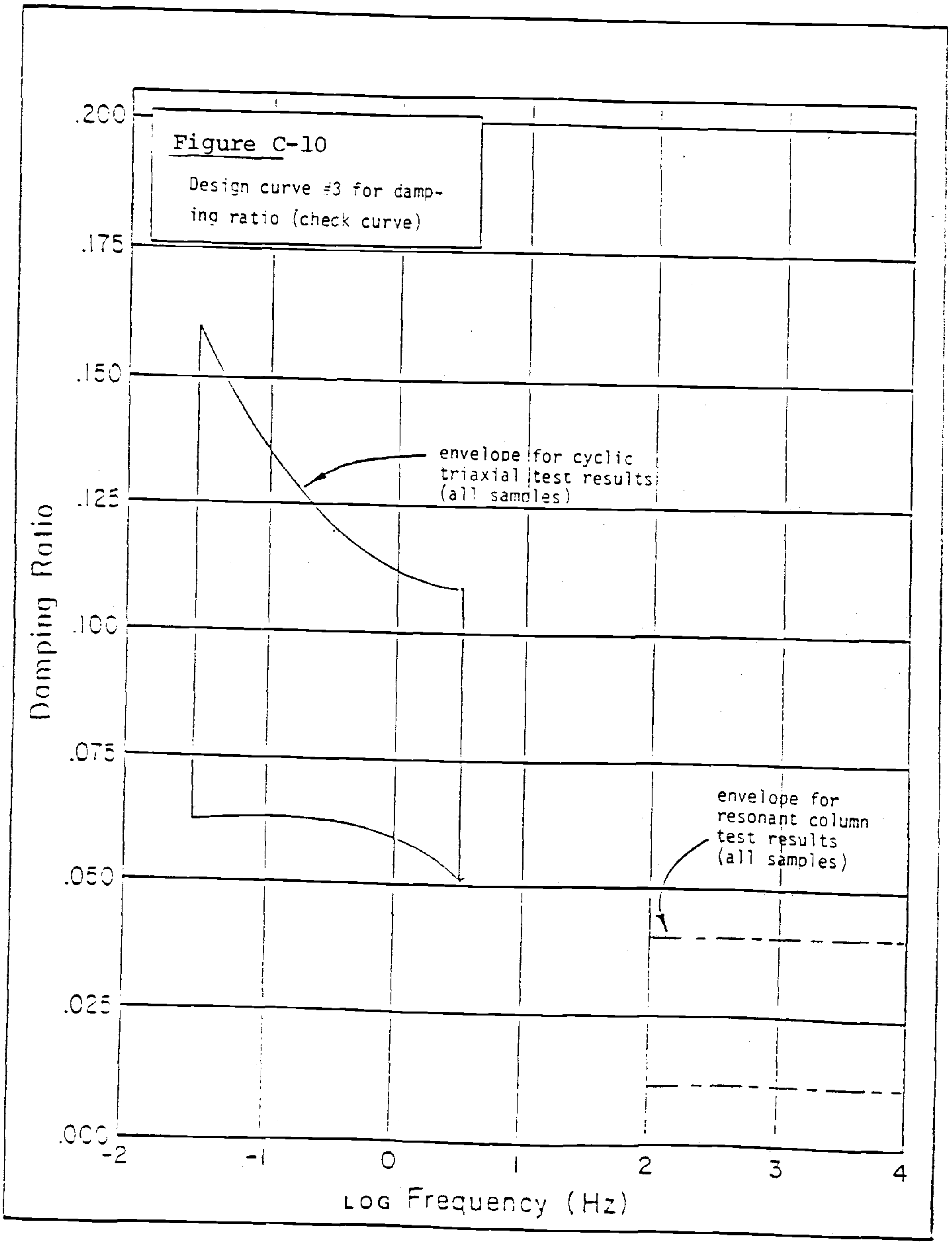
Figure C-10
Design curve #3 for damping ratio (check curve)
Damping Ratio
.200
.175
.150
.125
.100
.075
.050
.025
.000
-2
-1
0
1
2
3
4
Log Frequency (Hz)
envelope for cyclic triaxial test results (all samples)
envelope for resonant column test results (all samples)

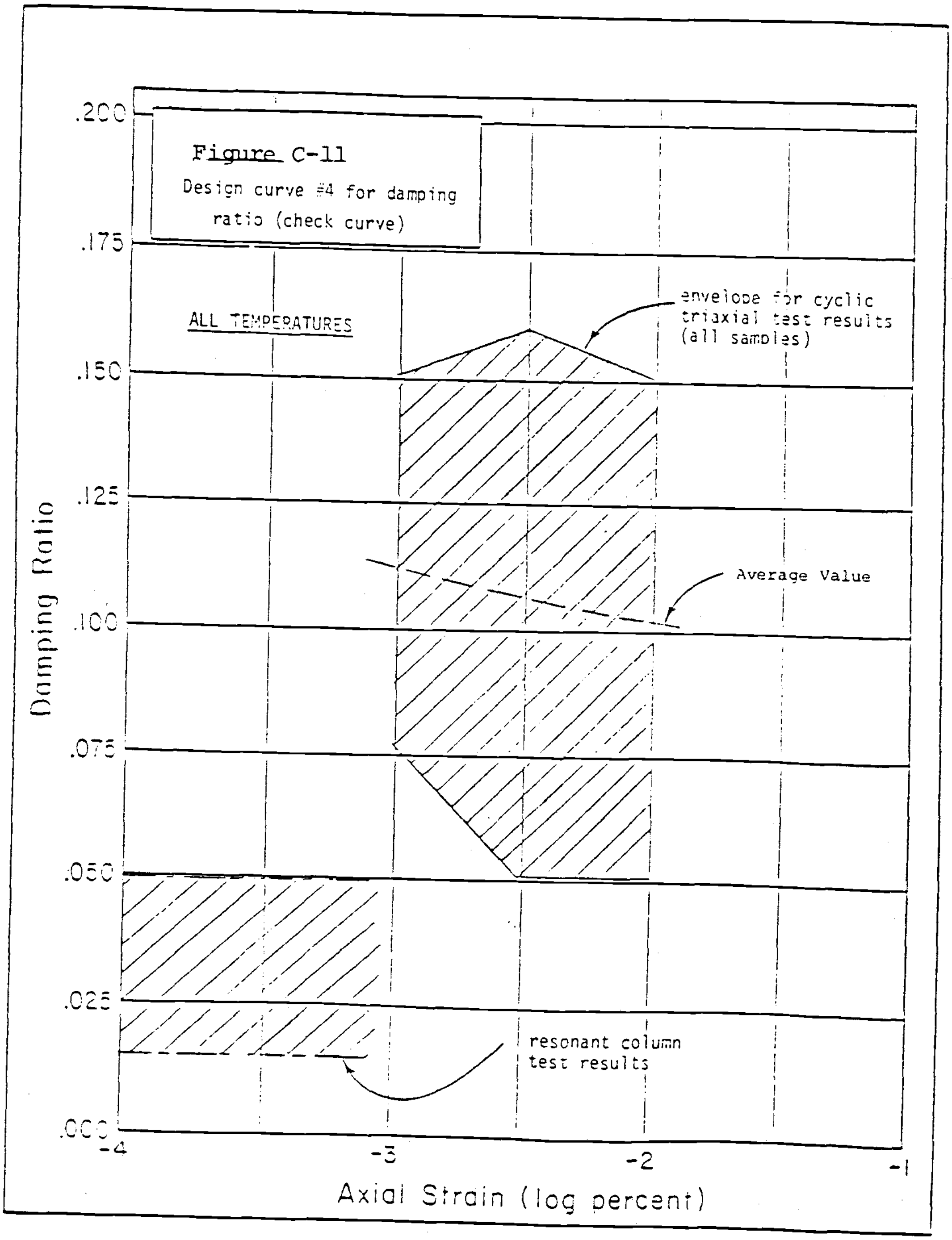
Figure C-11
Design curve #4 for damping ratio (check curve)
ALL TEMPERATURES
envelope for cyclic triaxial test results (all samples)
Average Value
resonant column test results
Damping Ratio
.200
.175
.150
.125
.100
.075
.050
.025
.000
-4
-3
-2
-1
Axial Strain (log percent)